THE UNIVERSITY OF CALGARY

Multiphase Chemical and Polymer Phase Equilibria Calculations

by

Aaron Phoenix

A DISSERTATION
SUBMITTED TO THE FACULTY OF GRADUATE STUDIES
IN PARTIAL FULFILMENT OF THE REQUIREMENTS FOR THE
DEGREE OF DOCTOR OF PHILOSOPHY

DEPARTMENT OF CHEMICAL AND PETROLEUM ENGINEERING

CALGARY, ALBERTA
JUNE, 1998

National Library of Canada
Acquisitions and Bibliographic Services
395 Wellington Street
Ottawa ON K1A 0N4
Canada

Bibliothèque nationale du Canada
Acquisitions et services bibliographiques
395, rue Wellington
Ottawa ON K1A 0N4
Canada

Your file Votre référence

Our file Notre référence

0-612-34692-7

Canada

ABSTRACT

A stoichiometric and a non-stoichiometric multiphase reactive flash algorithm were developed. These algorithms used a successive substitution mechanism to update fugacity coefficients in an outer loop. A nested inner loop solved the elemental balances and reaction equilibria requirements with a Newton-Raphson procedure. The inner loops in both cases were convex and quickly converged. Average chemical potentials for each species were used to define the reference phase chemical potentials.

The reactive flash routines were initiated with the maximum number of phases: one more than the number of components. Phases were combined as they became identical at each iteration. The tangent plane distance was incorporated into the unnormalized mole fractions of each phase so that phase stability could easily be examined during each iteration of the outer loop. This feature allowed incipient phases to be determined.

Both algorithms performed well in predicting the multiphase equilibria of methanol synthesis from carbon dioxide and hydrogen. An excess free energy mixing rule for a cubic equation of state was developed and used with the non-stoichiometric algorithm to calculate the conversion of methanol and isobutene to MTBE over a range of compositions. An association model for sulfur allotropes and sulfanes was used with the non-stoichiometric technique to successfully predict sulfur vapour pressures, enthalpies of vapourization and sulfur solubilities in hydrogen sulfide.

An algorithm to calculate isobaric lines of constant phase fraction in a polydisperse polymer/solvent system was developed. When a phase fraction of 0 or 1 was used, the lines represented the cloud and shadow point curves. A functional approach to continuous thermodynamics was employed using the Sanchez-Lacombe equation of state to model the components. Five scalar equations defined a single point on a curve and could be solved quickly using a Newton-Raphson method. Required integrations were done using a fifth order Runge-Kutta technique or a Gaussian quadrature technique.

The cloud point curves for a polyethylene/n-hexane system ($M_n = 8000$, $M_w = 177000$) showed an unstable critical point and a LLL point when the polyethylene was modeled with a log-normal distribution. Polyethylene modeled with the Shultz-Flory distribution did not show the same three phase point nor the unstable critical point.

A preliminary investigation into a multiphase polymer flash using continuous thermodynamics was done. The Sanchez-Lacombe equation of state was used to represent the components. Both a successive substitution approach and a Newton-Raphson approach were used to solve the scalar equations that defined the equilibrium. The development of the algorithm allowed incipient phases to be determined.

It was found that a damped successive substitution method was more reliable than using a combination of the successive substitution and Newton-Raphson techniques. Additional studies into initiation techniques and the effective use of a Newton-Raphson step to decrease convergence time are recommended.

ACKNOWLEDGEMENTS

I would like to acknowledge and thank my supervisor, Dr. Robert Heidemann, for his guidance, assistance and support in completing this work. Time and time again, his insight was beneficial in overcoming many of the computational and conceptual hurdles encountered in this work.

I would also like to thank my many friends and colleagues at the University of Calgary. They quite often helped me to step back, examine my objectives and then return to my tasks with a renewed vigour and a fresh approach.

Funding for this work was provided by the Natural Sciences and Engineering Council of Canada and the Izaak Walter Killam Foundation. It is greatly appreciated.

Dedicated to my family

Their unconditional support of my endeavours has always been the cornerstone of my success.

TABLE OF CONTENTS

LIST OF TABLES

LIST OF FIGURES

LIST OF SYMBOLS

Scalar Variables (Roman)

$\hat{A}$	-	component independent porition of $\hat{\phi}_i$ in Chapter 6
A_K	-	component independent portion of ln $K_B(r)$ defined by equation (5.17)
A_i	-	chemical formula of component i in Chapter 2
A_j	-	component independent portion of ln ϕ_{ij} and ln $\phi_{ij}(r)$ in Chapter 6
A_f	-	component independent portion of ln $K_B(r)$ defined by equation (5.18)
A_{ij}	-	Wilson activity coefficient model parameters (cal/mol) in Chapter 3
A_{ij}	-	NRTL activity coefficient model parameters (mol/cal) in Appendix A
a	-	equation of state parameter
$\tilde{a}, \tilde{a}_i$	-	Sanchez-Lacombe equation of state parameters using continuous thermodynamics
a_i	-	parameters in the Runge-Kutta integration routine
a_{ki}	-	amount of element k in component i
B_K	-	coefficient of r in the definition of ln $K_B(r)$ defined by equation (5.17)
B_f	-	coefficient of r in the definition of ln $K_B(r)$ defined by equation (5.19)
$\hat{B}_i$	-	coefficient of r in the definition of $\hat{\phi}_i$ in Chapter 6
B_{ij}	-	coefficient of r in the definitions of ln ϕ_{ij} and ln $\phi_{ij}(r)$ in Chapter 6
b	-	equation of state parameter
$\tilde{b}, \tilde{b}_i$	-	Sanchez-Lacombe equation of state parameters using continuous thermodyanamics
b_k	-	total moles of element k
b_{tot}	-	total moles of elements in modified feed vector, $\mathbf{z}^*$
C	-	number of components
C_d	-	number of discrete components in the discretized system of Chapter 6
C_1, C_2	-	coefficients in temperature dependent expression of K_{eq}
c	-	Trebble-Bishnoi equation of state parameter in Appendix A
c_i, c_i^*	-	coefficients in the 5th order Runge-Kutta integration routine in Chapter 4
c_i	-	Mathias-Copeman coefficients in Appendix A
c_{ij}	-	cubic extrapolation coefficients in cloud point curve calculations
D_j	-	tangent plane distance of test phase j
D_j	-	Villar's (1959) deviation from reaction equilibrium
$DG(\delta_r)$	-	Gâteaux derivative of the Gibbs free energy in the direction of δ_r.
d	-	Trebble-Bishnoi equation of state parameter in Appendix A
E_i	-	weighted sum of K values for component i, equations (2.43) and (6.21)
F	-	total Gibbs free energy
$f(r)$	-	generic function in integration routine definitions
f_1, f_2	-	equations (A.25) and (A.26) defining the zero pressure standard state in Appendix A

$\hat{f}_i$	-	reference phase fugacity of component i
f_i^0	-	standard state fugacity of pure component i
f_{ij}	-	fugacity of component i in phase j
G	-	total Gibbs free energy
g_i	-	residues in the cloud point curve algorithm of Chapter 5
g_{ij}	-	error in equilibrium criteria in Chapters 2 and 6
g_{Aj}, g_{Bij}	-	errors in the successive substitution routine in Chapter 6
$H(u)$	-	George *et al.* (1976) molar transformation function
h	-	standard state compressibility in Appendix A
h	-	step size in Runge-Kutta integration routine
h_j, l_k	-	optimality criteria defined by equations (2.50) and (2.51)
h_{Aj}	-	error in ln K_{Aj} values in Chapter 6
h_{Bij}	-	error in ln K_{Bij} values in Chapter 6
K_A	-	segmental K value for solvent in Chapter 5
$K_B(r)$	-	segmental K value for polymer in Chapter 5
K_{Dij}	-	interaction parameter for d parameter in the Trebble-Bishnoi equation of state
K_{ij}	-	thermodynamic distribution variable of component i in phase j (K value)
K_k	-	reaction equilibrium constant for reaction k
K_{eq}	-	sulfane reaction equilibrium constant
k	-	Mathias-Copeman coefficient in Appendix A
k_i	-	intermediate variables in the Runge-Kutta integration routine
k_{ij}	-	interaction parameter
l_j	-	summation requirement residues in Chapter 6
ℓ	-	Lagrangian function
ln K_{Aj}	-	component independent portion of ln K_{ij} and ln $K_{ij}(r)$ in Chapter 6
ln K_{Bij}	-	coefficient of r in the definitions of ln K_{ij} and ln $K_{ij}(r)$ in Chapter 6
M	-	number of elements
M_0	-	molecular weight distribution parameter used by Koak (1997)
M_B	-	mass fraction polymer
M_n	-	number average molecular weight
M_w	-	mass average molecular weight
m	-	successive substitution damping factor in Chapter 6
N	-	number of quadrature points
N_i	-	initial guess for total number of moles of component i in the stoichiometric algorithm
NS	-	number of source components in the association model
$\bar{n}$	-	total number of segments in a disperse system
n_d	-	number of discrete components in a semi-continuous system
n_i	-	total moles of component i
n_i^0	-	initial moles of component i
$\bar{n}_i$	-	total number of segments of component i in a disperse system
$\bar{n}_{r'}$	-	differential variable representing a change in the number of segments at r'

n_T	-	total number of moles in a system
n_{Tj}	-	total number of moles in phase j
n_{ij}	-	moles of component i in phase j
P	-	absolute pressure
P_C	-	critical pressure (MPa)
P_i^*	-	pure component Sanchez-Lacombe pressure parameter
Q	-	objective function to be minimized
q_i	-	Brinkley's (1947) modified feed composition of component i
R	-	gas constant
R	-	number of reactions (in indices).
r	-	ration of methanol to isobutene in the feed for production of MTBE
r	-	segment count of polymer molecules
$\bar{r}$	-	number average number of segments
$\hat{\bar{r}}$	-	reference phase number average number of segments
r_0	-	segmental distribution parameter
r_i	-	segment count of solvent i
S	-	damping parameter in the Newton-Raphson step of the non-stoichiometric algorithm
S	-	specification parameter in Chapter 5
T	-	absolute temperature
T_b	-	normal boiling point (K)
T_C	-	critical temperature (K)
T_i^*	-	pure component Sanchez-Lacombe temperature parameter
T_{ref}	-	temperature of NRTL correlation in Appendix A
t	-	limit variable in the Gâteaux derivative
tol	-	convergence tolerance in the successive substitution routine of Chapter 6
u	-	George *et al.* (1976) molar transformation variable
V_i	-	specific volume of component i (cm^3/mol)
v	-	specific volume
v_{ij}	-	Sanchez-Lacombe volume parameter
$W(r)$	-	intensive segmental distribution function
$\hat{W}(r)$	-	reference phase segmental distribution function
$w(r)$	-	extensive segmental distribution function
X	-	transformation variable in the integration routines
X_{ij}	-	unnormalized mole fraction of component i in phase j
$\hat{x}_i$	-	reference phase mole fraction of component i
x_{ij}	-	mole fraction of component i in phase j
z_i	-	initial mole fraction of component i in the feed

Scalar Variables (Greek)

α - *a/bRT* in Appendix A

α_i - composition independent portion of chemical potentials, equation (2.49)

α_i - specification variable in Chapter 5

α_{12} - NRTL model parameter in Appendix A

β - segmental distribution parameter

β - extrapolation coefficient in Appendix A

β_j - number of moles in phase *j* in Chapters 2 and 3

β_j - segmental phase fraction of phase *j* in Chapter 6

χ - extrapolation parameter in Appendix A

δ - defined by equation (A.14) in Appendix A

$\delta_{r'}(r)$ - Dirac delta function centered at r'

Δ_{max} - maximum tolerance in the Runge-Kutta integration routine

ΔA^E - excess Helmholtz free energy

ΔG^E - excess Gibbs free energy

$\Delta H_{f(0)}$ - enthalpy of formation at 0 K (kJ/mol)

Δn_i - small change in the number of moles of component *i*

ε_1, ε_2 - parameters in the Runge-Kutta integration routine

ε_{ij} - Sanchez-Lacombe energy parameter

ϕ - phase segment fraction in Chapter 5

$\hat{\phi}_i$ - reference phase fugacity coefficient

ϕ_{ij} - fugacity coefficient of component *i* in phase *j*

ϕ_{ij}^0 - initial guess for the fugacity coefficient for component *i* in phase *j* within the non-stoichiometric algorithm

Λ_{ij} - Wilson activity coefficient model parameters

γ_i, $\gamma_i(r)$ - segment-molar activity coefficient in Chapters 4-6

γ_{ij} - activity coefficient of component *i* in phase *j*

κ - mass of a polymer segment

λ - damping parameter in cloud point curve calculations

λ_j - Lagrange multiplier associated with element *j*

$\overline{\mu}$ - segmental chemical potential

$\hat{\mu}_i$ - reference phase chemical potential of component *i*

μ_i^0 - standard state chemical potential of component *i*

μ_{ij} - chemical potential of component *i* in phase *j*

ν_{ij} - stoichiometric coefficient of component *i* in reaction *j*

π - number of phases

θ_j - dimensionless tangent plane distance of test phase *j*

ρ_i^* - pure component Sanchez-Lacombe density parameter

σ - divergence parameter

τ - reduced temperature
τ_{ij} - NRTL parameter
ω - acentric factor
ω_k - weighting factor for node k in quadrature integration
ω_{ij} - slack variable
$\Omega(r)$ - weighting function in quadrature integration
ξ - dimensionless zero pressure standard state density in Appendix A
ξg - defined by equations (A.16) and (A.17) in Appendix A
ξ_j - reaction extent of reaction j
ξ_j^0 - initial guess for the reaction extent of reaction j
Ψ - unnormalized segment fraction
ψ - normalized segment fraction
$\hat{\psi}$ - reference phase segment fraction
ψ_l, ψ_l - defined on page 195 of Appendix A

Matrices and Vectors (Roman)

A - elemental composition matrix
A* - modified elemental composition matrix
b - elemental abundance vector
b* - modified elemental abundance vector
g - vector of the residues in the cloud point curve algorithm in Chapter 5
H - Hessian matrix
h, **l** - vectors of optimality criteria defined by equations (2.50) and (2.51)
$\mathbf{h_A}$, $\mathbf{h_B}$ - vectors of errors in ln K_{Aj} and ln K_{Bij} values in Chapter 6
I - identity matrix
J - Jacobian matrix
l - vector of summation requirement residues in Chapter 6
ln $\mathbf{K_A}$ - vector of ln K_{Aj} values
ln $\mathbf{K_B}$ - vector of ln K_{Bij} values
N - matrix of reaction stoichiometric coefficients
n - vector of total number of moles
$\mathbf{n_T}$ - vector of the total number of moles in each phase
V - symmetric decomposition of the Hessian matrix
Z - ($M \times R$) full matrix defined by equation (2.63)
z - vector of initial feed compositions
z* - modified feed composition vector

Matrices and Vectors (Greek)

α	-	vector of independent variables in Chapter 5
β	-	vector of phase mole numbers in Chapters 2 and 3
$\Delta\alpha$	-	Newton-Raphson change in the cloud point curve independent variables
λ	-	vector of Lagrange multipliers
ν_j	-	vector of stoichiometric coefficients of reaction *j*
ξ	-	vector of reaction extents

Subscripts

A	-	solvent
B	-	polymer
i, j, k, l, m	-	indices
r	-	reference phase
r'	-	segment count which Dirac delta function is centered upon

Superscripts

I	-	phase I
II	-	phase II
F	-	feed
L	-	liquid
V	-	vapour

1. INTRODUCTION

"In an extensive program of computations, the author has employed clerical personnel in all numerical portions of the work." (Brinkley, 1947)

1.1 Motivation

In Brinkley's 1947 paper on the computation of chemical equilibrium in homogeneous systems and heterogeneous systems with pure solids, repetitive calculations were performed using a number of clerical personnel. Techniques to calculate chemical equilibrium had to be simple and robust because of the slow and tedious nature of the work. Since 1947, the development of powerful, fast computers has made the use of clerical personnel obsolete, but the goal to increase the speed of the computations and to improve the confidence in their results remains the same.

This dissertation looks at two different areas of computational thermodynamics: reactive flash algorithms and polymer phase equilibrium calculations. The goal is to briefly review the current techniques used to perform these calculations and to develop alternative approaches which may provide additional information about the equilibrium solutions.

1.2 Reactive Flash Algorithms

Reactive distillation columns are examples of unit operations where simultaneous phase and reaction equilibria occur. These columns combine traditional reactors and distillation columns into one unit, resulting in lower capital and operational costs. By combining the reactor and separators into one column, separation azeotropes may be avoided and higher conversions may be achieved (Doherty and Buzad, 1992). The production of methyl tertiary butyl ether (MTBE) and methyl acetate are two processes which may use reactive distillation columns.

In an ideal situation, the vapour and liquid leaving each tray in a reactive distillation column are in chemical equilibrium. Therefore, each tray can be modeled by a reactive flash calculation. The equilibrium solution sets limits on the total conversion and separation achieved on each tray. In the case of non-ideal trays, the equilibrium solution can still be used to establish the driving forces in the simulation's mass transfer relationships. Many reactive flash calculations may be needed to model the complete distillation column. As more calculations are required, the efficiency and reliability of the algorithm become more important.

A reactive flash algorithm can be used to model any reactive system with the potential of forming multiple phases. Esterification reactions and low temperature reactors that produce methanol are two additional cases where both phase and reaction equilibrium may be important.

Equilibrium solutions are important in simulations, but significant information can also be found in knowledge of the system's incipient phases. That is, knowing how close potential phases are to being in equilibrium gives insight into the nature of the equilibrium solution and how changes in system parameters might cause an additional phase to evolve.

In this work, two multiphase reactive flash algorithms were developed. One uses a stoichiometric method and the other uses a non-stoichiometric method to enforce the elemental balances. In the algorithms, incipient phases are calculated at the same time

the equilibrium solution is found. This development is covered in chapter 2 and the algorithms are analyzed using a methanol production example, a MTBE synthesis example and a sulfur association example in chapter 3.

1.3 Continuous Thermodynamics

Polymer systems usually contain a distribution of molecular weights instead of easily identifiable discrete components. Therefore, it becomes important to determine how best to characterize the polymer species when modeling polymer systems. A standard approach is to discretize the polymer molecular weight distribution into a specified number of pseudocomponents which are then used in thermodynamic calculations. In this dissertation, the integrity of the molecular weight distribution is maintained by using a segmental distribution function to describe the polymer rather than a finite set of discrete components. By using a function to represent the distribution, the extended tails of the molecular weight distribution are included in the thermodynamic calculations and are not neglected as they might be if the distribution were discretized. It will be seen that these tails can have a significant affect on the phase behaviour of polymer systems.

This continuous thermodynamic approach has been studied by Rätzsch and coworkers (1985, 1986, 1989) and by Cotterman, Bender and Prausnitz (1985) to name two groups of workers. The development of the theory of continuous thermodynamics is covered in chapter 4.

1.4 Cloud and Shadow Point Calculations

In polymer systems, the cloud and shadow point curves are analogous to multicomponent bubble- and dew-point curves. If the pressure and composition of a system is fixed, a cloud point is the temperature at which a polymer solution first shows two phase behaviour. The corresponding shadow point is the temperature and composition of the incipient phase. If the temperature is fixed, the cloud and shadow point pressure is the pressure where two phases first appear. The locus of points formed

as the composition of the cloud point is varied are called the cloud and shadow point curves.

The disperse nature of polymer molecular weights leads to cloud and shadow point curves which reflect very interesting phase behaviour. The curves can show three phase points, stable and unstable critical points, lower and upper precipitation threshold temperatures, multiple liquid-liquid regions and a liquid-vapour region. A detailed discussion of these curves is given in chapter 5.

The potential complex behaviour shown by polymer systems requires robust algorithms to calculate the complete cloud and shadow point curves. Chapter 5 develops an algorithm for finding isobaric lines of fixed phase fraction in a polymer system. When the phase fraction is 0 or 1, the lines correspond to cloud and shadow curves.

1.5 Polymer Flash Algorithms

Polymer flash calculations are in the early development stages. They are used to model polymer fractionation procedures and to determine polymer solubilities in various solvents. Because of the large molecular weights and broad molecular weight distributions, polymer/solvent systems are very asymmetrical. That is, it is very likely to find phases with extremely low quantities of the polymer in them. The asymmetry of the system makes it difficult for flash procedures to converge to even a two phase solution unless a very good initial guess is supplied.

The majority of polymer flash algorithms in the literature deal with two phase equilibria. A typical way of achieving convergence in a two phase polymer flash is to discretize the polymer distribution and, with a reasonable initial guess, use a damped successive substitution technique to solve the thermodynamic equations (Koak, 1997). This approach works but convergence can be very slow. An alternative approach could be to utilize a second order procedure like the Newton-Raphson technique to solve all the necessary equations at the same time and expedite the convergence.

In chapter 6 of this work, the necessary equations for a multiphase polymer flash algorithm are developed within a continuous thermodynamics framework. The equations are developed such that incipient and stable phases are found simultaneously. The initial solution procedure uses a damped successive substitution technique. A preliminary investigation into the use of a Newton-Raphson procedure to solve all the equilibrium equations simultaneously is also performed.

1.6 Dissertation Overview

The dissertation can be thought of as containing two distinct parts. The first part focuses on multiphase reactive flash calculations for non-polymer systems (chapters 2 and 3). The second section contains the development of polymer phase equilibria procedures using continuous thermodynamics (chapters 4-6). These two divisions are completely independent of each other and can each stand on their own.

Appendix A outlines an investigation into an excess free energy mixing rule for cubic equations of state. It is not directly related to either of the two thesis sections but could be used to calculate the fugacity coefficients required for the reactive flash calculations.

Appendix B lists the derivatives used in the cloud and shadow curve algorithm outlined in chapter 5. Appendix C gives the derivatives required for both the successive substitution and Newton-Raphson polymer flash routines discussed in chapter 6.

This thesis describes a number of tools that can stand on their own or be used as an integral part of a larger simulator. For example, the reactive flash algorithms proposed could be used to model kinetically limited reactive systems by adding a time dependent constraint on the conversion. The restricted chemical equilibrium algorithm could then become part of a larger module used to simulate a kinetically controlled multiphase reactor. The framework by which the tools presented could be used in simulators is not discussed.

2. REACTIVE FLASH ALGORITHMS

2.1 Introduction

There is an extensive literature on phase and chemical equilibria calculations, most of which concentrates on ideal gas systems with a possibility of pure condensed, or solid, phases. Non-ideal systems have been a concern, but not a focus, in the computational aspects of chemical equilibria until recently when computers and the algorithms became sophisticated enough to deal with the non-linearity presented in non-ideal systems. The driving force behind much of the initial research was the need to have a fast, reliable means of calculating the equilibrium state of combustion products from rocket fuels. Currently, the motivation for this area of research is the accurate design and reliable control of chemical process units involving chemical reactions.

This chapter focuses on the development of two non-ideal multiphase reactive flash algorithms: one using a stoichiometric technique, the other a non-stoichiometric technique. Each algorithm is based upon Abdel-Ghani's (1995) multiphase flash which uses an average chemical potential over all the phases present as a reference phase and initiates the flash with the number of phases equal to the number of components in the system plus one. After a review of the subject terminology and the developments in reactive flash algorithms within the literature, the multiphase stoichiometric reactive flash algorithm and then the non-stoichiometric algorithm will be described. An emphasis is

placed upon the problem of initiation and computational concerns. Specific examples will be given and analyzed in the following chapter.

2.2 Terminology and Equilibrium Requirements

2.2.1 General

To clarify the discussion of phase and chemical equilibria algorithms, some terminology needs to be defined. Each chemical compound within a system being studied, regardless of which phase or state it is in, will be termed a *component* or *constituent* of that system, and the number of components will be represented by C. Each component is composed of *elements*, the total moles of these elements in the system being conserved. The number of different types of elements will be termed M. a_{ki} will represent the number of times element k appears in constituent i, and the matrix

$$\mathbf{A} = \begin{bmatrix} a_{11} & a_{12} & \cdots & a_{1C} \\ a_{21} & a_{22} & \cdots & a_{2C} \\ \vdots & \vdots & \ddots & \vdots \\ a_{M1} & a_{M2} & \cdots & a_{MC} \end{bmatrix} \tag{2.1}$$

will be called the elemental composition matrix. Some of the components may react with each other to form the other components. It may be assumed that $(C-M)$ of the components can be formed in $(C-M)$ linearly independent reactions using the M remaining constituents as reactants, one component being formed from each reaction (Brinkley, 1946). The M reactant constituents will be called the *base components* of the system while the $(C-M)$ product constituents will be termed the *derived components*. The procedures to define the elements, base components, derived components and the reactions relating them, will be discussed in later sections.

2.2.2 Reactions, Reaction Extents and Elemental Balances

Brinkley (1946) showed that the chemical formulae for the $(C-M)$ derived components could be generated through a linear combination of the base component formulae:

$$A_{M+j} = \sum_{i=1}^{M} \nu_{ij} A_i \quad ; \; 1 \le j \le C - M \tag{2.2}$$

where A_k represents the chemical formula for the k^{th} constituent. These $(C-M)$ combinations are, in essence, reactions between the base components to form the derived components and ν_{ij} is called the *stoichiometric coefficient* of component i in reaction j. Within this dissertation a reaction such as equation (2.2) will be rewritten as

$$\sum_{i=1}^{C} \nu_{ij} A_i = 0 \quad ; \; 1 \le j \le C - M . \tag{2.3}$$

In such a form, the stoichiometric coefficients will be positive for products of the j^{th} reaction, negative for reactants and zero for constituents not involved in the reaction.

ξ_j is said to be the *reaction extent* of the j^{th} reaction if, for a reaction written in the form of equation (2.3), the number of moles of constituent i, A_i, which has been *produced* through reaction j is equal to $\xi_j \nu_{ij}$.

Regardless of the reactions occurring in the system or their reaction extents, the *elemental abundance constraints* of the system must be satisfied. These constraints are given by:

$$\mathbf{An} - \mathbf{b} = \mathbf{0} \tag{2.4}$$

$$\mathbf{n} = \{n_1, n_2, \ldots, n_C\}^T \tag{2.5}$$

$$\mathbf{b} = \{b_1, b_2, \ldots, b_M\}^T \tag{2.6}$$

where n_i represents the total number of moles of constituent i in the system and b_k represents the total number of moles of element k in the system and is invariant. If an initial composition of the system and the $(C-M)$ reactions within the system are known, the elemental abundance constraint can be reformulated as

$$n_i = n_i^0 + \sum_{j=1}^{C-M} \nu_{ij} \xi_j \quad ; \; 1 \le i \le C \tag{2.7}$$

where n_i^0 is the initial number of moles of component i.

In the case of a multiphase system the constituents are distributed amongst different phases. The elemental abundance constraint, equation (2.4), must still be satisfied, but in a multiphase system the n_i in equation (2.5) are the sum of the moles of component i in all the phases. That is

$$n_i = \sum_{j=1}^{\pi} n_{ij} \quad ; \quad 1 \le i \le C \tag{2.8}$$

where n_{ij} represents the number of moles of the i^{th} component in the j^{th} phase and there are π phases. If β_j is the total number of moles in the j^{th} phase and x_{ij} is the mole fraction of the i^{th} constituent in the j^{th} phase, then equation (2.8) can be written as

$$n_i - \sum_{j=1}^{\pi} \beta_j x_{ij} = 0 \quad ; \quad 1 \le i \le C. \tag{2.9}$$

2.2.3 Equilibrium Requirements

Each component in the system will have a chemical potential associated with it of the form

$$\mu_{ij} = \mu_i^0 + RT \ln\left(f_{ij} / f_i^0\right) \tag{2.10}$$

where μ_i^0 is the standard state chemical potential of pure component i and f_{ij} is its fugacity in phase j. f_i^0 is the pure component reference fugacity which equals 1 bar for ideal gas species. The fugacity, f_{ij}, is a function of temperature, pressure and composition of phase j. It can be found through ideal approximations, activity coefficient models or equations of state to name only a few of the methods available.

At constant temperature and pressure, the total Gibbs free energy of the system can be expressed as

$$G = \sum_{j=1}^{\pi} \sum_{i=1}^{C} n_{ij} \mu_{ij} \, . \tag{2.11}$$

At equilibrium, this energy will be at a global minimum and the elemental balance constraints, equation (2.4), will be satisfied.

Gibbs (1876) showed that at this minimum, the chemical potential, and thus, the fugacities of each component i must be the same in all the phases where it appears. That is,

$$\mu_{ij} = \hat{\mu}_i \quad ; \; 1 \le i \le C \quad \forall \; j \text{ where component } i \text{ exists.}$$

In terms of fugacities, this can be written as

$$f_{ij} = \hat{f}_i \quad ; \; 1 \le i \le C \quad \forall \; j \text{ where component } i \text{ exists.} \tag{2.12}$$

where $\hat{\mu}_i$ is the common chemical potential and $\hat{f}_i$ is the common fugacity of component i.

Gibbs (1876) also showed that at this minimum, the *reaction affinity* must be zero. That is, the stoichiometrically weighted sum of the chemical potentials of reactants must equal the stoichiometrically weighted sum of the chemical potential of the products. In the case of reactions written in the form of equation (2.3) this equilibrium criteria can be stated as

$$\sum_{i=1}^{C} \nu_{ik} \hat{\mu}_i = 0 \quad ; \; 1 \le k \le C - M . \tag{2.13}$$

Substituting equation (2.10) into equation (2.13) yields the familiar mass action relationship:

$$\frac{1}{RT} \sum_{i=1}^{C} \nu_{ik} \mu_i^0 = -\ln\left(\prod_{i=1}^{C} \left[\hat{f}_i / f_i^0 \right]^{\nu_{ik}} \right) = -\ln K_k \quad ; 1 \le k \le C - M \tag{2.14}$$

where K_k is the reaction equilibrium constant of the k^{th} reaction at system temperature and pressure.

It is important to note that in a reactive multiphase system if the equal fugacity requirements stated in equation (2.12) are met and the reaction equilibrium condition

given by equation (2.13) or equation (2.14) is satisfied, the reaction equilibrium condition will be satisfied in all the phases where the reactive components exist.

2.2.4 Stoichiometric and Non-Stoichiometric Methods

When developing a computer algorithm to determine reactive phase equilibria, the necessary conditions of equilibrium may be developed using the method of Lagrange multipliers to minimize the free energy subject to the elemental balance constraints or by equating the chemical potentials of each component between each phase where the elemental balance constraints are written in terms of the reaction stoichiometry, equations (2.7) and (2.8). These two approaches have been called the *stoichiometric method* and the *non-stoichiometric method* respectively (Smith, 1980), and can be shown to be identical in nature (Smith and Missen, 1982). This classification of computational algorithms differs slightly from van Zeggeren and Storey (1970) who chose to classify chemical equilibria computations into either minimization techniques or non-linear equation techniques. For the most part, what van Zeggeren and Storey (1970) term a minimization technique, Smith and Missen (1982) call a non-stoichiometric technique, and the algorithms that van Zeggeren and Storey categorize as non-linear equation techniques, Smith and Missen classify as stoichiometric techniques.

2.3 Literature Review of Chemical and Phase Equilibria Calculations

2.3.1 Literature Review

There are many review papers on methods of calculating chemical and phase equilibria. Zeleznik and Gordon (1968) reviewed the methods prior to 1968, van Zeggeren and Storey (1970) published the first monograph dedicated to this area, Smith (1980) wrote an additional review of the material just prior to Smith and Missen's (1982) compilation of a second text dedicated to chemical and phase equilibria calculations. Additional reviews include those by Seider *et al.* (1980), Mather (1986) and, most recently, the review by Seider and Widagdo (1996).

Brinkley (1947) gave an outline of what is considered to be the first algorithm for calculating general chemical and phase equilibria. The algorithm described could be used for calculations of multiphase, non-ideal systems. It was what now is considered to be a non-stoichiometric technique where the reaction equilibrium relationships are satisfied on each iteration while convergence is defined upon the material balances. Multiple phases were accounted for by the use of different standard state chemical potentials, μ_{ij}^0, for constituents in each phase. After determining which constituents were to be used as base components and which were to be considered derived components, reactions of the form of equation (2.2) were formed. The elemental abundance constraints were rewritten as

$$\sum_{k=1}^{\pi}\left\{n_{jk} + \sum_{i=M+1}^{C} \nu_{ij} n_{ik}\right\} = q_j \quad ; \quad 1 \le j \le M \tag{2.15}$$

where

$$\sum_{j=1}^{M} a_{ij} q_j = b_i . \tag{2.16}$$

The set of q_j may be thought of as the number of moles of component j required to satisfy the elemental abundance constraints if there are no derived components in the system. A detailed description of the procedures used to choose the components and the reactions is given by Kandiner and Brinkley (1950).

A reference phase is chosen for each constituent, not necessarily the same phase for all constituents and identified by a subscript r. A thermodynamic distribution coefficient is then defined for each species in each phase.

$$\ln K_{jk} = \left[\mu_{jr}^0 - \mu_{jk}^0\right] / RT \quad ; \quad 1 \le j \le C \tag{2.17}$$

The mole fractions of the constituents in each phase can then be expressed as

$$x_{jk} = \frac{K_{jk}\gamma_{jr}}{\gamma_{jk}} x_{jr} \tag{2.18}$$

where γ_{jk} is the activity coefficient of the j^{th} constituent in the k^{th} phase.

The reaction equilibrium constants, K_j, can be written as

$$\ln K_j = \frac{1}{RT}\left[\sum_{i=1}^{M} \nu_{ij}\mu_{ir}^0 - \mu_{jr}^0\right] \quad ; \quad M+1 \le j \le C \tag{2.19}$$

and the mole fractions of the derived components are rewritten in terms of the reaction equilibrium constants:

$$x_{jr} = K_j \prod_{i=1}^{M}\left(\frac{\left[x_{ir}\gamma_{ir}\right]^{\nu_{ij}}}{\gamma_{jr}}\right) \quad ; \quad M+1 \le j \le C. \tag{2.20}$$

By substituting equation (2.20) into equation (2.18) all of the mole fractions of the derived components are in terms of the mole fractions of the base components and the reaction equilibrium constants. In this manner, the Brinkley algorithm ensures that at each iterative step the reaction equilibrium equations are satisfied.

If β_k is the number of moles in phase k then the mole numbers of each constituent, n_{ik}, in equations (2.15) can be rewritten as $\beta_k x_{ik}$ and equations (2.15) plus constraints that the mole fractions of each phase must sum to unity give $M + \pi$ equations in $M + \pi$ unknowns, β_j and x_{ir}. Brinkley (1947) suggested solving for these unknowns using two nested loops: a *primary loop* which used the composition estimates to determine the activity coefficients and a *secondary loop* contained within the primary loop to solve for β_j and x_{ir} using a Newton-Raphson procedure. Brinkley suggested using ideal activity coefficients on the first iteration of the primary loop and subsequent iterations would be the equivalent of a successive substitution algorithm. In the case of an ideal system, only one pass through the primary loop would be required. In either situation, ideal or non-ideal, this algorithm has difficulties converging when constituents have mole numbers close to zero.

Kandiner and Brinkley (1950) simplified Brinkley's original algorithm to one of an ideal gas system with pure condensed phases and suggested using a successive substitution method to solve for the mole numbers in the gas phase. They also pointed out the inherent difficulties of trying to 'guess' which condensed phases may be present.

Guessing a solid phase to be absent when in reality it was present would not show up in the calculations at all. Guessing a solid phase to be present when it was not would lead to a negative molar amount of solid. Boll (1961) removed this difficulty by proposing that the equality constraints on the mole fraction summation be changed to an inequality of the form

$$\sum_{i=1}^{C} x_{ij} \leq 1 \quad ; \quad 1 \leq j \leq \pi . \tag{2.21}$$

Initially, all phases were to be considered present and if the sum of the mole fractions for a phase dropped below one during the course of the iterations, that phase was removed from consideration.

Krieger and White (1948) rewrote the expression for the derived components in terms of their logarithms and used the mole fractions instead of mole numbers in an ideal system. Using the logarithms of the mole fractions is important because it helps eliminate the problems of constituents with small mole numbers and the mole fractions are easier to approximate than the mole numbers.

White, Johnson and Dantzig (1958) proposed a different approach to solving the reaction equilibrium problem in an ideal gas system. Their method has become known as the RAND algorithm. The primary difference between the Brinkley algorithm and the RAND algorithm is that at each iteration in the Brinkley Algorithm the reaction equilibrium equations are satisfied and the mass balance equations are the equations being solved whereas in the RAND algorithm, the material balance constraints are satisfied at each iteration while the reaction equilibrium equations are iteratively solved. The RAND algorithm is considered to be a non-stoichiometric technique.

The RAND algorithm is formulated as a constrained minimization problem where the function to be minimized is the Gibbs free energy of the system. For the ideal system considered, the Gibbs free energy is expressed as

$$F(n_1, n_2, \ldots, n_C) = \sum_{i=1}^{C} n_i \left(\frac{\mu_i^0}{RT} + \ln P + \ln \frac{n_i}{n_T} \right) \tag{2.22}$$

subject to the elemental abundance constraint, equation (2.4),

where $$n_T = \sum_{i=1}^{C} n_i \,. \tag{2.23}$$

Equation (2.22) is expanded in a Taylor series about a point that satisfies the elemental balances and truncated after the first order terms. The expansion is minimized subject to the elemental abundance constraints given in equation (2.4) using the method of Lagrangian multipliers. One Lagrangian multiplier, λ_j, was used for each of the M constraints. In essence, the method of Lagrangian multipliers converts the constrained minimization in C independent variables into an unconstrained minimization problem of $C + M$ independent variables:

$$\min Q(n_1, n_2, \ldots, n_C, \lambda_1, \ldots \lambda_M) = F(n_1, n_2, \ldots, n_C) - \sum_{j=1}^{M} \lambda_j \left(\sum_{i=1}^{C} a_{ji} n_i - b_j \right).$$

Setting $(\partial Q / \partial n_i) = 0$ gives an expression for the mole numbers of each constituent in terms of the Lagrange multipliers and the total number of moles, n. Substituting these expressions into the elemental abundance constraints plus equation (2.23) give $M + 1$ linear equations in the $M + 1$ unknowns, λ_j and n. These are solved to give the next iteration's approximations to λ_j and n. Convergence is enhanced through the use of a line search along the independent variable's direction of change, a line search which can also be utilized to ensure that mole numbers remain positive.

White, Johnson and Dantzig (1958) recognized that the Lagrangian multipliers corresponding to the elemental abundance constraints may be thought of as reduced chemical potentials for the elements of the system. They suggest using this fact to give better estimates of the moles of trace constituents not considered in the original computation through the equation:

$$n_i = n \exp\left\{ -\frac{\mu_i^0}{RT} - \ln P + \sum_{j=1}^{M} a_{ji} \lambda_j \right\}. \tag{2.24}$$

Boynton (1960) extends the RAND algorithm to include condensed phases and suggests calculating the free energy of multiple trials with different combinations of condensed phases in order to determine which set of condensed phases should actually be included in the final solution.

In the White *et al.* paper (1958), an algorithm is also given for the computation of chemical equilibrium through a linear approximation of the Gibbs free energy surface and through the use of standard simplex linear programming techniques to arrive at an estimate of the final solution.

Villars (1959) first proposed a stoichiometric technique for the solution of ideal gas systems containing multiple reactions. This method has been termed the method of *successive reaction adjustments*. Given the initial moles of the constituents in a system and a set of reactions with their reaction equilibrium constants, K_j, the material balance constraints are incorporated into the problem through the use of reaction extents as given in equation (2.7). At any composition, the $K_{j,calc}$ are found from the expressions for the reaction equilibrium constants and the deviation of each reaction from equilibrium is found from

$$D_j = \frac{K_{j,calc}}{K_j} - 1. \tag{2.25}$$

The reaction corresponding to the deviation, D_j, with the largest absolute value is forced to satisfy the equilibrium relationship by modifying its reaction extent until $K_{j,calc}$ equals the numerical K_j. This adjustment is done while keeping all other reaction extents constant. The new constituent mole numbers are recalculated, a new set of reaction deviations are found and the process continues until the absolute value of all the reaction deviations as found from equation (2.25) are less than a specified tolerance. Precautions must be taken to avoid negative mole numbers and the convergence of this method can be extremely slow when intermediate reaction constituents have small mole numbers.

Cruise (1964) modified Villars' approach by automatically choosing the base components at each iteration to be the linearly independent constituents present in the

greatest amounts. Cruise also updated the reaction extents for all condensed derived components upon each iteration using a Newton-Raphson step. The mole count of gaseous derived components were updated every fourth iteration. Smith and Missen (1968) built upon the changes Cruise had proposed by using a linear programming procedure to determine the base components and initial compositions by minimizing the linear system

$$G = \sum_{i=1}^{C} n_i \mu_i^0 \tag{2.26}$$

with respect to n_i. With this change, the process of choosing the base components need only be done once at the start of the computations. Villars' technique (1959) as modified first by Cruise (1964) and then by Smith and Missen (1968) is referred to in the literature as the VCS method.

Another significant approach to multiphase reaction equilibrium was developed through NASA research by Huff, Gordon and Morrell (1951). The primary difference between the NASA algorithm and the RAND and Brinkley algorithms is that within the NASA algorithm, the base components are chosen to be the elemental species and at each iteration, neither the elemental abundance constraints nor the chemical equilibrium relationships are satisfied. Lagrange multipliers are not used in the 1951 version of the algorithm. Instead, a Newton-Raphson technique is used to zero the error functions generated from the elemental abundance constraints and the equilibrium relationships. The iteration variables were the mole numbers of the base components and the logarithm of the mole numbers of the derived components. Zeleznik and Gordon (1968) give a good review of the NASA equations and how they relate to the RAND equations.

Gordon and McBride (1971) generalized the original NASA algorithm such that the base components were not necessarily the elements and such that Lagrange multipliers were used in a similar fashion to the RAND algorithm to ensure that the elemental abundance constraints were satisfied. The iteration variables were the mole

numbers of the derived components, the logarithms of the base component mole numbers, the total number of moles in the system and the Lagrange multipliers.

The Brinkley, NASA and RAND algorithms form the basis of many non-stoichiometric computer algorithms used to calculate phase and chemical equilibrium. These algorithms are similar enough that Smith and Missen (1982) have termed them the BNR algorithm. The BNR algorithms were primarily developed for calculations with an ideal gaseous phase however Smith and Missen (1988) describe a modification to the BNR algorithm (primarily the NASA algorithm) to allow their use for non-ideal systems.

Sanderson and Chien (1973) proposed a two phase stoichiometric method and included a detailed description of how to include non-ideal phases by using an activity coefficient model for liquid phases and an equation of state for the vapour phase. They suggested that at each iteration of a reactive flash, new reaction extents, ξ_j, and total number of moles first be determined from the current estimates of the fugacity coefficients and activity coefficients while neglecting the phase equilibria. Given these new reaction extents, the phase compositions and vapour fraction could then be calculated using a non-reactive flash. The new compositions could be used to update activity coefficients and fugacity coefficients before the next iteration started. They determined the reaction extents and total number of moles by minimizing a penalty function using Marquardt's method. Xiao *et al.* (1989) modified Sanderson and Chien's stoichiometric algorithm by rearranging the iterative loops: the outer loop solved the phase equilibrium equations while the inner loop solved the reaction equilibrium for ξ_k and the total number of moles in the system using Marquardt's unconstrained minimization technique. Both these techniques separated the phase equilibrium calculation from the chemical equilibrium calculation.

George *et al.* (1976) eliminated the non-negativity constraints on the constituents through the use of a variable transformation

$$n_i = n_i^0 H(u_i) \tag{2.27}$$

where $$H(u) = \frac{1}{1+e^{-u}}. \tag{2.28}$$

With this transformation, the non-stoichiometric equations are minimized with respect to u_i using Powell's method in either a one, two or three phase system. Castillo and Grossmann (1981) state that the transformation given in equations (2.27) and (2.28) can lead to ill-conditioned matrices at lower temperatures.

In their paper, Castillo and Grossmann (1981) also outline a non-stoichiometric method for performing a reactive flash calculation using a non-linear programming technique. It is initiated with a maximum number of phases which are kept throughout the computations. Phase fractions for unstable phases are set to 10^{-10} instead of 0 but become stable if the Kuhn-Tucker conditions indicate that doing so would lower the total Gibbs free energy of the system.

Myers and Myers (1986) present a second order stoichiometric technique for ideal, single phase systems. They focus on describing an initialization technique which chooses the system's components such that each linearly independent reaction associated with the system has a reaction equilibrium constant, K_j, less than 1. In this fashion, the equilibrium reactions extents will be small and positive, the initial guess of $\xi_j = 0$ is a good one and numerical problems are avoided during calculations.

A non-stoichiometric algorithm for multiphase ideal solutions was presented by Michelsen (1989). He sets up the equations for the Gibbs free energy in terms of a different standard state chemical potential for each component in each phase, and through the use of Lagrange multipliers, λ_j, converts the constrained problem into an unconstrained one. By use of a duality transformation, the iteration variables are then switched from n_{ik} and λ_j to λ_j and β_k, the phase amounts. The transformed problem is then minimized using one of two techniques both of which are initiated with Smith and Missen's (1968) linear programming technique. The first technique is to use a few successive substitution iterations to improve the initial guess in the Lagrange multipliers by assuming that the phase mole numbers are fixed and then complete the convergence

using a full Newton-Raphson technique. The second method utilizes a penalty function with the original first estimates. Both these methods were documented to work well.

Castier, Rasmussen and Fredenslund (1989) developed a stoichiometric technique using Michelsen's (1982a) stability check to see if additional phases should be added. They initialized their reaction extents with a modification to the Myers and Myers (1986) initiation to suit the needs of non-ideal, multiphase systems, and they initialized the phase splits using the method proposed by Michelsen (1982a, b). Convergence in the initiation procedure was achieved by iterating through inner and outer loops: the inner loop was used to update the mole numbers of components in each phase given constant partitioning coefficients, K_{ij}, and reaction extents, ξ_k, and the outer loop was used to update the reaction extents, phase fractions and partitioning coefficients. Initially, ξ_k was found using successive substitution for the first 5 iterations of the outer loop and after additional phases were added, the outer loop alternated between successive substitution and general dominant eigenvalue methods. The inner loop, which performed the phase split calculations used Rachford-Rice type equations with a Newton-Raphson algorithm. Final convergence was found by minimizing the Gibbs free energy of the system with respect to the reaction extents and the phase fractions using the second order Murray minimization technique (1972) while checking for phase stability at each iteration.

In 1991, Gupta, Bishnoi and Kalogerakis outlined a stoichiometric technique which incorporated the reactive/non-reactive flash and phase stability calculations into a single set of coupled non-linear equations. They selected a reference phase, indicated by a phase index r, and chose to minimize the function

$$G = \sum_{i=1}^{C} z_i \mu_{ir} + \sum_{\substack{j=1 \\ j \neq r}}^{\pi} n_{ij} \left(\mu_{ij} - \mu_{ir} \right) + \sum_{k=1}^{R} \sum_{i=1}^{C} \nu_{ik} \xi_k \mu_{ir} \qquad (2.29)$$

subject to an additional constraint on the phase fraction:

$$\beta_r = 1 - \sum_{\substack{j=1 \\ j \neq r}}^{\pi} \beta_j \quad ; \beta_j = \sum_{i=1}^{C} n_{ij} \Big/ n_T \quad . \tag{2.30}$$

Using Lagrangian multipliers, equations (2.29) and (2.30) form the equation

$$G^* = G + \sum_{\substack{j=1 \\ j \neq r}}^{\pi} \lambda_j \left(\beta_j - \sum_{i=1}^{C} n_{ij} \Big/ n_T \right) \tag{2.31}$$

which is minimized with respect to n_{ij}, ξ_k and β_j. λ_j / n_T can be related to the tangent plane distance of phase j and either β_j or λ_j must be zero. This condition can be written as

$$\begin{aligned} &\beta_j \theta_j = 0 \\ &\theta_j = \frac{\lambda_j}{n_T RT} \geq 0 \quad ; \beta_j \geq 0 \end{aligned} \tag{2.32}$$

They solved these equations using nested loops: the inner loop solving for β_j, θ_j and ξ_k given composition independent fugacity coefficients and the outer loop using the n_{ij} from the inner loop to calculate the new mole fractions and new fugacity coefficients and to combine identical phases.

Smith *et al.* (1993) used the definition of a system's Gibbs free energy subject to elemental constraints to define a reactive tangent plane criteria for reactive phase equilibria and stability. This criteria is similar to the tangent plane criteria used to describe phase equilibrium by Gibbs (1876), Baker *et al.* (1982) and Michelsen (1982a).

Greiner (1991) gives a description of a full Newton-Raphson method for calculating phase and reaction equilibrium in non-ideal systems. The technique is a minimization of the Gibbs free energy which has been developed for both stoichiometric and non-stoichiometric methods. Because it is a full Newton-Raphson technique and does not contain any mechanism to eliminate or add phases during the computations, it requires a good initial guess of the equilibrium compositions and number of phases as determined from a generalized linear programming solution.

Michelsen (1994) describes a method for calculating equilibrium reaction extents, phase fractions and compositions given composition independent fugacity coefficients and a set of reactions. Because of the form of the equations used, Michelsen was able to show that the objective function used was convex and thus its one global minimum was easily found using a Newton-Raphson technique. The number of unknowns in the problem was equal to the number of independent reactions plus the number of non-pure phases.

Hildebrandt and Glasser (1994) discuss the use of a geometric approach using convex hulls to find the global minimum of a system's free energy. A stoichiometric technique was used for reactive systems but few examples or calculation details were given. Another geometric look into reactive flashes was outlined by Jiang *et al.* (1996) where they noted that the mathematical formulation describing a reactive flash was similar to the formulation of the tangent plane criteria for a non-reactive flash. They formulated the reactive flash problem such that a non-reactive flash was a special case and showed that the presence of reaction stoichiometry gave additional constraints on the placement of the equilibrium tangent planes.

Ung and Doherty (1995) have developed a set of transformations to give a set of reaction independent composition variables. These variables can be used to eliminate extra dimensions when visualizing reactive phase diagrams and they can be used to assist in determining where reactive azeotropes may exist.

McDonald and Floudas (1995) have given a detailed description of a minimization algorithm and variable transformation that can be used when a NRTL model is used for liquid phases and the vapour phase is ideal. The method guarantees convergence to a global minimum in the Gibbs free energy using a Global Optimization Procedure. A procedure that is too complex to cover in this work.

Recently, Cisneros *et al.* (1997) have derived a new approach to a multiphase, non-ideal reactive flash by rewriting the equations in the same form as a traditional multiphase flash. In this case, elements are treated like components and the necessary

conditions of equilibrium are the chemical potentials of these elements are identical over all the phases and that the total number of moles of each element is conserved.

2.3.2 Comments

All of the reactive flash algorithms mentioned in the previous section are either directly minimizing the Gibbs free energy of a multicomponent system subject to elemental constraints or solving the equations which describe multiphase reactive equilibrium. With this in mind, the differences in the procedures lie in their formulation of the equilibrium or minimization equations, their choice of independent variables, their methods of initiating and solving the equations and their methods chosen to check for the stability of phases.

The earlier BNR algorithms and the methods of Myers and Myers (1986) and Michelsen (1989) were second order minimizations for ideal gaseous systems. However, the BNR algorithms and Michelsen's 1989 algorithm were also developed for the presence of pure condensed (solid) phases. More recently, non-ideal multiphase reactive flashes were described by the algorithms of Sanderson and Chien (1973), Castillo and Grossmann (1981), Castier *et al.* (1989), Gupta *et al.* (1991) and Cisneros *et al.* (1997), to name a few. Many of the algorithms first minimize the Gibbs free energy of an ideal system using a linear programming technique to determine an initial guess for their flash routine as outlined by Smith and Missen (1982).

A robust way to set up the equations for a non-ideal reactive flash involves nesting two loops to solve the required system of equations. The inner loop assumes composition independent fugacity coefficients and solves the pseudo-ideal flash problem, potentially with the method described by Michelsen (1994). The outer loop updates the fugacity coefficients. (See the papers by Brinkly, 1947, and Gupta *et al.*, 1991, to name two.)

The main drawbacks of the current algorithms for multiphase reactive flashes are that they require phase stability checks after each converged solution to see if an additional phase should be added (Castier *et al.*, 1989; Cisneros *et al.*, 1997) and/or they

require the algorithm to choose one of the phases to act as a reference phase which at some point might disappear from the active set of phases (Castier *et al.*, 1989; Gupta *et al.*, 1991; Cisneros *et al.*, 1997). The following sections address both of these problems in the development of a stoichiometric and a non-stoichiometric reactive flash algorithm. The flashes are initiated with a number of phases equal to the number of components plus one and the stability of each phase is determined from the sum of the unnormalized mole fractions in the phase. By weighting the chemical potentials of each component in a phase by the phase fraction, a weighted average chemical potential is used as the reference chemical potential in both algorithms. Thus, the reference chemical potentials are not defined to be from a single active phase in the system.

2.4 The Stoichiometric Algorithm

2.4.1 System Definition and Algorithm Objectives

Consider a system at constant temperature and pressure, T and P. Assume that the system contains π phases and C components which define an elemental composition matrix of rank M. The objective of this section is to develop a stoichiometric reactive flash algorithm which will perform a PT reactive flash given an initial feed composition, pressure and temperature without *a priori* knowledge of the final solution. The converged solution will contain information about the equilibrium phases and phase amounts as well as information about incipient phases. The algorithm will automatically determine a linearly independent set of R reactions ($R = C\text{-}M$) given the elemental compositions of the components.

Like Abdel-Ghani's flash algorithm (1995), the reactive flash algorithm consists of two nested loops. In the outer loop, the thermodynamic properties of the phases are updated using a successive substitution technique and in the inner loop the phase mole numbers, phase compositions and reaction extents are found assuming composition independent fugacity coefficients. The development of the algorithm follows the development proposed by Michelsen (1994) for a multiphase reactive flash but is

modified to account for a novel choice in the reference phase chemical potentials and to facilitate phase stability calculations.

2.4.2 The Reference Phase Chemical Potentials

Following Abdel-Ghani (1995), the reference chemical potential for component i is the average of the chemical potential of component i over all the phases of the system, each potential being weighted by its phase fraction. That is:

$$\hat{\mu}_i = \sum_{j=1}^{\pi} \beta_j \mu_{ij} \Big/ \sum_{n=1}^{\pi} \beta_n \tag{2.33}$$

where β_j is the number of moles in phase j.

With equation (2.10), the reference fugacities can be found from:

$$\ln \hat{f}_i = \ln \hat{x}_i \hat{\phi}_i P = \sum_{j=1}^{\pi} \beta_j \ln f_{ij} \Big/ \sum_{n=1}^{\pi} \beta_n \,. \tag{2.34}$$

If a phase is incipient, that is it does not exist, it has a phase mole number, β_j, equal to zero and will not contribute to the reference fugacity. As will be shown shortly, the reference phase composition, $\hat{x}_i$, is found from the material balances. The reference phase fugacity coefficient, $\hat{\phi}_i$, can be found from equation (2.34) and a knowledge of the reference phase composition.

In terms of the new reference phase, the condition of equality of chemical potentials between the phases, equation (2.12), can be rewritten as

$$f_{ij} = \hat{f}_i \quad ; \quad 1 \le i \le C \tag{2.35}$$

for each phase j which exists ($\beta_j > 0$). The condition of zero reaction affinity, equation (2.13), can be expressed as

$$\sum_{i=1}^{C} \nu_{ik} \hat{\mu}_i = 0 \quad ; \quad 1 \le k \le C - M \,. \tag{2.36}$$

If equation (2.36) holds for the reference phase and equation (2.35) is also true, then the reaction affinity condition will be satisfied in all the phases with positive phase amounts.

2.4.3 Tangent Plane Stability Criteria

Michelsen (1982a) describes a mechanism for determining phase stability using tangent plane criteria. An apparent equilibrium is defined by a plane that is tangent to the free energy surfaces. This is the "reference" tangent plane. If the distance from the reference tangent plane to the free energy surface is greater than zero at each point on the surface, the reference equilibrium is stable. But if the distance is less than zero at any point, the reference equilibrium is unstable and the free energy of the system can be further reduced with a different combination of phases.

In terms of the chemical potentials, this criteria can be written as

$$D_j = \sum_{i=1}^{C} x_{ij}\left(\mu_{ij} - \hat{\mu}_i\right) \geq 0 \quad ; \; 1 \leq j \leq \pi . \tag{2.37}$$

It is difficult to scan the entire Gibbs free energy surface for compositions that result in a negative tangent plane distance. Michelsen (1982a) shows that it is sufficient to determine that the minimum values of the tangent plane distance (stationary points) are all positive in order to determine that the reference equilibrium is stable. The stationary points can be thought of as points along the Gibbs free energy surfaces that have a tangent plane parallel to the tangent plane of the reference equilibrium and D_j is the distance from the tangent plane that defines the equilibrium and the Gibbs free energy of the stationary point.

Mathematically the stationary points can be found by minimizing equation (2.37) with respect to the mole fractions, x_{ij}, subject to the constraint that the sum of the mole fractions must be one. The unconstrained Lagrangian of this minimization problem is

$$\ell\left(x_{ij}, \theta_j\right) = D_j / RT - \theta_j\left(\sum_{i=1}^{C} x_{ij} - 1\right).$$

Therefore, the conditions for the stationary point of D_j are

$$\left(\frac{\partial \ell}{\partial x_{ij}}\right) = \left(\mu_{ij} - \hat{\mu}_i\right)/RT - \theta_j = 0 \quad ; \; 1 \le i \le C$$

Note that θ_j is independent of the component and is a property of the stationary point. It can easily be shown that $\theta_j = D_j/RT$. In the procedures developed, these stationary points are found through successive substitution, a procedure which results in the desired minima being found rather than potential maxima or saddle points.

If there are π stationary points, in terms of the fugacities, the tangent plane stability criteria can be expressed as

$$\begin{aligned} &\ln f_{ij} - \ln \hat{f}_i - \theta_j = 0 \quad ; \; 1 \le i \le C, \; 1 \le j \le \pi \\ &\theta_j = D_j / RT \ge 0 \qquad ; \; 1 \le j \le \pi \end{aligned} \quad . \tag{2.38}$$

If phase j is present, $\beta_j > 0$ and $\theta_j = 0$, and if phase j is incipient, $\beta_j = 0$ and $\theta_j > 0$.

2.4.4 Phase Distribution Variables and Material Balances

Starting from the tangent plane criteria, equation (2.38) and inserting the definition of fugacities in terms of mole fractions and fugacity coefficients results in equation (2.39).

$$K_{ij} = \frac{x_{ij}}{\hat{x}_i} \exp\left(-\theta_j\right) = \frac{X_{ij}}{\hat{x}_i} = \frac{\hat{\phi}_i}{\phi_{ij}} \tag{2.39}$$

The phase distribution variable, K_{ij}, determines the partitioning of component i into phase j and the X_{ij} are the unnormalized mole fractions equal to $x_{ij}\exp(-\theta_j)$. Knowing the unnormalized mole fractions, the normalized mole fractions, x_{ij}, can be found from

$$x_{ij} = X_{ij} \Big/ \sum_{n=1}^{C} X_{nj} \; . \tag{2.40}$$

Assuming that the $C - M = R$ linearly independent reactions of the system are known, the total number of moles of component i in the system using the stoichiometric formulation is given by

$$n_i = n_i^0 + \sum_{m=1}^{R} \nu_{im} \xi_m \tag{2.41}$$

where n_i^0 is the initial number of moles of component i, and ν_{im} is the stoichiometric coefficient which corresponds to the i^{th} component in the m^{th} reaction. The exact procedure for determining the independent reactions will be covered in the section on initiation.

Recognizing that the mole fractions, x_{ij} can be defined using equation (2.39), the conservation of species i over all the phases can be expressed as

$$\sum_{j=1}^{\pi} \beta_j x_{ij} = \sum_{j=1}^{\pi} \beta_j K_{ij} \hat{x}_i \exp\left(\theta_j\right) = n_i . \tag{2.42}$$

Since $\hat{x}_i$ is independent of the phase index and $\beta_j \exp(\theta_j)$ always equals β_j, the reference phase compositions can be defined to be

$$\hat{x}_i = \frac{n_i}{\sum_{i=1}^{\pi} \beta_j K_{ij}} = \frac{n_i}{E_i} . \tag{2.43}$$

The normalized mole fractions and unnormalized mole fractions can then be written in terms of the distribution variables as is shown in equations (2.44) and (2.45) respectively.

$$x_{ij} = \exp\left(\theta_j\right) K_{ij} n_i / E_i \tag{2.44}$$

$$X_{ij} = K_{ij} n_i / E_i \tag{2.45}$$

Since $\sum_{i=1}^{C} x_{ij} = 1$, it should be noted that if phase j is incipient ($\theta_j > 0$), $\sum_{i=1}^{C} X_{ij} < 1$. The value of θ_j can be found from the unnormalized mole fractions:

$$\theta_j = -\ln\left(\sum_{i=1}^{C} X_{ij}\right) . \tag{2.46}$$

2.4.5 The Inner Loop

The purpose of the inner loop in the algorithm is to return phase amounts, mole fractions and reaction extents given composition independent K_{ij} values, an initial feed composition and the reaction stoichiometry. Since the unnormalized mole fractions are a function of K_{ij} and β_j, if there are π phases and $R = C - M$ reactions, the inner loop finds $\pi + R$ unknowns, β_j and ξ_k. The equations used to solve for these variables are the π mole fraction constraints:

$$1 - \sum_{i=1}^{C} X_{ij} \begin{cases} = 0 & ; \ \beta_j > 0 \\ > 0 & ; \ \beta_j = 0 \end{cases} \quad ; \ 1 \le j \le \pi \tag{2.47}$$

and the R reaction affinity requirements:

$$\sum_{i=1}^{C} \nu_{ik} \hat{\mu}_i = 0 \quad ; \ 1 \le k \le R \cdot \tag{2.36}$$

Insight into this non-linear set of equations can be gained by looking at Michelsen's (1994) objective function for determining β_j and ξ_k given composition independent K_{ij} values. By reformulating his objective function to account for the use of an average reference phase and for the use of unnormalized mole fractions, the solution to equations (2.47) and (2.36) can be thought of as finding the minimum point of the scalar objective function:

$$Q(\beta, \xi) = \sum_{j=1}^{\pi} \beta_j + \sum_{i=1}^{C} n_i \left(\alpha_i + \ln n_i - \ln E_i + \ln \hat{\varphi}_i - 1 \right) \tag{2.48}$$

where

$$\alpha_i = \frac{\mu_i^0}{RT} + \ln P \, . \tag{2.49}$$

The fact that the minimum of equation (2.48) and the solution of equations (2.47) and (2.36) are the same can be seen by calculating the optimality criteria of (2.48):

$$h_j \equiv \left(\frac{\partial Q}{\partial \beta_j}\right) = 1 - \sum_{i=1}^{C} \frac{n_i K_{ij}}{E_i} = 1 - \sum_{i=1}^{C} X_{ij} \begin{cases} = 0 & ; \ \beta_j > 0 \\ > 0 & ; \ \beta_j = 0 \end{cases} \tag{2.50}$$

$$l_k \equiv \left(\frac{\partial Q}{\partial \xi_k}\right) = \sum_{i=1}^{C} \nu_{ik} \left(\alpha_i + \ln\left[\frac{n_i \hat{\phi}_i}{E_i}\right]\right) = \sum_{i=1}^{C} \nu_{ik} \hat{\mu}_i = 0 \tag{2.51}$$

The significance of this new formulation is that by examining the objective function's Hessian matrix, **H**, in the same fashion as Michelsen (1994), it can be shown that $Q(\beta, \xi)$ is a convex function.

The Hessian matrix, **H**, has the form

$$\mathbf{H} = \begin{bmatrix} \left(\frac{\partial \mathbf{h}}{\partial \beta}\right) & \left(\frac{\partial \mathbf{h}}{\partial \xi}\right) \\ \left(\frac{\partial \mathbf{l}}{\partial \beta}\right) & \left(\frac{\partial \mathbf{l}}{\partial \xi}\right) \end{bmatrix}$$

where $\mathbf{h} = \{h_1, h_2, \ldots, h_\pi\}$, $\mathbf{l} = \{l_1, l_2, \ldots, l_R\}$,

$$\left(\frac{\partial h_j}{\partial \beta_k}\right) = \sum_{i=1}^{C} X_{ij} X_{ik} / n_i \,, \tag{2.52}$$

$$\left(\frac{\partial h_j}{\partial \xi_k}\right) = \left(\frac{\partial l_k}{\partial \beta_j}\right) = -\sum_{i=1}^{C} \nu_{ik} X_{ij} / n_i \,, \tag{2.53}$$

and

$$\left(\frac{\partial l_k}{\partial \xi_m}\right) = \sum_{i=1}^{C} \nu_{ik} \nu_{im} / n_i \,. \tag{2.54}$$

Therefore, it is easily shown that $\mathbf{H} = \mathbf{V}\mathbf{V}^{\mathrm{T}}$ where **H** is a $(\pi + R) \times (\pi + R)$ matrix and **V** is a $(\pi + R) \times C$ matrix with elements

$$\begin{aligned} V_{ki} &= X_{ik} / \sqrt{n_i} && ; \ 1 \le k \le \pi \\ V_{kj} &= -\nu_{i,k-\pi} / \sqrt{n_i} && ; \ \pi < k \le R + \pi \end{aligned}$$

Since any square matrix which can be written as the product of another matrix and its transpose is at least positive semi-definite, the Hessian matrix must be at least positive

semi-definite. Therefore, the objective function, $Q(\beta, \xi)$ must be convex with a unique minimum corresponding to a unique solution of the original problem.

The convexity of Q can be exploited in the inner loop by using a Newton-Raphson procedure to quadratically converge to the unique solution of equations (2.50) and (2.51). The Jacobian needed in the Newton-Raphson procedure is the same as the Hessian matrix and is easily calculated using equations (2.52) through (2.54).

2.4.6 The Outer Loop

The objective of the outer loop is to update the K_{ij} values, the reference phase and the number of phases based upon the new phase amounts and mole fractions returned from the inner loop. Since the inner loop guarantees that the reaction equilibrium will be satisfied, establishing that the necessary conditions for phase equilibrium are met in the outer loop is sufficient to ensure both phase and reaction equilibrium has been reached.

With the new phase amounts and mole fractions, a thermodynamic model is used to calculate the new fugacity coefficients and the reference phase chemical potentials are recalculated using equation (2.34). The updating procedure for the K_{ij} values is a successive substitution method that can be derived from the tangent plane criteria stated in equation (2.38):

$$g_{ij} = \ln f_{ij} - \ln \hat{f}_i - \theta_j \tag{2.55}$$

$$g_{ij} = \ln\left(\frac{x_{ij}\phi_{ij}}{\hat{x}_i\hat{\phi}_i}\right) - \theta_j = \ln\left(\frac{x_{ij}}{\hat{x}_i}\exp\left(-\theta_j\right)\right) - \ln\left(\frac{\hat{\phi}_i}{\phi_{ij}}\right) = \ln K_{ij}^{(k)} - \ln K_{ij}^{(k+1)} \tag{2.56}$$

which can be written as

$$\ln K_{ij}^{(k+1)} = \ln K_{ij}^{(k)} - g_{ij}\,. \tag{2.57}$$

In equation (2.57) the superscripts represent the iteration count and g_{ij} are the residuals of the equations being solved.

If two phases in the inner loop become identical, the Jacobian matrix used in the Newton-Raphson procedure becomes singular. To avoid this problem, after updating the K_{ij} values in the outer loop the new phase distribution variables and specific volumes of each phase are compared. If there are two or more phases where all distribution variables and the specific volumes are within 5%, the phases are combined before the K_{ij} values are passed to the inner loop.

The outer loop terminates when the scaled sum of the square of the residuals is less than a specified tolerance, say 10^{-12}:

$$\sum_{i=1}^{C}\sum_{j=1}^{\pi} g_{ij}^2 \Big/ (\pi C) < 10^{-12}. \tag{2.58}$$

2.4.7 Initiation

Given a normalized feed composition, $\mathbf{z} = \{z_1, z_2, ..., z_C\}^T$, the ideal gas chemical potentials at the system temperature, $\mu^0 = \{\mu_1^0, \mu_2^0, ..., \mu_C^0\}^T$, and the elemental composition matrix **A**, as defined by equation (2.1), the initiation procedure must determine the number of linearly independent reactions within the system, an initial reaction extent for those reactions, the number of phases to consider and the K_{ij} value for each component in each phase. The problem of choosing the linearly independent reactions will be discussed first and will be followed by a description of how to find initial reaction extents, phases and distribution variables.

To find a set of linearly independent reactions, the linear programming technique as described by Smith and Missen (1968) is used. If the system energy is assumed to be a linear combination of the ideal gas standard state potentials, minimizing the Gibbs free energy subject to the linear elemental balance and the non-negativity constraints will result in a modified feed vector, $\mathbf{z}^*$, which can be considered an approximation to the overall composition after chemical reaction equilibrium has been established. Specifically, an initial elemental abundance vector $\mathbf{b} = \mathbf{A}\mathbf{z}$ is found and

$$G(\mathbf{z}) = \mathbf{z}^T \mu^0 \tag{2.59}$$

is minimized with respect to $\mathbf{z}$ subject to the equality constraints

$$\mathbf{Az} = \mathbf{b} \tag{2.60}$$

and the non-negativity constraints

$$\mathbf{z} \geq \mathbf{0}. \tag{2.61}$$

Equations (2.59) to (2.61) define a linear system with linear constraints and is solved using the linear programming method outlined in Chapter 10 of Fraleigh and Beauregard (1990). The solution consists of a modified feed vector, $\mathbf{z}^*$, a modified elemental abundance vector, $\mathbf{b}^*$, and a modified elemental composition matrix $\mathbf{A}^*$ which obey the relationship

$$\mathbf{A}^*\mathbf{z}^* = \mathbf{b}^*. \tag{2.62}$$

The rank of the modified vector, $\mathbf{b}^*$, and matrix will be less than the rank of their originals if two or more of the constituent equations were linearly dependent. The linear programming procedure was modified to detect this singularity and remove any degenerate elements from the problem and modify the constituent equation count, M, accordingly. The number of linearly independent reactions in the system is then found to be $R = C - M$. The discussion from this point forward assumes that there are M linearly independent constituent equations.

The modified feed vector, $\mathbf{z}^*$, is representative of the components that will be the most abundant in the equilibrium mixture of an ideal gas system. There will be M non-zero elements in this vector. The M columns of $\mathbf{A}^*$ which correspond to the M non-zero components of $\mathbf{z}^*$ will form a $M \times M$ identity matrix and $\mathbf{A}^*$ can be rearranged through column interchanges to have the form

$$\mathbf{A}^* = [\mathbf{I} \mid \mathbf{Z}] \tag{2.63}$$

where $\mathbf{I}$ is the $M \times M$ identity matrix and $\mathbf{Z}$ is a $M \times R$ full matrix. The first M columns of the $\mathbf{A}^*$ matrix shown in equation (2.63) correspond to the non-zero components in the modified feed and represent the base components. The R remaining columns of $\mathbf{A}^*$

correspond to the components with a zero mole number in modified feed which are the derived components in the system.

As described in Chapter 2 of Smith and Missen (1982), the stoichiometric coefficients of the R independent reactions can be found easily by forming the $C \times R$ matrix

$$\mathbf{N} = \begin{bmatrix} -\mathbf{Z} \\ \mathbf{I} \end{bmatrix}. \tag{2.64}$$

The i^{th} row of **N** corresponds to the same component as the i^{th} column of $\mathbf{A}^*$ in equation (2.63). The j^{th} column of **N**, denoted $\nu_j = \{\nu_{1j}, \nu_{2j}, ..., \nu_{Cj}\}^T$, represents the stoichiometric coefficients of the j^{th} independent reaction, ν_{ij} being positive for products and negative for reactants. Because the base components correspond to the first M rows of **N**, equation (2.64) indicates that each of the R independent reactions defined by **N** represents the formation of one of the R derived components from the set of M base components. Thus, the number of moles of the derived components will be equal to the reaction extent of their corresponding formation reaction.

With the reaction stoichiometry and feed compositions defined, an initial guess of the reaction extents can be found through an ideal gas approximation to the reaction affinity requirements:

$$\xi_j^0 = b_{tot} \exp\left\{ K_j - \sum_{i=1}^{M} \nu_{ij} \ln \frac{b_i^*}{b_{tot}} \right\} \tag{2.65}$$

where

$$b_{tot} = \sum_{i=1}^{M} b_i^* \tag{2.66}$$

and

$$K_j = -\sum_{i=1}^{C} \nu_{ij} \alpha_i \,. \tag{2.67}$$

The overall mole numbers used to initiate the non-ideal stoichiometric Gibbs free energy minimization can then be found from

$$N_i = z_i^* + \sum_{j=1}^{R} v_{ij}\xi_j \quad ; \; 1 \le i \le C \tag{2.68}$$

and $\mathbf{n}^0$, the initial feed mole numbers for the flash, are defined by

$$n_i^0 = \frac{N_i}{\sum_{j=1}^{C} N_i} \quad ; \; 1 \le i \le C. \tag{2.69}$$

A check should be done to ensure that all the component mole numbers remain positive when forming the initial compositions. If the reaction extents are such that a mole number becomes negative, all the reaction extents should be multiplied by a scaling factor to eliminate this problem. Because of the minimization which was done to determine the base and the derived components, the final mole numbers of the derived components should be small and therefore their corresponding reaction extents should be small. This should help eliminate the numerical difficulties of catastrophic cancellation.

Once the reactions and initial feed composition has been established, to initiate the non-ideal stoichiometric flash algorithm, the number of initial phases is set equal to the number of components plus one. According to the Gibbs phase rule, this number gives a non-reacting system one degree of freedom. As well, this allows the program to initiate the reactive flash with C liquid phases each phase being rich in one of the components and an additional vapour phase having the same composition as the feed determined by equation (2.69). To ensure that material balances are satisfied, the initial phase fractions, β_j, and mole factions, x_{ij}, are set to be

$$\beta_j = \begin{cases} 1/(C+1) & ; \; j = 1 \\ n_{j-1}^0 C/(C+1) & ; \; 2 \le j \le C+1 \end{cases} \tag{2.70}$$

$$x_{ij} = \begin{cases} n_i^0 & ;\ j = 1;\ 1 \le i \le C \\ 0.99 + 0.01 n_i^0 & ;\ 2 \le j \le C+1;\ i = j-1 \\ 0.01 n_i^0 & ;\ 2 \le j \le C+1;\ i \ne j-1 \end{cases} \tag{2.71}$$

Using the compositions as defined by equation (2.71) to determine initial fugacity coefficients, ϕ_{ij}, the initial phase distribution variables are defined by

$$K_{ij} = 1/\phi_{ij} \cdot \tag{2.72}$$

With the initial guess defined by equations (2.65) through (2.72) the stoichiometric reactive flash will be started with reaction extents close to the equilibrium extents and with a phase distribution covering all the corners in composition space.

2.4.8 Computational Concerns

The outer loop of the stoichiometric reactive flash is a straight forward successive substitution routine. Like all successive substitution flash routines, near a critical point it converges quite slowly. By using an acceleration routine as Abdel-Ghani (1995) did, the convergence rate may be improved. Other alternatives would be to switch to a single loop, full Newton-Raphson technique as is done in the polymer flash described in Chapter 6. However, a full Newton-Raphson technique requires a very good initial guess to achieve convergence to the proper solution, and the more robust successive substitution routine is adequate for all the flash calculations performed in the examples of the following chapter.

Precautions need to be taken within the inner loop to ensure that a Newton-Raphson step in the solution of equations (2.50) and (2.51) does not result in more than one phase becoming incipient at a time and that no mole numbers become negative. This is accomplished by using a single variable to scale the changes in independent variables calculated at each Newton-Raphson step. The value of the scaling parameter is initially set to 1 and then decreased if either the total number of moles of a component as calculated by (2.68) is negative or more than one phase amount, β_j, becomes less than zero. If a phase amount is to become negative, the scaling variable is set to a value such

that the phase amount becomes only slightly negative, say a value of -10^{-4}. If after the Newton-Raphson step, a phase amount is less than zero, the phase amount is set to zero and the phase is considered incipient during the next iteration. If the Newton-Raphson step results in a phase amount becoming positive, the phase is considered to be active during the next iteration.

At each iteration within the inner loop, care must be taken to ensure that incipient phases do not affect the changes in the independent variables associated with the active phases. This is accomplished by setting all the elements of a column in the Jacobian associated with an incipient phase to zero save for the element along the diagonal before the Newton-Raphson step is calculated.

2.5 The Non-Stoichiometric Algorithm

2.5.1 System Definition and Algorithm Objectives

The non-stoichiometric reactive flash algorithm performs a flash calculation under the same conditions as the stoichiometric algorithm and has the same objectives except that a set of independent reactions which characterize the system does not need to be found. Instead, the algorithm uses the elemental balances as written in equation (2.4) to constrain a minimization of the system's Gibbs free energy. The proposed algorithm is closely related to Michelsen's (1989) ideal non-stoichiometric chemical equilibrium algorithm but incorporates non-ideality and multiple mixed phases. Once again, the reference chemical potentials are weighted averages as described by equations (2.33) and (2.34). Phase stability is based upon the tangent plane criteria of section 2.4.3 and is determined by the sum of the unnormalized mole fractions in each phase.

Like the stoichiometric algorithm, the non-stoichiometric algorithm consists of two nested loops. Again, the outer loop updates thermodynamic properties using a successive substitution technique and the inner loop solves for phase mole numbers and phase compositions using composition independent fugacity coefficients supplied by the outer loop. The primary difference in the inner loop is that it does not calculate reaction

extents. In fact, no set of reactions are determined at all. Additionally, phase distribution variables, K_{ij}, are not used in this formulation.

2.5.2 The Inner Loop

The inner loop minimizes the Gibbs free energy of a multiphase system given the system feed composition and composition independent fugacity coefficients. It is formally the same as the ideal solution minimization problem solved in Michelsen's non-stoichiometric algorithm (1989). The Gibbs free energy of a multiphase system can be expressed as

$$\frac{G(\mathbf{n})}{RT} = \sum_{j=1}^{\pi}\sum_{i=1}^{C} n_{ij}\left(\frac{\mu_i^0}{RT} + \ln\left[n_{ij}\phi_{ij}P/n_{T,j}\right]\right) \tag{2.73}$$

subject to the constraints

$$\begin{aligned} \mathbf{A}\mathbf{n}_T - \mathbf{b} &= \mathbf{0} \\ \mathbf{n} &\geq \mathbf{0} \end{aligned} \tag{2.74}$$

where

$$n_{T,j} = \sum_{i=1}^{C} n_{ij}$$

$\mathbf{n}_T = \{n_1, n_2, \ldots, n_C\}^T$ and $\mathbf{n} = \{n_{11}, n_{21}, \ldots, n_{C1}, n_{12}, \ldots, n_{C\pi}\}^T$. n_i represents the total number of moles of component i in the system:

$$n_i = \sum_{j=1}^{\pi} n_{ij} \ .$$

If α_i is defined as in equation (2.49), and we use the method of Lagrange multipliers to convert the minimization of equation (2.73) subject to the constraints (2.74) into an unconstrained minimization problem, the resulting objective function, ℓ, is given by

$$\ell(\mathbf{n}, \ , \ ) = \sum_{j=1}^{\pi}\sum_{i=1}^{C} n_{ij}\left(\alpha_i + \ln X_{ij}\phi_{ij}\right) - \sum_{k=1}^{M}\lambda_k\left(\sum_{j=1}^{\pi}\sum_{i=1}^{C} A_{ki}n_{ij} - b_k\right) - \sum_{j=1}^{\pi}\sum_{i=1}^{C} n_{ij}\omega_{ij} \tag{2.75}$$

where the Lagrange multipliers associated with the elemental balances are λ_k and the slack variables ω_{ij} can be used to enforce the non-negativity constraints on the mole numbers. For brevity, n_{ij}/n_{Tj} has been replaced by the unnormalized mole fraction, X_{ij}, for reasons that will be become apparent shortly. In all the calculations, n_{ij} are forced to be positive; therefore ω_{ij} is assumed to be zero and the final term of equation (2.75) will be dropped from further discussions.

This problem contains $C\pi + M$ unknowns, $\mathbf{n}$ and λ. Recalling that in the inner loop, the fugacity coefficients are assumed to be independent of composition, at its minimum, the derivatives of (2.75) with respect to $\mathbf{n}$ and λ will equal:

$$\left(\frac{\partial \mathcal{L}}{\partial n_{ij}}\right) = \frac{\mu_{ij}}{RT} - \sum_{k=1}^{M} \lambda_k A_{ki} = \alpha_i + \ln X_{ij} + \ln \phi_{ij} - \sum_{k=1}^{M} \lambda_k A_{ki} = 0 \tag{2.76}$$

$$\left(\frac{\partial \mathcal{L}}{\partial \lambda_k}\right) = b_k - \sum_{j=1}^{\pi} \sum_{i=1}^{C} A_{ki} n_{ij} = 0. \tag{2.77}$$

The middle expression in equation (2.76) shows that the elemental Lagrange multipliers, λ_k, can be thought of as reduced elemental potentials: linear combinations of the reduced elemental potentials determine the reduced chemical potentials of all the components.

To reduce the number of variables in the system a duality transformation can be made. Rearranging equation (2.76) to isolate $\ln X_{ij}$ yields the following equation:

$$\ln X_{ij} = \sum_{k=1}^{M} \lambda_k A_{ki} - \alpha_i - \ln \phi_{ij}. \tag{2.78}$$

Substituting this into equation (2.75) results in a new objective function to be minimized:

$$Q(\lambda) = -\sum_{k=1}^{M} \lambda_k b_k \tag{2.79}$$

which is subject to the constraints

$$1-\sum_{i=1}^{C} X_{ij} \geq 0 \quad ; \quad 1 \leq j \leq \pi \tag{2.80}$$

and where X_{ij} is defined by equation (2.78). Using Lagrange multipliers for the constraints in equation (2.80) gives a new Lagrangian function:

$$\ell(\lambda,\beta) = -\sum_{k=1}^{M} \lambda_k b_k - \sum_{j=1}^{\pi} \beta_j \left(1-\sum_{i=1}^{C} X_{ij}\right). \tag{2.81}$$

This problem is one containing only $M+\pi$ equations, in $M+\pi$ unknowns, $\lambda = \{\lambda_1, \lambda_2, \ldots, \lambda_M\}$ and $\beta = \{\beta_1, \beta_2, \ldots, \beta_\pi\}^T$. It should be noted that the X_{ij} defined by equation (2.78) are unnormalized mole fractions.

The optimality conditions are given by

$$\frac{\partial \ell}{\partial \lambda_k} = -b_k + \sum_{j=1}^{\pi} \beta_j \left(\sum_{i=1}^{C} A_{ki} X_{ij}\right) = 0 \tag{2.82}$$

and

$$\frac{\partial \ell}{\partial \beta_j} = \sum_{i=1}^{C} X_{ij} - 1 \begin{cases} = 0 & ; \ \beta_j > 0 \\ < 0 & ; \ \beta_j = 0 \end{cases}. \tag{2.83}$$

The two possible right hand sides of equation (2.83) are a result of the Kuhn-Tucker conditions of constrained optimization problems. The Lagrange multipliers, β_j, must be positive if the constraint is active and they must be 0 if the constraint is inactive. Otherwise, the objective function could be further minimized (Fletcher, 1981). Examining equation (2.82) reveals that the Lagrange multiplier β_j is representative of the total number of moles in phase j.

Since it can be shown that the Gibbs function with constant fugacity coefficients is convex, the dual problem given in equation (2.81) must also be convex and contain a unique minimum. Therefore a Newton-Raphson procedure is a good choice to solve equations (2.82) and (2.83) to find the Gibbs free energy minimum. The derivatives used to form the Jacobian can be found readily and are given in equations (2.84) through (2.86).

$$\frac{\partial^2 \ell}{\partial \lambda_j \partial \lambda_m} = \sum_{i=1}^{C} A_{ji} A_{mi} n_i \quad ; \quad n_i = \sum_{k=1}^{\pi} \beta_k X_{ik} \tag{2.84}$$

$$\frac{\partial^2 \ell}{\partial \lambda_j \partial \beta_k} = \sum_{i=1}^{C} A_{ji} X_{ik} \tag{2.85}$$

$$\frac{\partial^2 \ell}{\partial \beta_k \partial \beta_l} = 0 \tag{2.86}$$

Like the stoichiometric algorithm, each Newton-Raphson step should be scaled to ensure that at most only one phase becomes incipient during a single iteration. Convergence is achieved when the sum of the square of the residues, given by equation (2.82) and the active phases of equation (2.83), is smaller than a specified tolerance. After converging, the θ_j values are calculated using equation (2.46) and the normalized mole fractions, x_{ij}, are determined and returned to the outer loop.

2.5.3 The Outer Loop

The purpose of the outer loop in the non-stoichiometric algorithm is the same as the outer loop of the stoichiometric method: it updates the fugacity coefficients to reflect the new phase compositions returned from the inner loop and determines the overall convergence of the calculation. A thermodynamic model is used with the compositions returned from the inner loop to calculate the new fugacity coefficients and fugacities. The new fugacities and phase fractions are used to calculate the reference fugacities using equation (2.34) and the residuals are determined using equation (2.55). Convergence is defined as it was in equation (2.58). If the sum of the squares of the residuals exceeds the tolerance, the inner loop is executed with the new fugacity coefficients. In a similar fashion as the stoichiometric algorithm, before entering the inner loop, phases which have compositions and specific volumes within 5% are combined.

2.5.4 Initiation

To initiate the non-stoichiometric procedure, the linear programming solution which Michelsen (1989) suggested is used with some small modifications. This

technique is the same as the linear programming initiation described for the stoichiometric algorithm, but instead of only minimizing with respect to C variables, this linear programming problem is one involving $C\pi$ variables, one for each component in each phase. The initial number of potential phases is set equal to the number of components plus one. The objective function being minimized is

$$G(\mathbf{z}) = \mathbf{z}^T \mu^0$$

subject to the linear constraints $\mathbf{Az} = \mathbf{b}$ and the normal non-negativity constraints. The difference between this problem and the linear programming problem described for the stoichiometric problem is that the feed vector $\mathbf{z}$ and the standard state chemical potential vector, μ^0, contain one element for each component in each phase, and the elemental composition matrix, $\mathbf{A}$, also has one column for each component in each phase.

To determine the $C\pi$ ranked standard state chemical potential vector, initial fugacity coefficients for each component in each phase are found based upon the inital composition guess defined by equation (2.71). The elements in the expanded standard state chemical potential vector are found from

$$\frac{\mu_{ij}^{0*}}{RT} = \frac{\mu_i^0}{RT} + \ln \phi_{ij}^0 P \tag{2.87}$$

and the multiphase, linear system is minimized.

The linear programming procedure returns a modified feed vector, $\mathbf{z}^*$, of a dimension equal to $C\pi$, but where only M of the elements of the vector are non-zero, and a modified elemental composition matrix, $\mathbf{A}^*$, where the leading $M \times M$ matrix is an identity matrix. The M non-zero elements of $\mathbf{z}^*$ can be used to determine an initial guess at the number of active phases present, the moles in the phases and the compositions of the phases. That is, from $\mathbf{z}^*$ initial estimates of β and $\mathbf{n}$ can be found. An initial guess for the Lagrange multipliers is the chemical potentials of the first M components:

$$\lambda_k = \frac{\mu_k^0}{RT} + \ln \phi_{kj}^0 x_{kj} P \quad ; \; 1 \le k \le M . \tag{2.88}$$

Note that these base components do not need to be in the same phase and care must be taken within the linear programming procedure to ensure that component and phase indices associated with the base components are properly recorded.

New compositions for each phase are found from equation (2.78), normalized and then used in a thermodynamic model to give the initial fugacity coefficients passed to the inner loop.

2.5.5 Computational Concerns

Before each Newton-Raphson step in the inner loop is calculated, the effect of the incipient phases on the active phases is eliminated by setting each element in the columns associated with the incipient phase amounts equal to zero save for the diagonal elements. Care must also be taken during calculations to ensure that not more than M phases have positive phase amounts at any one time otherwise the Jacobian becomes singular and the calculation procedure fails.

As in the stoichiometric algorithm, the Newton-Raphson step within the inner loop is scaled. Unlike the stoichiometric method, two independent scaling variables are used: one to control the change in the phase amounts and the other to control the change in the Lagrange multipliers. The Newton-Raphson step taken on any iteration is controlled to ensure that at most only one phase becomes incipient at a time. A phase becomes incipient if its β_j becomes negative or zero after an iteration. If $\beta_j < 0$, it is set equal to zero. The change in the Lagrange multipliers is scaled to ensure that each multiplier does not vary by more than 10% of its value upon each Newton-Raphson step. That is, a factor $S \leq 1$ is chosen to scale the changes in the Lagrange multipliers such that

$$S\left|\frac{\Delta\lambda_k}{\lambda_k}\right| \leq 0.10 \quad ; \; 1 \leq k \leq M.$$

A phase becomes active when the sum of the unnormalized mole fractions in that phase is greater than 1, the sum is the greatest of all the phase mole fraction sums and, by its addition, the number of active phases will not surpass M. In the case where a phase becomes active, its phase amount, β_j, is set equal to 10^{-6}.

2.6 Summary

The stoichiometric and non-stoichiometric algorithms developed in this chapter are similar in structure but differ in their implementations of the elemental constraints. Both use successive substitution in an outer loop to update thermodynamic properties of the phases and a Newton-Raphson procedure in the inner loop to determine phase amounts and mole fractions. In both algorithms, the inner loop is certain to converge to a unique solution due to the convex form of the problem. The inner loop of the stoichiometric method has $(C\text{-}M) + \pi$ unknowns while the non-stoichiometric algorithm only uses $M + \pi$ unknowns in its inner loop. This difference in the number of independent variables is important when deciding which algorithm to use and will be discussed more in the following chapter where multiple examples of the utility of these algorithms will be given and analyzed.

3. REACTIVE FLASH CALCULATIONS

3.1 Introduction

This chapter uses both the stoichiometric and non-stoichiometric reactive flash algorithms to study three multiphase reactive systems. The first example is the simple reaction between carbon monoxide, carbon dioxide and hydrogen to produce methanol and water. The reaction is also carried out in the presence of an inert heavy hydrocarbon to illustrate three phase reaction equilibrium. The second example illustrates the use of the non-stoichiometric algorithm to calculate the phase and reaction equilibrium when methyl *tert*-butyl ether (MTBE) is produced from methanol and isobutene in the presence of inert n-butane. The third example shows the use of a reactive flash algorithm to predict the properties and solubilities of an associating compound such as sulfur which can exist as S_x (commonly, x = 1, 2, ..., 8).

3.2 Methanol Synthesis

The production of methanol from carbon dioxide and water has the potential to show multiphase behaviour. Using the pure component properties shown in Table 3-1 and Table 3-2, two example methanol synthesis calculations were performed using the SRK equation of state with conventional mixing rules. The interaction parameters reported by Castier *et al.* (1989) were used in these calculations and shown in Table 3-3.

The Gibbs function of the pure component ideal gas standard states were fitted to the polynomial shown in Table 3-2 in order to determine the standard state chemical potentials over a broad temperature range.

The calculations were based on methanol production from synthesis gas in the presence of inert methane. The feed to the system consisted of CH_4, CO, H_2, CO_2, and,

Species	T_C (K)	P_C (MPa)	ω	$\Delta H^0_{f(0)}$ (kJ/mol)
CH_4	190.40	4.60	0.011	-66.505
CO	132.90	3.50	0.066	-113.820
H_2(eq)	33.20	1.30	-0.218	0.000
CO_2	304.10	7.38	0.239	-393.140
CH_3OH	512.60	8.09	0.556	-190.121
H_2O	647.30	22.12	0.344	-238.915
$C_{18}H_{38}$	748.00	1.20	0.790	-317.920

Table 3-1 - Pure Component Critical Properties, Acentric Factors and Enthalpies of Formation. Data from Reid, Prausnitz and Poling (1985).

T (K)	300	400	500	600	700	800
CH_4	-152.88	-162.67	-170.62	-177.44	-183.59	-189.20
CO	-168.62	-177.00	-183.51	-188.85	-193.40	-197.37
H_2(eq)	-102.35	-110.55	-116.93	-122.18	-126.62	-130.49
CO_2	-182.45	-191.77	-199.43	-206.04	-211.88	-217.15
CH_3OH	-201.58	-212.93	-222.33	-230.59	-238.09	-245.04
H_2O	-155.71	-165.28	-172.76	-178.92	-184.19	-188.82
$C_{18}H_{38}$	-581.84	-669.12	-747.95	-821.46	-891.58	-957.94

Gibbs Function fit to: $[G^0-\Delta H^0_{f(0)}]/T = A_1/T + A_2 ln\, T + A_3 + A_4 T + A_5 T^2 + A_6 T^3$

Table 3-2 - Pure Component Ideal Gas Gibbs Function. Values in J/mol (Marsh, 1985).

when three phase behaviour was examined, $C_{18}H_{38}$. Including the products, CH_3OH and H_2O, in the list of species, the problem can be seen to have six components and four elements when octadecane is omitted ($C = 6$, $M = 4$), and seven components and five elements when it is included ($C = 7$, $M = 5$). The reactions used in the stoichiometric algorithm were determined by the methods described in the previous chapter.

A reactive flash done at 30 MPa and 473.15 K, without octadecane resulted in a vapour and liquid phase as indicated in Table 3-4. The results agree well with those of Castier *et al.* (1989) and with the vapour phase predictions by Gupta *et al.* (1991). The small deviations seen are most likely due to differences in pure component chemical potentials. The liquid phase predictions by Gupta *et al.* are notably different from both the work of Castier *et al.* and from this work. It is unknown why this discrepancy exists.

Table 3-4 also shows the two reactions used to initiate the stoichiometric flash algorithm and their corresponding equilibrium reaction extents. Methanol is classified as a reactant because the linear programming initiation procedure determined that methanol, hydrogen and water would be the components present in greatest quantities at equilibrium. The linear programming solution redefined the feed in terms of these three base components plus the inert methane before establishing the reactions required to derive the remaining two components, carbon dioxide and carbon monoxide. The small reaction extents, 1.92×10^{-5} and 2.18×10^{-4}, indicate that the initial choice of reactions, base components, and derived components were close to the equilibrium solution. An ineffective initial guess would have resulted in larger values of the equilibrium reaction extents.

	CH_4	CO	H_2	CO_2	CH_3OH	H_2O
CO	0.0322					
H_2	-0.0222	0.0804				
CO_2	0.0933	-0.0315	-0.3426			
CH_3OH	-0.2500	-0.2881	0.0000	0.0148		
H_2O	0.5000	0.0603	-0.2500	0.0737	-0.0789	
$C_{18}H_{38}$	0.0000	0.0000	0.0000	0.0000	0.0000	0.4000

Table 3-3 - SRK Interaction Parameters. Data from Castier *et al.* (1989).

		Vapour			Liquid		
Species	Feed	Castier	Gupta	Current	Castier	Gupta	Current
CH_4*	3.00	8.78	9.15	8.80	2.46	1.56	2.44
CO	15.00	0.01	0.01	0.01	0.00	0.00	0.00
H_2	74.00	65.89	66.93	66.06	9.62	4.02	9.44
CO_2	8.00	0.06	0.04	0.06	0.02	0.01	0.02
CH_3OH	0.00	20.52	20.40	20.38	63.54	67.09	63.69
H_2O	0.00	4.73	3.47	4.69	24.36	27.32	24.41
Phase Fraction:		0.4889	0.5258	0.4890	0.5111	0.4742	0.5110
Compressibility:		1.0290	1.0190	1.0320	0.4588	0.3006	0.4585
Reaction:		$CH_3OH \leftrightharpoons CO + 2H_2$			$H_2O + CH_3OH \leftrightharpoons CO_2 + 3H_2$		
Extents:		1.92E-05			2.18E-04		
Iterations:		Stoichiometric - 21			Non-Stoichiometric - 20		
Equilibrium Moles/Feed Moles: 0.5405					* Inert Species.		

Table 3-4 - Methanol Synthesis at 30 MPa and 473.15 K. Values given are mole percentages.

		Vapour		Liquid I		Liquid II	
Species	Feed	Castier	Current	Castier	Current	Castier	Current
CH_4*	2.14	5.46	5.38	0.04	0.04	1.92	1.89
CO	10.71	0.11	0.10	0.00	0.00	0.02	0.02
H_2	52.86	57.31	57.35	0.58	0.56	11.59	11.48
CO_2	5.71	5.34	5.50	0.24	0.24	2.70	2.78
CH_3OH	0.00	14.41	14.30	22.05	21.86	27.53	27.37
H_2O	21.43	17.22	17.22	77.09	77.31	11.16	11.17
$C_{18}H_{38}$*	7.15	0.15	0.15	0.00	0.00	45.07	45.29
Phase Fraction:		0.4671	0.4740	0.3136	0.3082	0.2193	0.2178
Compressibility:		0.9623	0.9635	0.0978	0.0976	0.7515	0.7534
Reactions:		$H_2 + CO_2 \rightleftharpoons H_2O + CO$			$CO_2 + 3H_2 \rightleftharpoons H_2O + CH_3OH$		
Extents:		3.79E-04			1.40E-01		
Iterations:		Stoichiometric - 25			Non-Stoichiometric - 17		
Equilibrium Moles/Feed Moles: 0.7197					* Inert Species.		

Table 3-5 - Methanol Synthesis with Octadecane at 10.13 MPa and 473.15 K. Values given are mole percentages.

A reactive flash with octadecane in the feed was done at 10.13 MPa and 473.15 K. The results, shown in Table 3-5, indicate a vapour phase, an aqueous phase and a heavy hydrocarbon phase present at equilibrium. The reactions calculated for the stoichiometric technique were different than the ones found in the previous example. The base components in this case were hydrogen, carbon dioxide, water and the inerts were methane and octadecane. Methanol and carbon monoxide were the derived species.

As the table indicates, the reaction extent associated with the production of CO was small (3.79×10^{-4}), but the reaction extent associated with the production of methanol was significant (1.40×10^{-1}). This may account for the 25 iterations required by

the stoichiometric technique in this case whereas the non-stoichiometric technique only took 17 iterations. Again, the results agreed well with Castier *et al.* (1989).

The outer loop iteration count for both the 6 component (no octadecane) and the 7 component (with octadecane) example were evaluated. The 6 component system was flashed at 30 MPa and 473.15 °K while the 7 component system was flashed at pressures from 0.1 MPa to 65 MPa. The 7 component system showed both 2 phase and 3 phase regions over the pressure range studied. As listed in Table 3-6 and illustrated in Figure 3-1, at pressures below 8 MPa, a vapour-hydrocarbon liquid region exists. The vapour is rich in hydrogen. As the pressure increases past 8 MPa, the water and hydrocarbon liquid becomes unstable and a region containing a hydrogen-rich vapour phase, an aqueous liquid phase and a hydrocarbon liquid phase evolves. As the pressure continues to increase, the hydrogen-rich vapour is absorbed into the hydrocarbon liquid until the vapour phase completely disappears into the hydrocarbon phase at a pressure of 40 MPa. The aqueous liquid and hydrocarbon liquid are stable at the higher pressures tested.

Increasing the pressure increased the equilibrium conversion of carbon dioxide to methanol. However, at a pressure of 30 MPa, almost all of the carbon content is converted into methanol. Further pressure increases showed negligible improvements in conversion. At this pressure, the majority of the methanol was held in the aqueous phase and hydrocarbon phases.

Figure 3-1 shows the presence of incipient phases during the calculation. The dotted line gives the value of the stability variable, θ, corresponding to an incipient phase. Recall that the stability variable is positive for incipient phases and 0 for phases that are present in non-zero amounts. At pressures below 8 MPa, it is evident from observing the incipient stability variable that as the pressure increases the incipient phase becomes closer to being stable. That is, as the pressure increases, θ approaches 0. At 8 MPa, θ becomes zero and the aqueous phase appears. Conversely, at a pressure of 40 MPa, the hydrogen rich vapour becomes incipient as θ becomes positive. At pressures above

	Iterations		Methanol	Reaction	Reaction	Vapour	Aqueous	HC
P (MPa)	St.	NSt.	Produced	Extent 1	Extent 2	Phase	Phase	Phase
0.1	6	7	0.0000	3.86E-03	3.82E-05	0.9654	(0.0079)[c]	0.0347
0.5	7	7	0.0010	3.82E-03	1.02E-03	0.9346	(0.0410)	0.0654
1	8	7	0.0040	3.64E-03	4.00E-03	0.9292	(0.0840)	0.0708
2	10	6	0.0138	3.08E-03	1.38E-02	0.9223	(0.1824)	0.0777
4	12	11	0.0376	2.03E-03	3.76E-02	0.9068	(0.4348)	0.0932
6	13	12	0.0599	1.36E-03	5.99E-02	0.8858	(0.7367)	0.1142
8	18	14	0.0867	9.24E-04	8.67E-02	0.8111	0.0415	0.1474
10	25	17	0.1381	4.05E-04	1.38E-01	0.4899	0.2957	0.2145
10.13	25	17	0.1402	3.79E-04	1.40E-01	0.4740	0.3082	0.2178
12	20	17	0.1553	1.64E-04	8.72E-03	0.3374	0.4133	0.2493
14	21	23	0.1601	8.51E-05	3.98E-03	0.2760	0.4552	0.2688
16	21	21	0.1620	5.07E-05	2.14E-03	0.2397	0.4755	0.2848
18	21	21	0.1629	3.28E-05	1.28E-03	0.2128	0.4876	0.2996
20	21	21	0.1634	2.25E-05	8.18E-04	0.1903	0.4956	0.3141
25	21	22	0.1639	1.04E-05	3.31E-04	0.1421	0.5078	0.3501
30	22	23	0.1640	5.65E-06	1.63E-04	0.0982	0.5147	0.3871
35	23	24	0.1641	3.40E-06	9.05E-05	0.0552	0.5194	0.4254
40	22	24	0.1641	2.20E-06	5.51E-05	0.0120	0.5227	0.4653
45	23	25	0.1642	1.64E-06	3.87E-05	(0.9794)	0.5295	0.4705
50	31	31	0.1642	1.29E-06	2.90E-05	(0.9554)	0.5370	0.4630
55	43	42	0.1642	1.05E-06	2.23E-05	(0.9358)	0.5437	0.4563
60	24	27	0.1642	8.58E-07	1.75E-05		0.5496	0.4504
65	23	25	0.1642	7.14E-07	1.39E-05		0.5550	0.4450

Feed - CH_4: 0.0214 CO: 0.1071 H_2: 0.5286 CO_2: 0.0571
CH_3OH: 0.0000 H_2O: 0.2143 $C_{18}H_{38}$: 0.0715

Temperature is 473.15 K and methane is inert in all runs.

[a] Subsequent Reactions are: $H_2+CO_2 \rightleftharpoons CO+H_2O$ $3H_2+CO_2 \rightleftharpoons CH_3OH+H_2O$

[b] Subsequent Reactions are: $CH_3OH \rightleftharpoons CO+2H_2$ $CH_3OH+H_2O \rightleftharpoons 3H_2+CO_2$

[c] Parenthesis indicate an incipient phase, the number being the sum of the mole fractions.

Table 3-6 - Methanol Synthesis Iteration Counts.

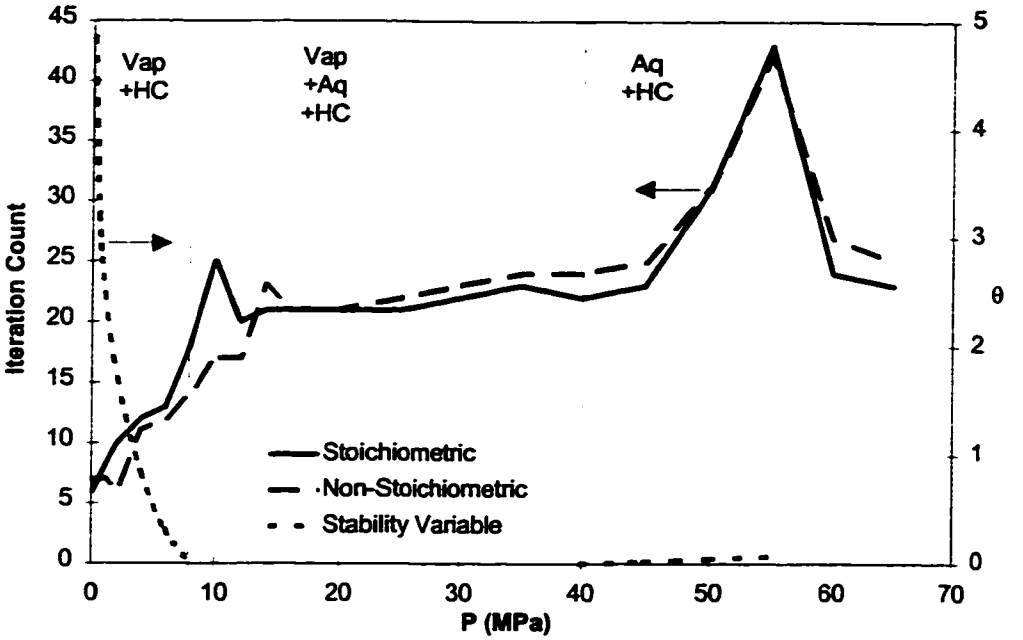

Figure 3-1 - Comparison of Stoichiometric and Non-Stoichiometric Algorithms in Methanol Synthesis. Methane is inert. Temperature is 473.15 K.

55 MPa, the composition belonging to the incipient vapour phase becomes locally unstable and no longer appear in the calculations.

The stability variable can be used to judge how close a phase is to being in equilibrium. Analyzing change of this variable as system conditions are modified gives an indication of how the system conditions can be varied to either make the incipient phase appear or to ensure that it does not become stable. As well, by examining the composition and volume of the incipient phase, the type of phase it represents can be determined.

In Figure 3-1, outer loop iteration counts are plotted for the stoichiometric and non-stoichiometric algorithms over the pressure range studied. It is apparent from the figure that the outer loop iteration count is comparable between the two techniques at all pressures except around 10 MPa.

At 10.13 MPa, the stoichiometric algorithm converges in 25 outer loop iteration whereas the non-stoichiometric algorithm converges in only 17. This difference can be

attributed to the reactions defined in the stoichiometric algorithm. At pressures below 12 MPa, the linear programming procedure discussed in the previous chapter determined that hydrogen, carbon dioxide and water would be the components present in the greatest quantities at equilibrium. As a result, the two reactions defining the system were

$$H_2 + CO_2 \leftrightharpoons H_2O + CO \quad \text{and} \quad CO_2 + 3H_2 \leftrightharpoons H_2O + CH_3OH.$$

As given in Table 3-5, the reaction extent corresponding to the second reaction at 10.13 MPa was high enough to account for the conversion of almost all of the carbon in the system to methanol. This is an indication that the choice of base components was wrong and methanol would have been a better choice than carbon dioxide as a base component. The ideal gas minimization used to determine the base components did not recognize this fact.

On the positive side, as soon as the pressure exceeded 12 MPa, the linear programming procedure gave methanol, water and hydrogen as the two reacting base components. The reactions associated with them were

$$CH_3OH \leftrightharpoons CO + 2H_2 \quad \text{and} \quad CH_3OH + H_2O \leftrightharpoons 3H_2 + CO_2.$$

These two reactions resulted in reaction extents of 1.64×10^{-4} and 8.72×10^{-3}, two values that indicate that methanol was a good choice for a base component. The stoichiometric algorithm iteration count dropped to 20 due to this change, a value close to the non-stoichiometric's 17.

The outer loop iteration count for both the stoichiometric and non-stoichiometric peaked just over 40 iterations at a pressure of 55 MPa. This corresponds to the point were the incipient vapour phase becomes locally unstable. This instability is the likely cause of the high iteration count at this point.

It is difficult to conclude that either of the algorithms is superior given the iteration counts in these examples. However, outer loop iterations is only one criteria which can be used to rank the procedures. To gain a better picture of the relative

performance of these two algorithms, the outer loop iterations can be considered along with the total computational time needed for convergence under a number of conditions.

Table 3-7 shows the time required to reach convergence for the two algorithms at 473.15 °K and different pressures. The 6 component system refers to the methanol synthesis example without octadecane while the 7 component system refers to the methanol example including octadecane. The table indicates that the non-stoichiometric

Calculation Technique	6 Component	7 Component System			
	P = 30 MPa	P = 5 MPa	10.13 MPa	30 MPa	50 MPa
Stoichiometric	129.250	143.919	306.790	193.904	266.315
Non-Stoichiometric	132.481	138.366	182.162	219.515	263.446

Table 3-7 - Stoichiometric and Non-Stoichiometric Computation Times. Times are in milliseconds and calculated on a 100 MHz Intel Pentium Processor.

Temperature is 473.15 °C.

System	P (MPa)	Iterations		Iteration Average			
		Outer Loop	Ave. Inner Loop	Inner Loop Time	Therm. Package Calls	Time Therm. Package	Time Book-Keeping
A	30.0	21/20	4.7/3.6	0.415/0.459	2.8/3.8	0.489/0.508	2.44/2.71
B	5.0	13/11	4.0/4.7	0.595/0.704	4.2/5.6	0.715/0.588	4.98/5.09
B	10.13	25/17	3.8/4.5	0.507/0.768	3.7/5.0	0.717/0.584	7.36/3.62
B	30.0	22/23	4.4/4.1	0.579/0.837	4.3/5.3	0.577/0.611	3.10/2.35
B	50.0	31/31	3.6/4.1	0.655/0.823	4.2/5.0	0.642/0.569	3.10/2.31

Table 3-8 - Iteration Count and Break Down of Computer Time. Times are in milliseconds on a 100 MHz Intel Pentium Processor.

(Stoichiometric/Non-Stoichiometric)
System A - 6 Component Methanol Synthesis Example (T = 473.15 °K).
System B - 7 Component Methanol Synthesis Example (T = 473.15 °K).

technique was faster than the stoichiometric technique except for the flashes of the 6 component system at 30 MPa and of the 7 component system at 30 MPa.

The deviation between the convergence time for the two algorithm was within 15% except for the 7 component flash at 10.13 MPa. At this pressure the stoichiometric algorithm was 68% slower than the non-stoichiometric algorithm. The longer convergence time is likely due to the 25 outer loop iterations required by the stoichiometric algorithm compared to the 17 needed by the non-stoichiometric technique. The cause of the increased iteration count at this point was discussed earlier.

Table 3-8 can be used to analyze the performance of the inner loops and to contrast the three main time consuming elements in the algorithms. It lists the outer loop iterations and the average number of inner loop iterations per outer loop pass. It displays the average number of calls to the thermodynamic package during each outer loop iteration and the average time for each call. Finally, it gives the average time for each inner loop iteration and the average time spent bookkeeping per outer loop iteration.

The inner loops of both algorithms are using an average of 4 - 5 iterations to converge. In actuality, the inner loops are repeated around 10 - 15 times in the early stages of the equilibrium computation but quickly drop to around 3 iterations as equilibrium is neared. In both cases, the inner loop solves the material balances and reaction equilibrium relationships using initial guesses from the previously converged solution and equations that are at least positive semi-definite. These two factors give rise to the quick convergence of the inner loop.

The average time per inner loop iteration is noticeably higher for the non-stoichiometric algorithm. This is a result of the problem formulation. The inner loop of the stoichiometric algorithm solves for $R + \pi$ variables where R is the number of reactions and π is the number of phases. In all the above calculations, $R = 2$. The inner loop of the non-stoichiometric technique solves for $M + \pi$ variables where M is the number of elements. In the 7 component system, $M = 5$. Therefore, since the number of phases are the same, the inner loop of the stoichiometric algorithm has to solve for an

additional 3 variables. Consequently, the time per iteration of its inner loop is greater. If the number of independent reactions, $R = C - M$, was larger than the number of elements, the inner loop of the stoichiometric algorithm would be slowest.

A call is made to the thermodynamic package each time the fugacities of a single phase need to be determined. The average number of calls to the thermodynamic package per outer loop iteration is therefore a good indication of the average number of phases included in the computation. Table 3-8 shows that the non-stoichiometric technique has an average of one more phase per outer loop iteration than the stoichiometric technique. Since both routines are initiated with $C + 1$ phases, the phases in the non-stoichiometric technique must not have merged to similar compositions and volumes as quickly as in the stoichiometric technique. It should be noted that more computational time is required in both the inner and outer loops if more phases are present.

The average bookkeeping time per outer loop iteration gives an idea of the amount of general work required to maintain the information flow in the algorithms. "Bookkeeping" includes keeping track of phase indices, initiation and combining identical phases. There is no real trend in the time required for these activities which is readily apparent from the table.

The average time for a call to the thermodynamics package turns out to be a significant factor in the analysis of these two algorithms in this case. Comparing the overall computational times in Table 3-7 to the average call times to the thermodynamic package, it becomes apparent that the algorithm with the faster thermodynamic package had the faster overall convergence time. This might not be the case when the number of equations to be solved in the inner loop of the stoichiometric algorithm is drastically different from the number in the non-stoichiometric algorithm. In this case, however, the difference is not significant, and the speed of the calls to the thermodynamic package are important.

In the calculations performed, the same thermodynamics package was used for both algorithms. This implies that the time difference for the calls to the package must be

the result of some overhead inherent in the two algorithms. By determining what this overhead is and reducing it, the computational speed of the algorithms could be improved.

The stoichiometric and non-stoichiometric algorithms spend about 28% of their computational time in the inner loop, 28% in the thermodynamic package and 40% with bookkeeping. The significant time spent in these three areas indicates that improvements in the variable management to reduce bookkeeping time or improvements in the speed of the thermodynamics package would substantially reduce the computation time of both algorithms. Thus, the need for fast, efficient thermodynamic models and proper coding procedures. Emphasis was not placed upon optimizing the computational time of these algorithms in this work.

3.3 MTBE Production

Methyl *tert*-butyl ether (MTBE) is a fuel additive used to reduce engine knock. It is synthesized from the reaction between methanol and isobutene and is usually carried out in the presence of inert C_4's like n-butane. Papers have been presented by Barbosa and Doherty (1988), Doherty and Buzad (1992), DeGarmo *et al.* (1992), Jacobs and Krishna (1993), Ung and Doherty (1995) and Okasinski and Doherty (1997), to name a few, which look at the behaviour of this reacting system and how it can be modeled within reacting distillation columns. An important aspect of modeling the production of MTBE in a reactive distillation column is the calculation of simultaneous phase and reaction equilibrium on each reactive tray of the column. The stoichiometric and non-stoichiometric algorithms are both well suited to this task.

Chemical and phase equilibrium calculations of systems containing methanol, isobutene, MTBE and n-butane where performed to illustrate the reactive flash calculations required when modeling a reactive distillation column used to produce MTBE. The non-stoichiometric algorithm was used with the SRK equation of state. Because methanol forms strong lower temperature azeotropes with MTBE and isobutene, standard equations of state can not accurately represent the liquid activity coefficients.

For these systems, activity coefficients correlated in the low pressure region give much more accurate phase equilibrium predictions at low pressures than an equation of state alone. As a result, the modified Heidemann-Kokal excess free energy mixing rule outlined in Appendix A was used to determine the mixture *a* parameter in the equation of state. This mixing rule allows an activity coefficient model to be used in conjunction with an equation of state to improve the low pressure liquid-vapour equilibrium while maintaining consistency between the liquid and vapour models.

Wilson's activity coefficient model was used in the Heidemann-Kokal mixing rule with parameters taken from Ung and Doherty (1995). Ung and Doherty used the Wilson model to represent the liquid phase and assumed an ideal vapour, a procedure which could lead to inconsistencies between the liquid and vapour models at higher pressures and temperatures.

Pure component critical properties were taken from Reid *et al.* (1987). All the pure component information and activity model parameters are given in Table 3-9 and Table 3-10. The ideal gas standard state chemical potentials were calculated from the Gibbs Function values given in Table 3-11 and the correlation function given in Table 3-2.

At first glance, a system composed of MTBE, methanol, isobutene and an inert n-butane would seem to contain 4 components and 4 elements (C, O, H and n-butane). However, the elemental composition of MTBE is a linear combination of the elemental composition of methanol and isobutene and the elemental abundance matrix is of rank 3, not 4. Thus there is one independent reaction in the system describing the formation of MTBE from methanol and isobutene:

$$CH_3OH + CH_2C(CH_3)_2 \rightleftharpoons CH_3\text{-}O\text{-}C(CH_3)_3$$
$$\text{(Methanol)} + \text{(Isobutene)} \rightleftharpoons \text{(MTBE)}$$

Component	T_C (K)	P_C (MPa)	ω	T_b (K)	$\Delta H_{f(0)}$ (kJ/mol)	V_i (cm^3/mol)
MTBE	496.4	3.37	0.2690	328.3	0.000	118.80
Methanol	512.6	8.09	0.5560	337.7	-190.120	44.44
Isobutene	417.9	4.00	0.1940	266.2	4.100	93.33
n-butane	425.2	3.80	0.1990	272.7	-97.150	100.39

Table 3-9 - Pure Component Properties for MTBE Production.

Critical properties, acentric factors and normal boiling points from Reid *et al.* (1987).
Molar volumes from Ung and Doherty (1995).
Enthalpies of formation from TRC Thermodynamic Tables (Marsh, 1985).
($\Delta H_{f(0)}$ for MTBE arbitrarily assigned.)

	MTBE	Methanol	Isobutene	n-butane
MTBE	0.0000	-406.3902	271.5669	$\Lambda_{14} = 1.00$
Methanol	1483.2478	0.0000	2576.8532	2283.8726
Isobutene	-30.2477	169.9953	0.0000	$\Lambda_{34} = 1.00$
n-butane	$\Lambda_{41} = 1.00$	382.3429	$\Lambda_{43} = 1.00$	0.0000

Table 3-10 - Wilson Model A_{ij} and Λ_{ij} Parameters. A_{ij} Parameters in cal/mol. (Ung and Doherty, 1995). $A_{ij} = 0$ or $\Lambda_{ij} = 1$ implies ideal binary mixture.

Component	200 K	273.15 K	298.15 K	300 K	400 K	500 K
MTBE			-1108.84	-1104.88	-950.53	-865.93
Methanol	-186.38	-198.01	-201.25	-201.58	-212.93	-222.33
Isobutene			-236.27	-236.65	-254.80	-271.00
n-butane	-221.84		-245.31	-245.68	-265.94	-284.34

Table 3-11 - Ideal Gas Gibbs Function Values for MTBE Synthesis Components. Values in J/mol and from the TRC Thermodynamic Tables (Marsh, 1985).

Values for MTBE were back calculated from reaction ΔG^0 values given by Ung and Doherty (1995).

Suppose that the reactive MTBE, methanol, isobutene and n-butane system contains 2 phases. According to the Gibbs phase rule with reactions there will be $F = C - \pi + 2 - R = 4 - 2 + 2 - 1 = 3$ degrees of freedom. If pressure is fixed, the degrees of freedom becomes 2. If the system is further constrained by stating that the vapour fraction is either 0 or 1 (bubble point and dew point respectively), the degrees of freedom is 1, and a single temperature will be defined for each overall composition. In fact, if there is no MTBE in the feed and the mole fractions of methanol and isobutene in the feed are fixed to a specific ratio, *r*, a pseudobinary plot can be made of the equilibrium dew and bubble point temperatures as a function of feed n-butane. Figure 3-2 shows a series of these dew and bubble point plots at 1 atmosphere and at feed methanol to isobutene mole fraction ratios of 0.7, 1.0 and 1.4.

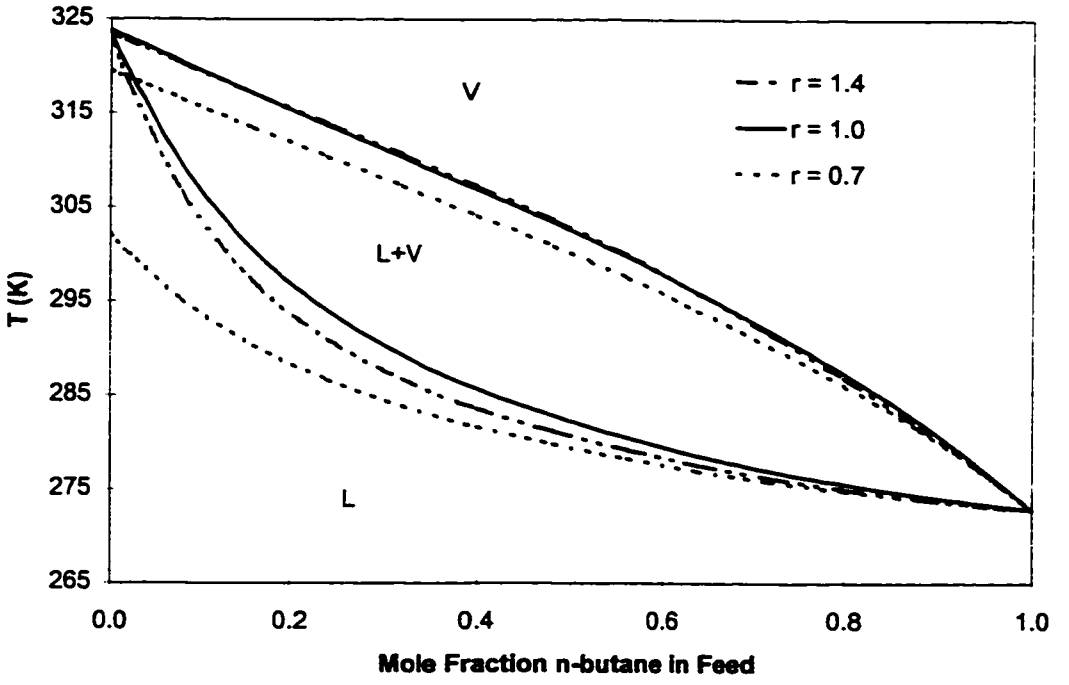

Figure 3-2 - MTBE Production Dew and Bubble Point Curves.
P = 101.325 kPa

$r = \left(z_{MeOH} / z_{Isobutene}\right)$

The figure indicates that as the mole fraction of inert n-butane in the feed increases, as expected, both the dew and bubble point temperatures approach the pure n-butane vapour pressure. However, the behaviour of the curve in the lean concentrations of n-butane is dependent upon the ratio of the reactants in the feed. The dew and bubble point temperatures in systems lean in n-butane are the highest when the reactants are fed in stoichiometric proportions ($r = 1.0$). The dew and bubble points are the lowest when the feed contains excess isobutene ($r = 0.7$) rather than excess methanol ($r = 1.4$). The figure also shows a possible liquid-vapour equilibrium in the reactive system when there are no inerts and the ratio of feed methanol to isobutene is 0.7. At all points the temperatures are below the normal boiling point of MTBE (328.3 K) and of methanol (337.7 K).

Examining the dew and bubble point curves when the n-butane mole fraction in the feed is 0.20 helps explain this behaviour. Table 3-12 lists the principle and incipient phase compositions, temperatures and total MTBE yield per mole of feed at the three methanol/isobutene ratios tested. The table shows that the highest yield of MTBE occurs when the reactants are fed in stoichiometric proportions. Stoichiometric proportions minimizes the wasted reactants. When the ratio of methanol to isobutene in the feed is 0.7, the principle phase at both the dew and bubble point contains over 20 mole per cent isobutene. The low boiling point of isobutene (266.2 K) significantly lowers the dew and bubble point temperatures below their values when the feed was stoichiometric. Conversely, when the feed contains an excess of methanol, the equilibrium dew and bubble point compositions have over 20 mole per cent methanol. As seen in Table 3-9, methanol has a boiling point that is over 9 degrees higher than MTBE's boiling point. The depression in the dew and bubble point curves with a methanol rich feed cannot be ascribed to Raoult's Law, but can be attributed to the minimum boiling azeotrope observed in binary mixtures of MTBE and methanol (Ung and Doherty, 1995).

Dew Point	$r = 0.7$		$r = 1.0$		$r = 1.4$	
	x	y	x	y	x	y
MTBE	0.8282	0.4697	0.8582	0.5543	0.5986	0.4726
Methanol	0.0072	0.0144	0.0387	0.0674	0.3495	0.2146
Isobutene	0.0797	0.2219	0.0222	0.0674	0.0036	0.0182
n-butane	0.0849	0.2940	0.0808	0.3109	0.0483	0.2945
MTBE Yield	0.320		0.357		0.321	
Temp. (K)	311.92		315.42		315.55	

Bubble Point	$r = 0.7$		$r = 1.0$		$r = 1.4$	
	x	y	x	y	x	y
MTBE	0.4905	0.1043	0.6386	0.2047	0.4963	0.1469
Methanol	0.0005	0.0006	0.0168	0.0192	0.2019	0.0665
Isobutene	0.2109	0.3592	0.0168	0.0329	0.0025	0.0058
n-butane	0.2981	0.5359	0.3277	0.7431	0.2993	0.7808
MTBE Yield	0.329		0.390		0.332	
Temp. (K)	288.48		297.06		293.93	

Table 3-12 - MTBE Dew and Bubble Point Curve Data. P = 101.325 kPa.
$z_{\text{n-butane}} = 0.20$

$r = \left(z_{MeOH} / z_{Isobutene}\right)$

The amount of MTBE produced per mole of feed increased as the amount of inert n-butane in the system decreased. The primary reason for this increase is the additional reactants in the feed. The inerts can not be eliminated entirely because they help absorb the heat of the reaction in the reactive distillation column and they, along with any excess methanol, reduce any polymerization of the isobutene. If a reactive distillation column were to be simulated, the reactive flash algorithms proposed could be used in conjunction with enthalpy balances, material transport relationships between plates and even kinetics to optimize the composition of the feed, the number of equilibrium plates needed, the

feed location in the column and how many reactive zones would be needed. The algorithms presented are one of many components necessary to model a complex chemical process such as a reactive distillation column.

3.4 Sulfur-Hydrogen Sulfide Systems

3.4.1 Introduction to Sulfur Chemistry

The utility of a reactive flash can be seen by looking at a sulfur/hydrogen sulfide system. Sulfur is an interesting compound because under process conditions it can be present in allotropes from S_1 up to S_8 where the association of sulfur atoms to form an S_x allotrope can be thought of as a reaction. Since the total amount of each allotrope is usually not known and the relationship between the allotropes can be written as reactions, phase equilibrium calculations involving sulfur systems are well suited for reactive flash algorithms. Specifically, in H_2S-sulfur systems where there are only 2 independent elements but many association reactions between sulfur allotropes and H_2S, the non-stoichiometric algorithm can be used to reduce the number of equation solved in the inner loop.

The association of sulfur molecules to form short chains leads to interesting thermodynamic properties of the pure compound. West and Menzies (1929) found that pure sulfur exhibited a minimum in its enthalpy of vapourization due to the dissociation of the allotropes. This minimum value of 281 kJ/kg occurred around a temperature of 640 K. It has been found that a sulfur model that neglects the associative nature of the molecules is not able to reproduce this interesting behaviour (Karan *et al.*, 1998).

Brunner and Woll (1980) measured the solubility of sulfur in H_2S. They found that the solubility increased with decreasing temperature at pressures below 40 MPa while it increased with increasing temperature at higher pressures. They attributed this property to the changing density of hydrogen sulfide.

Another interesting property of sulfur chemistry is that it can associate with other gas molecules to produce polysulfides. Hyne *et al.* (1966) have established that sulfur

can combine with H_2S to form sulfanes ($H_2S + S_x \leftrightharpoons H_2S_{x+1}$). This additional association reaction could affect the solubility of sulfur in H_2S and vice versa.

Karan *et al.* (1998) have examined the ability of the Peng-Robinson equation of state to match sulfur vapour pressure and sulfur/hydrogen sulfide solubilities. They considered only the S_8 form of sulfur and matched the sulfur vapour pressure by correlating the equation of state *a* parameter. As stated above, they found that their non-associative model was unable to reproduce the minimum observed in the sulfur enthalpy of vapourization curve. They also found that their model under predicted the solubility of sulfur in H_2S at low pressures but showed the proper qualitative behaviour as described by Brunner and Woll (1980).

The following example uses the non-stoichiometric reactive flash algorithm to expand on the work by Karan *et al.* (1998). S_x molecules are considered to be formed from reactions with S_8, one reaction for each molecule S_x. The *a* parameter of the Peng-Robinson equation of state will be matched to sulfur vapour pressure data and the enthalpies of vapourization will be calculated. The solubilities of sulfur in H_2S will then be calculated taking into account the potential association between sulfur and H_2S.

3.4.2 The Sulfur Association Model

An association model can be used to represent the sulfur species S_1 to S_8. If S_8 is considered the main component, the remaining sulfur species, S_x, can be considered as the product of the molecular decomposition of S_8:

$$\frac{x}{8} S_8 \leftrightharpoons S_x.$$

Assuming that a cubic equation of state is used as a thermodynamic model, the equation of state parameters, *a* and *b*, for the derived components S_x can be derived from the S_8 parameters. Using the technique developed by Heidemann and Prausnitz (1976) for associating systems, the equation of state parameters for S_x are

$$a_{S_x} = \left(\frac{x}{8}\right)^2 a_{S_8}$$

and

$$b_{S_x} = \frac{x}{8} b_{S_8}.$$

a is the temperature dependent attractive term in a cubic equation of state while b is the hard sphere volume. b is not usually temperature dependent.

Karan *et al.* (1998) modeled sulfur systems using the Peng-Robinson equation of state:

$$P = \frac{RT}{v-b} - \frac{a(T)}{v^2 + 2bv - b^2}.$$

They estimated the value of b_{S_8} by simultaneously matching both a_{S_8} and b_{S_8} to the sulfur liquid density and vapour pressure at 413.15 K. They found that $b_{S_8} = 0.13122 \times 10^{-3}$ m^3/mol. The same b value was used for S_8 in this work while the a value was re-correlated over a range of vapour pressures. In mixtures the a and b parameters were found from the following mixing rules:

$$a = \sum_{i=1}^{C}\sum_{j=1}^{C} x_i x_j a_{ij} \quad ; \quad a_{ij} = \sqrt{a_i a_j}\left(1 - k_{ij}\right) \tag{3.1}$$

$$b = \sum_{i=1}^{C} x_i b_i. \tag{3.2}$$

The interaction parameter, k_{ij}, between sulfur allotropes was 0.

The ideal gas chemical potentials for S_1 to S_8 can be found in the JANAF Thermochemical Tables (1985). These 8 sulfur components are related through 7 reactions. If pure sulfur with these allotropes exists in two phases, it will only have one degree of freedom. That is, at a specified temperature, two phases will exist at a single pressure. Therefore, a reactive flash algorithm can be used to determine the vapour pressure and sulfur compositions at a specified temperature by adjusting the pressure until a two phase system appears. It should be noted that a point on a vapour pressure line is

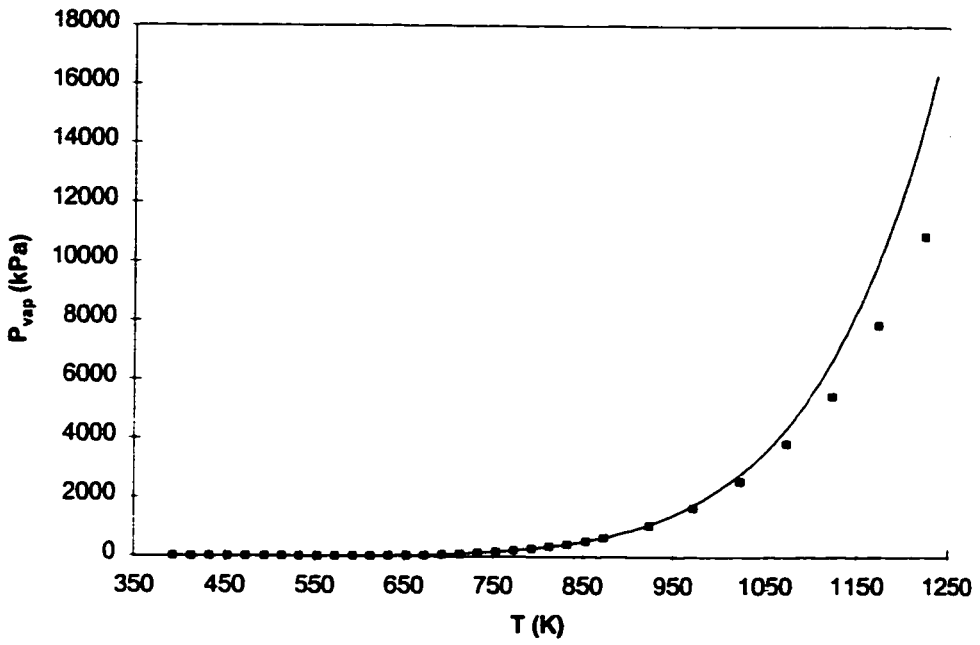

Figure 3-3 - Pure Sulfur Vapour Pressures. Data from West and Menzies (1929) and Rau *et al.* (1973).

difficult to find, but can be located quickly by changing the pressure such that the stability variable associated with an incipient phase approaches zero. Since b_{S_i} is known, a_{S_i} can be adjusted such that the calculated vapour pressure matches experimental data.

Using this technique, the sulfur vapour pressures of West and Menzies (1929) were used to determine a_{S_i} values for temperatures from 393.15 K to 873.15 K. The set of a_{S_i} values found were then fit to an expansion of inverse temperature to give:

$$a_{S_i} = 12.371 - \frac{4772.5}{T} + \frac{3.5631 \times 10^6}{T^2} - \frac{8.7494 \times 10^8}{T^3} + \frac{9.1054 \times 10^{10}}{T^4}$$

A plot of the pure sulfur vapour pressures found using this correlation and the S_1 through S_8 association model is shown in Figure 3-3. The vapour pressure data of West and Menzies (1929) and high temperature data of Rau *et al.* (1973) are also plotted. The correlation predicts the vapour pressure well up to 900 K but over-predicts the saturation pressure at higher temperatures where $a(T)$ is extrapolated.

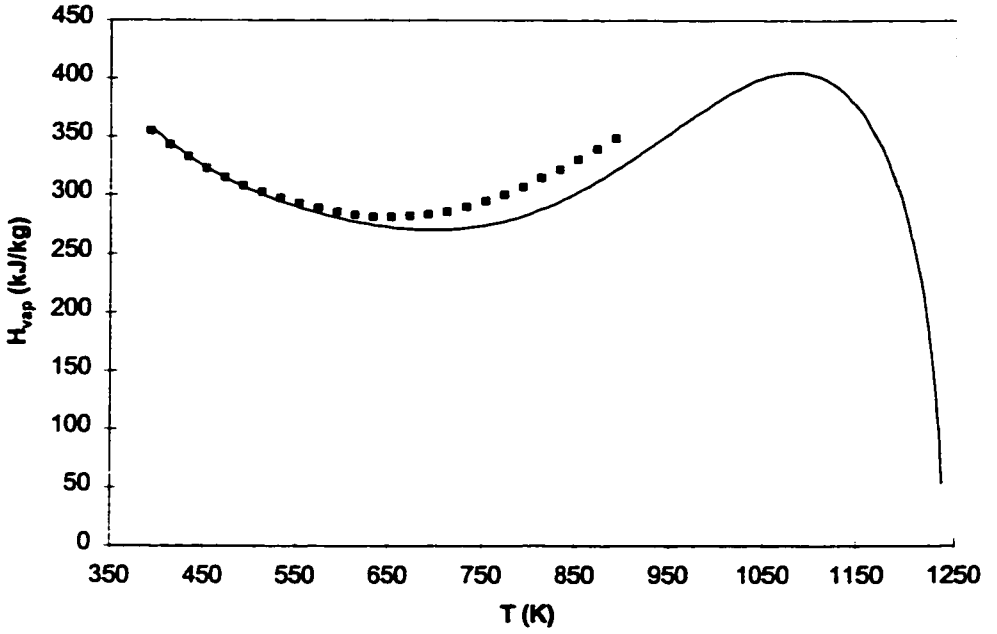

Figure 3-4 - Pure Sulfur Enthalpy of Vapourization. Data from West (1950).

The enthalpies of each component in each phase can be found from enthalpies of formation and standard departure functions. These enthalpies can be used to calculate an enthalpy of vapourization. A plot of the enthalpy of vapourization versus temperature is given in Figure 3-4 for a system of pure sulfur allotropes using an association model. Like West and Menzies (1929), a minimum in the enthalpy of vapourization is observed. The minimum occurs at 703 K with a value of 270.6 kJ/kg compared to West and Menzies' 640 K and 281 kJ/kg. The fit to the data is acceptable.

Extrapolating the enthalpies to higher temperatures shows a maximum in the enthalpy of vapourization of 405.3 kJ/kg at 1083 K. At even higher temperatures, the enthalpy of vapourization quickly approaches zero as a critical point is reached. The reported critical temperature ranges from 1209 K to 1314.2 K (Rau *et al.*, 1973) while the critical pressure varies from 11.75 MPa (West, 1950) to 18.2 MPa (Rau *et al.*, 1973). The critical temperature and pressure of sulfur using the association model are about 1236 K and 16.4 MPa respectively.

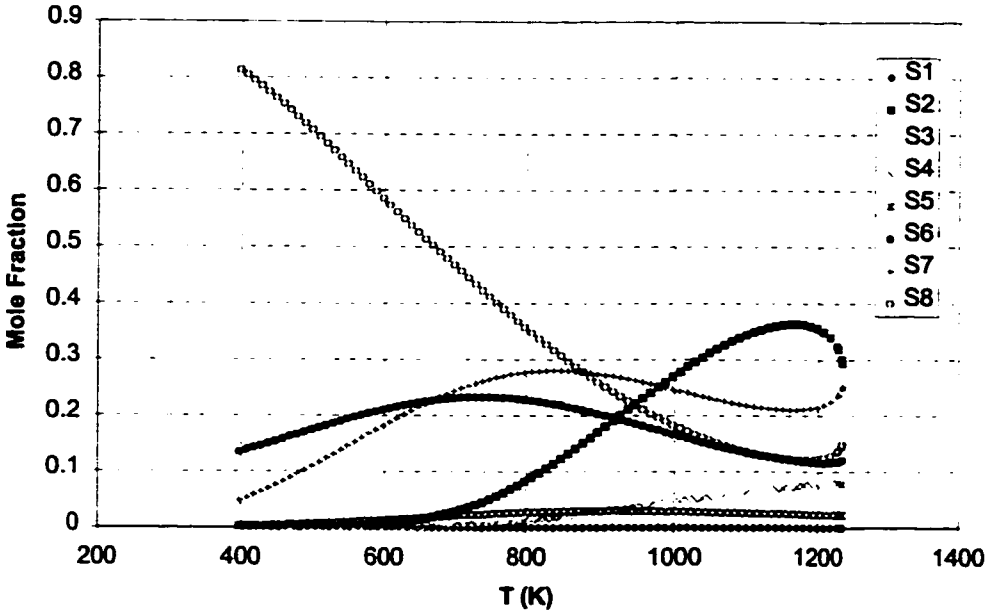

Figure 3-5 - Pure Sulfur Vapour Compositions.

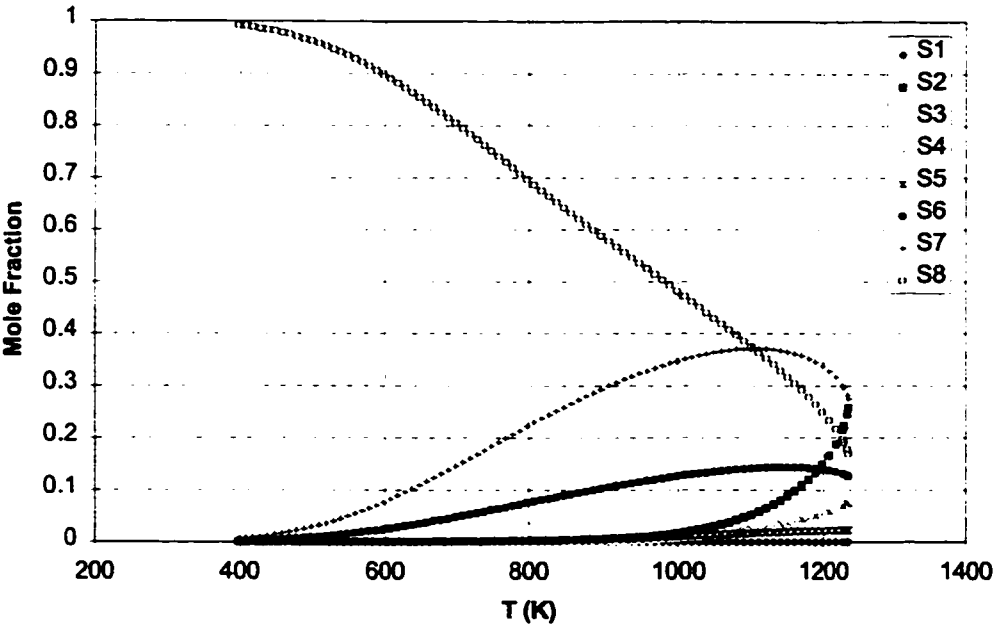

Figure 3-6 - Pure Sulfur Liquid Compositions.

The compositions of both liquid and vapour phase can also be examined along the pure sulfur liquid-vapour saturation line. Figure 3-5 and Figure 3-6 show the saturated vapour phase and saturated liquid phase compositions as a function of temperature. At temperatures below 850 K, S_8 is the dominant species in the vapour phase. At higher temperatures, S_2 has the highest saturated mole fraction. The liquid phase is rich in S_8 at temperatures below 1100 K after which S_7 becomes the dominant liquid species. Finding that S_8 is the dominant component in both liquid and vapour phases at lower temperatures justifies the common approximation that sulfur is all S_8 at low temperatures. The liquid and vapour phase compositions approach each other as the critical point is neared.

3.4.3 Sulfur Solubility in Hydrogen Sulfide

Adding hydrogen sulfide to the pure sulfur system increases the degrees of freedom by one. Therefore, in a two phase mixture of sulfur and H_2S at fixed pressure and temperature, the compositions of the two phases will be fixed. This allows solubility of sulfur in a H_2S vapour to be calculated using a two phase flash algorithm.

Treating H_2S as an inert species, the association model described above was used to model a sulfur-H_2S system. The non-stoichiometric reactive flash algorithm was used to determine the composition of the equilibrium vapour phase and, thus, the sulfur solubility in H_2S. The interaction parameter between sulfur and H_2S, k_{ij}, was found to be 0.08206 by matching the predicted solubility of sulfur in H_2S vapour at 393.15 K and 40 MPa to 0.09960 g S/g (Brunner and Woll, 1980). Increasing the interaction parameter decreased the solubility of sulfur in the vapour phase.

Figure 3-7 plots the solubility of sulfur in a H_2S vapour at 393.15 K, 413.14 K and 433.15 K over a pressure range of 5 MPa to 60 MPa. The experimental solubilities found by Brunner and Woll (1980) are also shown. It is clear that the model under-predicts the solubility at pressures below 40 MPa. It does, however, show that the solubility decreases with increasing temperature at pressures below 40 MPa and that the solubility increases with increasing temperature at higher pressures. This is the same qualitative behaviour observed by Brunner and Woll in their experiments (1980).

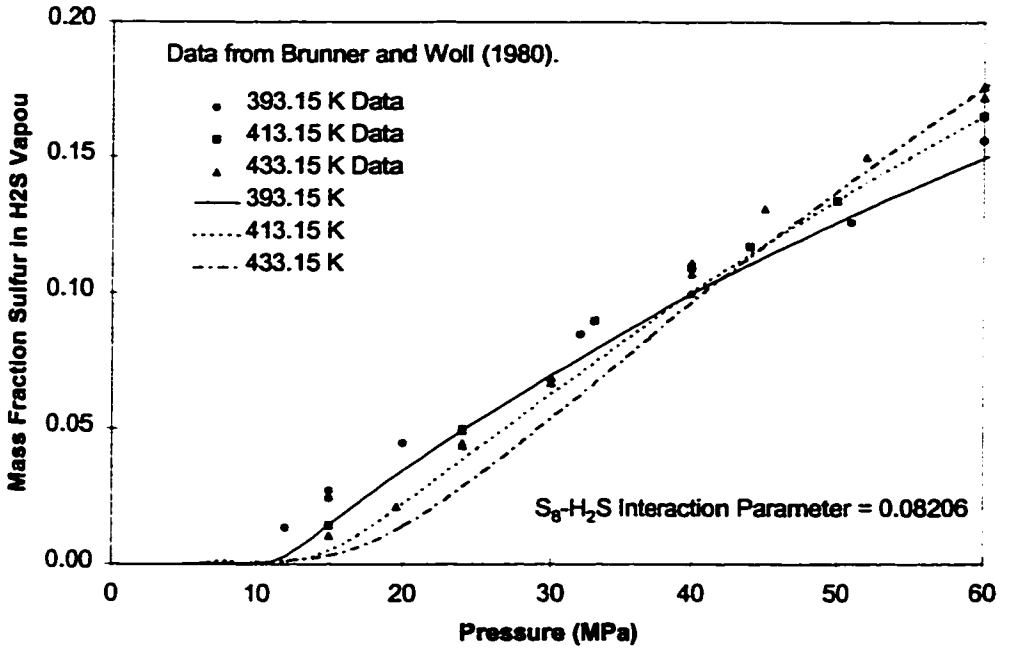

Figure 3-7 - Solubility of Sulfur in Hydrogen Sulfide. Without Sulfanes.

Karan *et al.* (1998) show that by modeling sulfur with only the S_8 allotrope the same general predictions are observed. The solubility of sulfur in H_2S was under-predicted at pressures below 40 MPa. The solubility decreased with increasing temperatures when the pressure was below 40 MPa and it increased with increasing temperature when the pressure was above 40 MPa. The similarity between the association model and the pure S_8 model is easily explained by noting that the association model predicts that pure liquid sulfur is over 95 mole % S_8 and pure sulfur vapour is over 80 mole % S_8 at 400 K.

There has been experimental evidence for the presence of sulfanes or polysulfides (H_2S_x) in sulfur/H_2S systems (Hyne *et al.*, 1966). It is possible to include these components in the model generating chemical reactions which form H_2S_{x+1} from H_2S and S_8:

$$H_2S + xS_8/8 \rightleftharpoons H_2S_{x+1}. \tag{3.3}$$

The pure component a and b parameters plus the cross terms used to determine the mixture a parameter, a_{ij}, can be found from the pure component properties of S_8 and H_2S. In general, consider there to be NS source components from which all the other components are derived. Reactions which describe the formation of both source and derived components can be written as

$$A_j = \sum_{i=1}^{NS} \nu_{ij} A_i \quad ; \; NS+1 \le j \le C. \tag{3.4}$$

When A_j refers to a source component, $\nu_{jj} = 1$ and $\nu_{ij} = 0$ for $i \neq j$.

The pure component and cross terms for the a parameter were calculated as

$$a_{ij} = \sum_{k=1}^{NS} \sum_{l=1}^{NS} \nu_{ki} \nu_{lj} \sqrt{a_k a_l} \left(1 - k_{kl}\right) \tag{3.5}$$

and the b parameter was found from

$$b_i = \sum_{j=1}^{NS} \nu_{ij} b_j \,. \tag{3.6}$$

It is important to note that the cross terms a_{ii} represent the a parameter for pure component i.

This method of determining the a_{ij} and b_i terms used in the mixing rules presented in equations (3.1) and (3.2) is a modification of the mixing rule for associating fluid proposed by Heidemann and Prausnitz (1976) to incorporate binary interaction parameters between source components. It is the same technique used by Heidemann and Rizvi (1986) for associating ammonia-water systems but more generalized. These rules imply that the covolume parameter of the associated molecules, b_i, are the linear sum of the covolumes of the molecule's source components. They also state that the pure component energy terms, a_{ii}, and energy cross terms, a_{ij}, are functions only of the interactions between the source components constituting the associated molecules. That is, there are no energy effects due to association that are not already included in the interactions between source components. Hendriks *et al.* (1997) used this notion that the

a parameter of a mixture of associating monomers can be determined from the interactions of the monomers alone to develop a mixing rule for his generalized association model.

In the case of the sulfane reaction shown in equation (3.3), the source components can be taken as H_2S and S_8. The stoichiometric coefficients associated with H_2S and S_8 in equation (3.4) will be 1 and x/8 respectively. The only interaction parameter needed is the H_2S-S_8 interaction parameter. Similar reactions can be written for the production of S_x from S_8. In these reactions, the stoichiometric coefficient associated with the hydrogen sulfide will be 0.

All equation of state parameters are defined either by the source component parameters, or by equations (3.5) and (3.6) and conventional mixing rules. The only additional information needed to define a non-stoichiometric reactive flash are the ideal gas chemical potentials of the sulfanes.

There is no information available on the ideal gas chemical potential of sulfanes. In this work, these chemical potentials were calculated by assuming that a single reaction equilibrium constant, K_{eq}, could be used to define each sulfane reaction equilibrium constant. If a value for K_{eq} is chosen, the ideal gas chemical potential of H_2S_{x+1} can be calculated from:

$$\mu^0_{H_2S_{x+1}} = -RT \ln K_{eq} + \mu^0_{H_2S} + \mu^0_{S_x} .$$

Assuming that a single reaction equilibrium constant can be used for all sulfane formation reactions, is the equivalent of assuming that adding a single sulfur molecule to either S_x or H_2S_{x+1} will result in identical changes in the Gibbs free energy of the two molecules. This assumption keeps the number of adjustable parameters to a minimum.

Conceptually, there is one reaction added to the system for each sulfane species added. Therefore, the total degrees of freedom of the system is not changed and a two phase system at a specified temperature and pressure will have fixed compositions. The solubility of sulfur in H_2S can be found by examining the total elemental sulfur, less the

H_2S sulfur, held in the vapour phase. Isothermal solubility curves similar to those shown in Figure 3-7 can be found by analyzing the vapour phase compositions during a series of reactive flash calculations over a range of pressures.

If three sulfanes, H_2S_2, H_2S_3 and H_2S_4, are included in the solubility calculations, the solubility curves found for a sulfur-H_2S system are shown in Figure 3-8. The figure was generated using the a parameter correlation for S_8 covered in the last section. The a and b parameters for H_2S were calculated from its critical properties listed in Reid, Prausnitz and Poling (1985) using the standard procedures listed in the same reference.

The two remaining adjustable parameters, k_{ij} and K_{eq}, were found by fitting the solubility curves to the experimental data of Brunner and Woll (1980). K_{eq} is assumed to be related to temperature through two constants, C_1 and C_2:

$$\ln K_{eq} = C_1 + C_2/T .$$

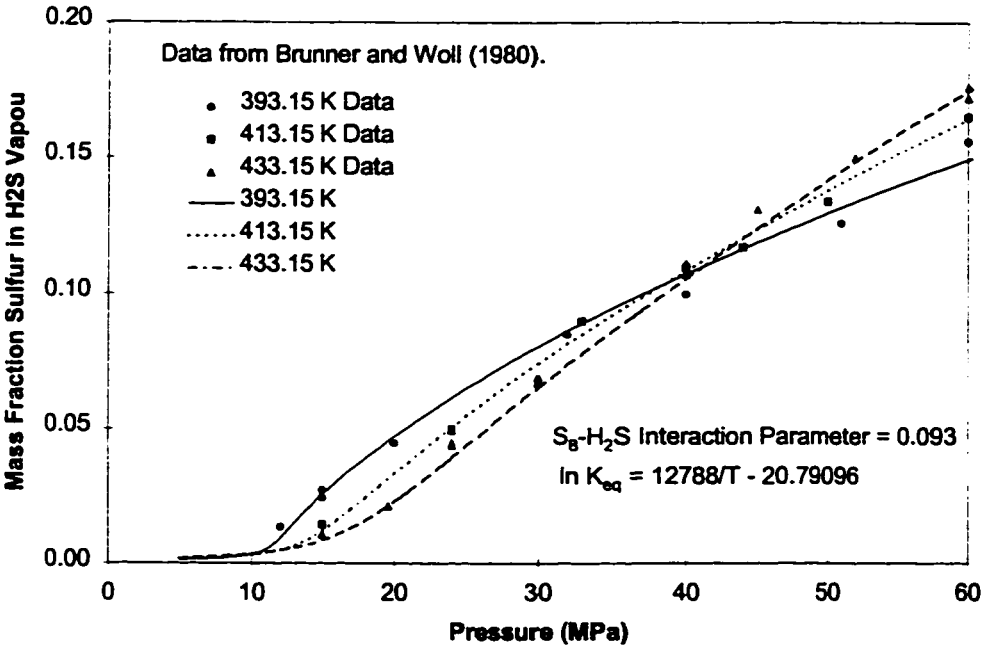

Figure 3-8 - Solubility of Liquid Sulfur in Hydrogen Sulfide. With Sulfanes. H_2S_2, H_2S_3 and H_2S_4 included in calculations.

The interaction parameter, $k_{ij} = 0.093$, and one value of K_{eq} at 433.15 K were found by matching the calculated solubilities at 433.15 K to the experimental ones at 19.6 MPa and 60 MPa. A second value for K_{eq} was then found by matching the calculated and experimentally measured solubility at 393.15 K and 15 MPa. The two values of K_{eq} were used to determine C_1 and C_2. The final expression for $\ln K_{eq}$ is

$$\ln K_{eq} = -20.791 + 12\,788/T.$$

The solubility curves in Figure 3-8 match the experimental data better than the solubility curves produced without including sulfanes components. At lower pressures, the sulfane molecules, H_2S_2, H_2S_3 and H_2S_4 are light enough that the additional solvating power provided by the hydrogen sulfide molecule is enough to favourably partition the sulfanes into the vapour phase. This partitioning increases the sulfur content in the vapour, correcting for the under prediction of the solubilities without sulfanes. If heavier sulfanes are used, this favourable partitioning is not observed.

At higher pressures, the reactions favour the production of the heavier S_8 molecules due to Le Chatelier's principle. This reduces the amount of light sulfanes in the system. Since the S_8 selectively partitions into the liquid phase, the result is that the sulfur solubility in H_2S at the higher pressure is not significantly greater than if no sulfanes were considered at all. It should be noted that if the H_2S_9 sulfane had been included in the model, higher pressures would have favoured its production. This heavy sulfane would partition into the vapour phase at high pressures and increased the overall solubility of sulfur in H_2S at high pressures.

The focus of the current section was not to analyze the performance of the reactive flash algorithms, but to show their utility in calculating phase equilibria in complex systems. No difficulties were encountered in any of the calculations performed using the non-stoichiometric technique.

3.5 Summary

The stoichiometric and non-stoichiometric multiphase reactive flash algorithms presented were able to quickly perform non-ideal chemical and phase equilibrium calculations using fugacity coefficients from conventional thermodynamic models like the SRK equation of state (methanol synthesis example) or more sophisticated models such as the SRK with an excess free energy mixing rule (MTBE example). The example calculations involving methanol synthesis gave a good indication that both algorithms could quickly predict multiphase equilibrium while accounting for possible incipient phases. Considering that each flash was initiated with a phase count equal to the number of components plus one, the low outer loop iteration counts can attest that reasonably effective initiation procedures were used.

Systems that self-associate, such as the sulfur systems discussed, are important areas for the application of reactive flash algorithms since the association of similar species can be modeled as a reaction. It was shown that the association model for sulfur predicted complex thermodynamic properties of the pure element such as the minimum point in the enthalpy of vapourization curve. As well, the association of sulfur and hydrogen sulfide to form sulfanes could be used to help predict the solubilities of sulfur in a hydrogen sulfide vapour.

In general, the two examples showed that the reactive flash algorithms developed in chapter 2 can be used to perform phase and reaction equilibrium on complex, non-ideal systems. No clear advantage of one algorithm over the other was seen in the methanol synthesis example, but it is recommended that the algorithm which results in the fewest number of inner loop equations to be solved should be used. That is, if $C - M = R$ (the number of reactions) is greater than M (the number of elements), the non-stoichiometric technique is recommended. Otherwise, the stoichiometric technique should be used.

4. CONTINUOUS THERMODYNAMICS OF POLYMER SYSTEMS

4.1 Introduction

Systems containing heavy oils, asphaltenes or polymers may contain a very large number of components with similar structure. It is quite often difficult to determine the exact mole fractions of these components or to even determine their structures. Even if the components could be characterized exactly, it would be impractical to perform phase boundary or flash calculations on a system with an infinite number of individual species. Typically, the characterization of these disperse compounds is accomplished by looking at the distribution of a physical property of the components. For example, the boiling point distribution of a heavy oil or a molecular weight distribution of a polymer sample may be used.

The two alternatives for modeling the system are to either choose a fixed number of discrete pseudocomponents or to use a continuous function of the distributed property, r, to represent the disperse component. The latter technique is called *continuous thermodynamics*. If the system contains both discrete and continuous species, the technique is called *semi-continuous thermodynamics*. In the following chapters, the term *continuous thermodynamics* will refer to both a continuous and a semi-continuous system.

This chapter will discuss the history of continuous and semi-continuous thermodynamics and will introduce the terminology used in the two subsequent chapters. As well, this chapter will describe the numerical integration routines used, the two distribution functions employed and the continuous form of the Sanchez-Lacombe equation of state. Chapter 5 will cover the development of an algorithm to determine the cloud and shadow point curves of polymer/solvent system and Chapter 6 will describe a multiphase flash for continuous and semi-continuous systems.

4.2 Literature Review

The development of continuous thermodynamics has taken two distinct branches. Phase equilibrium and material balance equations are solved either using the method of moments or the more rigorous functional method. Both approaches are still in use but the functional method has become the technique of choice in the current literature. A review of both frameworks for continuous thermodynamics is given by Cotterman and Prausnitz (1991).

4.2.1 Method of Moments

In the method of moments, thermodynamic properties and material balances of the system are defined in terms of the moments of a distribution. The continuous component in each phase is assumed to have a specific distribution and the equilibrium relationships and material balances are solved using distribution parameters as the independent variables.

Consider a system that contains a single dispersed component characterized by a distribution $W(r; \alpha, \beta, \ldots)$ and a discrete solvent. $W(r; \alpha, \beta, \ldots)$ represents the distribution of a conserved quantity such as number of moles, r is the distribution variable and $\alpha, \beta, \ldots$ are the distribution parameters. If ψ_B is the overall fraction of dispersed component B in a phase, the material balance for B in a two phase mixture can be written as

$$\psi_B^F W^F\left(r; \alpha^F, \beta^F, \ldots\right) = \phi\psi_B^V W^V\left(r; \alpha^V, \beta^V, \ldots\right) + \left(1-\phi\right)\psi_B^L W^L\left(r; \alpha^L, \beta^L, \ldots\right). \qquad (4.1)$$

Multiplying equation (4.1) by r^n and integrating over the range of r results in a material balance equation in terms of the n^{th} moment of $W(r)$:

$$\psi_B^F M_n^F(\alpha^F, \beta^F, \ldots) = \phi\psi_B^V M_n^V(\alpha^V, \beta^V, \ldots) + (1-\phi)\psi_B^L M_n^L(\alpha^L, \beta^L, \ldots). \quad (4.2)$$

The superscripts, F, V and L refer to either the feed, vapour or liquid phases respectively and ϕ indicates the equilibrium vapour fraction. A standard, discrete, material balance is used for the solvent.

Since the chemical potential of the disperse component must be the same in each phase, the following equilibrium relationship must hold:

$$\psi_B^V W^V(r; \alpha^V, \beta^V, \ldots)\varphi_B^V(r) = \psi_B^L W^L(r; \alpha^L, \beta^L, \ldots)\varphi_B^L(r) \quad (4.3)$$

where $\varphi_B(r)$ represents the fugacity coefficient of the disperse component. $\varphi_B(r)$ can be found from any suitable thermodynamic model. A similar, discrete, expression holds for the solvent.

If the distribution function, $W(r)$, contains k parameters, the solution technique usually involves using k moment balance equations, equation (4.2), to determine the relationship between the feed, vapour and liquid distribution parameters. ϕ, ψ_B^V and ψ_B^L are found from the solvent material balance and the equality of chemical potential requirements.

Cotterman and Prausnitz (1985) and Cotterman *et al.* (1985) developed a flash algorithm using this framework and gave an example calculation using a petroleum mixture and a cubic equation of state. They assumed that the feed, liquid and vapour phase distributions were three parameter gamma distributions. When the ratio of fugacity coefficients for the disperse component could be written as

$$\ln\frac{\varphi_B^L(r)}{\varphi_B^V(r)} = C_1 + C_2 r$$

the ratio, ψ_B^V/ψ_B^L, could be found analytically.

Willman and Teja (1986) used the same approach as Cotterman *et al.* (1985) to determine the dew points of natural gas and petroleum mixtures. They used a bivariate log-normal distribution function with the boiling point and specific gravity as the distribution variables. They also used a two parameter gamma function with an effective carbon number as the distribution variable (1987a, b). They first used an ideal solution approximation (1987a) and then improved upon it using a virial expansion and regular solution theory (1987b).

Du and Mansoori (1986) formulate an expression for the Gibbs free energy of a two phase system. Their Gibbs free energy is a function of the distribution parameters and molar volumes of each phase. The equilibrium state is found by minimizing the Gibbs free energy with respect to the distribution parameters and ensuring that the pressures of both phases equal the system pressure.

It has been shown that the method of moments fails to satisfy both the material balances and thermodynamic equilibrium at all values of the distribution variable (Luks *et al.*, 1990; Liu and Wong, 1997). By assuming that the distribution in each of the phases are identical in form, the material balances cannot be satisfied and the equality of chemical potential criteria can not be met over the complete range of the distribution variable. Despite these shortcomings, the method of moments is used as a reasonably efficient and accurate technique to calculate phase equilibria (Lira-Galeana *et al.*, 1991).

4.2.2 Functional Approach

To eliminate the inconsistent material balances and chemical potential inequalities associated with the method of moments, a functional approach can be used. Unlike the method of moments, in a functional approach a specific distribution function is chosen for the disperse components in the feed stream only. The phase distributions are found from the material balances and by equating the chemical potentials of the disperse and discrete components over the entire range of the distribution variable.

Aris and Gavalas (1966) first used functional analysis theory to define a functional form for the chemical potential of a continuous component, $\mu(r)$. Their work

looked at single phase, ideal systems and focused on the functional relationships which define an infinite number of reactions in the system. Kramarz and Wyczesany (1993) have also looked at reactions in continuous mixtures by using functions to represent the chemical properties of homologous series of alkanes and alkenes. Otherwise, the focus of continuous thermodynamics has shifted away from reactions and to the problem of phase equilibrium.

The equations which describe phase equilibrium in a semi-continuous system are the material balances for the discrete and the disperse components and the equality of the chemical potential of components in each phase. For a disperse species, B, the material balance in a LV flash is given by equation (4.1) and the equality of chemical potentials can be expressed as

$$\mu_B^L(r) = \mu_B^V(r). \tag{4.4}$$

That is, in the functional method, the chemical potentials are equated over the entire range of the distribution variable.

Kehlen *et al.* (1985) used functional analysis to derive the continuous thermodynamic expressions of state variable, molar properties and partial molar properties. They also derived continuous forms of Raoult's law, the NRTL model and the Flory-Huggins model for polymer systems.

Rätzsch and Kehlen (1985) used the methods described by Kehlen *et al.* (1985) to examine the effect of polydispersivity on the liquid-liquid behaviour of polymer/solvent solutions. Rätzsch *et al.* (1986) and Rätzsch *et al.* (1989) looked at polymer/polymer systems and copolymer/copolymer blends, respectively. A review of their work in these areas is given by Rätzsch and Kehlen (1989).

Rätzsch and coworkers characterize a polydisperse polymer by a segmental distribution, $W(r)$. In a segmental distribution, $W(r)\mathrm{d}r$ represents the fraction of polymer segments in the polymer molecules having segment counts between r and $r + \mathrm{d}r$.

Polymer chemical potentials are defined in terms of an ideal solution Flory-Huggins model and a deviation from that ideality, $RT\ln\gamma_i$:

$$\mu_i(r) = \mu_i^0(r,T,P) + RT\left[\ln\psi_i W_i(r) + 1 - \frac{r}{\bar{r}}\right] + rRT\ln\gamma_i(r). \tag{4.5}$$

$\mu_i^0(r,T,P)$ is the pure component chemical potential, the second term is the Flory-Huggins contribution for an ideal polymer solution and ψ_i is the overall segment fraction of component *i*. $\bar{r}$ is the number average number of segments that a molecule within a phase would contain. In the case of a polymer(B)/solvent(A) system, it can be shown to be

$$\frac{1}{\bar{r}} = \frac{\psi_A}{r_A} + \int_r \frac{\psi_B W_B(r)}{r} dr \tag{4.6}$$

For a polymer/solvent system, they developed the equations to calculate cloud point curves in terms of the independent variables, ψ_B^{II}, $\bar{r}^{II}$ and the cloud point temperature. The superscript *II* indicates that the variables refer to the incipient phase. In the two phase flash routine that they developed, the independent variables were ψ_B^{II}, $\bar{r}^{II}$ and the phase fraction ϕ. Rätzsch and Kehlen (1985) state that using continuous thermodynamics reduces computation time by 10 - 20% over methods using pseudocomponents to characterize the polymer.

Cotterman and Prausnitz (1985) developed a practical way to perform equilibrium calculations for a continuous system using Gaussian quadrature methods. If the integrand of an integral can be written as the product of a standard weighting function, $\Omega(r)$, and a function, $f(r)$, then the integral can be approximated by a summation:

$$\int_r \Omega(r) f(r) dr \cong \sum_{k=1}^{N} \omega_k f(r_k). \tag{4.7}$$

In equation (4.7), N is the number of quadrature points, ω_k is a weighting factor and r_k is the discrete r value corresponding to the weighting ω_k. For a specified weighting

function and number of quadrature points, tables of optimum values of ω_k and r_k are available (Abramowitz and Stegun, 1972).

As proposed by Cotterman and Prausnitz (1985), if the disperse component in the feed can be represented by a distribution function, Gaussian quadrature can be used to determine an appropriate set of pseudocomponents and mole fractions to best represent the system. The pseudocomponents are defined by the values of r_k and their mole fractions can be related to ω_k. Their routine is the same as characterizing a disperse system by a set of discrete components; however any arbitrariness in the choice of pseudocomponents has been removed.

After a set of discrete pseudocomponents have been found to represent the disperse component in the feed, flash and phase boundary calculations can be done with conventional algorithms. The number of equations is directly related to the number of quadrature points used.

Peng *et al.* (1987) used the quadrature technique to predict the dew points of oil reservoir fluid systems. They modeled the fluid with a gamma distribution and used the Peng-Robinson equation of state as a thermodynamic model. They concluded that quadrature techniques did not perform well in this case since the dew point temperature varied with the number of quadrature points used. They attributed this behaviour to the higher molecular weight components included in the computation when higher orders of quadrature were used.

Distribution variables typically range from 0 to infinity. Cotterman *et al.* (1986) and Shibata *et al.* (1987) have looked at using truncated distribution functions with the quadrature method to find the dew point pressures of hydrocarbon mixtures. These truncated distributions could be used to eliminate pseudocomponents with unrealistically high or low molecular weights.

Polymers systems have often been modeled using the quadrature method. Sako *et al.* (1989) have used it with a modified cubic equation of state to model high pressure polyethylene/ethylene systems. More recently, Koak (1997) has used quadrature to

determine pseudocomponents of a disperse polyethylene system to perform flash and cloud point calculations. Although he does not classify his technique as continuous thermodynamics, the method is identical to the quadrature technique described by Cotterman and Prausnitz (1985).

Another functional approach to continuous thermodynamics is the work by Ying and coworkers. Ying *et al.* (1989) developed a method of fitting distributions with cubic splines. The cubic splines allowed easy integration of the necessary phase equilibrium equations and allowed more versatility than standard distribution functions. Ying *et al.* (1989) successfully applied cubic spline fits to a hydrocarbon system using a cubic equation of state for thermodynamic properties. The computation times were comparable to quadrature and pseudocomponent techniques when the same number of nodes were used. Hu *et al.* (1993) used cubic spline fits to predict cloud point curves and critical points of polymer systems.

Moore and Anthony (1989) introduced a method of approximating distributions with a Fourier series expansion. Required integrals became the sum of Fourier series expansion terms. This has applications when looking at chromatographic characterization of petroleum fractions.

Similarly, Liu and Wong (1997) expanded distributions into series of orthogonal polynomials. They showed how these series could reduce to the same quadrature technique as proposed by Cotterman and Prausnitz (1985). They also demonstrate the errors in the material balances and equality of chemical potential when the method of moments and cubic spline methods are used to represent a continuous hydrocarbon distribution.

Kincaid *et al.* (1987) and Schlijper (1987) both developed a perturbation method to solve the continuous flash problem. In essence, they divided the disperse component into a number of discrete pseudocomponents which were used in a standard flash calculation to give a reference solution. The effect of polydispersity on the solution was found through a perturbation expansion of the thermodynamic models about the

pseudocomponent approximation. Schlijper's results were comparable to the quadrature technique when first order expansions were used.

Hendriks (1987) published an important paper which showed how the number of equations required for a continuous thermodynamic flash could be minimized. He grouped components (discrete or disperse) into families. Families were groups of components that had a zero interaction parameter within their family but shared constant interaction parameters between families. If there were k families, the maximum number of equations for a two phase PT flash was $3k + 1$. This number was reduced if families consisted of a single discrete component. The independent variables in the equations were the liquid fraction, the ratio of the vapour fraction of a family to its liquid fraction and the similar ratio of the family-averaged equation of state parameters. Integration was performed through Gaussian quadrature methods. An important aspect of the work was that the number of equations was independent of the number of quadrature points used. Hendriks developed the equations for a two parameter equation of state and compared his results to the petroleum example given by Cotterman *et al.* (1985).

4.3 Terminology

The terminology used in this dissertation will closely follow the notation used by Rätzsch and coworkers (Rätzsch and Kehlen, 1985; Rätzsch and Kehlen, 1989).

4.3.1 The Segmental Distribution Function

A polymer system can be composed of both discrete components and polydisperse polymer components. In the following discussion, a system is considered to be composed of C components, n_d discrete components and $C - n_d$ polymers. For notational purposes, when indexing species, the first n_d components will be the discrete ones. A polymer species is considered to be a single component because its disperse nature will be described by a single distribution function.

A polymer may be considered to be constructed of a number of identical segments. Sometimes these segments correspond to the repeating unit of the polymer

chain, sometimes they do not. In most cases the size of the segment is defined by the thermodynamic model used to represent the polymer. The thermodynamic model can also be used to define the number of segments which constitute a discrete component in the system. Segment sizes are not necessarily the same for discrete and polymer species.

Polydisperse polymer systems in this dissertation will be modeled with segmental distribution functions. The segment count, r, is the number of segments which a molecule contains and is considered to range from zero to infinity. An extensive segmental distribution function, $w(r)$, is defined such that $w(r)dr$ represents the total number of polymer segments contained in polymer molecules having segment counts between r and $r + dr$.

Each polymer species on a solvent free basis has its own distribution function. The total number of segments which belong to a polymer i can be calculated from

$$\bar{n}_i = \int_{r=0}^{\infty} w_i(r)dr \quad ; \; n_d < i \le C. \tag{4.8}$$

The number of segments associated with a discrete component is given by

$$\bar{n}_i = n_i r_i \quad ; \; 1 \le i \le n_d$$

where n_i represents the number of moles of component i and r_i is the number of segments which constitute that component.

The total number of segments in the system is found from

$$\bar{n} = \sum_{i=1}^{C} \bar{n}_i \,. \tag{4.9}$$

An intensive distribution function, $W(r)$, can be defined such that $W(r)dr$ is the fraction of a polymer's segments contained in molecules having segment counts between r and $r + dr$. It is the normalized extensive segmental distribution function.

$$W_i(r) = w_i(r)/\bar{n}_i \quad ; \; n_d < i \le C \tag{4.10}$$

The integral of $W(r)$ over the range of r is 1.

A segment fraction ψ_i is defined as

$$\psi_i = \frac{\bar{n}_i}{\bar{n}} \tag{4.11}$$

and represents the fraction of all segments which are associated with component *i*. The sum of all segment fractions must be 1.

Let $n_i(r)dr = w_i(r)dr/r$ represent the number of polymer molecules with segment counts between r and $r + dr$. As well, let n represent the total number of molecules in a system. The number average number of segments in a system, $\bar{r}$, can then be found as follows.

$$\bar{r} = \left[\sum_{i=1}^{n_d} r_i n_i + \sum_{i=n_d+1}^{C} \int_{r=0}^{\infty} r n_i(r) dr\right] \Big/ n = \left[\sum_{i=1}^{n_d} r_i n_i + \sum_{i=n_d+1}^{C} \int_{r=0}^{\infty} w_i(r) dr\right] \Big/ n$$

$$\frac{1}{\bar{r}} = n \Big/ \sum_{i=1}^{C} \bar{n}_i = n/\bar{n}$$

$$= \frac{1}{\bar{n}} \sum_{i=1}^{n_d} \frac{\bar{n}_i}{r_i} + \frac{1}{\bar{n}} \sum_{i=n_d+1}^{C} \int_{r=0}^{\infty} \frac{w_i(r)}{r} dr$$

$$= \sum_{i=1}^{n_d} \frac{\bar{n}_i}{r_i} \frac{\bar{n}}{} + \sum_{i=n_d+1}^{C} \int_{r=0}^{\infty} \frac{\bar{n}_i}{\bar{n}} \frac{w_i(r)}{r} \frac{\bar{n}_i}{} dr$$

and by equations (4.10) and (4.11)

$$\frac{1}{\bar{r}} = \sum_{i=1}^{n_d} \frac{\psi_i}{r_i} + \sum_{i=n_d+1}^{C} \int \frac{\psi_i W_i(r)}{r} dr \tag{4.12}$$

4.3.2 Chemical Potentials

For a discrete multicomponent system, the total Gibbs free energy can be written as

$$G(T, P, n_i) = -TS + PV + \sum_{i=1}^{C} \mu_i n_i \,. \tag{4.13}$$

The chemical potential, μ_i, is defined to be the partial derivative of the Gibbs free energy with respect to the moles of component i:

$$\mu_i = \left(\frac{\partial G}{\partial n_i}\right)_{T,P,n_{j\neq i}} = \lim_{\Delta n_i \to 0} \frac{G(T,P,n_1,\ldots,n_i+\Delta n_i,\ldots n_C) - G(T,P,n_1,\ldots,n_C)}{\Delta n_i}. \quad (4.14)$$

Now consider a polymer system where the polymer segment distribution is defined by a segmental distribution function, $w(r)$. The Gibbs free energy of the system now becomes a functional of w:

$$G(T,P;w) = -TS + PV + \int_{r=0}^{\infty} \bar{\mu}(r)w(r)dr. \quad (4.15)$$

The segmental chemical potential, denoted by $\bar{\mu}(r)$, can be related to the Gâteaux derivative of the Gibbs free energy with respect to a change in the number of segments associated with molecules of segment count r.

If $\delta_{r'}(r)$ represents the Dirac delta function centered at r', $w(r)+t\delta_{r'}(r)$ represents the addition of t segments to the segmental distribution function at r' (since $\int_0^{\infty} t\delta_{r'}(r)dr = t$). The Gâteaux derivative of G in the direction of $\delta_{r'}(r)$ is defined as (Tapia, 1971):

$$DG(\delta_{r'}) = \lim_{t\to 0} \frac{G(T,P;w+t\delta_{r'}) - G(T,P;w)}{t}.$$

By inserting equation (4.15) into the above definition and assuming that $\bar{\mu}(r)$ is independent of w, the relationship between the Gâteaux derivative and the segmental chemical potential can be seen:

$$DG(\delta_{r'}) = \lim_{t\to 0} \frac{\int_0^\infty \bar{\mu}(r)[w(r)+t\delta_{r'}(r)]dr - \int_0^\infty \bar{\mu}(r)w(r)dr}{t}$$

$$= \lim_{t\to 0} \frac{\int_0^\infty \bar{\mu}(r)t\delta_{r'}(r)dr}{t} = \lim_{t\to 0} \int_0^\infty \bar{\mu}(r)\delta_{r'}(r)dr$$

$$= \bar{\mu}(r')$$

Given an expression for the Gibbs free energy of a continuous system, the segmental chemical potentials can be found from the limiting process used above. An alternative, more practical method would be to take the derivative of the Gibbs free energy with respect to an increase of segments at r', $(\partial G/\partial \bar{n}_{r'})_{T,P}$, use the chain rule, and replace $(\partial w(r)/\partial \bar{n}_{r'})_{T,P}$ with $\delta_{r'}(r)$, the Dirac delta function (Kehlen *et al.*, 1985). $(\partial G/\partial \bar{n}_{r'})_{T,P}$ will be equal to $\bar{\mu}(r')$.

Rätzsch and Kehlen (1989) have defined the segment-molar activity coefficients for discrete and continuous components, γ_i and $\gamma_i(r)$ respectively, by

$$\bar{\mu}_i = \frac{\mu_i}{r_i} = \bar{\mu}_i^\bullet + RT\left[\frac{1}{r_i}\ln\psi_i + \frac{1}{r_i} - \frac{1}{\bar{r}}\right] + RT\ln\gamma_i \qquad (4.16)$$

and

$$\bar{\mu}_i(r) = \frac{\mu_i(r)}{r} = \bar{\mu}_i^\bullet + RT\left[\frac{1}{r}\ln\psi_i W_i(r) + \frac{1}{r} - \frac{1}{\bar{r}}\right] + RT\ln\gamma_i(r). \qquad (4.17)$$

These equations are written in the format of the original Flory-Huggins expression where volume fractions have been replaced by segment fractions. As is evident in these equations, the segmental chemical potentials, $\bar{\mu}_i$, can be thought of as the molar chemical potential per segment.

The second terms on the right hand side of equations (4.16) and (4.17) are the athermal Flory-Huggins contributions and the third terms on the right hand side represent the deviations from the athermal Flory-Huggins model. These segment-molar activity

coefficients depend upon the thermodynamic model used to represent the components of the system.

Equations (4.16) and (4.17) will be the form of the segmental chemical potentials that will be used in this dissertation.

4.4 Distributions

In this thesis, two different distributions were used to represent polymer distributions: the log-normal distribution and the Shultz-Flory distribution. Both distributions were defined such that $W(r)dr$ represents the fraction of polymer segments that are contained in molecules with segment counts between r and $r + dr$.

4.4.1 Log-normal Distribution

The log-normal segmental distribution has the form

$$W(r) = \frac{1}{r\beta\sqrt{\pi}} \exp\left\{-\left(\frac{\ln r - \ln r_0}{\beta}\right)^2\right\} \tag{4.18}$$

where r_0 is related to the mode of the distribution and β to its breadth. If κ is the mass of a segment, the number average molecular weight, M_n, and weight average molecular weight, M_w, of the polymer described by the distribution are

$$M_n = \kappa r_0 \exp\left\{-\beta^2/4\right\} \tag{4.19}$$

and

$$M_w = \kappa r_0 \exp\left\{\beta^2/4\right\}. \tag{4.20}$$

If M_n and M_w of a polymer sample are known, these relationships can be used to find the log-normal parameters, β and r_0:

$$\beta = \sqrt{2\ln\left(M_w/M_n\right)} \tag{4.21}$$

$$r_0 = M_n \exp\left\{\beta^2\ 4\right\}/\kappa \tag{4.22}$$

Koak (1997) also uses the number average and mass average molecular weights to find the parameters of a log-normal molecular weight distribution. His log-normal distribution, $F(M)$, was defined such that $F(M)d(\ln M)$ represented the fraction of polymer molecules with molecular weights between M and $M + dM$. His distribution parameters were β and M_0 where β was given by equation (4.21) but the value for M_0 was given by

$$M_0 = M_n \exp\{-\beta^2/4\} \neq \kappa\sigma_0 .$$

M_0 does not equal $\kappa\sigma_0$ because $F(M)d(\ln M)$ represents a number of molecules whereas $W(r)dr$ represents a number of segments. $W(r)dr/r$ represents a number of molecules. The two distributions are related in the following manner:

$$\frac{F(M)}{M} = \frac{F(r\kappa)}{r\kappa} = \frac{1}{r\kappa\beta\sqrt{\pi}} \exp\left\{-\left(\frac{\ln r\kappa - \ln M_0}{\beta}\right)^2\right\} = \frac{W(r)\,r}{\int_{r=0}^{\infty} W(r')dr'\;r'} \qquad (4.23)$$

Since the denominator of equation (4.23) is equal to $\exp\{\beta^2/4\}/r_0$, the relationship between $F(M)$ and $W(r)$ can be simplified to

$$F(M)/M = F(r\kappa)/r\kappa = r_0\, W(r) \exp\{-\beta^2\ \ 4\}/r .$$

After substituting in the definition of a log-normal distribution and some algebraic manipulation, the relationship between r_0 and M_0 is found to be

$$\kappa\sigma_0 = M_0 \exp\{\beta^2/2\} .$$

The log-normal distribution is *divergent*. That is, the distribution converges more slowly than the exponential, $\exp(-\sigma r)$ where σ is any positive value (Šolc, 1970). Using limits, this behaviour can also be described by

$$\lim_{r\to\infty} W(r)\exp(\sigma r) = \infty \quad \forall\ \sigma : \sigma > 0 .$$

As will be shown in the following chapter, many integrals associated with the calculation of cloud point curves have the factor $W(r)\exp(\sigma r)$ in their integrand. Because the log-

normal distribution is divergent, cloud point calculations using it will have to be approximated using flash calculations.

4.4.2 Shultz-Flory Distribution

An example of a convergent distribution is the Shultz-Flory distribution given in equation (4.24). It is a two parameter gamma distribution.

$$W(r) = \left(\frac{r}{r_0}\right)^{\beta} \frac{\beta^{\beta+1}}{r_0 \Gamma(\beta+1)} \exp\left\{-\frac{\beta r}{r_0}\right\} \tag{4.24}$$

Like the log-normal distribution, this form has two parameters which can be defined by the polymer sample's M_n and M_w:

$$M_n = \kappa r_0 \tag{4.25}$$

and

$$M_w = \kappa\left(\frac{\beta+1}{\beta}\right) r_0 . \tag{4.26}$$

The parameters, β and r_0 as functions of M_n and M_w are given in equations (4.27) and (4.28) respectively.

$$\beta = 1 \Big/ \left(\frac{M_w}{M_n} - 1\right) \tag{4.27}$$

$$r_0 = M_n / \kappa \tag{4.28}$$

4.4.3 Distribution Comparison

Table 4-1 gives the log-normal and Shultz-Flory distribution parameters for polyethylene with a number average molecular weight of 8000 and a weight average molecular weight of 177 000. Using the Sanchez-Lacombe equation of state as described in a later section, the mass per mol of segments is $\kappa = 11.477$. These parameters are those used in the following chapter to represent a polyethylene distribution and will be used to compare the log-normal and the Shultz-Flory distribution in the following discussion.

Parameter	Log-Normal Distribution	Shultz-Flory Distribution
r_0	3278.7	697.04
β	2.4886	0.0473
$\Gamma(\beta+1)$	n/a	0.9748

Table 4-1 - Distribution Parameters for Polyethylene. $M_n = 8000$, $M_w = 177\ 000$. $\kappa = 11.477$ using the Sanchez-Lacombe equation of state.

Figure 4-1 plots the log-normal and Shultz-Flory distributions versus the logarithm of dimensionless molecular weight. It can be seen that the Shultz-Flory distribution is a much flatter one with more of the segments found in the lower molecular weight region. In order to better view the behaviour of the two distributions at higher molecular weights a log-log plot was made. Figure 4-2 shows this plot. It is evident from this plot that the Shultz-Flory distribution converges to 0 at higher molecular weights much more quickly than the divergent log-normal distribution.

The number of molecules corresponding to a segment count of r is equal to $W(r)dr/r$. Figure 4-3 shows a graph of the molecule count versus the molecular weight. It is important to note that the log-normal distribution is bounded at $r = 0$ whereas the Shultz-Flory distribution shows a singularity at the origin if $\beta < 1$. This fact is important in numerical integration routines where difficulties occur near singular points. The singularity could be avoided by formally truncating the distribution at a finite lower value of r or by using a three parameter gamma distribution. As well, the singularity would not exist if the distribution was chosen to represent the number of molecules instead of the number of segments. However, the unmodified Shultz-Flory distribution was used in this work.

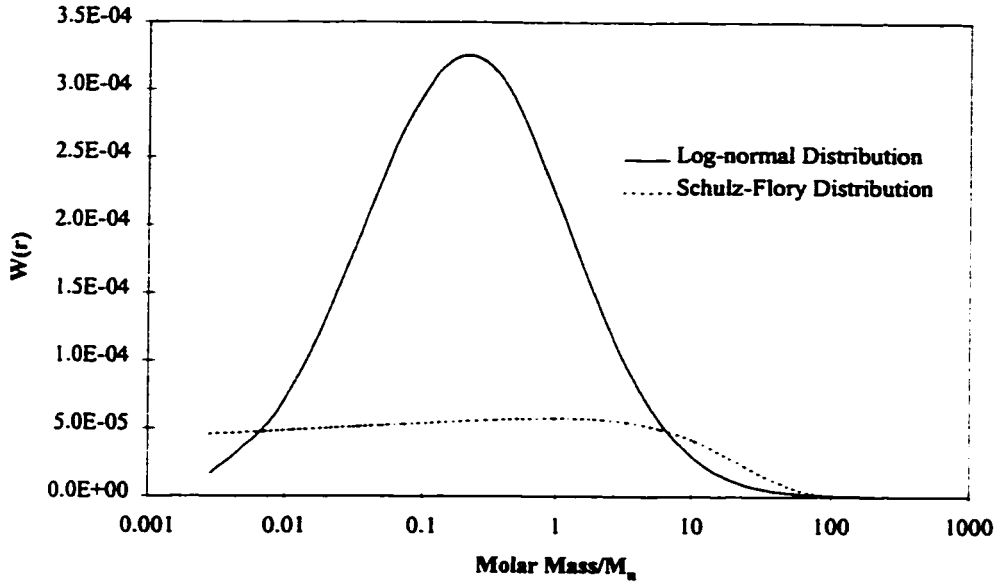

Figure 4-1 - Log-Normal and Shultz-Flory Distributions. Semi-Log Plot. (Polyethylene with M_n = 8000 and M_w = 177 000)

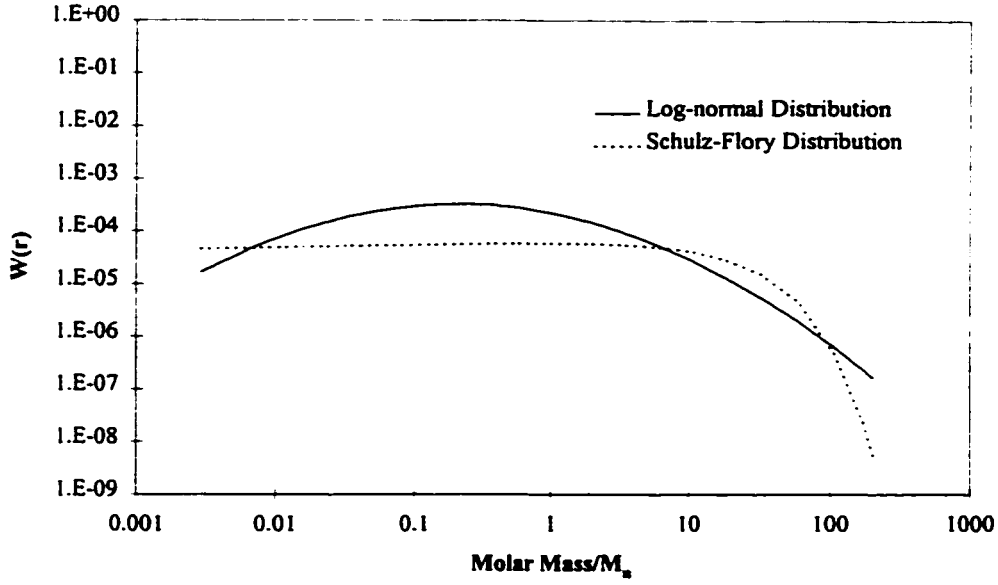

Figure 4-2 - Log-Normal and Shultz-Flory Distributions. Log-Log Plot. (Polyethylene with M_n = 8000 and M_w = 177 000)

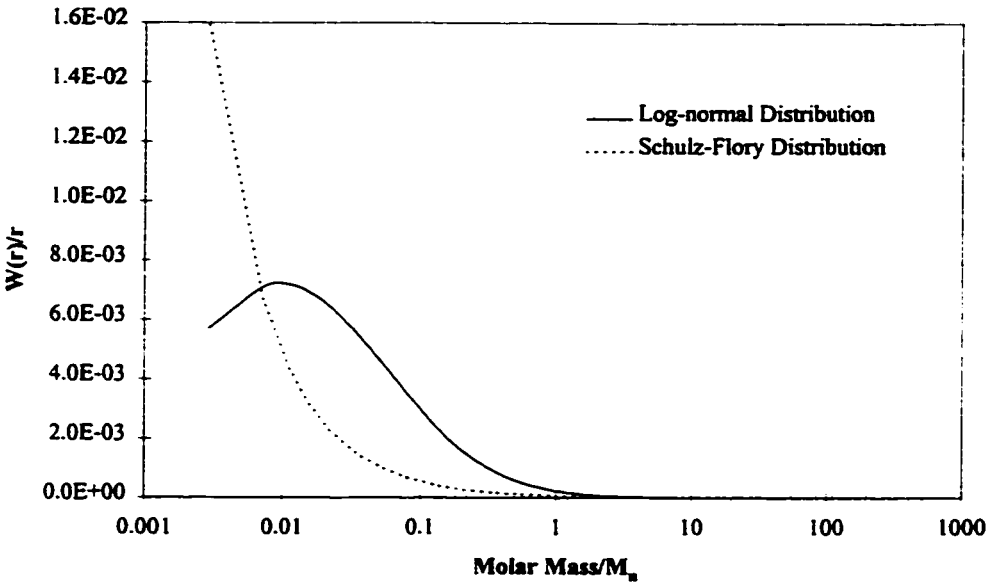

Figure 4-3 - Molecule Count of Log-Normal and Shultz Distributions. (Polyethylene with M_n = 8000 and M_w = 177 000)

4.5 Integration Routine

Euler's method, Rhomberg's method, Runge-Kutta techniques of various orders and Gaussian quadrature were initially evaluated for the necessary numerical integration in this work. Two algorithms were chosen: a high precision fifth order Runge-Kutta algorithm was used for high precision integration and a Gaussian quadrature technique was used for less accurate, but much faster, integration.

4.5.1 High Precision Routine

A fifth order Runge-Kutta integration routine with adaptive step size control was used for high precision integration. The theory of the routine and the exact algorithm can be found in the text by Press *et al.* (1992).

The integral $y = \int f(x)dx$ is treated as the solution of the ordinary differential equation

$$(dy/dx) = f(x) \quad ; \; x \in [s,t]$$

Initial Condition: $x = s \Rightarrow y = 0$.

The fifth order Runge-Kutta method determines successive values of y, y_{n+1}, which correspond to the integral from s up to x_{n+1}. y_{n+1} is based upon six evaluations of the derivative, $f(x)$, and the prior value of y, y_n:

$$y_{n+1} = y_n + c_1 k_1 + c_2 k_2 + c_3 k_3 + c_4 k_4 + c_5 k_5 + c_6 k_6 + O(h^6)$$

where

$$\begin{aligned} k_1 &= hf(x_n) \\ k_2 &= hf(x_n + a_2 h) \\ &\vdots \\ k_6 &= hf(x_n + a_6 h) \end{aligned}$$

h is a step size parameter and the constants a_i are dependent upon the development of the fifth order routine. The Cash-Karp parameters were used (Press *et al.*, 1992):

$$\{a_2, a_3, \ldots, a_6\} = \{1/5, 3/10, 3/5, 1, 7/8\}.$$

The step size, h, indicates the amount the variable x is changed at each step. That is, $x_{n+1} = x_n + h$.

The benefit of this format is that a fourth order Runge-Kutta method is embedded within the same formulation. That is, a fourth order approximation to y_{n+1} can be found from the same k_i used in the fifth order method.

$$y^*_{n+1} = y_n + c^*_1 k_1 + c^*_2 k_2 + c^*_3 k_3 + c^*_4 k_4 + c^*_5 k_5 + c^*_6 k_6 + O(h^5)$$

The parameters for both c_i and c_i^* are given in Table 4-2.

i	c_i	c_i^*
1	$\frac{37}{378}$	$\frac{2825}{27648}$
2	0	0
3	$\frac{250}{621}$	$\frac{18575}{48384}$
4	$\frac{125}{594}$	$\frac{13525}{55296}$
5	0	$\frac{277}{14336}$
6	$\frac{512}{1771}$	$\frac{1}{4}$

Table 4-2 - Cash-Karp Parameters for Runge-Kutta Method

This fourth order approximation is used to give an estimate of the error in the fifth order approximation, $\Delta \equiv y_{n+1} - y_{n+1}^*$. If this error is larger than a set tolerance, Δ_{max}, the step size, h, can be decreased. Conversely, if the error is smaller than desired, h can be increased. The adaptive step size allows the integration routine to take smaller steps when the integrand is complex, but still allows large step sizes when the integrand is well behaved.

The upper and lower limits of integration in this thesis are typically 0 and infinity and the integrands sometimes are not defined at either limit. If the integral being calculated has the form,

$$I = \int_{r=0}^{\infty} f(r)dr, \tag{4.29}$$

the upper limit of integration can be changed to a finite value using the transformation $X = r/(r_0 + r)$. The resulting integral becomes

$$I = \int_{X=0}^{1} \frac{r_0 f(Xr_0, 1-X)}{(1-X)^2} dX. \tag{4.30}$$

For practical calculations, the limits of integration are taken to be $s = 0 + \varepsilon_1$ and $t = 1 - \varepsilon_2$. These limits and the maximum error allowed at each integration step were manipulated so that the numerically calculated weight average and number average molecular weights of the distribution in question were within 0.5% of the analytical solutions. An additional criteria was that the number average segment count of the feed had to be within 0.1% of the analytic solution. The tolerances used are given in Table 4-3. For the log-normal distribution, these parameters give values for M_n, M_w and $\bar{r}$ within 0.01% accuracy. For the Shultz-Flory distribution, the small value of ε_1 was needed because the integrand required to find M_n, $W(r)/r$, had a strong singularity near $r = 0$ (see Figure 4-3). However, in this case, it was found that setting $\varepsilon_1 = 1\times10^{-12}$ did not change the calculated cloud and shadow point curves significantly.

Distribution	Δ_{max}	ε_1	ε_2
Log-Normal	1×10^{-10}	1×10^{-10}	1×10^{-10}
Shultz-Flory	1×10^{-12}	1×10^{-40}	1×10^{-10}

Table 4-3 - Integration Tolerances

4.5.2 Gaussian Quadrature

Cheney and Kincaid (1985) review the fundamental theory of Gaussian quadrature. The main result of Gaussian quadrature is that for specific weighting functions, $\Omega(x)$, the integral of $\Omega(x)f(x)$ can be approximated by a summation of N points. That is,

$$I = \int_x \Omega(x) f(x) dx \cong \sum_{i=1}^{N} \omega_i f(x_i). \tag{4.31}$$

The summation is exactly equal to the integral if $f(x)$ is a polynomial of degree less than or equal to $2N - 1$. The weighting factors, ω_i, and quadrature points, x_i, are dependent upon the weighting function and the number of quadrature points.

If $\Omega(x) = \exp(-x^2)$, the quadrature technique used is called Gauss-Hermite quadrature. If $\Omega(x) = \exp(-x)$, the technique is called Gauss-Laguerre quadrature. The weighting factors and quadrature points for both of these techniques can be found in texts (Abramowitz and Stegun, 1972) or through calculation methods as outlined by Press *et al.* (1992). The computational approach was used in this work.

Gauss-Hermite quadrature was used when the log-normal distribution was employed. If an integral to be calculated has the form

$$I = \int_{r=0}^{\infty} f(r)W(r)dr = \frac{1}{\beta\sqrt{\pi}} \int_{r=0}^{\infty} \frac{f(r)}{r} \exp\left\{-\frac{\ln^2(r\ r_0)}{\beta^2}\right\} dr,$$

the variable transformation, $u = \ln(r/r_0)/\beta$, results in

$$I = \frac{1}{\sqrt{\pi}} \int_{u=-\infty}^{\infty} f(r(u))e^{-u^2} du. \tag{4.32}$$

This last equation has the same form as equation (4.31) when the weighting function equals $\exp\{-u^2\}$. It shows that as long as the integrand contains the log-normal distribution function, the integral can be approximated using Gauss-Hermite quadrature.

Similarly, when the distribution function is the Shultz-Flory distribution given by equation (4.24), a variable transformation, $u = \beta r/r_0$, gives the following integral:

$$I = \frac{1}{\Gamma(\beta+1)} \int_{u=0}^{\infty} f(r(u))u^{\beta}e^{-u} du.$$

This integral also has the form of equation (4.31) if the weighting function is $\exp\{-u\}$. Thus all integrals using the Shultz-Flory distribution can be approximated with Gauss-Laguerre quadrature.

An important point to note about Gaussian quadrature techniques is that they only give good approximations to an integral if the function $f(x)$ can be closely approximated with a polynomial. That is, they work best with smooth functions. Since the weightings and quadrature points depend only on the weighting function, these values only have to be calculated once at the start of the main program. After this initial calculation, the same weightings and quadrature points can be used for each required integral.

The number of quadrature points used in this thesis was 10 unless otherwise stated.

4.6 The Sanchez-Lacombe Equation of State

The Sanchez-Lacombe equation of state (Sanchez and Lacombe,1976; Sanchez and Lacombe, 1978) is a mean field lattice gas equation of state where pressure effects are introduced through the use of "holes" in the lattice.

Starting with the Sanchez-Lacombe equation of state as given by Koak and Heidemann (1996) for discrete thermodynamics,

$$\frac{P}{RT} = \frac{(1-\tilde{r})}{v} - \frac{\tilde{r}^2}{b}\ln\left(\frac{v-b/\tilde{r}}{v}\right) - \frac{a\ RT}{v^2}, \tag{4.33}$$

the chemical potentials for individual components are formulated as

$$\begin{aligned}\frac{\mu_k}{RT} = \ln\left(\frac{x_k RT}{v}\right) - 2\frac{\tilde{r}^2}{b}\left[\sum_{i=1}^{C} x_i b_{ik}/b - \frac{r_k}{\tilde{r}}\right]\left(v-\frac{b}{\tilde{r}}\right)\ln\left(\frac{v-b/\tilde{r}}{v}\right) \\ -\tilde{r}\left[2\sum_{i=1}^{C} x_i b_{ik}/b - \frac{r_k}{\tilde{r}}\right]\left[\ln\left(\frac{v-b/\tilde{r}}{v}\right)+1\right] - \frac{2}{RTv}\sum_{i=1}^{C} x_i a_{ik} \\ +\left[1+\ln\left(\frac{r_k b}{\tilde{r}^2 RT}\right)+2\left(\sum_{i=1}^{C} x_i b_{ik}/b - \frac{r_k}{\tilde{r}}\right)\right]\end{aligned} \tag{4.34}$$

where

$$b = \sum_{i=1}^{C}\sum_{j=1}^{C} x_i x_j b_{ij} \quad ; \quad b_{ij} = r_i r_j v_{ij} = r_i r_j \left(v_{ii}+v_{jj}\right)/2, \tag{4.35}$$

$$a = \sum_{i=1}^{C}\sum_{j=1}^{C} x_i x_j a_{ij} \quad ; \quad a_{ij} = r_i r_j a_{ij} = r_i r_j \varepsilon_{ij} \left(v_{ii} + v_{jj}\right)/2 , \tag{4.36}$$

and

$$\bar{r} = \sum_{i=1}^{C} x_i r_i . \tag{4.37}$$

The cross energy term, ε_{ij}, is related to the pure component energy parameters through

$$\varepsilon_{ij} = \left(1 - k_{ij}\right)\sqrt{\varepsilon_{ii}\varepsilon_{jj}} . \tag{4.38}$$

A pure component is defined by three parameters, namely r_i, v_{ii} and ε_{ii}, which can be found from the standard Sanchez-Lacombe parameters, T_i^*, P_i^* and ρ_i^* through the equations $\varepsilon_{ii} = RT_i^*$, $v_{ii} = \varepsilon_{ii}/P_i^*$ and $r_i = M_i/\rho_i^* v_{ii}$.

Recall the previous section on segmental distributions, section 4.4. The mass per segment, κ, was defined such that a molecule of mass M_i and a segment count r_i were related by

$$M_i = \kappa r_i . \tag{4.39}$$

By comparing equation (4.39) to the definition of r_i given by the Sanchez-Lacombe equation of state parameters, the definition of κ for the Sanchez-Lacombe equation of state is $\kappa = \rho_i^* v_{ii}$.

Suppose a system contains n_d discrete components and $(C - n_d)$ polymers with continuous distributions. The above equations are rewritten for the continuous components by replacing a mole fractions with segment fractions through the following equations:

$$x_i = \bar{r}\frac{\psi_i}{r_i} \quad ; \; 1 \le i \le n_d$$

$$x_i(r) = \bar{r}\frac{\psi_i W_i(r)}{r} \quad ; \; n_d < i \le C$$

These definitions are inserted into equations (4.33) through (4.36) and the summation signs in equations are replaced with integration when a disperse component is considered. The result is a continuous form of the Sanchez-Lacombe equation of state:

$$\frac{P}{RT} = \frac{1-\bar{r}}{v} - \frac{1}{\tilde{b}}\ln\left(\frac{v-\bar{r}\tilde{b}}{v}\right) - \frac{\tilde{a}}{v^2}\frac{RT}{} \tag{4.40}$$

The expression for the number average number of segments, equation (4.37), is replaced with equation (4.12).

Assuming that v_{ii} and ε_{ii} are independent of the concentration and distribution of polymer, the equation of state parameters become

$$\tilde{a} = \bar{r}^2 \sum_{i=1}^{C}\sum_{j=1}^{C} \psi_i \psi_j \varepsilon_{ij} v_{ij} \,, \tag{4.41}$$

$$\tilde{b} = \sum_{i=1}^{C}\sum_{j=1}^{C} \psi_i \psi_j v_{ij} \,, \tag{4.42}$$

$$\tilde{a}_i = \sum_{j=1}^{C} \psi_j \varepsilon_{ij} v_{ij} \,, \tag{4.43}$$

and $$\tilde{b}_i = \sum_{j=1}^{C} \psi_j v_{ij} \,. \tag{4.44}$$

The continuous form of the chemical potentials per segment are given by

$$\frac{\bar{\mu}_i}{RT} = \frac{\mu_i}{r_i RT} = \frac{1}{r_i}\ln\psi_i + \frac{1}{r_i} - \frac{1}{\bar{r}} + \ln\gamma_i \quad ; \; 1 \le i \le n_d \tag{4.45}$$

$$\frac{\bar{\mu}_i(r)}{RT} = \frac{\mu_i(r)}{rRT} = \frac{1}{r}\ln\psi_i W_i(r) + \frac{1}{r} - \frac{1}{\bar{r}} + \ln\gamma_i(r) \quad ; \; n_d < i \le C \tag{4.46}$$

where

$$\ln\gamma_i = \frac{1}{r_i}\ln\left(\frac{\bar{r}\tilde{b}}{v}\right) - \frac{2}{\bar{r}\tilde{b}}\left[\frac{\tilde{b}_i}{\tilde{b}} - 1\right]\left(v - \bar{r}\tilde{b}\right)\ln\left(\frac{v-\bar{r}\tilde{b}}{v}\right) - \left(\frac{2\tilde{b}_i}{\tilde{b}} - 1\right)\left[\ln\left(\frac{v-\bar{r}\tilde{b}}{v}\right) + 1\right] - \frac{2\tilde{a}_i\bar{r}}{vRT} + \frac{2\tilde{b}_i}{\tilde{b}\bar{r}} - \frac{1}{\bar{r}} \quad ; \; 1 \le i \le n_d \tag{4.47}$$

and

$$\ln\gamma_i(r) = \frac{1}{r}\ln\left(\frac{\bar{r}\tilde{b}}{v}\right) - \frac{2}{\bar{r}\tilde{b}}\left[\frac{\tilde{b}_i}{\tilde{b}} - 1\right]\left(v - \bar{r}\tilde{b}\right)\ln\left(\frac{v-\bar{r}\tilde{b}}{v}\right) - \left(\frac{2\tilde{b}_i}{\tilde{b}} - 1\right)\left[\ln\left(\frac{v-\bar{r}\tilde{b}}{v}\right) + 1\right] - \frac{2\tilde{a}_i\bar{r}}{vRT} + \frac{2\tilde{b}_i}{\tilde{b}\bar{r}} - \frac{1}{\bar{r}} \quad ; \; n_d < i \le C \tag{4.48}$$

Equations (4.47) and (4.48) are the segment molar activity coefficients as defined by Rätzsch and Kehlen (1989) and represent the deviation of the thermodynamics from the Flory-Huggins model. All thermodynamic pressure dependencies are contained within these values.

It is important to note that the equation of state parameters given in the above equations do not depend upon the details of the segmental distributions of the polymer species. They only depend upon the segment fractions of each component and the number average number of segments as defined by equation (4.12). That is, if the segment fractions and the $\bar{r}_i$ are known for a particular phase, the equation of state parameters can be found. This independence on the details of the segmental distributions results from the assumption that segment-segment interactions are independent of the size of the polymer chains involved. The interactions are dependent only upon the average distributions of the different segments throughout the system: average distributions which are described by the segment fractions.

With the equation of state parameters determined, equation (4.40) can be solved for a molar volume, v, which can be used in equations (4.47) and (4.48) to calculate the segment molar activity coefficients. The following section describes the volume solver.

4.7 The Volume Solver

The method used to solve the Sanchez-Lacombe equation of state for a volume root is the same as used by Koak (1997). The solver returns either a liquid root or a

vapour root. It is passed the temperature, pressure, equation of state parameters and type of root to find. The procedure first determines the number of roots which exist and then uses a Newton-Raphson technique to find the liquid or vapour root desired.

The number of roots is found by first calculating a critical temperature from the parameters given:

$$T_C = 2\tilde{a}/\bar{r}\tilde{b}R\left(1+\sqrt{\bar{r}}\right)^2 .$$

If the temperature is above the critical temperature, only one root exists and it is assumed to be vapour-like. If the temperature is below the critical temperature, three roots may exist. To determine if there are three roots, the limits of mechanical stability are found by locating the two volumes where $\left(\partial P/\partial v\right)_T = 0$ using a Newton-Raphson procedure. The initial guess to find the higher mechanical stability limit volume is 1.1 times the critical volume:

$$v_C = \bar{r}\tilde{b}\left(1+\sqrt{\bar{r}}\right).$$

The initial guess to find the lower mechanical stability limit volume is 1.1 times the hard sphere limit, $v = \bar{r}\tilde{b}$. These two volumes define the upper and lower mechanical stability limits on pressure and if the system pressure is between them, three roots exist. Otherwise, if the pressure is above the upper mechanical stability limit pressure, a liquid-type root is sought, and if the pressure is below the lower mechanical stability limit pressure a vapour-type root is sought.

The volume returned from the volume solver is found using a standard Newton-Raphson procedure. If a vapour-type root is being found the Newton-Raphson procedure is initiated with volume guess of $v = 0.9RT/P$. If a liquid-type root is being found, an initial guess of $v = 1.1\bar{r}\tilde{b}$ is used. This technique worked without trouble in almost all cases; however, it was found that the Newton-Raphson step size had to be monitored when finding a liquid root to ensure that the volume did not become smaller than the hard sphere volume.

4.8 Summary

Of the two techniques for continuous thermodynamic calculations, the functional approach is used the most. The Gaussian quadrature technique developed by Cotterman and Prausnitz (1985) is the most practical of these methods. This technique uses Gaussian quadrature to divide a polydisperse component into pseudocomponents which can then be utilized in traditional multicomponent calculations. The more quadrature points used, the more equations need to be solved.

The following two chapters differ from the quadrature method by developing cloud point curve calculations and multiphase flash calculations without dividing the disperse polymer into pseudocomponents. Instead, functional objective functions and residues will be developed. This eliminates a number of equations that would be necessary if a pseudocomponent method was used. Even if a Gaussian quadrature technique is employed to perform the integration within the functionals, the number of equations to be solved will be unaffected by the number of quadrature points used.

5. CLOUD AND SHADOW POINT CURVE CALCULATIONS IN POLYMER SYSTEMS

5.1 Introduction

As a vapour cools at constant pressure, the temperature at which the first drop of liquid forms is called the dew point temperature. At this temperature, the vapour phase will have the same composition as the initial vapour had, but the liquid phase will likely have a very different composition. The liquid phase has negligible mass and is called the incipient or conjugate phase.

An analogous development can be made for varying the temperature of a liquid phase until it splits into two liquids. The temperature at which two phases first appear is called the cloud point temperature. The liquid corresponding to the initial phase is called the cloud phase whereas the liquid present in negligible amounts is named the shadow phase. The cloud phase has the same composition as the initial, or feed, liquid and the shadow phase will likely have a different composition. By plotting the cloud point temperature versus the cloud phase composition, a cloud point curve is formed. The corresponding plot of cloud point temperature versus shadow phase composition is the shadow point curve.

It is important to recognize that liquid-liquid instabilities can occur on decreasing the temperature and/or on increasing the temperature. If the liquid-liquid split occurs as

the temperature decreases, the system can be described as following UCST (Upper Critical Solution Temperature) type behaviour. If the liquid-liquid split occurs as the temperature increases, the system can be described as following LCST (Lower Critical Solution Temperature) type behaviour. It is quite possible for a polymer system to show both LCST and UCST types of behaviour.

Figure 5-1 shows some representative cloud and shadow point curves. Part (a) is an example of LCST type behaviour while part (b) is UCST type behaviour. Because polymer systems contain a distribution of molecular weights and molecules with very high molecular weights, these cloud and shadow point curves can show very interesting behaviour. Part (a) in Figure 5-1 shows a cloud point curve having a three phase point (indicated by a crossover of the cloud point curve with itself), an unstable critical point (intersection of cloud and shadow point curves) and two liquid-liquid regions (above and below the three phase point). Part (b) illustrates a cloud point curve having a stable critical point at the intersection of the cloud and shadow point curves. A potential liquid-

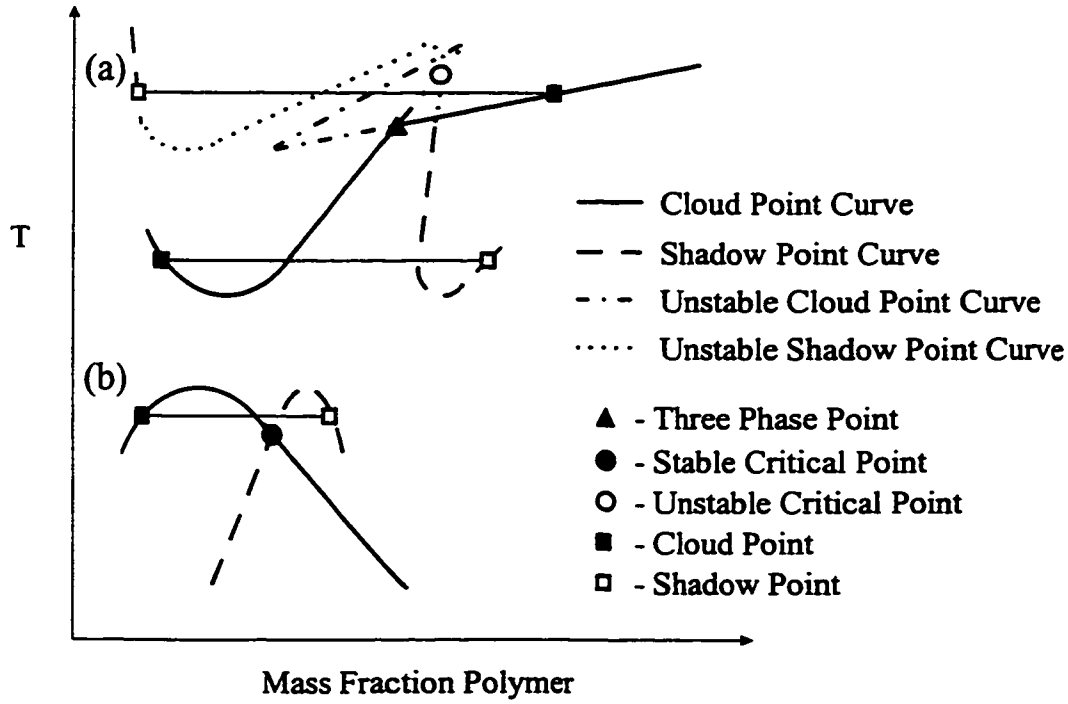

Figure 5-1 - Representative Polymer Cloud Point Curves.

vapour region is not shown in the figure but may appear at higher temperatures (Koak, 1997).

This chapter formulates a method for finding lines of constant phase segment fraction, ϕ, in polymer/solvent systems using the continuous thermodynamic form of the Sanchez-Lacombe equation of state (see section 4.6). The curves are generated at a fixed pressure, but in principle, the pressure could be used as an independent variable in the following development. The algorithm is designed using the functional approach to continuous thermodynamics and is developed in a fashion which results in only five equations in five unknown variables. When $\phi = 0$ or $\phi = 1$, the curves found correspond to cloud and shadow point curves.

5.2 Algorithm Development

5.2.1 Background

A review of developments in continuous thermodynamics was given in the previous chapter. Cloud and shadow point calculations with a functional approach to continuous thermodynamics were covered in depth by Rätzsch and Kehlen (1989). Their calculations were meant to find curves at a fixed phase segment fraction of $\phi = 0$ or $\phi = 1$. The independent variables of their formulation were the polymer segment fractions, ψ_B, and the number average number of segments in the shadow phase, $\bar{r}$. No information on how complete curves were generated was given for cases when numerical integration was necessary in the Rätzsch and Kehlen publications.

Michelsen (1980) developed an algorithm for calculating phase envelopes of hydrocarbon systems at constant composition. With a specified feed composition, his method used a Newton-Raphson procedure to converge on points of a fixed phase fraction. The independent variables that he used were the logarithms of the distribution variables, the temperature and pressure ($\ln K_i$, $\ln T$ and $\ln P$). $C + 1$ equations were formed for these $C + 2$ variables from the equilibrium requirements and the material balance constraints. The remaining equation was found by choosing one of the

independent variables to be a *specification variable*, α_i, which was forced to a value, $\alpha_i = S$, where S is a specified constant. The curves corresponding to fixed phase fractions were traced by finding points corresponding to incremental values of S. The choice of specification variable could change along the length of a curve by examining the derivatives of the independent variables with respect to the specification constant, S. The variable with largest magnitude derivative with respect to the specification constant became the specification variable. Initial guesses for consecutive points along the curve were found from a cubic extrapolation of the independent variables using values of the independent variables and their derivatives at two previous points.

Koak (1997) used the same principles to develop an algorithm for calculating the phase boundary of discretized polymer systems at constant pressures. However, in Koak's work the mass fraction of polymer in the feed could be used as a specification variable.

5.2.2 Problem Definition

The terminology introduced in the previous chapter can be written for a polymer/solvent system. In this case the number of discrete components is 1 and the total number of components is 2. The solvent is denoted by A and the polydisperse polymer by B. The number average number of segments, $\bar{r}$, can be calculated from equation (4.12) in the form:

$$\frac{1}{\bar{r}} = \frac{\psi_A}{r_A} + \int \frac{\psi_B W_B(r)}{r} dr . \tag{5.1}$$

If the entire system is considered as a single phase, it can be thought of as the feed phase. The overall polymer segment fraction, ψ_B^F, and intensive polymer segmental distribution function, $W_B^F(r)$, define the feed phase composition. The solvent segment fraction in the feed phase is simply $\psi_A^F = 1 - \psi_B^F$. If the feed phase splits into two phases at a specified temperature and pressure, the two phases can be designated phase I and phase II. Variables associated with either the feed phase, phase I or phase II will be

denoted by the superscripts F, I and II respectively. The fraction of the total system segments that are in phase II is called the phase fraction, $\phi = \bar{n}^{II}/(\bar{n}^{I} + \bar{n}^{II}) = \bar{n}^{II}/\bar{n}^{F}$. As in chapter 4, the overbar indicates that n is a segmental value as opposed to a molecular value.

Consider that the feed has split into two phases. Assume that the phase fraction, ϕ, is fixed and that the pressure and feed polymer distribution are specified. The remaining variables that define the composition, polymer distribution and temperature of the system are ψ_B^F, ψ_A^I, ψ_B^I, ψ_A^{II}, ψ_B^{II}, T, $W_B^I(r)$, and $W_B^{II}(r)$. These are 6 scalar variables and 2 functions that need to be determined. That means 6 scalar equations and 2 functional equations are needed to fully define the system. It can be shown that 2 scalar equations and 1 functional equation result from the polymer and solvent segment balances, 2 scalar equations and 1 functional equation come from the equilibrium requirements and 1 scalar equation results from the requirement that the segment fractions in a phase must sum to unity. This totals 5 scalar equations and 2 functional equations for 6 scalar variables and 2 functions, leaving one degree of freedom in the system. Therefore, if the composition of one phase were fixed, the temperature and the composition of the second phase in equilibrium with the first could be found. A plot of the equilibrium temperature versus the compositions of the two phases would result in two distinct lines of constant phase fraction in the isobaric temperature-composition plane.

Given an isobaric polymer/solvent system, the objective of the following sections is to develop an algorithm capable of finding the equilibrium temperature-composition curves corresponding to a constant phase fraction. Three criteria need to be met: the total number of solvent segments must be conserved, the total number of polymer segments at each value of r must be conserved and the chemical potentials of both solvent and polymer must be the same in each of the two phases.

5.2.3 Segmental Balances

If the feed splits into two phases, the number of segments of solvent must be conserved:

$$\bar{n}_A^F = \bar{n}_A^I + \bar{n}_A^{II}. \tag{5.2}$$

Dividing equation (5.2) by $\bar{n}^F$, the total segments in the feed, yields

$$\frac{\bar{n}_A^F}{\bar{n}^F} = \frac{\bar{n}_A^I}{\bar{n}^I}\frac{\bar{n}^I}{\bar{n}^F} + \frac{\bar{n}_A^{II}}{\bar{n}^{II}}\frac{\bar{n}^{II}}{\bar{n}^F}$$

which can be simplified to

$$\psi_A^F = 1 - \psi_B^F = \psi_A^I(1-\phi) + \psi_A^{II}\phi \tag{5.3}$$

The segmental balance for the polymer can be expressed in terms of the extensive segmental distributions as

$$w_B^F(r) = w_B^I(r) + w_B^{II}(r). \tag{5.4}$$

This equality is written such that the segmental balance must be satisfied over the entire range of r. By dividing equation (5.4) by $\bar{n}^F$ and noting that

$$\frac{w_B(r)}{\bar{n}} = \frac{\bar{n}_B}{\bar{n}}\frac{w_B(r)}{\bar{n}_B} = \psi_B W_B(r),$$

equation (5.4) can be rewritten as

$$\psi_B^F W_B^F(r) = (1-\phi)\psi_B^I W_B^I(r) + \phi\psi_B^{II} W_B^{II}(r). \tag{5.5}$$

Equations (5.3) and (5.5) are the two segmental balances of the system.

5.2.4 Defining the Segment Fractions and Distributions

A segmental distribution variable, K, can be defined as the ratio of a component's segment fraction in phase *II* to its segment fraction in phase *I*. The K values for the solvent and polymer species are given by equations (5.6) and (5.7) respectively.

$$K_A = \psi_A^{II}/\psi_A^I \tag{5.6}$$

$$K_B(r) = \frac{\psi_B^{II} W_B^{II}(r)}{\psi_B^{I} W_B^{I}(r)} \tag{5.7}$$

Note that K_B is a function of the polymer segment count, r, and not a scalar value. In essence, equation (5.7) defines a K value for each value of r. These K values are analogous to the K values in traditional discrete flash calculations, but instead of mole fractions, they use segment fractions.

If ψ_A^I and ψ_B^I are fixed and sum to one, arbitrary K_A and $K_B(r)$ values define in ψ_A^{II} and ψ_B^{II} values which do not necessarily sum to one and *vice versa*. It is advantageous to write equations (5.6) and (5.7) in terms of unnormalized segment fractions, Ψ, instead of the normalized segment fractions, ψ. The constraint that the sum of the segment fractions in each phase must sum to unity then becomes an additional equation to be solved.

The segment fractions and segmental distribution functions can be expressed in terms of the K values by using the segmental balances. Recognizing that $\Psi_A^{II} = K_A \Psi_A^I$, equation (5.3) can be solved for the unnormalized segment fractions Ψ_A^I and Ψ_A^{II}:

$$\Psi_A^I = \frac{1 - \psi_B^F}{1 + \phi\left[K_A - 1\right]} \quad ; \quad \Psi_A^{II} = \frac{\left(1 - \psi_B^F\right) K_A}{1 + \phi\left[K_A - 1\right]}. \tag{5.8}$$

Similarly, since $\psi_B^{II} W_B^{II}(r) = K_B(r) \psi_B^I W_B^I(r)$, the polymer segmental balance given by equation (5.5) can be used to find expressions for $\Psi_B W_B(r)$:

$$\Psi_B^I W_B^I(r) = \frac{\psi_B^F W_B^F(r)}{1 + \phi\left[K_B(r) - 1\right]} \quad ; \quad \Psi_B^{II} W_B^{II}(r) = \frac{\psi_B^F W_B^F(r) K_B(r)}{1 + \phi\left[K_B(r) - 1\right]}. \tag{5.9}$$

Because the integrals of $W_B^I(r)$ and $W_B^{II}(r)$ over the range of r must be unity, the unnormalized polymer segment fractions in each phase can be found by integrating equations (5.9):

$$\Psi_B^I = \int_{r=0}^{\infty} \frac{\psi_B^F W_B^F(r)}{1+\phi\left[K_B(r)-1\right]} dr \;\; ; \;\; \Psi_B^{II} = \int_{r=0}^{\infty} \frac{\psi_B^F W_B^F(r) K_B(r)}{1+\phi\left[K_B(r)-1\right]} dr \tag{5.10}$$

If the K values, the feed composition and the feed polymer distribution function are known, equations (5.8) and (5.10) can be used to calculate the unnormalized solvent and polymer segment fractions. Inserting the polymer segment fractions into equation (5.9) gives the segmental distributions in each phase:

$$W_B^I(r) = \frac{\psi_B^F W_B^F(r)\ \Psi_B^I}{1+\phi\left[K_B(r)-1\right]} \;\; ; \;\; W_B^{II}(r) = \frac{\psi_B^F W_B^F(r) K_B(r)\ \Psi_B^{II}}{1+\phi\left[K_B(r)-1\right]}. \tag{5.11}$$

The unnormalized segment fractions cannot be used in thermodynamic models and must be normalized. These ψ values are found before using a thermodynamics model from equation (5.12).

$$\psi_i^I = \Psi_i^I \Big/ \left(\Psi_A^I + \Psi_B^I\right) \;\; ; \;\; \psi_i^{II} = \Psi_i^{II} \Big/ \left(\Psi_A^{II} + \Psi_B^{II}\right). \tag{5.12}$$

Definitions for the segmental distribution functions can be inserted into equation (5.1) to give expressions for the number average number of segments in phase I and phase II. Because the number average number of segments is based upon the normalized segment fractions and the expressions for $W_B^I(r)$ and $W_B^{II}(r)$ are in terms of the unnormalized fractions, each term in the expression for $\bar{r}$ must contain a normalizing factor:

$$\begin{aligned} \frac{1}{\bar{r}^I} &= \left(\frac{\Psi_A^I}{r_A} + \int_{r=0}^{\infty} \frac{\psi_B^F W_B^F(r)\, r}{1+\phi\left[K_B(r)-1\right]} dr \right) \Big/ \left(\Psi_A^I + \Psi_B^I\right) \\ \frac{1}{\bar{r}^{II}} &= \left(\frac{\Psi_A^{II}}{r_A} + \int_{r=0}^{\infty} \frac{\psi_B^F W_B^F(r) K_B(r)\, r}{1+\phi\left[K_B(r)-1\right]} dr \right) \Big/ \left(\Psi_A^{II} + \Psi_B^{II}\right) \end{aligned} \tag{5.13}$$

With ψ_A, ψ_B, $W_B(r)$ and $\bar{r}$ defined for both phases in terms of the K values, the K values need to be defined in a useful form. The chemical equilibrium requirements allow this form to be found.

5.2.5 Equality of Chemical Potentials

A necessary condition for two phase equilibrium is that the chemical potential of the solvent must be the same in both phases and the chemical potential of the polymer must be the same in both phases for every value of r. This is equivalent to stating that the chemical potential per segment is the same in both phases:

$$\begin{aligned} \bar{\mu}_A^I &= \bar{\mu}_A^{II} \\ \bar{\mu}_B^I(r) &= \bar{\mu}_B^{II}(r) \end{aligned} \tag{5.14}$$

Inserting the definitions of the segmental chemical potentials as given by equations (4.45) and (4.46) into equation (5.14), the two K values, K_A and $K_B(r)$, can be written as:

$$\ln K_A = \ln \psi_A^{II} - \ln \psi_A^I = r_A\left[\frac{1}{\bar{r}^{II}} - \frac{1}{\bar{r}^I} - \ln \gamma_A^{II} + \ln \gamma_A^I\right] \tag{5.15}$$

$$\ln K_B(r) = \ln \psi_B^{II} W_B^{II}(r) - \ln \psi_B^I W_B^I(r) = r\left[\frac{1}{\bar{r}^{II}} - \frac{1}{\bar{r}^I} - \ln \gamma_B^{II}(r) + \ln \gamma_B^I(r)\right] \tag{5.16}$$

Combining equation (5.16) with the Sanchez-Lacombe segment molar activity coefficient, equation (4.48), it can be seen that $K_B(r)$ has the form

$$\ln K_B(r) = A_K + rB_K = A_f + r\left(B_f^I - B_f^{II}\right) \tag{5.17}$$

where

$$A_f = \ln\left(\frac{\bar{r}^I \tilde{b}^I}{v^I}\right) - \ln\left(\frac{\bar{r}^{II} \tilde{b}^{II}}{v^{II}}\right), \tag{5.18}$$

and

$$\begin{aligned} B_f^i = \frac{2\tilde{b}_B^i}{\tilde{b}^i \bar{r}^i} - \frac{2\tilde{a}_B^i \bar{r}^i}{v^i RT} - \frac{2}{\bar{r}^i} - \frac{2}{\bar{r}^i \tilde{b}^i}\left[\frac{\tilde{b}_B^i}{\tilde{b}^i} - 1\right]\left(v^i - \bar{r}^i \tilde{b}^i\right)\ln\left(\frac{v^i - \bar{r}^i \tilde{b}^i}{v^i}\right) \\ - \left(\frac{2\tilde{b}_B^i}{\tilde{b}^i} - 1\right)\left[\ln\left(\frac{v^i - \bar{r}^i \tilde{b}^i}{v^i}\right) + 1\right] \end{aligned} \tag{5.19}$$

Noting that the definitions of $\ln \gamma_A$, A_f and B_f are independent of the segment count, r, and the segmental distribution function, the rightmost equality in equation (5.17) allows

$K_B(r)$ to be defined by two scalar equations for two new independent variables, A_K and B_K.

Equations (5.15) and (5.17) now define three scalar equations in five scalar unknowns, $\ln K_A$, A_K, B_K, $\ln T$ and $\ln \psi_B^F$:

$$g_1\left(\ln K_A, A_K, B_K, \ln T, \ln \psi_B^F\right) = A_K - A_f = 0 \tag{5.20}$$

$$g_2\left(\ln K_A, A_K, B_K, \ln T, \ln \psi_B^F\right) = B_K + B_f^{II} - B_f^{I} = 0 \tag{5.21}$$

$$g_3\left(\ln K_A, A_K, B_K, \ln T, \ln \psi_B^F\right) = \ln K_A - r_A\left\{\frac{1}{\bar{r}^{II}} - \frac{1}{\bar{r}^{I}} - \ln\left(\gamma_A^{II}/\gamma_A^{I}\right)\right\} = 0 \tag{5.22}$$

The logarithms of temperature and feed polymer segment fraction are used as variables to help scale the variables.

If equations (5.20) and (5.21) are satisfied, the chemical potentials of all polymer molecules are equal in both phases. When equation (5.22) equals 0, the chemical potential of the solvent is equal in both phases.

5.2.6 Summation Requirement

The summation of the unnormalized polymer and solvent segmental fractions must be unity in both phase *I* and phase *II*. Because the *K* values and material balances relate the compositions of one phase to the composition of the other, the two summation restraints (one for each phase) are linearly dependent. Therefore, a single summation requirement is formulated in the same fashion as was proposed by Rachford and Rice (1952). This summation forms a fourth scalar equation:

$$g_4\left(\ln K_A, A_K, B_K, \ln T, \ln \psi_B^F\right) = \left(\Psi_A^{I} - \Psi_A^{II}\right) + \left(\Psi_B^{I} - \Psi_B^{II}\right) = 0.$$

Inserting equations (5.8) and (5.10) into this equation gives

$$g_4 = \frac{\left(1-\psi_B^F\right)\left(1-K_A\right)}{1+\phi\left[K_A - 1\right]} + \psi_B^F \int_{r=0}^{\infty} \left\{\frac{W_B^F(r)\left[1-K_B(r)\right]}{1+\phi\left[K_B(r)-1\right]}\right\} dr = 0. \tag{5.23}$$

When equation (5.23) is satisfied, the sum of the segment fractions in both phases will equal 1 and the segmental balance constraints used to define ψ_A and ψ_B in terms of the K values will be met.

5.2.7 The Specification Variable

Up to this point, equations g_1, g_2, g_3 and g_4 define four scalar equations in 5 scalar unknowns. The final equation needed to define the system is formulated to fix one of the independent variables to a specified value, S. The variable chosen to be fixed is called the specification variable and the value, S, is called the specification parameter. By repeated solution of the equilibrium equations at incremental values of the specification parameter, the constant phase fraction curves can be drawn. This is similar to the techniques used by Michelsen (1980) and by Koak (1997).

If the independent variables are placed in a vector $\alpha = \{\ln K_A,\ A_K,\ B_K,\ \ln T,\ \ln \psi_B^F\}^T$, the i^{th} independent variable is α_i. For example, B_K is α_3. Since the specification variable can be any of the independent variables, the generic form of the remaining scalar equation can be written as

$$g_5 = \alpha_i - S = 0. \tag{5.24}$$

The choice of the initial specification variable is arbitrary. The feed polymer segment fraction was used as the specification variable in most of the calculations performed because it was a value with easily described physical significance. However, as will be noted, the temperature and solvent K value were also at times used as the specification variable. The method used for choosing an incrementing S to trace curves is described in a later section.

5.2.8 Updating Procedure

The five scalar, non-linear equations which define the fixed phase fraction equilibrium problem for the Sanchez-Lacombe equation of state are given by:

$$g_1(\alpha) = A_K - A_f = 0 \tag{5.25}$$

$$g_2(\alpha) = B_K + B_f^{II} - B_f^{I} = 0 \tag{5.26}$$

$$g_3(\alpha) = \ln K_A - r_A\left\{\frac{1}{\tilde{r}^{II}} - \frac{1}{\tilde{r}^{I}} - \ln\left(\gamma_A^{II}/\gamma_A^{I}\right)\right\} = 0 \tag{5.27}$$

$$g_4(\alpha) = \frac{\left(1-\psi_B^F\right)\left(1-K_A\right)}{1+\phi\left[K_A-1\right]} + \psi_B^F \int_{r=0}^{\infty}\left\{\frac{W_B^F(r)\left[1-K_B(r)\right]}{1+\phi\left[K_B(r)-1\right]}\right\}dr = 0 \tag{5.28}$$

$$g_5(\alpha) = \alpha_i - S = 0 \tag{5.29}$$

The vector $\alpha = \{\ln K_A, A_K, B_K, \ln T, \ln\psi_B^F\}^T$ holds the five independent scalar unknowns. The five equations to be zeroed is represented by the vector $\mathbf{g}(\alpha) = \{g_1, g_2, g_3, g_4, g_5\}^T$.

To solve this system of equations, a Newton-Raphson procedure can be used. The Newton-Raphson procedure is a second order technique for the solution of non-linear equations. It works by finding successive approximations to the solution using a linear approximation of the problem. A single Newton-Raphson iteration is written as

$$\alpha^{(n+1)} = \alpha^{(n)} + \Delta\alpha^{(n)} \tag{5.30}$$

$$\mathbf{J}^{(n)}\Delta\alpha^{(n)} = -\mathbf{g}\left(\alpha^{(n)}\right). \tag{5.31}$$

$\Delta\alpha$ is the change in the independent variables during a single Newton step. The superscripts in parenthesis represent the iteration count. **J** represents the Jacobian, a matrix containing the derivatives of **g** with respect to the independent variables. The structure of the Jacobian is shown below.

$$\mathbf{J} = \left(\frac{\partial \mathbf{g}}{\partial \alpha}\right) = \begin{bmatrix} \left(\frac{\partial g_1}{\partial \alpha_1}\right) & \left(\frac{\partial g_1}{\partial \alpha_2}\right) & \cdots & \left(\frac{\partial g_1}{\partial \alpha_5}\right) \\ \left(\frac{\partial g_2}{\partial \alpha_1}\right) & \left(\frac{\partial g_2}{\partial \alpha_2}\right) & \cdots & \left(\frac{\partial g_2}{\partial \alpha_5}\right) \\ \vdots & \vdots & \ddots & \vdots \\ \left(\frac{\partial g_5}{\partial \alpha_1}\right) & \left(\frac{\partial g_5}{\partial \alpha_2}\right) & \cdots & \left(\frac{\partial g_5}{\partial \alpha_5}\right) \end{bmatrix} \tag{5.32}$$

The derivatives ($\partial g_i/\partial \alpha_j$) can be found in Appendix B.

On each iteration, the independent variables, $\alpha^{(n)}$, are used to calculate $\mathbf{g}^{(n)}$ and the Jacobian, $\mathbf{J}^{(n)}$. The change in the independent variables, $\Delta\alpha^{(n)}$, can be found from equation (5.31) using any routine to solve a set of linear equations. LU decomposition with back substitution was used in this work and is described in detail by Press *et al.* (1992).

Convergence is achieved when the error determined by $\mathbf{g}$ is smaller than an assigned tolerance. The error is defined to be the sum of the squares of g_i divided by the number of equations, 5:

$$Err = \mathbf{g}^T\mathbf{g}/5 \tag{5.33}$$

Newton-Raphson iterations continued until *Err* was less than 10^{-15}.

The Newton-Raphson technique gives second order convergence in regions near the actual solution. If initial guesses are not close to the solution, convergence may be slow or not happen at all. Sometimes the region of convergence can be improved by damping each Newton-Raphson step. This is accomplished by multiplying $\Delta\alpha_i$ with a scalar quantity, $\lambda_i < 1$, before updating α_i:

$$\alpha_i^{(n+1)} = \alpha_i^{(n)} + \lambda_i \Delta\alpha_i \,. \tag{5.34}$$

However, it should be noted that this scaling has the adverse affect of slowing convergence.

When seeking a solution using a poor initial guess, scaling the Newton-Raphson step with a factor of $\lambda_i = 0.1$ for changes in $\ln K_A$, A_K, B_K and $\ln \psi_B^F$ and with a factor of

$\lambda_i = 0.001$ for the changes in ln T, worked well. These damping factors were used for the first 20 iterations and at any time when the error was greater than 10^{-6}. The higher damping factor for temperature changes was needed due to the large changes introduced to temperature if α was far from the solution. If the initial guess was good (initiated with a prior solution), no scaling was required and convergence occurred in three to five iterations.

5.2.9 Specification Variable Progression

Solving equations (5.25) through (5.29) gives the compositions, segmental distributions and temperature corresponding to the specification parameter, S, and the constant phase fraction, ϕ. To generate the entire fixed phase fraction curves, the value of the parameter S can be changed after each individual equilibrium solution is found and repeated solutions will generate a locus of equilibrium points. The initial guess for the new solution can be found using the previous solution or by extrapolation of the independent variables. With enough points, the entire fixed phase fraction curves can be drawn.

If extrapolation of α is desired between points, one possible technique is cubic extrapolation as proposed by Michelsen (1980). It uses the current and previous values of α and the derivatives of α with respect to the specification parameter to determine the appropriate polynomial coefficients.

The derivatives of α can be found by taking the derivative of equation (5.31) with respect to S:

$$\mathbf{J}\left(\frac{d\alpha}{dS}\right) = -\left(\frac{d\mathbf{g}}{dS}\right). \tag{5.35}$$

Since $(d\mathbf{g}/dS) = \{0, 0, 0, 0, -1\}^T$, the vector $(d\alpha/dS)$ can quickly be determined using the same linear equation solver as used in the Newton-Raphson procedure. It is convenient, therefore to use the LU factorization method in the Newton-Raphson procedure since the

factorization of **J** at the converged solution can be used in equation (5.35) to determine $(d\alpha/dS)$.

A cubic extrapolation can be done for each independent variable. Consider an extrapolating polynomial with the form

$$\alpha_i(S) = c_{i0} + c_{i1}S + c_{i2}S^2 + c_{i3}S^3$$

where there is a distinct set of four coefficient, c_{ij}, for each independent variable. If equilibrium points have been found at two values of S, and values for both α and $(d\alpha/dS)$ are known at these points, enough information is known to find all of the extrapolations coefficients, c_{ij}. Consequently, if a new value of S is chosen, S_{new}, an initial guess of $\alpha = \alpha(S_{new})$ can be found from the polynomial.

It was found that cubic extrapolation did not yield good initial estimates for α in the polymer/solvent cloud point curve calculations. A linear extrapolation was tried but also resulted in poor initial guesses unless the step change in S was limited to very small values. The reasons for this deficiency were not examined. In the end, it was found that with small enough step changes in S, calculations along the cloud point curve were adequately initiated by the converged solution to the previous cloud point while neither extrapolation technique offered any particular benefit to the calculation procedure.

The size of the increments in S used to trace the fixed phase fraction curves can be changed after each equilibrium solution is found. By examining the number of iterations required to converge to the last solution, the step size can be increased if the previous number of iterations was too small, and it can be decreased if too many iteration were taken. It stands to reason that larger changes in S will result in greater error in the initial guess. If the initial guess is worse, more iterations will be required to reach the final solution. Therefore, by decreasing the step change in S when iteration counts are high and increasing the step change when iteration counts are low, a crude adaptive method can be implemented to optimize the change in S along the curves. A reasonable approach for the polymer/solvent system was to decrease the step size if more than 5 Newton-

Raphson iterations were needed and to increase the step size if less than 3 iterations were needed. The maximum step size allowed was 0.01, regardless of the specification variable chosen.

It is also possible to automatically switch between specification variables along the length of the fixed phase fraction curve (Michelsen, 1980). The choice of independent variable represented by α_i in equation (5.29) can change after finding each equilibrium point by examining the derivatives of the independent variables with respect to S. By selecting α_i to represent the variable with the largest magnitude derivative, $\partial\alpha_i/\partial S$, the change of the other independent variables between each equilibrium point would be minimized. This automated procedure was not used in this work, but it was found that the choice of specification variable could greatly affect the ease in which cloud point curves could be followed. This result will be discussed in more detail in the examples to follow.

5.2.10 Convergence of Integrals

Equations (5.10) are used to calculate segment fractions before normalization:

$$\Psi_B^I = \int_{r=0}^{\infty} \frac{\psi_B^F W_B^F(r)}{1+\phi\left[K_B(r)-1\right]}dr \quad ; \quad \Psi_B^{II} = \int_{r=0}^{\infty} \frac{\psi_B^F W_B^F(r) K_B(r)}{1+\phi\left[K_B(r)-1\right]}dr \tag{5.10}$$

The form of these two integrals is typical of all integrals in continuous thermodynamics. If the definition of K_B as given by equation (5.17) is inserted into these integrals, they can be rewritten as

$$\Psi_B^I = \int_{r=0}^{\infty} \frac{\psi_B^F W_B^F(r)}{1+\phi\left[C\exp\{rB_K\}-1\right]}dr \quad ; \quad \Psi_B^{II} = \int_{r=0}^{\infty} \frac{\psi_B^F W_B^F(r) C\exp\{rB_K\}}{1+\phi\left[C\exp\{rB_K\}-1\right]}dr \tag{5.36}$$

where $C=\exp\{A_K\}$. The true cloud and shadow point curves are represented by these equations when the phase fraction is either 0 or 1. In the case of $\phi=0$, equations (5.36) become

$$\Psi_B^I = \int_{r=0}^{\infty} \psi_B^F W_B^F(r)dr = \psi_B^F \quad ; \quad \Psi_B^{II} = \int_{r=0}^{\infty} \psi_B^F W_B^F(r) C \exp\{rB_K\} dr \tag{5.37}$$

and when $\phi = 1$, they become

$$\Psi_B^I = \int_{r=0}^{\infty} \psi_B^F W_B^F(r) \exp\{-rB_K\} dr / C \quad ; \quad \Psi_B^{II} = \int_{r=0}^{\infty} \psi_B^F W_B^F(r)dr = \psi_B^F . \tag{5.38}$$

The sign of B_K cannot be fixed as positive or negative. Therefore, equations (5.37) and (5.38) show that an integral defining Ψ_B along a phase boundary could have the form:

$$\Psi_B = C' \int_{r=0}^{\infty} W_B^F(r) \exp\{\sigma r\} dr \quad ; \quad \sigma > 0.$$

As covered in the previous chapter in the discussion about distribution functions, when $W_B^F(r)$ is a divergent distribution like the log-normal distribution, these integrals are unbounded as r approaches infinity. If the Shultz-Flory distribution is used, the integrals are convergent and can be found analytically (Rätzsch and Kehlen, 1989).

The integrals are also convergent when the log-normal distribution is used and the phase fraction is between 0 and 1 (Rätzsch and Kehlen, 1989). Therefore, to avoid possibly divergent integrals, the cloud and shadow point curves using a log-normal distribution can be approximated by performing the calculations at a fixed phase fraction close to the limiting values, say $\phi = 0.0001$ or $\phi = 0.9999$.

A segmental phase fraction of 0.9999 was used to approximate the cloud point curves found in this work. During numerical integration, the value $K_B(r)$ was calculated only if $\ln K_B(r) = A_K + rB_K$ was between -500 and 500. Otherwise the numerical limit of the integrand as $K_B \to 0$ was used when $\ln K_B(r) < -500$ and the limit as $K_B \to \infty$ was used when $\ln K_B(r) > 500$. No overflow or underflow errors were encountered during integration when this procedure was followed.

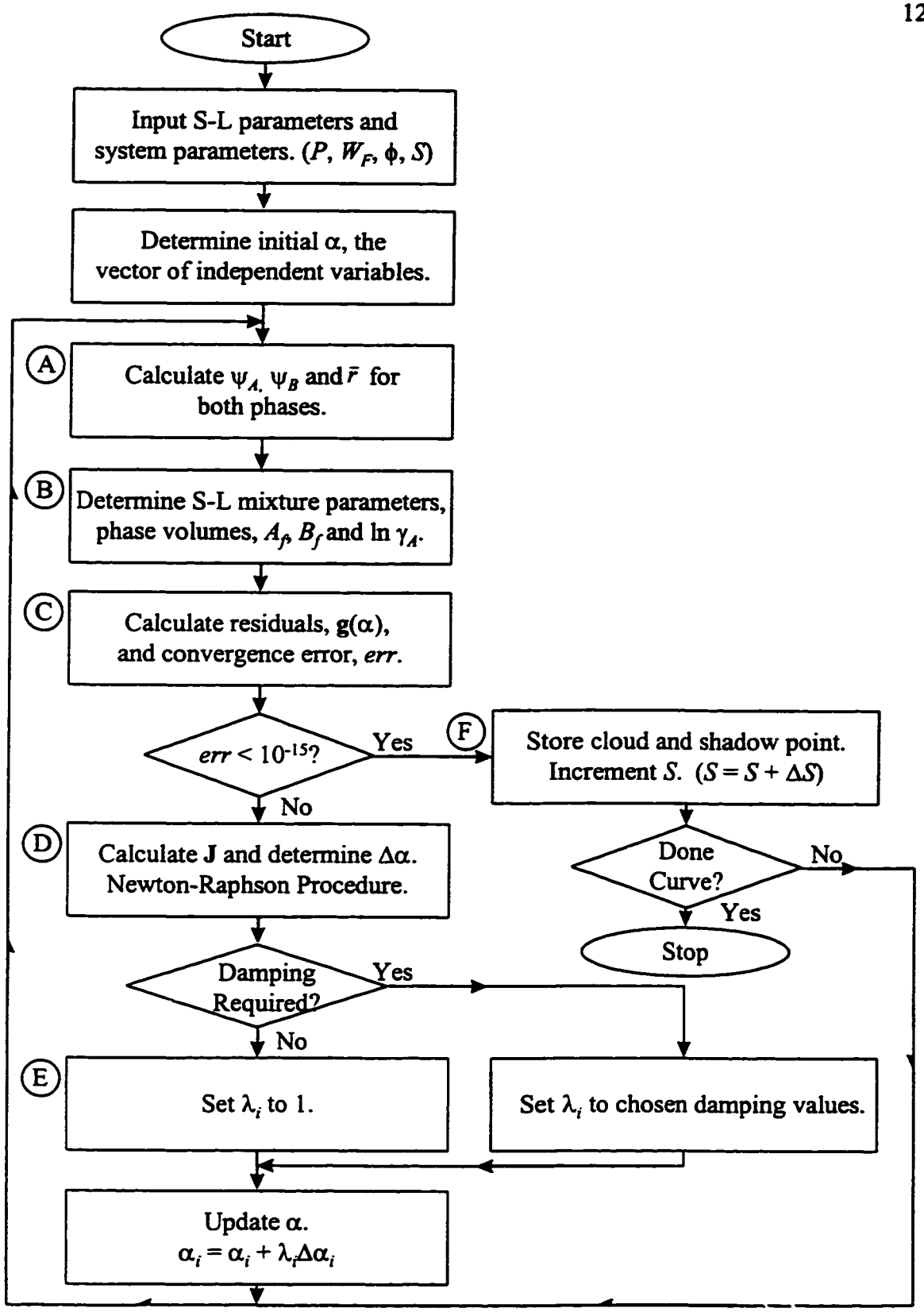

Figure 5-2 - Flowsheet of Cloud and Shadow Point Calculation Algorithm.

5.2.11 Program Overview

Figure 5-2 displays a flowsheet for the cloud and shadow point curve algorithm. It consists of two loops: an inner loop for determining a single equilibrium point and an outer loop to control the tracing of the curves. The inner loop is the Newton-Raphson procedure discussed in section 5.2.8 and the outer loop is the specification variable progression covered in the section 5.2.9.

The problem is initially defined by inputting the Sanchez-Lacombe parameters for the pure solvent and polymer. The system pressure, distribution function parameters, fixed phase fraction and starting specification parameter are also read from a file. The initial vector of independent variables, α, is usually determined from *a priori* information obtained from experimental results or a two phase flash algorithm. After the problem parameters have been defined and the initial guess determined, the outer and inner loops are entered.

Within the inner loop, the first task (box A in Figure 5-2) is to use the $\ln \psi_B^F$, $\ln K_A$, A_K and B_K values held in α to determine the segment fractions and number average number of segments in each phase. This is done using equations (5.8), (5.10), (5.12) and (5.13). These values are then used to determine the Sanchez-Lacombe equation of state parameters for each phase (box B). The equation of state can then be solved for the molar volumes of phase *I* and phase *II*, and subsequently, the values of A_f, B_f and $\ln \gamma_A$ in each phase can be determined from equations (5.18), (5.19) and (4.50) respectively. It should be noted that the volume root found depends on the type of phase being considered. That is, if a vapour phase is considered, the vapour root of the Sanchez-Lacombe equation of state is sought whereas if a liquid phase is of interest (as is normally the case for polymer systems), a liquid root is sought. The technique for finding the volume roots is discussed in section 4.7.

The residuals of the objective functions are calculated using equations (5.25) through (5.29) and the error as defined by equation (5.33) is found (box C). If the error is greater than the tolerance, 10^{-15}, the inner loop continues in box D where the Jacobian is

determined and the change in the independent variables is found from equation (5.31). The error and iteration count is examined to determine if the Newton-Raphson step needs to be scaled. The damping parameters λ_i are set in Box E using the technique described in the Updating Procedure section. The final step in the inner loop before returning to box A is to update the independent variables.

If the error calculated in box C is less than the tolerance, the inner loop has converged to an equilibrium point, and the outer loop increments the specification parameter, S (box F). This incrementing procedure is described in section 5.2.9. If the specification variable moves outside of a user defined set of bounds, the outer loop is stopped and the program terminated. Otherwise, the inner loop is reentered and an additional point along the fixed phase fraction curve is found.

Cloud and shadow point curves can be found in the above fashion by setting ϕ to 0.9999 or 0.0001. The integrations required can be done using one of the numerical techniques discussed in the previous chapter. Second order convergence was achieved when the independent variables are close to the final solution. Results from this algorithm in predicting the cloud and shadow point curves of a polyethylene/n-hexane system and a polyethylene/ethylene system are given in the following section.

Component	T^* (K)	P^* (bar)	ρ^* (kg/m^3)
n-hexane*	476	2980	775
Ethylene†	327	2026.5	515
Polyethylene*	649	4250	904

Table 5-1 - Sanchez-Lacombe Pure Component Parameters.

* Data from Sanchez and Lacombe (1978).

† Data from Kiszka *et al.* (1988).

5.3 *Examples*

5.3.1 Polyethylene/n-Hexane at 6 Bar

Koak (1997) modeled a mixture of n-hexane and polyethylene ($M_n = 8000$, $M_w = 177000$) using the Sanchez-Lacombe equation of state. He divided the disperse polymer into 10 initial pseudocomponents using the quadrature technique of Cotterman and Prausnitz (1985) to approximate the molecular weight distribution. He discarded the components with molecular weights lighter than the solvent.

In this work, a log-normal segmental distribution was used to model the polyethylene. The pure component parameters are shown in Table 5-1 and an interaction parameter of $k_{ij} = -0.1297$ was used (Koak, 1997). The number average molecular weight and mass average molecular weight were used to determine the log-normal parameters, $\beta = 2.4886$ and $r_0 = 3278.67$ (see Table 4-1). As discussed in the previous chapter, these log-normal distribution parameters are related algebraically to Koak's (1997) parameters, β and M_0, and result in exactly the same molecular weight distribution.

This system exhibited LCST type behaviour. The cloud and shadow curves found in the region of the lower precipitation threshold temperature (lowest temperature point on the cloud point curve) were calculated using the fifth order Runge-Kutta integration routine. These curves are shown in Figure 5-3. Because the log-normal distribution is divergent (Šolc, 1975), the cloud and shadow point curves were approximated by finding the boundary associated with a phase segment fraction of $\phi = 0.9999$. Once an initial point on the curve was found, the change in the specification parameter was adjusted such that each successive point on the curves was found in between 3 to 5 Newton-Raphson steps. The actual step size would depend upon the complexity of the curve being traced and the specification variable being used.

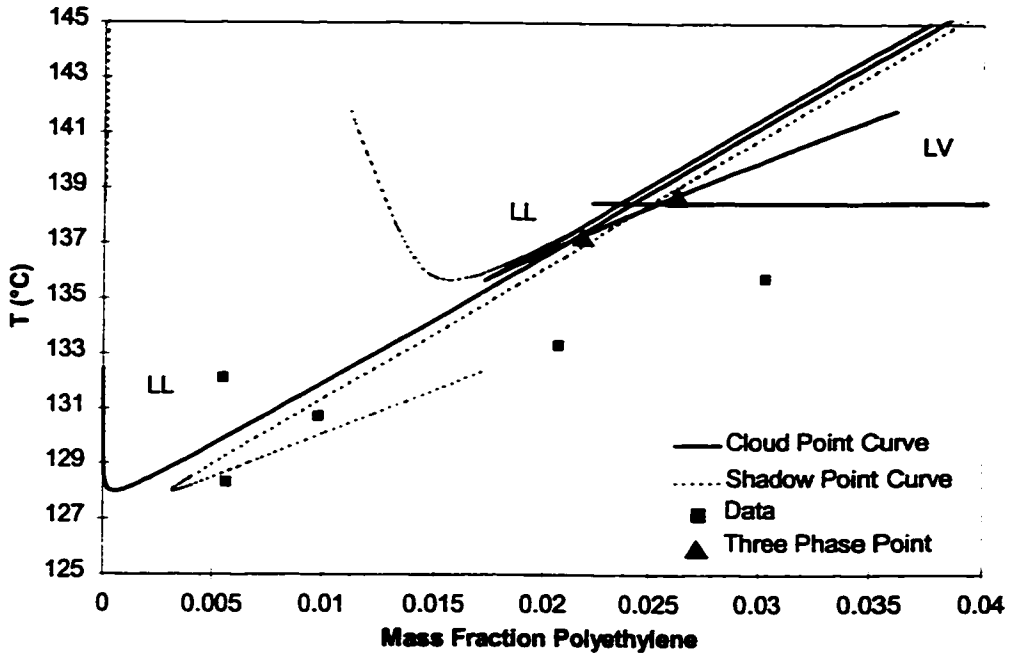

Figure 5-3 - Cloud and Shadow Curves of Polyethylene in n-Hexane. k_{ij} = -0.1297, P = 6 bar. Data from Kennis (1990).

Koak (1997) found the interaction parameter, -0.1297, by matching the precipitation threshold temperature of the discretized system with the experimental precipitation threshold found by Kennis (1990). As can be seen in Figure 5-3, the continuous system also matches the precipitation threshold temperature well with a temperature of 128 °C. A three phase liquid-liquid-liquid point is indicated on the figure at 137 °C by a crossover in the cloud point curve. This point separates two stable liquid-liquid equilibrium regions. A three phase liquid-liquid-vapour point can be seen at a temperature of 138.8 °C. At cloud point temperatures higher than this, the stable polymer rich liquid is in equilibrium with a solvent rich vapour shadow phase.

Metastable cloud points are indicated by extensions of the cloud point lines through the three phase points. The crossover at 137 °C extends to a metastable lower cusp at 135.8 °C. An upper cusp was difficult to locate because the associated cloud and shadow point curves slowly merged together. These lines were followed up to a temperature of 172 °C before calculations were ceased. Metastable liquid-liquid and

liquid-vapour lines are shown as the extensions of the cloud point curves to the left of the three phase point at 138.8 °C.

Koak (1997) found that the metastable upper cusp extending from the 137 °C three phase point is in the region of an unstable critical point. A critical point would be indicated in the figure by an intersection of the cloud and shadow point curves. As can be seen from Figure 5-3, the stable cloud points at temperatures below the 137 °C three phase point are leaner in polymer than their corresponding shadow points (the cloud points lie to the left of the shadow points). Also, the stable cloud points at temperatures above 137 °C are richer in polymer than their shadow points. This indicates that the cloud and shadow point curves must intersect in the metastable region above 137 °C supporting Koak's statement that an unstable critical point exists in the upper cusp. Figure 5-1 (a) shows how this unstable intersection might appear. Additionally, the cloud and shadow phases would have the same composition and molar volume at this unstable critical point. Identical phases would result in a singular Jacobian, accounting for the numerical difficulties encountered in finding the upper, metastable cusp.

It should be noted that Šolc (1975) observed similar phenomena using the Flory-Huggins model to represent a polymer solution. In their study of log-normal distributions of polymers exhibiting UCST type behaviour, depressions in the cloud point curve were observed near a liquid-liquid-liquid three phase point. As Šolc increased the maximum molecular weight which was included in his model, the metastable cloud point curve extending down from the three phase point merged with the shadow point curve. As well, the cusp formed by the metastable cloud point curve moved to lower and lower temperatures. This is analogous to the upper cusp of Figure 5-2 where the cloud and shadow point curves merge. The primary difference in Šolc's system is that it exhibited UCST type behaviour and the cusp which was difficult to find was not associated with an unstable critical point. From his analysis, Šolc concluded that the observed extension of the metastable cusp was due to the significant quantities of high molecular weight molecules inherent with a log-normal distribution.

Further calculations at higher temperatures showed that the Sanchez-Lacombe model results in a hypothetical liquid-vapour critical point at a temperature of 963°C. This complete phase envelope, with its shadow point curve, is given in Figure 5-4. Although it is evident that the polymer would degrade long before the high temperatures shown could be reached, the figure is given to indicate the ability of the algorithm and the model to predict high temperature liquid-vapour behaviour.

The segmental distribution of the polymer in both the cloud and shadow phases were examined at three separate temperatures along the cloud point curve. The segmental distributions corresponding to a liquid-vapour equilibrium at 145.8 °C, a liquid-liquid equilibrium at 138.3 °C and the left hand branch of the cloud point curve at 131.8 °C were plotted on a solvent free basis in Figure 5-5. The segmental distribution of the liquid cloud point in each case is identical and indicated by the solid line. The shadow phase segmental distributions are drawn with dashed lines.

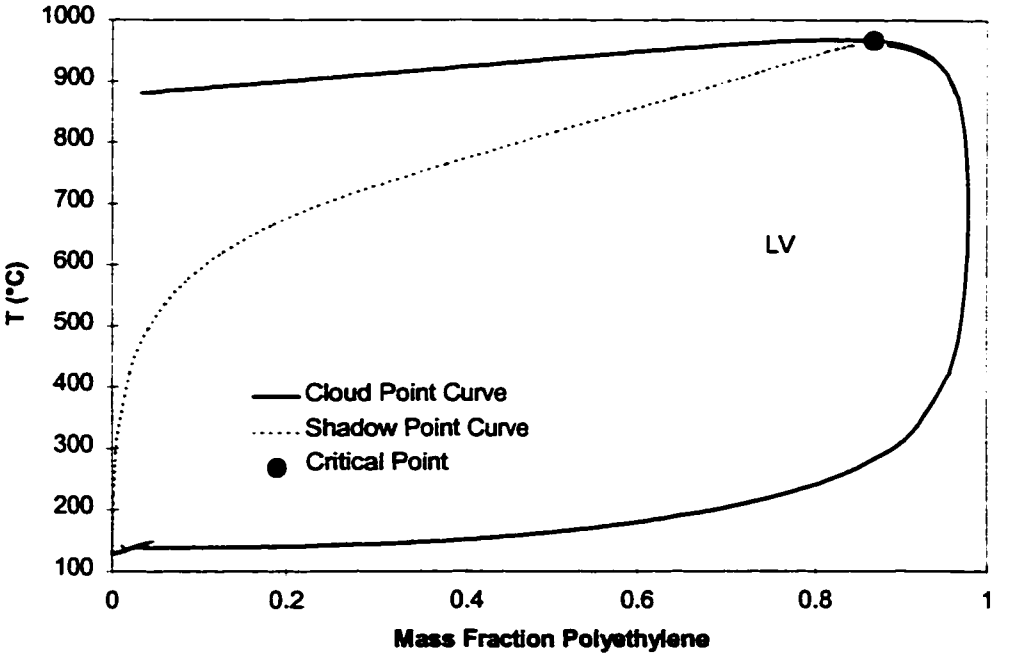

Figure 5-4 - Liquid-Vapour Cloud and Shadow Point Curves of Polyethylene in n-Hexane. $k_{ij} = -0.1297$, P = 6 bar.

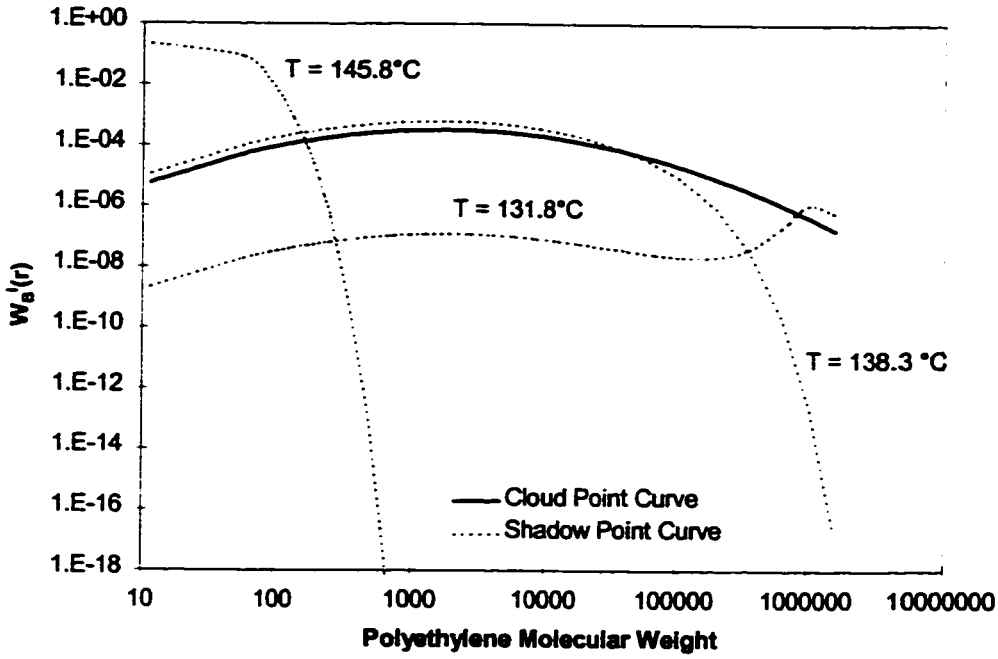

Figure 5-5 - Molecular Weight Distributions of Polyethylene in n-Hexane.

The polymer component in the incipient "vapour" phase at 145.8 °C is primarily the light polymer molecules, as is to be expected. The incipient liquid phase at 138.3 °C has a polymer distribution which is similar to the cloud point distribution but is especially lean in the higher molecular weight molecules. The segmental distribution of the incipient liquid phase at 131.8 °C indicates that it is enriched in the heavy polymer molecules. The polymer mass fraction, polymer segment fraction, number average number of segments and *K* values for these three points are shown in Table 5-2 and Table 5-3.

T(°C)	M_B^I	M_B^{II}	ψ_B^I	ψ_B^{II}	$\bar{r}_B^I$	$\bar{r}_B^{II}$
131.8	1.54×10^{-2}	5.62×10^{-6}	1.38×10^{-2}	5.18×10^{-6}	8.473	8.356
138.3	1.29×10^{-2}	2.47×10^{-2}	1.16×10^{-2}	2.22×10^{-2}	8.452	8.543
145.8	1.52×10^{-4}	0.323	1.36×10^{-4}	0.300	8.352	11.876

Table 5-2 - Cloud and Shadow Point Phase Properties.

Phase *I* is incipient phase. Phase *II* is the feed phase.
M_B is the mass fraction polymer.

T (°C)	$\ln K_A$	$\ln K_B(r) = A_K + rB_K$	
		A_K	B_K
131.8	1.39×10^{-2}	1.18×10^{-2}	-1.14×10^{-4}
138.3	-1.08×10^{-2}	-9.30×10^{-3}	1.67×10^{-4}
145.8	-3.57×10^{-1}	-3.59	0.788

Table 5-3 - Cloud and Shadow Point *K* Values.

It is clear from Table 5-2 and Table 5-3 that the shadow point (phase *I*) is richer in polymer than its cloud point (phase *II*) at 131.8 °C. It is leaner in polymer than its cloud points at the other two temperatures. This switch from a polymer rich shadow phase to a polymer lean shadow phase occurs at the unstable critical point. As the critical point is approached from the liquid-liquid region below 137 °C, $\ln K_A$ and A_K change from positive values to zero at the critical point and then become negative. The opposite holds true for B_K.

An interesting observation can be made by examining the cloud and shadow points at 131.8 °C. If the segmental distribution for phase *II* is plotted and compared against the feed segmental distribution which was plotted in Figure 5-5, the two show quite different behaviours at high molecular weights. Figure 5-6 illustrates that at high molecular weights phase *II* at 131.8 °C contains less high molecular weight polymer than the feed. Additionally, the polymer segment fraction in phase *II* is 5.18×10^{-6} whereas the segment fraction of the feed used was 5.04×10^{-6}, a deviation of 2.8%. If phase *II* were the true cloud point, its segmental distribution and polymer segment fraction would be the same as the feed distribution. This shortcoming is the result of the small polymer segment fraction in the feed and the fixed segmental phase fraction being 0.9999 instead of 1. The small polymer segment fraction in the feed reduces the significance of the polymer distribution in the calculations. As a result the error introduced by using a segmental phase fraction of 0.9999 instead of 1 is magnified.

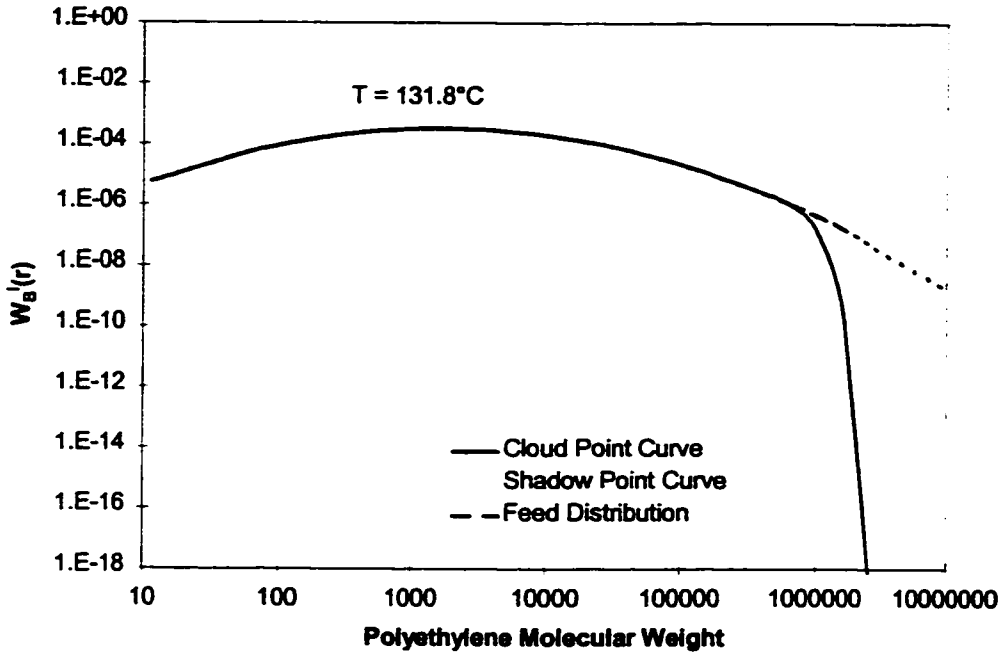

Figure 5-6 - Failure of Cloud Point Calculation with Log-Normal Distribution.

A statement should be made about the "light ends" in the polymer distributions. Each distribution was assumed to represent molecular weights extending from zero to infinity. In a real system, polymer molecules do not have molecular weights less than that of their repeating monomer unit, and the unrealistic range of molecular weights was chosen solely for mathematical convenience. As seen in Figure 5-5, these "light ends" partition into a vapour phase at higher temperatures leading to a potentially false impression that the polymer is more volatile than it is. These light ends would have more impact on vapour-liquid equilibria than on liquid-liquid equilibria. To avoid this misrepresentation of the polymer distribution, the distribution could be truncated at molecular weights below the weight of a single monomer by simply starting the integration at an r value corresponding to the molecular weight of the monomer and renormalizing $W(r)$.

The choice of specification variable dictated the ease by which the cloud and shadow point curves were found. The feed polymer segment fraction was used as the specification variable for all the cloud point curve calculations except in the region of the

near vertical cloud point curve between 300 °C and 900 °C (right hand side of Figure 5-4). In this region, the temperature was used as the specification variable because changing the temperature resulted in a comparatively small change in the other independent variables. Changing the feed polymer segment fraction would have resulted in significant changes in temperature and may have even forced the segment fraction outside of the phase envelope.

The different branches of the cloud point curve were found by tracing each branch separately and then plotting all the branches on a single figure. The initial guess for the branch of Figure 5-3 corresponding to the lower precipitation threshold was found by using the results published by Koak (1997). Initial guesses for the other branches were found by trial and error.

It is possible that one of either $\ln K_A$, A_K or B_K would be more effective as the specification variable in the metastable regions. As is visible in Figure 5-3, a single polymer segment fraction can represent four distinct cloud point lines. Each of these lines, however, has unique K values associated with it. This suggests that generating the curves in these complex regions using a K value as the specification variable might smoothly progress from one cloud point branch to another. This aspect of the calculations was not explored in this dissertation, but is an area to be examined in future work.

A Shultz-Flory distribution was also used to model the polyethylene/n-hexane system. The parameters, $\beta = 0.04734$ and $r_0 = 697.04$, were chosen such that the number average molar mass and mass average molar mass would equal 8000 and 177000 respectively (see Table 4-1). The cloud and shadow point curves in the region of the lower precipitation threshold temperature were found using a phase segment fraction of 0.9999. These liquid-liquid cloud and shadow curves are shown in Figure 5-7. Again, the fifth order Runge-Kutta integration technique was used. The obvious difference between the cloud point curves using the Shultz-Flory distribution and the log-normal distribution is that the former did not result in a second liquid-liquid instability. This is

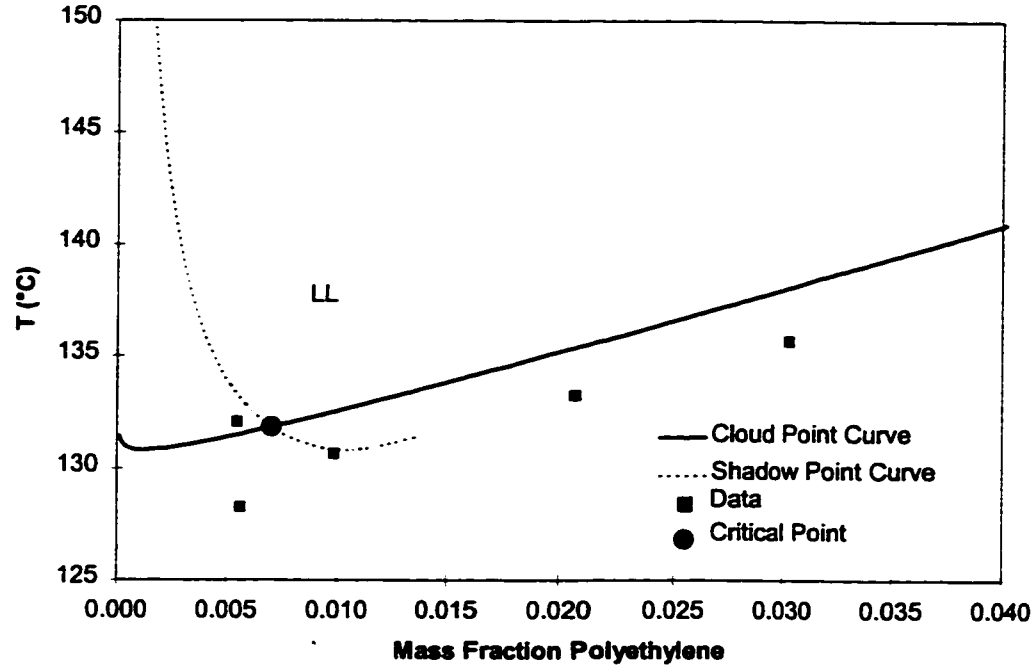

Figure 5-7 - Cloud and Shadow Point Curves for Polyethylene/n-Hexane Using a Shultz-Flory Distribution. $k_{ij} = -0.1297$, P = 6 bar. Data from Kennis (1990).

seen in the lack of a low temperature, liquid-liquid-liquid three phase point. Instead the cloud and shadow curves intersect in a stable critical point at a temperature of 131.7 °C. The lower precipitation threshold temperature is 130.8 °C, 2.8 ° higher than the log-normal distribution with the same M_n and M_w. Liquid-vapour equilibrium curves were not calculated for this example.

An interesting conclusion from this observation is that although the polyethylene sample modeled in each case showed the same M_n and M_w, the phase behaviour can be significantly affected by changes in the shape of the distribution. Indeed, Šolc (1975) noted the presence of three phase points on cloud point curves when log-normal distributions were used to model UCST type phase behaviour. This phenomenon was not visible when a convergent distribution such as the Shultz-Flory distribution was used. The additional liquid-liquid instability in the log-normal distributions can be attributed to the higher concentrations of large molecular weight polymers ($r \rightarrow \infty$) that exist because of the nature of the distribution.

The cloud and shadow point curves of this system were also found using a log-normal distribution and the Hermitian quadrature integration method. The quadrature points and weightings are found before calculations start and are used each time an integral appears in an equation. This is different from the quadrature technique used by Cotterman and Prausnitz (1985) and Koak (1997) because they used the quadrature technique to divide the feed distribution into pseudocomponents. In their technique, the number of equations solved was proportional to the number of quadrature points used. In this work, the number of quadrature points utilized has no effect on the number of equations.

Using a 10 point Hermitian quadrature technique to integrate, the cloud point curve around the lower precipitation threshold temperature was generated and it is shown in Figure 5-8. The graph compares the quadrature technique (solid line) to the fifth order Runge-Kutta technique (dashed line). It shows that the quadrature technique matches the

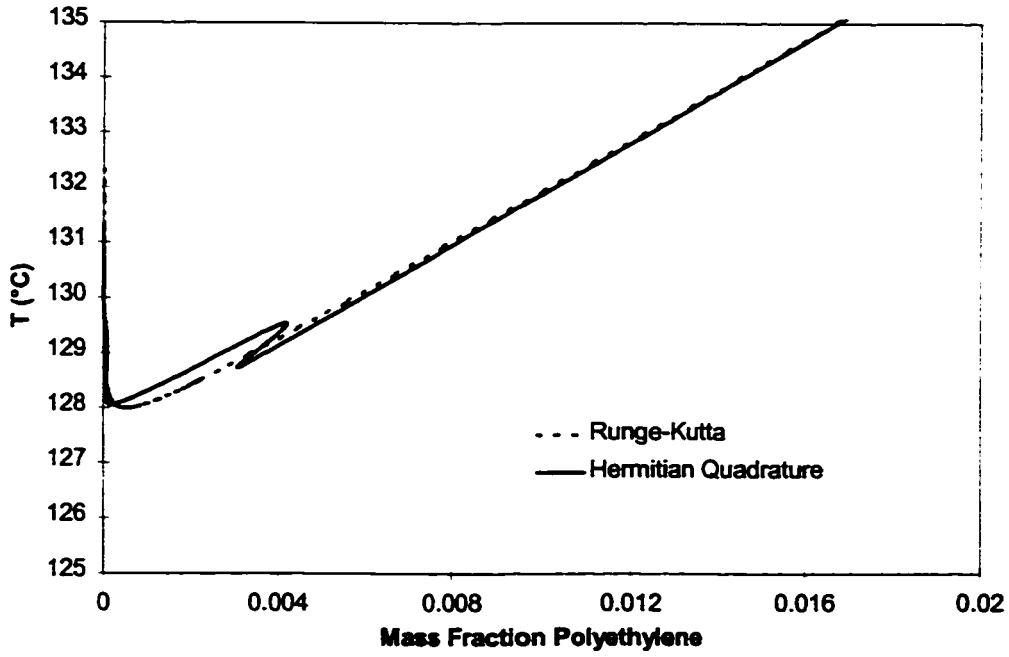

Figure 5-8 - Cloud Point Curve of Polyethylene in n-Hexane. 10 Point Hermitian Quadrature.

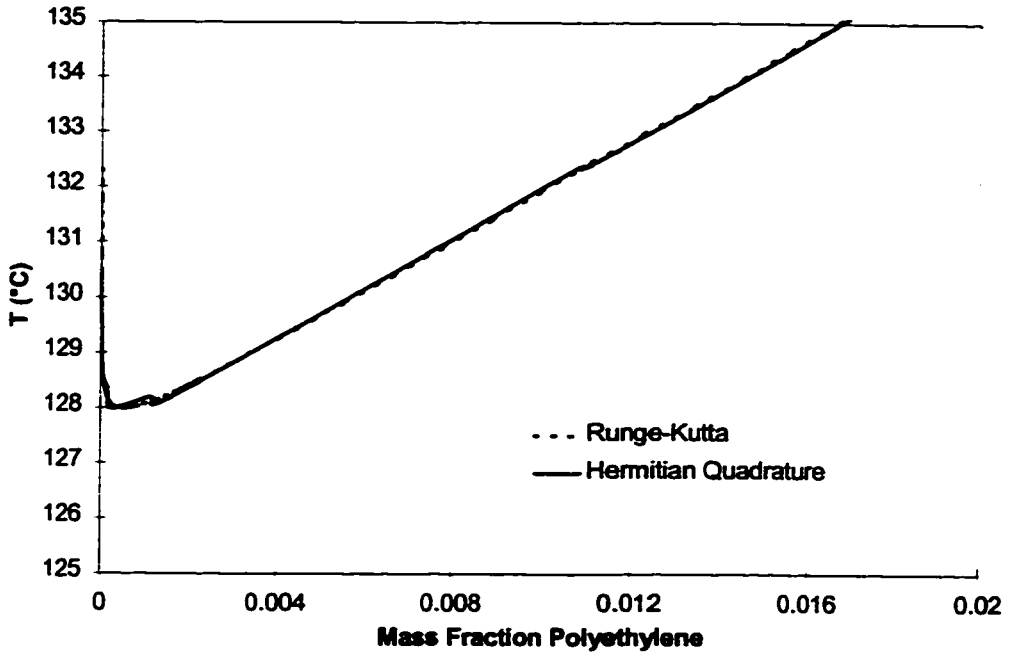

Figure 5-9 - Cloud Point Curve of Polyethylene in n-Hexane. 30 Point Hermitian Quadrature.

precipitation threshold temperature well, but shows a significant aberration in the cloud point line around a polymer mass fraction of 0.004. This "oscillation" about the high precision solution is apparent throughout the entire cloud and shadow point curve, even in the liquid-vapour region. It should be noted that the oscillation shown in Figure 5-8 is the most significant one.

For comparison, the cloud point curve was generated using Hermitian quadrature with 30 quadrature points. The curve around the lower precipitation threshold temperature is shown in Figure 5-9. Comparing the 10 node quadrature to the 30 node quadrature, it can be seen that the larger number of nodes improves the precision of the results (using the fifth order Runge-Kutta routine as the "exact" solution). The oscillation about the high precision solution is still present, but smaller. As well, the significant aberration apparent in Figure 5-8 has moved left to a polymer mass fraction of approximately 0.002. Smaller oscillations to the left of this point are also apparent. The cause of the oscillations was not determined, but the cloud and shadow point curves

found approached the fifth order Runge-Kutta solution as the number of quadrature nodes increased.

It is important to note that the Hermitian quadrature techniques were orders of magnitude faster than the Runge-Kutta technique. Table 5-4 compares the computation time required to complete one Newton-Raphson step using the three integration techniques examined. It displays the total time, the time spent performing the necessary integrations, the percentage of the total time devoted to integration and the "Integration Speed Ratio". The integration speed ratio compares the integration speed of each technique to that of the 10 node quadrature method. It is clear from this table that the 5^{th} order Runge-Kutta method is over 300 times slower than the 30 node quadrature method and over 600 times slower than the 10 node quadrature technique.

It is easy to see that this speed difference is a result of the number of integrand evaluations required to integrate a function. The number of integrand evaluations is directly related to the number of times the feed segmental distribution function was called. In the course of one Newton-Raphson step, the distribution function was evaluated 110 times when using the 10 node quadrature, 315 times when using the 30 node quadrature and 46851 times when using the Runge-Kutta technique. The extraordinary number of integrand evaluations occurring when the Runge-Kutta integration method is employed is a result of the adaptive step size used to ensure high precision. By decreasing the step size used in the integration to achieve the specified

Integration Technique	Total Time (ms)	Integration Time (ms)	% of Total Time in Integration	Integration Speed Ratio
10 Node Quadrature	89.651	3.993	4.5	1.0
30 Node Quadrature	103.205	7.539	7.3	1.9
5^{th} Order Runge-Kutta	2541.406	2457.23	96.7	615

Table 5-4 - Comparison of Integration Routines.

Computations performed on a 100MHz Intel Pentium Processor

tolerance, the number of steps required to complete the integration is increased thereby increasing the computation time.

In practical simulators, the time required to perform the integration using a fifth order Runge-Kutta technique is unacceptable. As well, the oscillations resulting from the use of the 10 node quadrature technique cast doubt upon the validity of the results. Therefore, more study needs to be directed towards finding an effective numerical integration routine for these problems. One possibility is to increase the number of quadrature nodes and find a compromise between accuracy and computational time. Another potential way to improve the accuracy of integration is to use the cubic spline techniques proposed by Hu and coworkers (1993, 1995). It may also be possible to reformulate the equations such that the quadrature technique does not result in oscillations around the high precision solution. The remaining results in this chapter were found using the fifth order Runge-Kutta technique in order to ensure that they best represented the model's true solution to the problem.

5.3.2 Polyethylene/Ethylene at 1750 Bar

As a final indication of this algorithm's performance, the cloud and shadow curves of a polyethylene/ethylene system were found. The polyethylene considered had a number average molecular weight of 56000 and a mass average molecular weight of 99000. It was modeled using a log-normal segmental distribution. The binary interaction parameter used was -0.0334 as suggested by Koak (1998). The calculated cloud and shadow point curves at a pressure of 1750 bar show a stable critical point at 163.6 °C and an upper precipitation threshold temperature of 176.2 °C. These curves are illustrated in Figure 5-10.

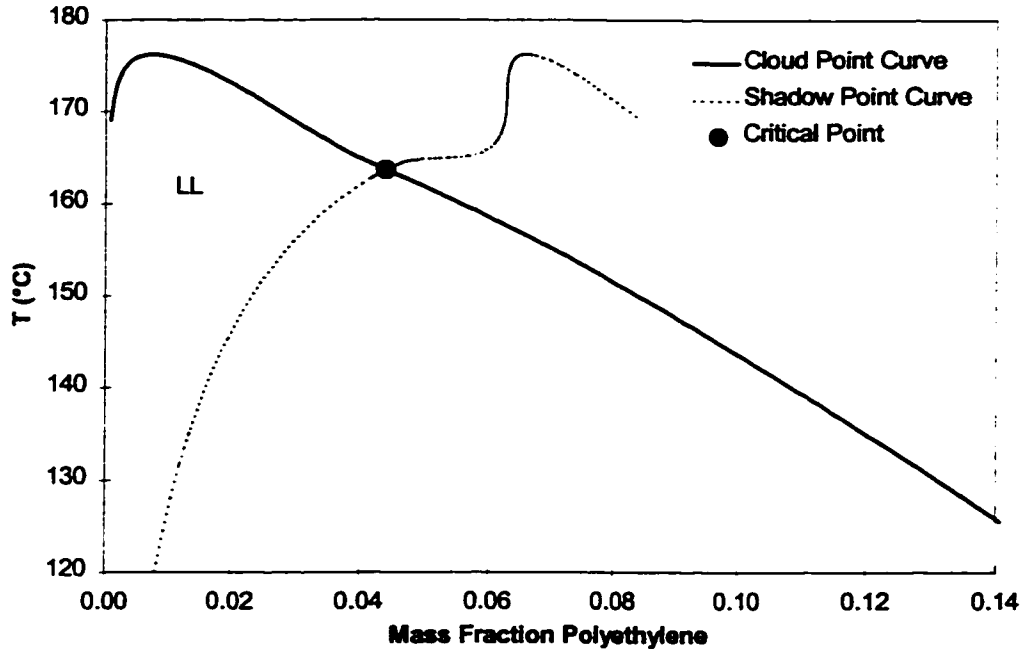

Figure 5-10 - Cloud and Shadow Point Curves for Polyethylene/ethylene. k_{ij} = -0.0334, P = 1750 bar.

The algorithm had little difficulties along the main branches of the curves, but care had to be taken near the critical point due to the ill conditioned Jacobian matrix at that point. The cloud and shadow point curves were found on the left and right hand sides of the critical point and extrapolated to find the intersection. The feed polymer segment fraction was used as the specification variable with no troubles.

5.4 Summary

The algorithm presented allows curves of fixed phase fraction to be traced for a disperse polymer/solvent system. The polymer can be modeled using a continuous thermodynamic form of the Sanchez-Lacombe equation of state. The Newton-Raphson formulation for locating one point along these curves consists of only 5 scalar equations in 5 scalar unknowns. The algorithm traces the curves by solving the set of 5 equations at each increment of an assigned specification parameter, *S*.

The algorithm located the cloud and shadow point curves of a polyethylene/n-hexane system exhibiting LCST type behaviour at 6 bar. It was also able to model the

UCST type behaviour of the polyethylene/ethylene system at 1750 bar. Complex phase behaviour such as three phase points, unstable and stable critical points were easily identified by the phase boundaries generated. The Sanchez-Lacombe model also predicted a hypothetical, high temperature liquid-vapour critical point in the polyethylene/n-hexane system.

It was found that when modeling the polyethylene/n-hexane system, the choice of the segmental distribution function affected the phase behaviour observed. When a divergent log-normal distribution was used, a liquid-liquid-liquid three phase point was present. This three phase point was not observed when polyethylene with the same polydispersity was modeled with the convergent Shultz-Flory distribution. This behavioural difference was attributed to the larger number of high molecular weight molecules present in a system modeled with the log-normal segmental distribution.

A fifth order Runge-Kutta integration routine was compared with 10 node and 30 node Hermitian quadrature integration methods. The Runge-Kutta technique was too slow to be of practical use, but gave more reliable results than the faster quadrature techniques. The "oscillation" observed when the quadrature methods were used decreased as the number of quadrature nodes increased. Further investigation is required to optimize the choice of integration routine.

The following chapter uses the same principles of continuous thermodynamics to develop a Newton-Raphson multiphase flash for polymer systems. It can be used to determine initial guesses for the cloud point calculations or to explore the phase behaviour around the boundaries determined by the cloud point algorithm.

6. A CONTINUOUS THERMODYNAMIC MULTIPHASE POLYMER FLASH PROCEDURE

6.1 Introduction

Knowing the phase boundaries of polymer/solvent systems is important in establishing feasible operating regions for polymer processes. The boundaries allow two phase regions to be located and avoided if necessary. However, it is also desirable to be able to perform polymer flash calculations. Given a defined feed composition, a PT-flash calculation determines the number of equilibrium phases, their compositions and quantities at a specified temperature and pressure. These flash calculations can be used with polymer systems in order to study polymer fractionation processes and solvent-polymer separation stages.

This chapter combines the principles of continuous thermodynamics developed in chapter 4 with the principles of a multiphase flash algorithm discussed in chapter 2. An algorithm to compute multiphase equilibrium in systems containing polymers is generated. Unlike the fixed phase fraction computation of chapter 5, the feed in the multiphase flash may contain numerous disperse polymers and numerous discrete components. Continuous thermodynamics is used to describe the disperse polymers. Again, the equations are developed for use with the Sanchez-Lacombe equation of state.

6.2 Algorithm Development

6.2.1 Background

Polymer systems can contain both large polymer molecules and small simple molecules. This disparity in molecular size can cause numerical difficulties in flash computations as the systems tend to be quite asymmetrical. Formulations which are based upon the mole fractions of the components can lead to numerical difficulties because of the extremely low polymer mole fractions which are often encountered. Using equations based upon segment fractions or mass fractions helps to avoid this numerical problem because the segment and mass fractions of the polymer will not be as small as their corresponding mole fractions.

Rätszch and coworkers published a number of papers describing a two phase polymer flash which utilizes a functional approach to continuous thermodynamics (Rätszch and Kehlen, 1985; Rätszch *et al.*, 1986; Rätszch and Kehlen, 1989). They established the equilibrium relationships for systems containing any number of discrete components and any number of polymers. The independent variables in their PT-flash equations were the segment fractions of each component, the number average number of segments in each phase and the phase fraction. They did not describe how integrals were calculated or how initial guesses to the solution were obtained.

Chen *et al.* (1993) developed a two phase flash for polymer/solvent/antisolvent systems where a disperse polymer is treated as a set of pseudocomponents. Components were modeled with the statistical associating fluid theory (SAFT). Their flash uses K values based upon mole fractions to define the distribution of each component between the phases. They state that the traditional technique of using two nested loops to solve the phase equilibrium requirements is not suited to polymer systems because the fugacity coefficients are highly dependent upon composition. As a result, they formulate their equilibrium requirements such that all the equations defining equilibrium are solved at the same time using a Newton-Raphson procedure. They divide the Jacobian of their system into blocks in order to allow the equations to be solved more quickly (Block-

Algebra technique). No information is given describing how an initial guess was formed for their iterative process.

Kosinski and Anderko (1996) describe a multiphase polymer flash algorithm. Their system of equations is based upon a disperse polymer being divided into pseudocomponents. Beginning with a single phase, they alternately used a modified version of Michelsen's tangent plane stability test to determine if a new phase should be added (Michelsen, 1982) and a successive substitution/free energy minimization method to determine the equilibrium phase compositions and amounts. The stability test determined initial guesses for new phases used in the equilibrium calculation. The flash calculation was a combination of nested loop successive substitution and direct Gibbs free energy minimization. In the successive substitution formulation, an outer loop updated fugacity coefficients while an inner loop solved the material balances using a Newton-Raphson procedure to solve the convex objective function defined by Michelsen (1994). The K values used in this procedure were based upon the mass fractions of each component. The reference phase for each component was chosen to be the phase where the component had the smallest mass fraction based activity coefficient. The number of equations to be solved was directly proportional to the number of pseudocomponents chosen to represent a disperse polymer. No example calculations were given in their paper.

Koak (1997) has also modified a multiphase flash algorithm for use with polymer systems. He modified the algorithm proposed by Abdel-Ghani *et al.* (1996) to use the Sanchez-Lacombe equation of state. Disperse polymers were characterized by pseudocomponents as determined by the quadrature method outlined by Cotterman and Prausnitz (1985). The number of equations solved was directly proportional to the number of quadrature points chosen to represent the system. K values were defined in terms of component mole fractions. The nested successive substitution algorithm needed to be heavily damped in order to converge.

The multiphase algorithm developed herein is also based upon the procedure described by Abdel-Ghani *et al.* (1996), but it has been developed using continuous thermodynamics and uses segment fractions as variables instead of mole fractions. It will be seen that the number of equations will be related only to the number of polymer species and discrete components in the system, not to the number of nodes used to perform the integrations.

6.2.2 Problem Definition

Suppose that a system contains n_d discrete components and n_c continuous components such that $n_d + n_c = C$. For indexing purposes, the first n_d components in the system will be the discrete components while the remaining $C - n_d$ components will have continuous distributions. Assume also that the system is divided into π phases. An intensive segmental distribution function, $W_{ij}(r)$, is associated with each continuous component i in each phase j. The extensive segmental distribution function, $w_{ij}(r)$, is defined to be $w_{ij}(r) = \bar{n}_{ij} W_{ij}(r) = \bar{n}_j \psi_{ij} W_{ij}(r)$ where $\bar{n}_{ij}$ is the total number of segments of component i in phase j, $\bar{n}_j$ is the total number of segments in phase j and ψ_{ij} is the segment fraction of component i in phase j. $\bar{r}_j$ represents the number average number of segments in phase j and is defined by equation (4.12). The segmental phase fraction, or phase fraction, of phase j will be denoted by β_j.

Given a feed composition defined by segment fractions for all components and an extensive segmental distribution function for each disperse polymer, the objective of the multiphase flash algorithm is to find the equilibrium number of phases, the compositions and quantities of those phases and the distributions of the disperse polymers in each of the equilibrium phases. The pressure and temperature are assumed to be fixed. Like the reactive flash algorithms, the multiphase polymer flash algorithm will also be capable of determining incipient phases (phases with a 0 phase fraction but a Gibbs free energy tangent parallel to the equilibrium Gibbs free energy tangent).

For phase equilibrium to be established, the segmental chemical potential of each component needs to be the same in each of the phases present. Additionally, the segmental balances for each of the components must be satisfied, and the segment fractions in each phase must sum to 1 if the phase fraction for that phase is greater than 0.

The algorithm is developed such that no single phase acts as a reference phase. Instead, the chemical potentials of each component are weighted according to the phase fraction of each phase and averaged to form the reference chemical potentials. In the development which follows, variables that describe the reference phase are denoted by a carat sign over the variable.

6.2.3 Equality of Chemical Potentials

The equality of chemical potentials of each component for all phases in which it is present can be written as

$$\left.\begin{aligned} \bar{\mu}_{ij} &= \hat{\bar{\mu}}_i \quad ; \ 1 \le i \le n_d \\ \bar{\mu}_{ij}(r) &= \hat{\bar{\mu}}_i(r) \quad ; \ n_d < i \le C \end{aligned}\right\} \text{ for all } j \text{ which contain component } i \tag{6.1}$$

where the carat sign denotes a common reference phase (defined below) and j denotes the phase index, $j = 1, \ldots, \pi$. Using the segmental chemical potentials as expressed in equations (4.45) and (4.46), these equations become

$$\begin{aligned} \ln\psi_{ij} - \frac{r_i}{\bar{r}_j} + r_i \ln\gamma_{ij} &= \ln\hat{\psi}_i - \frac{r_i}{\hat{\bar{r}}} + r_i \ln\hat{\gamma}_i \quad ; \ 1 \le i \le n_d \\ \ln\psi_{ij}W_{ij}(r) - \frac{r}{\bar{r}_j} + r\ln\gamma_{ij}(r) &= \ln\hat{\psi}_i\hat{W}_i(r) - \frac{r}{\hat{\bar{r}}} + r\ln\hat{\gamma}_i(r) \quad ; \ n_d < i \le C \end{aligned} \tag{6.2}$$

Equations (6.2) can be rewritten more compactly in terms of fugacities if a discrete and continuous fugacity coefficient can be defined by equations (6.3) and (6.4) respectively.

$$\ln\phi_{ij} = r_i\left(\ln\gamma_{ij} - 1/\bar{r}_j\right) + 1 \tag{6.3}$$

$$\ln\phi_{ij}(r) = r\left(\ln\gamma_{ij}(r) - 1/\bar{r}_j\right) + 1 \tag{6.4}$$

These fugacity coefficients allow the equal chemical potential requirement to be written as

$$\begin{aligned} \ln f_{ij} &= \ln \hat{f}_i \quad ; \ 1 \le i \le n_d \\ \ln f_{ij}(r) &= \ln \hat{f}_i(r) \quad ; \ n_d < i \le C \end{aligned} \tag{6.5}$$

where

$$f_{ij} = \psi_{ij}\phi_{ij} \tag{6.6}$$

and

$$f_{ij}(r) = \psi_{ij}W_{ij}(r)\phi_{ij}\,. \tag{6.7}$$

The discrete and continuous reference phase fugacities, $\hat{f}_i$, have the same definitions as equations (6.6) and (6.7) respectively.

The chemical potential can be written in terms of these fugacities as

$$\begin{aligned} \mu_{ij} &= \mu_i^{\bullet} + RT\ln f_{ij} \quad ; \ 1 \le i \le n_d \\ \mu_{ij}(r) &= \mu_i^{\bullet}(r) + RT\ln f_{ij}(r) \quad ; \ n_d < i \le C \end{aligned}$$

where $\mu_i^{\bullet}$ is a standard state chemical potential that drops out of the equations in the end.

6.2.4 Stability Criteria

As covered in chapter 2, Michelsen (1982a) defined a stability criterion for discrete systems with respect to the addition of phase j as

$$D_j \equiv \sum_{i=1}^{C} n_{ij}\left(\mu_{ij} - \hat{\mu}_i\right) \ge 0$$

Rewriting this criterion in terms of segment counts and using integration instead of summation for each continuous component, the stability criterion for a semi-continuous system using a segmental basis becomes

$$D_j \equiv \sum_{i=1}^{n_d} \frac{\overline{n}_{ij}}{r_i}\left(\mu_{ij} - \hat{\mu}_i\right) + \sum_{i=n_d+1}^{C} \int_{r=0}^{\infty} \frac{w_{ij}(r)}{r}\left(\mu_{ij}(r) - \hat{\mu}_i(r)\right)dr \ge 0 \tag{6.8}$$

where $\bar{n}_{ij}$ is the total number of segments of component i in phase j. $\bar{n}_{ij}/r$ represents the number of moles of discrete component i, and $w_{ij}(r)dr/r$ represents the number of moles of the continuous component i with segment counts between r and $r + dr$.

Michelsen shows that D_j must be non-negative at all stationary points for the system to be stable with respect to the addition of phase j. The stationary points can be found by locating the minimum points of D_j subject to the constraint that the sum of the total moles in the test phase j must be constant:

$$\sum_{i=1}^{n_d} \frac{\bar{n}_{ij}}{r_i} + \sum_{i=n_d+1}^{C} \int_{r=0}^{\infty} \frac{w_{ij}(r)}{r} dr = n_{const}$$

Using the method of Lagrange multipliers to convert the constrained minimization of D_j to an unconstrained minimization problem, gives the Lagrangian function, Q.

$$Q\left(\bar{n}_{ij}, w_{ij}, \theta\right) = D_j - \theta_j RT\left(\sum_{i=1}^{n_d} \frac{\bar{n}_{ij}}{r_i} + \sum_{i=n_d+1}^{C} \int_{r=0}^{\infty} \frac{w_{ij}(r)}{r} dr - n_{const}\right). \tag{6.9}$$

Recognizing that the derivatives of Q with respect to $\bar{n}_{ij}$ and w_{ij} must be 0 at a minimum gives the conditions for a stationary point:

$$\begin{aligned} &\mu_{ij} - \hat{\mu}_i = r_i\left(\bar{\mu}_{ij} - \hat{\bar{\mu}}_i\right) = \theta_j RT = D_j && ;\ 1 \le i \le n_d \\ &\mu_{ij}(r) - \hat{\mu}_i(r) = r\left(\bar{\mu}_{ij}(r) - \hat{\bar{\mu}}_i(r)\right) = \theta_j RT = D_j && ;\ n_d < i \le C \end{aligned}. \tag{6.10}$$

It should be noted that the value θ_j is independent of the component considered and the polymer segment count r. Geometrically, it represents the closest dimensionless distance from the tangent plane defined by the reference phase to the Gibbs free energy surface at the test phase j. θ_j can be used to determine the stability of phase j and is called the stability variable. If test phase j is in equilibrium with the reference phase, θ_j will be 0. If the test phase is incipient, θ_j will be greater than 0 and if the reference phase is unstable with respect to the addition of the test phase, θ_j will be less than 0. It should be noted when $\theta_j = 0$, equation (6.5) is satisfied.

Equations (6.10) give the relationship between the reference phase and stationary point composition as

$$\mu_{ij} = \hat{\mu}_i + \theta_j RT.$$

Since the segmental chemical potentials are related to the fugacities by

$$\mu_{ij} = \mu_i^* + RT \ln f_{ij},$$

the criteria for a phase j to be a stationary point with respect to the reference phase is

$$\begin{aligned} g_{ij} &= \ln f_{ij} - \ln \hat{f}_i - \theta_j = 0 \quad ; \ 1 \le i \le n_d \\ g_{ij}(r) &= \ln f_{ij}(r) - \ln \hat{f}_i(r) - \theta_j = 0 \quad ; \ n_d < i \le C \end{aligned} \tag{6.11}$$

where the first equation is a scalar expression used for the discrete components and the second equation is a function of the segment count r and is used for the continuous components. Once again, θ_j is independent of the component considered.

The algorithm proposed converges to the stationary points of the system. Each stationary point represents a potential phase. The values of the stability variables at these points indicate which phases are stable and which phases are incipient.

6.2.5 Normalized and Unnormalized Segment Fractions

The normalized segment fractions of each component in each phase can be found from equations (6.11) by inserting the definitions of f_{ij}:

$$\begin{aligned} \psi_{ij} &= \hat{\psi}_i K_{ij} \exp(\theta_j) \quad ; \ 1 \le i \le n_d \\ \psi_{ij} W_{ij}(r) &= \hat{\psi}_i \hat{W}_{ij}(r) K_{ij} \exp(\theta_j) \quad ; \ n_d < i \le C \end{aligned} \tag{6.12}$$

The K values are defined by

$$\begin{aligned} K_{ij} &= \hat{\phi}_i / \phi_{ij} \quad ; \ 1 \le i \le n_d \\ K_{ij}(r) &= \hat{\phi}_i(r) / \phi_{ij}(r) \quad ; \ n_d < i \le C \end{aligned} \tag{6.13}$$

and, if phase j is stable at equilibrium, K_{ij} will be equal to the ratio of the segment fraction of component i in phase j to the segment fraction of component i in the reference phase.

These K_{ij} are analogous to the K values used in chapter 5 where the reference phase was phase I.

Since the normalized segment fractions must sum to unity in each phase, for phase j,

$$\sum_{i=1}^{C} \psi_{ij} = \left(\sum_{i=1}^{n_d} \hat{\psi}_i K_{ij} + \sum_{i=n_d+1}^{C} \int_{r=0}^{\infty} \hat{\psi}_i \hat{W}_i(r) K_{ij}(r) dr \right) \exp\left(\theta_j\right) = 1. \tag{6.14}$$

Noting that $\theta_j \geq 0$, $\exp\left(\theta_j\right)$ is a quantity greater than 1. The exponential factor can be factored out of the right hand side of this equation and into the segment fractions in the left hand summation. The result is

$$\sum_{i=1}^{C} \psi_{ij} \exp\left(-\theta_j\right) = \sum_{i=1}^{C} \Psi_{ij} = \left(\sum_{i=1}^{n_d} \hat{\psi}_i K_{ij} + \sum_{i=n_d+1}^{C} \int_{r=0}^{\infty} \hat{\psi}_i \hat{W}_i(r) K_{ij}(r) dr \right) \leq 1, \tag{6.15}$$

where Ψ_{ij} are the unnormalized segment fractions defined by

$$\begin{aligned} \Psi_{ij} &= \hat{\psi}_i K_{ij} && ;\ 1 \leq i \leq n_d \\ \Psi_{ij} &= \int_{r=0}^{\infty} \hat{\psi}_i \hat{W}_i(r) K_{ij}(r) dr && ;\ n_d < i \leq C \end{aligned} \tag{6.16}$$

If the reference phase $\hat{\psi}_i$ and $\hat{W}_i(r)$ are known along with the K_{ij} values, equations (6.16) fully define the unnormalized segment fractions in each phase. The normalized segment fractions, ψ_{ij}, can be found from

$$\psi_{ij} = \Psi_{ij} \Big/ \sum_{k=1}^{C} \Psi_{kj} \tag{6.17}$$

Comparing equations (6.14) and (6.15), it can be seen that the sum of the unnormalized segment fractions for phase j defines the stability variable:

$$\theta_j = -\ln\left(\sum_{i=1}^{C} \Psi_{ij} \right). \tag{6.18}$$

It is apparent from equation (6.18) that when the unnormalized segment fractions of phase j sum to unity, θ_j will be zero and phase j is in equilibrium with the reference phase. When they sum to a value less than unity, θ_j will be greater than 0 and phase j will be an incipient phase.

Thus, the K values and reference phase define the unnormalized segment fractions which in turn can be used to find the stability variables. The stability variables can then be used to determine if a phase is in stable equilibrium or whether it is an incipient phase.

The K values also define the segmental distribution functions as

$$W_{ij}(r) = \hat{\psi}_i \hat{W}_i(r) K_{ij}(r) \quad ; \; n_d < i \le C .$$

6.2.6 *Segmental Balances and Summation Requirements*

The previous discussion has referred to an abstract, undefined reference phase. The segmental balances can be used to determine the reference phase composition and segmental distributions in terms of the K values, the feed composition and continuous component distributions.

Recall that β_j denotes the fraction of total feed segments present in phase j. Assume that the π phases of the system include both stable, present phases and incipient phases. The stable phases will have phase fractions greater than 0 while the incipient phases will have phase fractions of 0. Segmental balances on component i yield

$$\begin{aligned} \sum_{j=1}^{\pi} \beta_j \psi_{ij} &= \psi_{iF} && ; \; 1 \le i \le n_d \\ \sum_{j=1}^{\pi} \beta_j \psi_{ij} W_{ij}(r) &= \psi_{iF} W_{iF}(r) && ; \; n_d < i \le C \end{aligned} \tag{6.19}$$

where ψ_{iF} is the segment fraction of component i in the feed and $W_{iF}(r)$ is the intensive segment distribution function for component i in the feed. These equations are analogous to the segmental balances used in chapter 5 to develop the algorithm for fixed phase fraction equilibrium calculations.

The reference phase segment fractions and distributions can be determined from the material balances by substituting equations (6.12) into equations (6.19) and recognizing that $\beta_j \exp(\theta_j) = \beta_j$ since either β_j is zero or θ_j is zero.

$$\begin{aligned} \hat{\psi}_i &= \psi_{iF} / E_i && ;\ 1 \le i \le n_d \\ \hat{\psi}_i \hat{W}_i(r) &= \psi_{iF} W_{iF}(r) / E_i(r) && ;\ n_d < i \le C \end{aligned} \tag{6.20}$$

The E_i and $E_i(r)$ variables represent the weighted K value average for discrete and continuous components respectively:

$$\begin{aligned} E_i &= \sum_{j=1}^{\pi} \beta_j K_{ij} && ;\ 1 \le i \le n_d \\ E_i(r) &= \sum_{j=1}^{\pi} \beta_j K_{ij}(r) && ;\ n_d < i \le C \end{aligned} \tag{6.21}$$

Substituting the definition of the reference phase composition, equations (6.20), into equation (6.15) yields the following summation requirement on the segment fractions in each phase:

$$\begin{aligned} l_j &= 1 - \sum_{i=1}^{C} \Psi_{ij} \\ &= 1 - \left(\sum_{i=1}^{n_d} \psi_{iF} K_{ij} / E_i + \sum_{i=n_d+1}^{C} \int_{r=0}^{\infty} \frac{\psi_{iF} W_{iF}(r) K_{ij}(r)}{E_i(r)} dr \right) \begin{cases} = 0 & ;\ \beta_j > 0 \\ > 0 & ;\ \beta_j = 0 \end{cases} ;\ 1 \le j \le \pi \end{aligned} \tag{6.22}$$

The equality sign holds if phase j is present and the inequality holds if it is incipient. The independent variables in this equation are the discrete and continuous component K values and the phase fractions, β_j. Equation (6.22) is the continuous thermodynamic, segmental form of equation (2.50).

If the K_{ij} are known and assumed to be constant, equations (6.22) give π equations for π unknowns, β_j. This set of equations can be solved using a Newton-Raphson technique.

6.2.7 *Defining the Reference Phase Fugacity Coefficients*

The reference phase segment fractions, $\hat{\psi}_i$, and polymer segment fractions, $\hat{\psi}_i \hat{W}_i(r)$, are defined using the material balances and can be calculated from equations (6.20). However, the reference phase fugacity coefficients still need to be defined. To avoid the bookkeeping required if an existing phase is chosen as the reference phase, the average chemical potentials of each component over all the existing phases are used to define the reference phase chemical potentials. Doing so eliminates the problem of dealing with a reference phase becoming incipient.

The average chemical potential of each component is found by weighting the chemical potentials in a phase with their corresponding phase fraction. That is, the reference phase chemical potentials are defined as

$$\begin{aligned} \hat{\mu}_i &= \sum_{j=1}^{\pi} \beta_j \mu_{ij} \qquad ; \ 1 \le i \le n_d \\ \hat{\mu}_i(r) &= \sum_{j=1}^{\pi} \beta_j \mu_{ij}(r) \quad ; \ n_d < i \le C \end{aligned}$$

After inserting the definitions of a chemical potential, the resulting expressions for the reference phase fugacities are

$$\begin{aligned} \ln \hat{f}_i &= \sum_{j=1}^{\pi} \beta_j \ln f_{ij} \qquad ; \ 1 \le i \le n_d \\ \ln \hat{f}_i(r) &= \sum_{j=1}^{\pi} \beta_j \ln f_{ij}(r) \quad ; \ n_d < i \le C \end{aligned} \tag{6.23}$$

The reference phase fugacity coefficients can then be found from

$$\begin{aligned} \hat{\phi}_i &= \hat{f}_i / \hat{\psi}_i \qquad ; \ 1 \le i \le n_d \\ \hat{\phi}_i(r) &= \hat{f}_i(r) / \hat{\psi}_i \hat{W}_i(r) \quad ; \ n_d < i \le C \end{aligned} \tag{6.24}$$

6.2.8 *Eliminating the Functional Equations*

Consider a fixed temperature and pressure multiphase flash where the feed composition is fully defined and where the number of phases (both present and incipient)

is π. The unknown variables that define the equilibrium system are the π phase fractions, β_j, the $C\pi$ segment fractions, ψ_{ij}, and the $(C - n_d)\pi$ disperse component segment distributions, $W_{ij}(r)$. The $C\pi$ scalar and functional K values defined by equations (6.13) can be used to calculate the unnormalized segment fractions (equation (6.16)) and thus can replace the segment fractions as independent variables. The $(C - n_d)\pi$ functional K values for the polymers can also be used to define the polymer segmental distribution functions. Therefore, the unknowns that define the system become the π phase fractions, the $n_d\pi$ scalar K values and the $(C - n_d)\pi$ K value functions.

The summation requirements give π scalar equations. The remaining equations come from the stationary point requirements of equations (6.11):

$$g_{ij} = \ln f_{ij} - \ln \hat{f}_i - \theta_j = 0 \quad ;1 \le i \le n_d, 1 \le j \le \pi \tag{6.25}$$

$$g_{ij}(r) = \ln f_{ij}(r) + \ln \hat{f}_{ij}(r) - \theta_j = 0 \quad ;n_d < i \le C, 1 \le j \le \pi . \tag{6.26}$$

Equations (6.25) and (6.26) can be rewritten using the definitions of the scalar and functional fugacities:

$$g_{ij} = \ln\left(\frac{\psi_{ij}}{\hat{\psi}_i}\right) - \ln\left(\frac{\hat{\phi}_i}{\phi_{ij}}\right) - \theta_j = 0 \qquad ;1 \le i \le n_d$$

$$g_{ij}(r) = \ln\left(\frac{\psi_{ij} W_{ij}(r)}{\hat{\psi}_i \hat{W}_i(r)}\right) - \ln\left(\frac{\hat{\phi}_i(r)}{\phi_{ij}(r)}\right) - \theta_j = 0 \quad ;n_d < i \le C$$

Recognizing that $\ln(\psi_{ij}/\hat{\psi}_i)$ and $\ln(\psi_{ij} W_{ij}(r)/\hat{\psi}_i \hat{W}_i(r))$ are equal to $\ln K_{ij}$ and $\ln K_{ij}(r)$ respectively at equilibrium, these stationary criteria can be written in terms of the K values:

$$g_{ij} = \ln K_{ij} - \ln \hat{\phi}_i + \ln \phi_{ij} - \theta_j = 0 \quad ;1 \le i \le n_d, 1 \le j \le \pi \tag{6.27}$$

$$g_{ij}(r) = \ln K_{ij}(r) - \ln \hat{\phi}_i(r) + \ln \phi_{ij}(r) - \theta_j = 0 \quad ;n_d < i \le C, 1 \le j \le \pi . \tag{6.28}$$

Equation (6.28) is a functional equation and could be thought of as a set of scalar equations, one for each value of r. Computationally, an infinite number of equations is difficult to deal with.

However, equation (6.28) can be broken up into two scalar equations in two scalar unknowns using the same technique as was used in chapter 5. Combining the definition of the fugacity coefficients given in equations (6.3) and (6.4) with the definition for the Sanchez-Lacombe segment molar activity coefficient, equations (4.47) and (4.48), it is seen that both the discrete and functional forms of the fugacity coefficients have the form:

$$\ln\phi_{ij}(r) = \left\{\ln\left(\frac{\bar{r}_j\tilde{b}_j}{v_j}\right)+1\right\} + r\left\{2\frac{\tilde{b}_{ij}}{\tilde{b}_j\bar{r}_j} - \frac{2}{\bar{r}_j\tilde{b}_j}\left[\frac{\tilde{b}_{ij}}{\tilde{b}_j}-1\right]\left(v_j-\bar{r}_j\tilde{b}_j\right)\ln\left(\frac{v_j-r_j\tilde{b}_j}{v_j}\right) - \left(\frac{2\tilde{b}_{ij}}{\tilde{b}_j}-1\right)\left[\ln\left(\frac{v_j-\bar{r}_j\tilde{b}_j}{v_j}\right)+1\right] + \frac{2\tilde{a}_{ij}\bar{r}_j}{v_jRT} - \frac{2}{\bar{r}_j}\right\} \tag{6.29}$$

where the segment count r is replaced by r_i if component i is discrete. The first term on the right hand side of this expression is only dependent upon the phase considered, not the component of interest. The second term is the product of the segment count r and a factor only dependent upon the phase considered, the component considered and the mixture properties of the phase. That is, the terms in brackets do not depend upon the segment count, nor do they depend explicitly upon the form of a segmental distribution functions. Therefore, the expression for the fugacity coefficient can be compactly written as

$$\ln\phi_{ij}(r) = A_j + rB_{ij} \tag{6.30}$$

where, once again, r is replaced by r_i if component i is discrete.

A_j and B_{ij} in equation (6.30) are defined by:

$$A_j = \ln\left(\frac{\bar{r}_j\tilde{b}_j}{v_j}\right)+1 \tag{6.31}$$

$$B_{ij} = 2\frac{\tilde{b}_{ij}}{\tilde{b}_j \bar{r}_j} - \frac{2}{\bar{r}_j \tilde{b}_j}\left[\frac{\tilde{b}_{ij}}{\tilde{b}_j} - 1\right]\left(v_j - \bar{r}_j \tilde{b}_j\right)\ln\left(\frac{v_j - r_j \tilde{b}_j}{v_j}\right)$$

and

$$-\left(\frac{2\tilde{b}_{ij}}{\tilde{b}_j} - 1\right)\left[\ln\left(\frac{v_j - \bar{r}_j \tilde{b}_j}{v_j}\right) + 1\right] + \frac{2\tilde{a}_{ij}\bar{r}_j}{v_j RT} - \frac{2}{\bar{r}_j} \quad (6.32)$$

The equation of state parameters are the same as defined by equations (4.41) through (4.44) except that the phase index j has been added. It should be noted that equation (6.31) for A_j is only dependent upon the phase index j and is the same for all components in phase j, discrete or continuous.

Assume that the logarithms of the K values are linear functions of the segment count r:

$$\ln K_{ij} = \ln K_{Aj} + r_i \ln K_{Bij} \quad ; \; 1 \le i \le n_d$$

$$\ln K_{ij}(r) = \ln K_{Aj} + r \ln K_{Bij} \quad ; \; n_d < i \le C$$

Since equation (6.30) defines the logarithm of the fugacity coefficients as linear functions of r, it can be shown that the reference phase fugacity coefficients will be linear functions of r:

$$\ln \hat{\phi}_i(r) = \hat{A} + r\hat{B}_i. \quad (6.33)$$

where, assuming $\sum_{j=1}^{\pi} \beta_j = 1$,

$$\hat{A} = \sum_{j=1}^{\pi} \beta_j \left[\ln K_{Aj} + A_j + \theta_j\right] \quad (6.34)$$

and

$$\hat{B}_i = \sum_{j=1}^{\pi} \beta_j \left[\ln K_{Bij} + B_{ij}\right]. \quad (6.35)$$

Using these definitions of the fugacity coefficients and the reference phase fugacity coefficients, equations (6.27) and (6.28) become:

$$g_{ij} = \ln K_{Aj} + r_i \ln K_{Bij} - \hat{A} - r_i \hat{B}_i + A_j + r_i B_{ij} - \theta_j = 0 \quad ;1 \le i \le n_d \tag{6.36}$$

$$g_{ij}(r) = \ln K_{Aj} + r \ln K_{Bij} - \hat{A} - r\hat{B}_i + A_j + rB_{ij} - \theta_j = 0 \quad ;n_d < i \le C \tag{6.37}$$

Equations (6.36) and (6.37) can be seem to be linear in terms of the variables r_i and r respectively. Therefore, it is possible to replace the $n_d\pi$ scalar equations in (6.36) and the $(C - n_d)\pi$ functional equations in (6.37) by a total of $(C + 1)\pi$ scalar equations if terms of like powers of r_i and r in equations (6.36) and (6.37) are isolated and set equal to zero. The new scalar objective functions are

$$h_{Bij} = \ln K_{Bij} + B_{ij} - \hat{B}_i = 0 \quad ; \; 1 \le i \le C, \; 1 \le j \le \pi \tag{6.38}$$

$$h_{Aj} = \ln K_{Aj} + A_j - \hat{A} - \theta_j = 0 \quad ; \; 1 \le j \le \pi . \tag{6.39}$$

These two equations effectively eliminate the functional equations for $\ln K_{ij}(r)$ and replace them with manageable scalar equations.

If $\ln K_{Bij}$ and $\ln K_{Aj}$ are known, they can be used to find the segment fractions and segmental distribution functions within each phase. These values then determine the number average number of segments in all phases and the equation of state parameters for each phase. The equation of state is used to find the volumes of each phase which allows the fugacity coefficients of each component in each phase to be calculated.

6.2.9 Solving the Equations

Equations (6.38) and (6.39) are the objective functions that define the K values of the system. Equation (6.22) defines the objective functions due to the material balances and summation constraints. Together, these objective functions are $(C + 2)\pi$ scalar equations in $(C + 2)\pi$ scalar unknowns, $\ln K_{Bij}$, $\ln K_{Aj}$ and β_j. They can be solved using a variety of techniques including a Newton-Raphson technique or a successive substitution method.

The Newton-Raphson technique determines successive approximations to the solution of a non-linear set of equations using a linear approximation to the set of

equations. Let the residues defined by equations (6.38), (6.39) and (6.22) on any given iteration can be represented in vector notation by

$$\mathbf{h_B} = \left[h_{B11}, h_{B21}, \ldots, h_{BC1}, h_{B12}, \ldots, h_{BC\pi}\right]^T,$$

$$\mathbf{h_A} = \left[h_{A1}, h_{A2}, \ldots, h_{A\pi}\right]^T \text{ and}$$

$$\mathbf{l} = \left[l_1, l_2, \ldots, l_\pi\right]^T$$

respectively. As well, define three vectors of independent variables such that

$$\mathbf{lnK_B} = \left[\ln K_{B11}, \ln K_{B21}, \ldots, \ln K_{BC1}, \ln K_{B12}, \ldots, \ln K_{BC\pi}\right]^T,$$

$$\mathbf{lnK_A} = \left[\ln K_{A1}, \ln K_{A2}, \ldots, \ln K_{A\pi}\right]^T \text{ and}$$

$$\beta = \left[\beta_1, \beta_2, \ldots, \beta_\pi\right]^T.$$

The Newton-Raphson procedure for updating the independent variables can then be written as

$$\begin{bmatrix} \mathbf{lnK_B} \\ \mathbf{lnK_A} \\ \beta \end{bmatrix}^{(n+1)} = \begin{bmatrix} \mathbf{lnK_B} \\ \mathbf{lnK_A} \\ \beta \end{bmatrix}^{(n)} + \begin{bmatrix} \mathbf{\Delta lnK_B} \\ \mathbf{\Delta lnK_A} \\ \Delta\beta \end{bmatrix}^{(n)} \tag{6.40}$$

where the superscript in parenthesis indicates the iteration count. The rightmost term in this equation can be found by solving the linear set of equations defined by

$$\mathbf{J}^{(n)} \begin{bmatrix} \mathbf{\Delta lnK_B} \\ \mathbf{\Delta lnK_A} \\ \Delta\beta \end{bmatrix}^{(n)} = -\begin{bmatrix} \mathbf{h_B} \\ \mathbf{h_A} \\ \mathbf{l} \end{bmatrix}^{(n)}.$$

where the Jacobian, $\mathbf{J}^{(n)}$, has the structure

$$\mathbf{J} = \begin{bmatrix} \left(\frac{\partial h_B}{\partial \ln K_B}\right) & \left(\frac{\partial h_B}{\partial \ln K_A}\right) & \left(\frac{\partial h_B}{\partial \beta}\right) \\ \left(\frac{\partial h_A}{\partial \ln K_B}\right) & \left(\frac{\partial h_A}{\partial \ln K_A}\right) & \left(\frac{\partial h_A}{\partial \beta}\right) \\ \left(\frac{\partial l}{\partial \ln K_B}\right) & \left(\frac{\partial l}{\partial \ln K_A}\right) & \left(\frac{\partial l}{\partial \beta}\right) \end{bmatrix}. \tag{6.41}$$

The analytic derivatives required to determine each element of the Jacobian are given in Appendix C. Iterations are ceased when the sum of the squares of the residues is less than $(C+2)\pi \times 10^{-12}$. It should be noted that residues, l_j, are only included in the error evaluation if phase j is present ($\beta_j > 0$).

Since Newton-Raphson procedures only converge well with good initial guesses, a successive substitution technique may be used to provide a larger convergence region. The successive substitution approach is identical to the approach used in the stoichiometric reactive flash of chapter 2. An inner loop and an outer loop are used to solve the objective functions. The inner loop solves the material balances and summation constraints assuming composition independent K values using a Newton-Raphson procedure while the outer loop updates the K values.

The inner loop is given the K values and uses them to determine phase fractions, β_j. The objective functions and their residues in this inner loop are given by equation (6.22). The phase fractions are updated using $\beta^{(n+1)} = \beta^{(n)} + \Delta\beta^{(n)}$ where $\Delta\beta^{(n)}$ is found from the solution of $\mathbf{J}_\beta^{(n)}\Delta\beta^{(n)} = -\mathbf{l}$. $\mathbf{J}_\beta$ is defined by

$$\mathbf{J}_\beta = \left[\left(\frac{\partial l_i}{\partial \beta_j}\right)\right] \tag{6.42}$$

where the derivatives required are the same as those defined in Appendix C. Iterations continue until the sum of the square of the residuals for present phases is less than 10^{-8}.

The outer loop takes the phase fractions found from the inner loop and calculates the segment fractions and fugacities of each component in each phase. It uses the

fugacities found to update the $\ln K_{Aj}$ and $\ln K_{Bij}$ values for the next iteration. The updating formulae are determined from the definitions of the K values in the following manner. Consider the equal fugacity requirement as given in equation (6.11):

$$\begin{aligned} g_{ij} &= \ln f_{ij} - \ln \hat{f}_i - \theta_j \quad ; \ 1 \le i \le n_d \\ g_{ij}(r) &= \ln f_{ij}(r) - \ln \hat{f}_i(r) - \theta_j \quad ; \ n_d < i \le C \end{aligned} \tag{6.11}$$

A relationship between the residuals, g_{ij}, the segment fractions and the fugacity coefficients can be found by inserting the definition of fugacity into these equations.

$$\begin{aligned} \ln\left(\frac{\hat{\phi}_i}{\phi_{ij}}\right) &= \ln\left(\frac{\psi_{ij}}{\hat{\psi}_i}\right) - \theta_j - g_{ij} = 0 \quad ; \ 1 \le i \le n_d \\ \ln\left(\frac{\hat{\phi}_i(r)}{\phi_{ij}(r)}\right) &= \ln\left(\frac{\psi_{ij} W_{ij}(r)}{\hat{\psi}_i \hat{W}_i(r)}\right) - \theta_j - g_{ij}(r) = 0 \quad ; \ n_d < i \le C \end{aligned}$$

Let the iteration which defines g_{ij} be the n^{th} iteration. Equation (6.12) shows that the K values on the n^{th} iteration can be defined in terms of the segment fractions and tangent plane distances:

$$\begin{aligned} \ln K_{ij}^{(n)} &= \ln\left(\psi_{ij}/\hat{\psi}_i\right)^{(n)} - \theta_j^{(n)} \quad ; \ 1 \le i \le n_d \\ \ln K_{ij}^{(n)}(r) &= \ln\left(\psi_{ij} W_{ij}(r)/\hat{\psi}_i \hat{W}_i(r)\right)^{(n)} - \theta_j^{(n)} \quad ; \ n_d < i \le C \end{aligned}$$

The K values defined by the ratio of fugacity coefficients, equation (6.13), correspond to the next iteration's value. Thus, equation (6.11) can be written as

$$\begin{aligned} \ln K_{ij}^{(n+1)} &= \ln K_{ij}^{(n)} - g_{ij}^{(n)} \quad ; \ 1 \le i \le n_d \\ \ln K_{ij}^{(n+1)}(r) &= \ln K_{ij}^{(n)}(r) - g_{ij}^{(n)}(r) \quad ; \ n_d < i \le C \end{aligned} \tag{6.43}$$

Michelsen (1982b) showed that convergence of this successive substitution algorithm requires that the eigenvalues of the variable transformation matrix **H** should satisfy $|\lambda| < 1$, where **H** is defined by

$$\mathbf{H}=\begin{bmatrix} \left(\dfrac{\partial \ln \mathbf{K}^{(n+1)}}{\partial \ln \mathbf{K}^{(n)}}\right) & \left(\dfrac{\partial \ln \mathbf{K}^{(n+1)}}{\partial \ln \mathbf{K}^{(n)}(r)}\right) \\ \left(\dfrac{\partial \ln \mathbf{K}^{(n+1)}(r)}{\partial \ln \mathbf{K}^{(n)}}\right) & \left(\dfrac{\partial \ln \mathbf{K}^{(n+1)}(r)}{\partial \ln \mathbf{K}^{(n)}(r)}\right) \end{bmatrix}$$

and the successive substitution updating procedure is represented by

$$\begin{bmatrix} \ln \mathbf{K}^{(n+1)} \\ \ln \mathbf{K}^{(n+1)}(r) \end{bmatrix} = \mathbf{H} \begin{bmatrix} \ln \mathbf{K}^{(n)} \\ \ln \mathbf{K}^{(n)}(r) \end{bmatrix}.$$

Michelsen (1982b) also provided an explanation for the poor convergence of successive substitution near critical points where two eigenvalues of **H** approach $\lambda = 1$. Convergence in these cases is monotonic.

More recently, Heidemann and Michelsen (1995) identified a class of equilibrium problems where successive substitution can show oscillatory divergent behaviour. They showed that typical polymer-solvent equilibrium calculations can fail in this manner. The divergence results when one or more eigenvalues of **H** are less than -1 ($\lambda < -1$).

As Heidemann and Michelsen (1995) and Koak (1997) showed, the stability of the solution method can be improved by damping the updating procedure. If the damping factor is denoted by m ($m < 1$), the damped successive substitution procedure is

$$\begin{aligned} \ln K_{ij}^{(n+1)} &= \ln K_{ij}^{(n)} - m g_{ij}^{(n)} && ;\ 1 \le i \le n_d \\ \ln K_{ij}^{(n+1)}(r) &= \ln K_{ij}^{(n)}(r) - m g_{ij}^{(n)}(r) && ;\ n_d < i \le C \end{aligned} \qquad (6.44)$$

If the initial formulation has an eigenvalue represented by λ, equations (6.44) result in an effective eigenvalue of $\lambda_{eff} = 1 - m(1 - \lambda)$. As Koak (1997) points out, as m approaches 0, the effective eigenvalues of the variable transformation matrix approach unity and convergence slows, but there is a possibility of locating an "optimal" $0 < m < 1$ providing the "best" convergence behaviour.

The second equation of (6.44) is a functional equation and is inconvenient to use. Consider the fact that $\ln K_{ij}$ can be represented as

$$\ln K_{ij}^{(k)} = \ln K_{Aj}^{(k)} + r \ln K_{Bij}^{(k)}$$

and that g_{ij} may be written as

$$g_{ij}^{(k)} = \left\{ \ln K_{Aj}^{(k)} + A_j^{(k)} - \hat{A}^{(k)} - \theta_j^{(k)} \right\} + r \left\{ \ln K_{Bij}^{(k)} + B_{ij}^{(k)} - \hat{B}_i^{(k)} \right\}.$$

By substituting these expressions into equations (6.44) and grouping terms with similar dependencies on r together, (6.44) can be represented by two sets of scalar equations:

$$\left.\begin{aligned} \ln K_{Bij}^{(n+1)} &= (1-m) \ln K_{Bij}^{(n)} - m\left(B_{ij}^{(n)} - \hat{B}_i^{(n)} \right) \\ \ln K_{Aj}^{(n+1)} &= (1-m) \ln K_{Aj}^{(n)} - m\left(A_j^{(n)} - \hat{A}^{(n)} - \theta_j^{(n)} \right) \end{aligned}\right\} \; 1 \le i \le C; \; 1 \le j \le \pi . \qquad (6.45)$$

The error in the $\ln K_{Bij}$ and $\ln K_{Aj}$ can be calculated from

$$\left.\begin{aligned} g_{Bij}^{(k)} &= \ln K_{Bij}^{(k)} + B_{ij}^{(k)} - \hat{B}_i^{(k)} \\ g_{Aj}^{(k)} &= \ln K_{Aj}^{(k)} + A_j^{(k)} - \hat{A}^{(k)} - \theta_j^{(k)} \end{aligned}\right\} \; 1 \le i \le C; \; 1 \le j \le \pi . \qquad (6.46)$$

If the inner loop of a successive substitution routine returns a segment fractions and phase fractions which allow A_j, B_{ij} and θ_j values to be calculated, equation (6.45) can be used to determine the K values used for the next iteration.

Convergence is achieved when the sum of the square of the residuals associated with A and B are less than $(C + 1)\pi \times tol$, where tol is a specified tolerance.

6.2.10 Initiation

A good initial guess is important to the flash routine. The better the initial guess, the faster the equilibrium solution will be found. The proposed multiphase polymer flash algorithm was initiated using a preliminary successive substitution flash for a discretized system.

The $C - n_d$ continuous components were characterized by a set of 7 pseudocomponents. The segment count and molar mass of the 7 pseudocomponents were found through quadrature techniques described by Cotterman and Prausnitz (1985) and Koak (1997). The polymer pseudocomponents shared the same Sanchez-Lacombe

parameters and interaction parameters as the original continuous components. The segment fractions of the pseudocomponents summed to give the same segment fraction of their parent continuous component.

The new system contained $C_d = n_d + 7(C - n_d)$ discrete components and 0 continuous components. Using the equations as developed in the earlier sections of this chapter, the $\ln K_A$ and $\ln K_B$ values were defined for each component, and the successive substitution updating procedure was utilized to determine an approximation of the continuous equilibrium solution. Iterations proceeded until the error was less than $(C_d + 1)\pi \times 10^{-8}$.

The preliminary flash was initiated with the number of phases equal to the number of discrete components plus one. That is, $\pi = C_d + 1$. The compositions of the initial phases were chosen such that the first phase was a vapour with the feed composition, n_d phases were almost pure solvents (the original discrete components) and the remaining $C_d - n_d$ phases were each rich in one of the polymer pseudocomponents. Specifically, the initial segment fractions and phase fractions were given by:

$$\psi_{ij} = \begin{cases} \psi_i^F & ;\ j = 1;\ 1 \le i \le C_d \\ 0.99 + 0.01\psi_i^F & ;\ 2 \le j \le n_d + 1;\ i = j - 1 \\ 0.01\psi_i^F & ;\ 2 \le j \le n_d + 1;\ i \ne j - 1 \\ 0.30 + 0.70\psi_i^F & ;\ n_d + 1 < j \le \pi;\ i = j - 1 \\ 0.70\psi_i^F & ;\ n_d + 1 < j \le \pi;\ i \ne j - 1 \end{cases}$$

$$\beta = 1/\pi \quad ;\ 1 \le j \le \pi.$$

This initial guess worked better than starting with a phase in each corner of composition space because the polymer components rarely partition into a nearly pure polymer phase.

Once the approximate solution was found, the segment fractions of the pseudocomponents were combined to give the segment fractions of the original continuous component in all of the phases. These new segment fractions were used to initiate the continuous polymer flash.

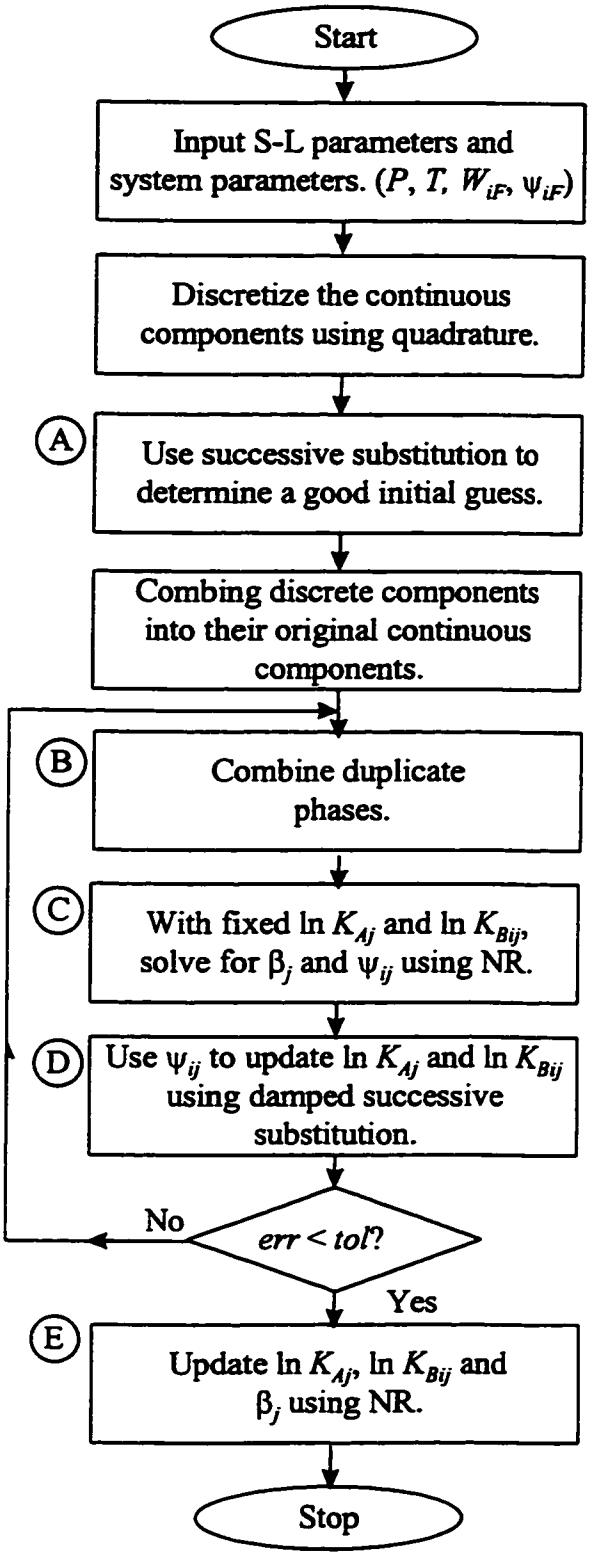

Figure 6-1 - General Flowsheet for Multiphase Polymer Flash.

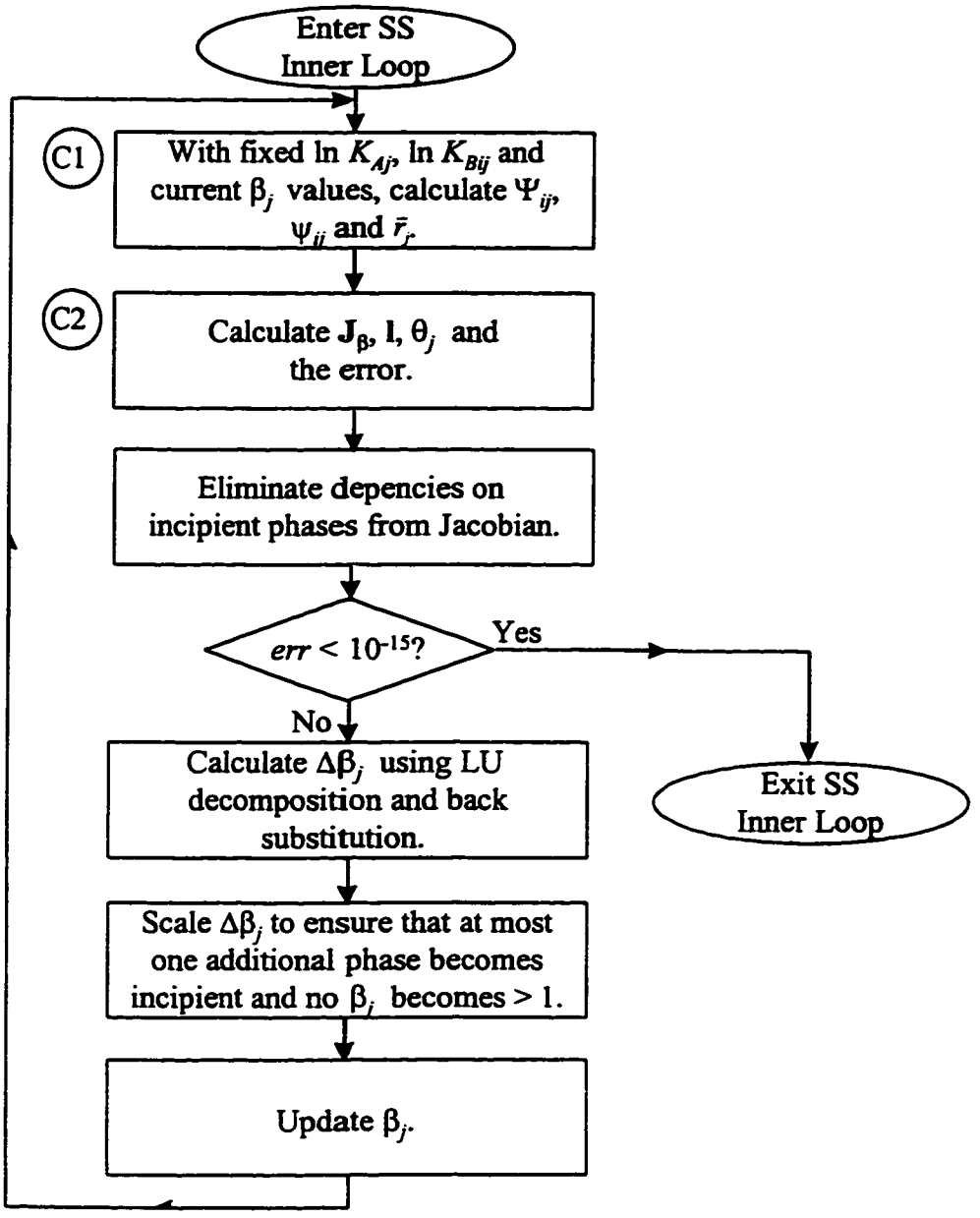

Figure 6-2 - Successive Substitution Inner Loop. Expansion of Block C from Figure 6-1.

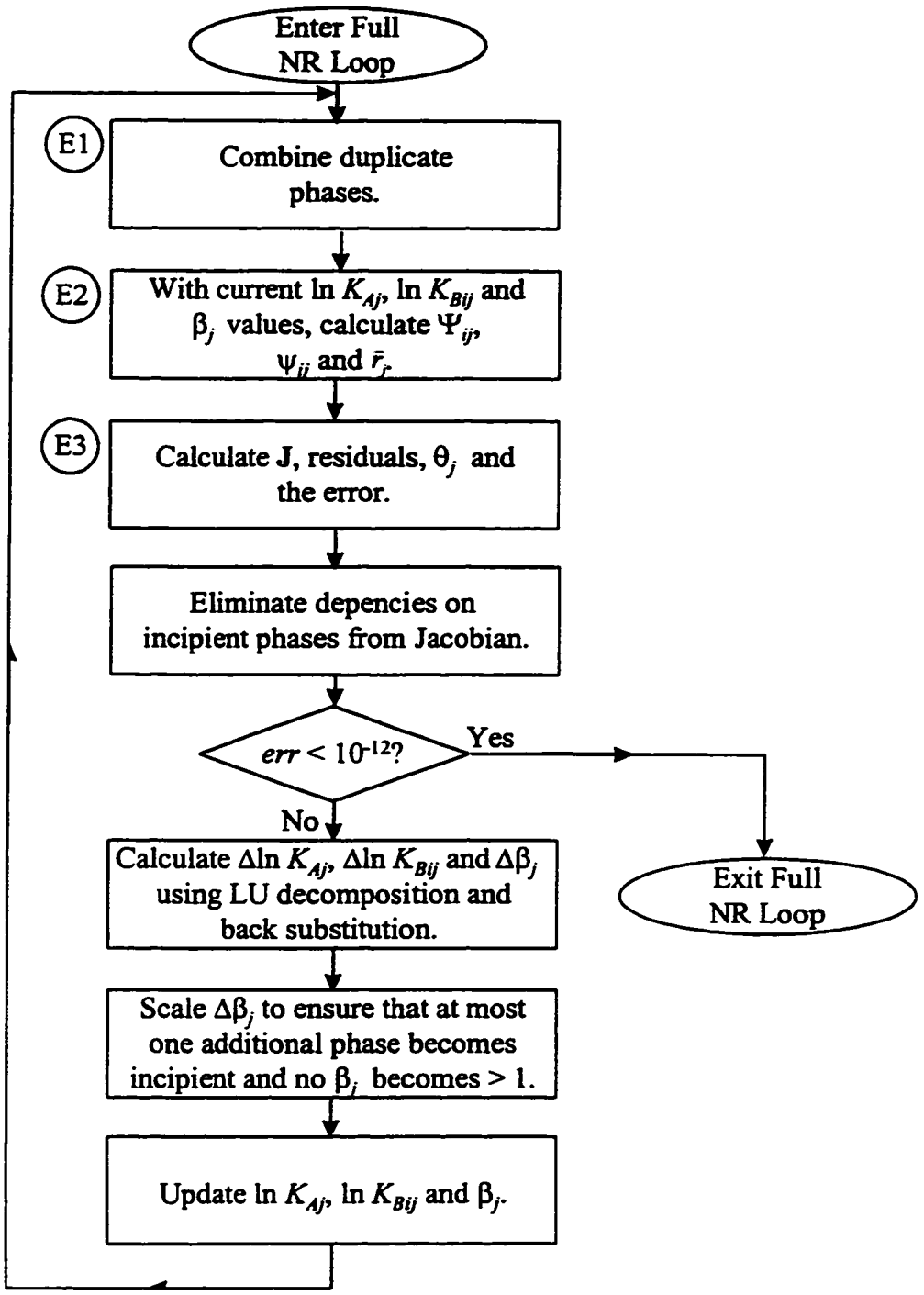

Figure 6-3 - Full Newton-Raphson Flowsheet. Expansion of Block E from Figure 6-1.

6.2.11 Procedure Overview

An flowsheet of the entire procedure is given in Figure 6-1. After inputting the system definition (P, T, ψ_{iF} and $W_{iF}(r)$), the disperse polymer components are temporarily discretized and the discrete system is passed to a successive substitution routine to gain a rough estimate of the equilibrium (Block A). The structure of this initial flash is the same as the continuous successive substitution routine described below.

The segment fractions and K values returned from the discrete successive substitution block are used to supply an initial guess to the continuous successive substitution procedure indicated by blocks B,C and D. This portion of the code consists of two nested loops: an inner loop shown by block C and an outer loop shown by blocks B, D and the convergence check.

The inner loop uses a Newton-Raphson procedure to solve for phase fractions at fixed K values. A flowsheet for this inner loop is given in Figure 6-2. Upon entering the inner loop, block C1 uses equations (6.16), (6.17) and (4.12) to calculate Ψ_{ij}, ψ_{ij} and $\bar{r}_j$ respectively. θ_j is found using equation (6.18). In block C2, the $\pi \times \pi$ Jacobian, $\mathbf{J}_\beta$, is found using equation (6.42) and the residuals are determined using equations (6.22). The inner loop error is defined to be the sum of the square of the residuals corresponding to phases with non-zero phase fractions. Because incipient phases should not affect the material balances of the phases that are present, the columns of the Jacobian corresponding to incipient phases are set to zero save for the diagonal elements.

If the error calculated is less than 10^{-15} the inner loop has converged and is exited. If the error is greater, $\Delta\beta$ is found by solving the linear Newton-Raphson equations using LU decomposition (see Press *et al.*, 1992). $\Delta\beta$ is scaled to ensure that, at most, one additional phase becomes incipient (phase fraction becomes 0) and to ensure that none of the β_j become greater than 1. The new approximations to β are found using the scaled $\Delta\beta$ values and the inner loop starts over at block C1.

Once the phase fractions and phase compositions are determined in the inner loop, the Sanchez-Lacombe parameters for each phase are found. The volume for each phase is found and A_j, B_{ij}, $\hat{A}$ and $\hat{B}_i$ are calculated from equations (6.31), (6.32), (6.34) and (6.35) respectively. The error in the outer loop is determined from

$$err = \sum_{j=1}^{\pi} \left\{ g_{Aj}^2 + \sum_{i=1}^{C} g_{Bij}^2 \right\} \Big/ (C+1)\pi$$

where g_{Aj} and g_{Bij} are defined by equation (6.46). If the error is less than a specified tolerance (10^{-8} is shown to work well in the next section), the full Newton-Raphson flash routine is entered (block E of Figure 6-1). Otherwise $\ln K_{Aj}$ and $\ln K_{Bij}$ are updated using equation (6.44). The outer loop checks compares the K values and molar volumes of any two phases and combines them into one phase if all of the values are within 1% (block B). The inner loop is reentered with the new K values.

Once the successive substitution routine is exited, the Newton-Raphson routine is entered at block E. The flowsheet of this program section is given in Figure 6-3. It is very similar to the inner loop of the successive substitution section except the K values are not considered fixed. At the top of each Newton-Raphson loop, the K values and molar volumes are compared and any phases with less than 1% difference in these variables are combined (block E1). The values Ψ_{ij}, ψ_{ij} and $\tilde{r}_j$ are calculated in block E1 and θ_j is determined from equation (6.18) in block E2. The Jacobian, **J**, in block E2 is a $(C+2)\pi \times (C+2)\pi$ matrix defined by equation (6.41) and the residuals are found from equations (6.22), (6.38) and (6.39). Once the Jacobian and residuals have been found, the Jacobian is modified so that the columns associated with zero phase fractions are zero except for the diagonal element. This eliminates the dependencies of the material balances on phases which do not exist.

The error in the loop is calculated from the sum of the square of the residuals:

$$err = \left[\sum_{j=1}^{\pi} \left\{ h_{Aj}^2 + \sum_{i=1}^{C} h_{Bij}^2 \right\} + \sum_{\substack{j=1 \\ \beta_j > 0}}^{\pi} l_j^2 \right] \Big/ (C+2)\pi .$$

If the error is less than 10^{-12} the procedure has converged and is exited. Otherwise the change in the independent variables are calculated using a LU decomposition and back substitution procedure. The changes to the phase fractions are scaled to ensure that, at most, one new phase becomes incipient ($\beta_j = 0$) and that no phase fraction exceeds 1. The independent variables are then updated and the top of the loop is reentered at block E1.

The converged solution will consist of a set of π phases representing the stationary points of the system with respect to reference phase. The phase stability variables and phase fractions will determine which of the phases are incipient and which are stable equilibrium phases.

6.3 Example Calculations

Example flash calculations were done on a polyethylene/n-hexane system similar to the one studied in chapter 5. The polyethylene had a polydispersivity of 22.125 ($M_n = 8000$, $M_w = 177000$) and was modeled with a log-normal distribution. The distribution parameters are given in Table 4-1 and the Sanchez-Lacombe equation of state parameters are shown in Table 5-1. All of the calculations were performed at a pressure of 6 bar and a feed n-hexane segment fraction of 0.9845 (1.7 wt% polyethylene). The flash calculations were done at temperatures of 120 °C, 127 °C, 129 °C, 133 °C, 137 °C and 141 °C. This temperature range covered a single liquid phase, a two liquid phase and a liquid-vapour phase region. All integration was performed using a 30 node Hermitian quadrature technique.

The damping factor used in the initiation procedure was $m = 0.1$. The discretized system converged to an error of 10^{-8} in about 70 iterations. At 120, 127 and 129 °C the discretized system converged to a stable liquid, an incipient liquid and an incipient vapour phase. At 133 °C and 137 °C, it converged to a stable liquid-liquid solution with an incipient vapour phase. At 141 °C, it converged to a stable liquid-vapour solution

with an incipient second liquid phase. These phases were used to initiate the continuous form of the successive substitution algorithm.

Table 6-1 shows the equilibrium solutions as found from the continuous successive substitution algorithm with a damping factor of $m = 0.5$. The tolerance of the routine was set to 10^{-12} so that no Newton-Raphson steps occurred after the successive substitution algorithm had converged. The solutions consisted of up to three phases and the table lists the mass fractions of n-hexane and polyethylene in each of the phases. As well, the phase fraction, β, is listed for phases that are present. The stability variable, θ, is listed in parenthesis for incipient phases.

It can be seen from the decreasing vapour phase stability variable that as the temperature is raised from 120 °C to 137 °C, the incipient vapour becomes closer to being stable. At 141 °C the vapour phase becomes stable with a phase fraction of 0.945. From 120 to 133 °C, the one stable phase is a liquid phase with the same composition as the feed. However at 133 °C, both an incipient vapour and an incipient liquid rich in solvent exist. At 137 °C, the second liquid phase becomes stable and a liquid-liquid equilibrium solution exists.

T	Vapour			Liquid			Liquid		
(°C)	M_{C6}	M_{PE}	$\beta(\theta)$	M_{C6}	M_{PE}	$\beta(\theta)$	M_{C6}	M_{PE}	$\beta(\theta)$
120	1.000	0.000	(0.171)	-	-	-	0.983	0.017	1.000
127	1.000	0.000	(0.104)	-	-	-	0.983	0.017	1.000
129	1.000	0.000	(0.085)	-	-	-	0.983	0.017	1.000
133	1.000	0.000	(0.048)	0.997	0.003	(<.01)	0.983	0.017	1.000
137	1.000	0.000	(0.013)	0.999	0.001	0.430	0.974	0.026	0.570
141	1.000	0.000	0.925	-	-	-	0.776	0.224	0.075

Table 6-1 - Polyethylene/n-Hexane Flash Calculations.

P = 6 bar
M_{C6}, M_{PE} - mass fractions n-hexane and polyethylene respectively
Feed: 98.3 wt% n-hexane, 1.7 wt% polyethylene
30 node Hermitian quadrature integration

These results agree with the cloud and shadow point curve shown in Figure 5-3. At a feed composition of 1.7 wt% polyethylene, a single liquid phase splits into two liquids phases around 135.5 °C, while a liquid-vapour equilibrium is stable at temperatures above 139 °C. It should be noted that the liquid-liquid solution found in the flash corresponds to the left hand branch of the cloud point curve at 137 °C; the branch running next to the ordinate axis. This left hand branch was more readily found than the right hand branch because the right hand branch is closer to the critical point and results in very similar compositions between the two equilibrium phases. Additional work needs to be done on the initiation process in order to find the solutions which are closer to the critical point. The three phase compositions in the same reason are also close to the critical point and were not found with the algorithm as presented.

The effect of varying the damping factor in the successive substitution routine can be seen by examining the first 5 columns of Table 6-2. This table lists two numbers in each cell, the first number being the total iterations and the second number being the total

T (°C)	$m = 0.3$ $tol=10^{-12}$	$m = 0.5$ $tol=10^{-12}$	$m = 0.7$ $tol=10^{-12}$	$m = 0.8$ $tol=10^{-12}$	$m = 0.5$ $tol=10^{-4}$	$m = 0.5$ $tol=10^{-8}$	$m = 0.5$ $tol=10^{-10}$
120	38/0	21/0	NC	NC	15/9	19/1	20/1
127	39/0	21/0	30/0	NC	16/10	20/1	21/1
129	41/0	54/0	NC	136/0	16/10	35/1	38/1
133†	53/0	51/0	NC	NC	9/3	40/3	48/2
137†	2323/0	1390/0	238/0	NC	9/3	18/4	866/5
141	NC	60/0	67/0	49/0	NC	88/9	89/1

Table 6-2 - Iteration Counts for Flash Calculations.

(Total Iterations/Newton-Raphson Iterations)
P = 6 bar
†Newton-Raphson converged to only 2 phases. Solvent rich liquid phase not found.

m = successive substitution damping factor
tol = error at which Newton-Raphson iterations are started
NC = no convergence

number of Newton-Raphson iterations. In the case of the first five columns, the convergence criteria for the successive substitution procedure was set to $tol = 10^{-12}$ and no Newton-Raphson iterations were performed.

When the damping factor was 0.3 the iteration counts were higher than when the damping factor was 0.5. An exception to this occurs at 129 °C where the former damping factor resulted in 10 fewer iterations. At 141 °C, the lower damping factor resulted in no noticeable change in the residuals after 200 iterations and calculations were ceased. The generally higher iteration count when a damping factor of 0.3 was used instead of 0.5 is due to the smaller eigenvalues of the damped system. The majority of iteration counts occurred as the error was reduced from 10^{-10} to 10^{-12}, particularly in the system at 137 °C where the iteration count surpassed 1000.

At higher damping factors, the successive substitution algorithm tended to oscillate. The errors in the outer loop often jumped from low values to extremely high values. This instability is likely due to the larger eigenvalues of the damped system. When trials at the larger damping factor converged, they resulted in higher iteration counts than when a damping factor of 0.5 was used because of the oscillations.

When studying the Newton-Raphson procedure, a damping factor of 0.5 was used in the leading successive substitution procedure to ensure that it would converge to the specified tolerance, *tol*. After the successive substitution algorithm converged, the Newton-Raphson iterations were run until the error was less than 10^{-12}. As can be seen from the right three columns of Table 6-2, the iteration count using the Newton-Raphson procedure was usually significantly lower than when the successive substitution algorithm alone was used.

In general, the more that the tolerance on the successive substitution algorithm was relaxed (*tol* becomes larger), the less total iterations were needed to converge to a solution. The exception to this statement can be seen at a temperature of 141 °C where $tol = 10^{-4}$. In this case, the Newton-Raphson iterations moved away from the solution and resulted in errors on the order 10^{6} within 3 iterations. It is likely that the initial guess

when $tol = 10^{-4}$ was not close enough to the actual solution at this temperature to validate using a Newton-Raphson procedure. It can also be seen that the total number of iterations required when the Newton-Raphson procedure was used at 141 °C increased over the number of iterations when only the successive substitution procedure was used. The increase is deceptive because it is due to an increased number of successive substitution iterations, not due to Newton-Raphson iterations. The reason why the successive substitution procedure required more iterations to converge to a less stringent tolerance was not found.

The number of Newton-Raphson iterations was usually quite low, ranging from 1 to 10. More steps were required when the Newton-Raphson procedure was initiated further from the equilibrium solution. This low number of iterations shows the ability of a Newton-Raphson procedure to quickly converge to a solution where the successive substitution technique might take much longer. However, it should be noted that the Newton-Raphson procedure did not converge to the liquid incipient phase at 133 °C, nor to the stable solvent rich liquid phase at 137 °C. The missing phase may possibly be located if a line search along the Newton-Raphson step direction ensured that the Gibbs free energy of the system was minimized by constraining the Newton-Raphson step size. These options were not explored in this work.

6.4 Summary

A multiphase polymer flash algorithm was developed which used continuous thermodynamics to model the polymer. The equations were formulated such that either a successive substitution technique and/or a Newton-Raphson procedure could be used. Incipient phases could be tracked through the use of a stability variable incorporated into the segment fraction variables.

Successful multiphase flashes were performed for a disperse polyethylene/n-hexane system over a range of temperatures. These flashes illustrated liquid-liquid and liquid-vapour equilibrium, and showed the development of a stable vapour phase from an incipient one.

The successive substitution algorithm tended to be more reliable than the rudimentary Newton-Raphson algorithm used, but it was also much slower. As this was a preliminary investigation into multiphase polymer flashes, a lot of additional work needs to be done to optimize the use of both successive substitution and Newton-Raphson procedures. In particular, initiation procedures need to be developed to ensure that difficult polymer equilibrium near the critical points can be found using a flash routine. An additional area of future research is to develop a technique to ensure that a Newton-Raphson step does not needlessly eliminate a phase from consideration.

7. CONCLUSIONS AND RECOMMENDATIONS

7.1 Introduction

There were two distinct focuses of this dissertation. Chapters 2 and 3 examined multiphase reactive flash algorithms while chapters 4 through 6 looked at continuous thermodynamics in polymer phase equilibrium calculations. The objective was to provide background on the current tools available in each of these areas and to develop new tools which could be used.

7.2 Reactive Flash Calculations

Two non-ideal multiphase flash algorithms for chemically reacting systems were developed in chapter 2 and tested in chapter 3. The first of these used a stoichiometric approach to deal with the elemental balances and track species conversions. The second used a non-stoichiometric approach to ensure the conservation of elements. The novelty of these two techniques lies in their use of an average of the chemical potentials to define reference phase chemical potentials and their ability to track incipient phases throughout a calculation. Calculations were initiated with a maximum number of phases which were then reduced as phases became identical.

It was found that both of the two algorithms worked well to predict phase and reaction equilibrium in a system where methanol was produced from synthesis gas. A

SRK equation of state with conventional mixing rules was used to model each of the phases. The algorithms were tested over a range of pressures which resulted in either two or three phase solutions. The incipient phases were successfully located and tracked as pressure was varied and they became stable.

The computational time of these algorithms were similar over all the calculations compared, but the non-stoichiometric technique was better on average. If the system contains many more reactions than elements, the non-stoichiometric algorithm would be preferred due to the smaller number of equations. Conversely, if the number of elements is high and the number of reactions low, the stoichiometric algorithm would be the method of choice as it would use less equations.

The modified Heidemann-Kokal excess free energy mixing rule developed in Appendix A was used with the Soave-Redlich-Kwong equation of state and the non-stoichiometric reactive flash algorithm to calculate the chemical equilibrium in MTBE synthesis reactions. The excess free energy mixing rule used the Wilson activity coefficient model to calculate the equation of state *a* parameter and improve low pressure liquid-vapour equilibrium predictions. The reactive flash calculations were able to show the equilibrium conversions of methanol and isobutene to MTBE in the presence of n-butane over a range of initial feed compositions. The equilibrium results showed that by using the excess free energy mixing rule, the negative deviations from Raoult's Law could be calculated in the methanol/MTBE mixtures. The maximum production of MTBE occurred when the methanol and isobutene were reacted in stoichiometric proportions.

It was also shown that the non-stoichiometric algorithm could be used with an association model to adequately predict sulfur vapour pressures and enthalpies of vapourization. The association model defined reactions between the different allotropes of pure sulfur, S_1 to S_8, and allowed the pure component properties of each allotrope to be determined from the properties of S_8. Additionally, associations between hydrogen sulfide and sulfur to produce sulfanes were easily included in this model. Including the

lower molecular weight sulfanes, H_2S_2, H_2S_3 and H_2S_4, in solubility calculations, improved the predictions of sulfur solubility in hydrogen sulfide vapour

7.3 Continuous Thermodynamics and Polymer Phase Equilibria

The common method of dealing with a components like disperse polymers is to divide the continuous distribution into a set of pseudocomponents using Gaussian quadrature techniques (Cotterman and Prausnitz, 1985). The number of equations to be solved in a standard flash or cloud point problem increases as the number of quadrature points increases.

A set of 5 scalar equations in 5 scalar unknowns was developed to describe isobaric two phase equilibrium at a fixed phase fraction in a polymer/solvent system. The equations developed were specific to the Sanchez-Lacombe equation of state. The algorithm described to solve these equations allowed temperature-mass fraction curves of constant phase fraction to be traced. If the fixed phase fraction was 0 or 1, the curves corresponded to the shadow and cloud point curves.

It was found that the choice of the distribution function chosen to represent the polymer was an important factor in the predicted phase behaviour. When polydisperse polyethylene was modeled with a log-normal distribution, the Sanchez-Lacombe equation of state accurately predicted the lower precipitation threshold temperature of a polyethylene/n-hexane system when the interaction parameter was -0.1297. The predicted cloud and shadow point curves also showed an unstable critical point, a liquid-liquid-liquid point, a liquid-liquid-vapour point and a hypothetical high temperature liquid-vapour critical point. When a polymer with the same M_n and M_w was modeled with a Shultz-Flory distribution the liquid-liquid-liquid three phase point was not seen and the lower precipitation threshold temperature was 2.8 °C higher.

Using the same principles as were used to develop the reactive flash algorithm, a multiphase polymer flash routine was developed for use with continuous thermodynamics. The algorithm is different from other polymer/solvent equilibrium methods because of the average chemical potential used as a reference phase chemical

potential and its ability to track incipient phases. The equilibrium equations were developed for the Sanchez-Lacombe equation of state, and both a successive substitution and a full Newton-Raphson procedure were developed to solve these equations. In a limited study of the two solution techniques in polyethylene/n-hexane flash calculations, it was found that the successive substitution method was more reliable than the Newton-Raphson technique. If the Newton-Raphson technique was not initiated with values close to the final solution, it could diverge. When the Newton-Raphson solution step was used, equilibrium phases were incorrectly eliminated from the final solution.

7.4 Future Work

The reactive flash algorithms developed in chapter 2 need to be optimized. It is possible for both of the techniques to be rewritten using a complete Newton-Raphson solution procedure instead of a nested successive substitution procedure. The procedures can also be modified to include solid precipitation. A multiphase reactive flash algorithm with solids capability could be useful for reactions which produce solids such as asphaltene precipitation and liquid phase coking.

The primary problem with polymer phase equilibrium calculations is in generating a good initial guess from which to start the solution routines. This was seen in both the cloud and shadow point curve calculations and in the multiphase polymer flash algorithm. An important area of future research in polymer thermodynamics is to find generic algorithms capable of determining good initial guesses for flash routines.

Integration techniques used in the continuous thermodynamic procedures need to be examined and optimized for accuracy and speed.

The means by which the specification parameter in the cloud and shadow point curve algorithm is incremented needs to be studied. A better extrapolation could be utilized to improve the initial guess between consecutive cloud points. More importantly, an automated procedure needs to be developed to switch between optimum choices in the specification variable as the curves are being generated. The proposal given by Michelsen (1980) would be a good starting point to approach this problem.

Further work on the multiphase polymer flash algorithm needs to be done in order to determine the optimum way to utilize a Newton-Raphson step. Techniques such as trust region methods or line searches along the Newton-Raphson step vector may help improve the reliability and speed.

LITERATURE CITED

Abdel-Ghani, R.M., 1995. EOS Mixing Rules For Multi-Phase Behaviour. M.Sc. Thesis. University of Calgary, Calgary.

Abdel-Ghani, R.M., Phoenix, A.V. and Heidemann, R.A., 1994. An Approach to Multiphase Equilibrium Computation. Paper presented at the 1994 AIChE Conference, San Francisco, CA, 1994.

Abramowitz, M. and Stegun, I.A., 1972. Handbook of Mathematical Functions. Dover, New York.

Aris, R. and Gavalas, G.R., 1966. On the Theory of Reactions in Continuous Mixtures. *Philos. Trans. R. Soc.*, **A260**: 351-393.

Baker, L.E., Pierce, A.C. and Luks, K.D., 1982. Gibbs Energy Analysis of Phase Equilibria. *Soc. Pet. Eng. J.*, **22**: 731-742.

Barbosa, D. and Doherty, M.F., 1988. The Influence of Equilibrium Chemical Reactions on Vapour-Liquid Phase Diagrams. *Chem. Eng. Sci.*, **43**: 529-540.

Barr-David, F. and Dodge, B.F., 1959. Vapor-Liquid Equilibrium at High Pressures - The Systems Ethanol-Water and 2-Propanol-Water. *J. Chem. Eng. Data*, **4**: 107-121.

Boll, R.H., 1961. Calculation of Complex Equilibrium with an Unknown Number of Phases. *J. Chem. Phys.*, **34**: 1108-1110.

Boynton, F.P., 1960. Chemical Equilibrium in Multicomponent Polyphase Systems. *J. Chem. Phys.*, **32**: 1880-1881.

Brinkley, S.R., 1946. Note on the Conditions of Equilibrium for Systems of Many Constituents. *J. Chem. Phys.*, **14**: 563-564.

Brinkley, S.R., 1947. Calculation of the Equilibrium Composition of Systems of Many Constituents. *J. Chem. Phys.*, **15**: 107-110.

Brunner, E. and Woll, W., 1980. Solubility of Sulfur in Hydrogen Sulfide and Sour Gases. *SPE J.*, 377-384.

Butcher, K.L. and Medani, M.S., 1968. Thermodynamic Properties of Methanol-Benzene Mixtures at Elevated Temperatures. *J. Appl. Chem.*, **18**(4): 100-107.

Castier, M., Rasmussen, P. and Fredenslund, A., 1989. Calculation of Simultaneous Chemical and Phase Equilibria in Nonideal Systems. *Chem. Eng. Sci.*, **44**: 237-248.

Castillo, J and Grossmann, I.E., 1981. Computation of Phase and Chemical Equilibria. *Computers chem. Engng.*, **5**: 99-108.

Chen, C.-K., Duran, M.A. and Radosz, M., 1993. Phase Equilibria in Polymer Solutions. Block-Algrebra, Simultaneous Flash Algorithm Coupled with SAFT Equation of State, Applied to Single-Stage Supercritical Antisolvent Fractionation of Polyethylene. *Ind. Eng. Chem. Res.*, **32**: 3123-3127.

Cheney, E.W. and Kincaid, D.R., 1985. Numerical Mathematics and Computing. Second Edition. Brooks/Cole Publishing, Monterey, California.

Cisneros, E.S.P., Gani, R. and Michelsen, M.L., 1997. Reactive Separation Systems - I. Computation of Physical and Chemical Equilibrium. *Chem. Eng. Sci.*, **52**: 527-543.

Cotterman, R.L., Bender, R. and Prausnitz, J.M., 1985. Phase Equilibria for Mixtures Containing Very Many Components. Development and Application of Continuous Thermodynamics for Chemical Process Design. *Ind. Eng. Chem. Process Des. Dev.*, **24**: 194-203.

Cotterman, R.L. and Prausnitz, J.M., 1985. Flash Calculations for Continuous or Semicontinuous Mixtures Using an Equation of State. *Ind. Eng. Chem. Process Des. Dev.*, **24**: 434-443.

Cotterman, R.L., Chou, G.F. and Prausnitz, J.M., 1986. Comments on Flash Calculations for Continuous and Semi-continuous Mixtures Using an Equation of State. *Ind. Engng. Chem. Process Des. Dev.*, **25**: 840-841.

Cotterman, R.L. and Prausnitz, J.M., 1991. Continuous Thermodynamics for Phase-Equilibrium Calculations in Chemical Process Design. In Kinetic and Thermodynamic Lumping of Multicomponent Mixtures. G. Astarita and S.I. Sandler, Eds. Elsevier Science Publishers, Amsterdam, The Netherlands.

Cruise, D.R., 1964. Notes on the Rapid Computation of Chemical Equilibria. *J. Phys. Chem.*, **68**: 3797-3802.

Dahl, S. and Michelsen, M.L., 1990. High-pressure Vapor-liquid Equilibrium with a UNIFAC-based Equation of State. *AIChE J.*, **36**: 1829-1836.

DeGarmo, J.L., Parulekar, V.N. and Pinjala, V., 1992. Consider Reactive Distillation. *Chem. Eng. Prog.*, **88**(3): 43-50.

DIPPR (Design Institute for Physical Property Data), 1984. *Data Compilation Tables of Properties of Pure Components*. Daubert, T.E. and Danner, R.P., Editors. AIChE, New York.

Doherty, M.F. and Buzad, G., 1992. Reactive Distillation By Design. *Trans IChemE*, **70A**: 448-458.

Du, P.C. and Mansoori, G.A., 1986. Phase Equilibrium Computational Algorithms of Continuous Mixtures. *Fluid Phase Equilibria*, **30**: 57-64.

Fletcher, R., 1981. Practical Methods of Optimization. Volume 2: Constrained Optimization. John Wiley & Sons, USA.

Fraleigh, J.B. and Beauregard, R.A., 1990. Linear Algebra. Second Edition. Addison-Wesley Publishing Company, New York.

George, B., Brown, L.P., Farmer, C.H., Buthod, P. and Manning, F.S., 1976. Computation of Multicomponent, Multiphase Equilibrium. *Ind. Eng. Chem. Process Des. Devel.*, **15**: 372-377.

Gibbs, J.W., 1876. On the Equilibrium of Heterogeneous Substances. *Trans. Conn. Acad.*, **3**: 108-248. As reprinted in The Scientific Papers of J. Willard Gibbs, Vol. 1, Dover, New York, 1961.

Gmehling, J. and Onken, U., 1977. *DECHEMA Chemistry Data Series, Vol. I, Part 1. Aqueous-Organic Systems*. DECHEMA, Frankfurt am Main, FRG.

Gmehling, J. and Onken, U., 1977. *DECHEMA Chemistry Data Series, Vol. I, Part 2a. Organic Hydroxy Compounds*. DECHEMA, Frankfurt am Main, FRG.

Gordon, S. and McBride, B., 1971. Computer Program for Calculation of complex Chemical Equilibrium Compositions, Rocket Performance, Incident and Reflected Shocks, and Chapman-Jouget Detonations. NASA SP-273.

Greiner, H., 1991. An Efficient Implementation of Newton's Method for Complex Nonideal Chemical Equilibria. *Computers chem. Engng*, **15**: 115-123.

Griswold, J. and Wong, S.Y., 1952. Phase Equilibria of the Acetone-Methanol-Water System From 100°C Into the Critical Region. *AIChE Symp. Ser.*, **48**: 18-34.

Gupta, A., Bishnoi, P.R. and Kalogerakis, N., 1991. A Method For The Simultaneous Phase Equilibria and Stability Calculations For Multiphase Reacting and Non-Reacting Systems. *Fluid Phase Equilibria*, **63**: 65-89.

Heidemann, R.A. and Kokal, S.L., 1990. Combined Excess Free Energy Models and Equations of State. *Fluid Phase Equilibria*, **56**: 17-37.

Heidemann, R.A., 1996. Excess Free Energy Mixing Rules for Cubic Equations of State. *Fluid Phase Equilibria*, **116**: 454-464.

Heidemann, R.A. and Michelsen, M.L., 1995. Instability of Successive Substitution. *Ind. Eng. Chem. Res.*, **34**: 958-966.

Heidemann, R.A. and Prausnitz, J.M., 1976. A van der Waals-type equation of state for fluids with associating molecules. *Proc. Natl. Acad. Sci. USA*, **73**: 1773-1776.

Heidemann, R.A. and Rizvi, S.S.H., 1986. Correlation of Ammonia-Water Equilibrium Data with Various Modified Peng-Robinson Equations of State. *Fluid Phase Equilibria*, **29**: 439-446.

Hendriks, E.M., 1987. Simplified Phase Equilibrium Equations for Multicomponent Systems. *Fluid Phase Equilibria*, **33**: 207-221.

Hendriks, E.M., Walsh, J., and van Bergen, A.R.D., 1997. A General Approach to Association Using Cluster Partition Functions. *J. Stat. Phys.*, **87**: 1287-1306.

Hildebrandt, D. and Glasser, D., 1994. Predicting Phase and Chemical Equilibrium Using the Convex Hull of the Gibbs Free Energy. *Chem. Eng. Journal*, **54**: 187-197.

Hu, Y., Ying, X., Wu, D.T. and Prausnitz, J.M., 1993. Liquid-Liquid Equilibria for Solutions of Polydisperse Polymers. Continuous Thermodynamics for the Close-Packed Lattice Model. *Macromolecules*, **26**: 6817-6823.

Hu, Y., Ying, X., Wu, D.T. and Prausnitz, J.M., 1995. Continuous Thermodynamics for Polydisperse Polymer Solutions. *Fluid Phase Equilibria*, **104**: 229-252.

Huff, V.N., Gordon, S. and Morrell, V.E., 1951. General Method and Thermodynamic Tables for Computation of Equilibrium Composition and Temperature of Chemical Reactions. *Nat'l Adv. Committee Aeronautics (NACA) Report 1037.*

Huron, M.-J. and Vidal, J., 1979. New Mixing Rules in Simple Equations of State For Representing Vapour-Liquid Equilibria of Strongly Non-Ideal Mixtures. *Fluid Phase Equilibria*, **3**: 255-271.

Hyne, J.B., Muller, E. and Wiewiorowski, T.K., 1966. Nuclear Magnetic Resonance of Hydrogen Polysulfides in Molten Sulfur. *J. Phys. Chem.*, **70**: 3733-3735.

Jacobs, R. and Krishna, R., 1993. Multiple Solutions in Reactive Distillation for Methyl *tert*-Butyl Ether Synthesis. *Ind. Eng. Chem. Res.*, **32**: 1706-1709.

JANAF Thermochemical Tables, 1985. *J. Phys. Chem. Ref. Data*, **14**, Supplement 1.

Jiang, Y., Chapman, G.R. and Smith, W.R., 1996. On the Geometry of Chemical Reaction and Phase Equilibria. *Fluid Phase Equilibria*, **118**: 77-102.

Kandiner, H.J. and Brinkley, S.R., 1950. Calculation of Complex Equilibrium Relations. *Ind. Eng. Chem.*, **42**: 850-855.

Karan, K., Heidemann, R.A. and Behie, L.A., 1998. Sulfur Solubility in Sour Gas: Predictions with an Equation of State Model. *Ind. Eng. Chem. Res.*, **37**: 1079-1684.

Kehlen, H., Rätzsch, M.T. and Bergmann, J., 1985. Continuous Thermodynamics of Multicomponent Systems. *AIChE J.*, **31**: 1136-1148.

Kennis, H.A.J., 1990. The Influence of Nitrogen on the Phase Behaviour of the System n-Hexane/Linear High Density Polyethylene. Thesis. Technical University of Delft, Delft, The Netherlands.

Kincaid, J.M., MacDonald, R.A. and Morrison, G., 1987. A Thermodynamic Perturbation Theory for Multicomponent and Polydisperse Mixtures. *J. Chem. Phys.*, **87**: 5425-5436.

Kiszka, M.B., Meilchen, M.A. and McHugh, M.A., 1988. Modeling High-Pressure Gas-Polymer Mixtures Using the Sanchez-Lacombe Equation of State. *J. Appl. Poly. Sci.*, **36**: 583-597.

Koak, N. and Heidemann, R.A., 1996. Polymer-Solvent Phase Behavior near the Solvent Vapor Pressure. *Ind. Eng. Chem. Res.*, **35**: 4301-4309.

Koak, N., 1997. Polymer Solution Phase Behaviour. Ph.D. Thesis. University of Calgary, Calgary.

Koak, N., 1998. Personal communication.

Kolár, P. and Kojima, K., 1993. Prediction of Vapor-Liquid Equilibria by Using Equations of State with Zero-pressure Excess Gibbs Energy Mixing Rules: the RKU2 Model for Moderate Temperatures. *J. Chem. Eng. Japan*, **26**: 166-172.

Kosinski, J.J. and Anderko, A., 1996. An Algorithm for Multiphase Equilibrium Calculations for Systems Containing Polymers. *Fluid Phase Equilibria*, **117**: 11-17.

Kramarz, J. and Wyczesany, A., 1993. Development and Application of Continuous Thermodynamics for Complex Chemical Equilibria Calculations. *Chem. Eng. Sci.*, **48**: 1665-1673.

Krieger, F.J. and White, W.B., 1948. A Simplified Method for Computing the Equilibrium Composition of Gaseous Systems. *J. Chem. Phys.*, **16**: 358-360.

Lira-Galeana, C., Najera-Blanco, A. and Ponce-Ramirez, L., 1991. Comments on "Asymptotic Effects Using Semicontinuous vis-à-vis Discrete Description in Phase Equilibrium Computations". *Ind. Eng. Chem. Res.*, **30**: 2360-2362.

Liu, J.L. and Wong, D.S.H., 1997. Rigorous Implementation of Continuous Thermodynamics Using Orthonormal Polynomials. *Fluid Phase Equilibria*, **129**: 113-127.

Luks, K.D., Turek, E.A. and Kragas, T.K., 1990. Asymptotic Effects Using Semicontinuous vis-à-vis Discrete Description in Phase Equilibrium Computations. *Ind. Eng. Chem. Res.*,**29**: 2101-2106.

Marsh, K.N. (Director), 1985. TRC Thermodynamic Tables, Thermodynamics Research Center, College Station, Texas.

Mather, A.E., 1986. Phase Equilibria and Chemical Reaction. *Fluid Phase Equilibria*, **30**: 83-100.

McDonald, C.M. and Floudas, C.A., 1995. Global Optimization For the Phase and Chemical Equilibrium Problem: Application to the NRTL Equation. *Computers chem. Engng.*, **19**: 1111-1139.

Michelsen, M.L., 1980. Calculation of Phase Envelopes and Critical Points for Multicomponent Mixtures. *Fluid Phase Equilibria*, **4**: 1-10.

Michelsen, M.L., 1982a. The Isothermal Flash Problem. Part I. Stability. *Fluid Phase Equilibria*, **9**: 1-19.

Michelsen, M.L., 1982b. The Isothermal Flash Problem. Part II. Phase-Split Calculation. *Fluid Phase Equilibria*, **9**: 21-40.

Michelsen, M.L., 1989. Calculation of Multiphase Ideal Solution Chemical Equilibrium. *Fluid Phase Equilibria*, **53**: 73-80.

Michelsen, M.L., 1990a. A Method for Incorporating Excess Gibbs Energy Models in Equations of State. *Fluid Phase Equilibria*, **60**: 47-58.

Michelsen, M.L., 1990b. A Modified Huron-Vidal Mixing Rule for Cubic Equations of State. *Fluid Phase Equilibria*, **60**: 213-219.

Michelsen, M.L., 1994. Calculation of Multiphase Equilibrium. *Computers chem. Engng*, **18**: 545-550.

Michelsen, M.L. and Heidemann, R.A., 1996. Some Properties of Equation of State Mixing Rules Derived From Excess Gibbs Energy Expressions. *Ind. Eng. Chem. Res.*, **35**: 278-287.

Mollerup, J., 1986. A Note on the Derivation of Mixing Rules From Excess Gibbs Energy Models. *Fluid Phase Equilibria*, **25**: 323-326.

Murray, W., 1972. Second Derivative Methods. In Numerical Methods for Unconstrained Minimization, W. Murray (Ed.). Academic Press, London. pp. 57-71.

Myers, A.K. and Myers, A.L., 1986. Numerical Solution of Chemical Equilibria With Simultaneous Reactions. *J. Chem. Phys.*, **84**: 5787-5795.

Okasinski, M.J. and Doherty, M.F., 1997. Thermodynamic Behaviour of Reactive Azeotropes. *AIChE J.*, **43**: 2227-2238.

Patel, N.C. and Teja, A.S., 1982. A New Cubic Equation of State for Fluids and Fluid Mixtures. *Chem. Eng. Sci*, **37**: 463-473.

Peng, D.-Y., Wu., R.S. and Batycky, J.P., 1987. Application of Continuous Thermodynamics to Oil Reservoir Fluid Syststems Using an Equation of State. *AOSTRA J. Res.*, **3**: 113-122.

Press, W.H., Teukolsky, S.A., Vetterling, W.T. and Flannery, B.P., 1992. Numerical Recipes in C - The Art of Scientific Computing. Second Edition. Cambridge University Press, Cambridge.

Rachford, H.H. Jr. and Rice, J.D., 1952. Procedure For Use of Electronic Digital Computers in Calculating Flash Vaporization Hydrocarbon Equilibrium. *J. Petrol. Technol.*, **195**: October, Section 1: page 19, Section 2: page 3.

Rätzsch, M.T., 1989. Continuous Thermodynamics. *Pure & Appl. Chem.*, **61**: 1105-1114.

Rätzsch, M.T. and Kehlen, H., 1985. Continuous Thermodynamics of Polymer Solutions: The Effect of Polydispersity on the Liquid-Liquid Equilibrium. *J. Macr. Sci. - Chem.*, **A22**: 323-334.

Rätzsch, M.T., Kehlen, H. and Thieme, D., 1986. Polymer Compatibility by Continuous Thermodynamics. *J. Macr. Sci. - Chem.*, **A23**: 811-822.

Rätzsch, M.T. and Kehlen, H., 1989. Continuous Thermodynamics of Polymer Systems. *Prog. Polym. Sci.*, **14**: 1-46.

Rätzsch, M.T., Wohlfarth, C., Browarzik, D. and Kehlen, H., 1989. Liquid-Liquid Equilibrium in Polydisperse Random copolymer Blends. *J. Macr. Sci. - Chem.*, **A26**: 1497-1523.

Rau, H., Kutty, T.R.N. and Guedes de Carvalho, J.R.F., 1973. High Temperature Saturated Vapour Pressure of Sulphur and the Estimation of its Critical Quantities. *J. Chem. Thermodynamics*, **5**: 291-302.

Reid, R.C., Prausnitz, J.M. and Poling, B.E., 1985. The Properties of Gases and Liquids. McGraw Hill, USA.

Salim, P.H. and Trebble, M.A., 1991. A Modified Trebble-Bishnoi Equation of State: Thermodynamic Consistency Revisited. *Fluid Phase Equilibria*, **65**: 59-71.

Sako, T. Wu, A.H. and Prausnitz, J.M., 1989. A Cubic Equation of State for High-Pressure Phase Equilibria of Mixtures Containing Polymers and Volatile Fluids. *J. Appl. Polym. Sci.*, **38**: 1839-1858.

Sanchez, I.C. and Lacombe, R.H., 1976. An Elementary Molecular Theory of Classical Fluids. Pure Fluids. *J. Phys. Chem.*, **80**: 2352-2362.

Sanchez, I.C. and Lacombe, R.H., 1978. Statistical Thermodynamics of Polymer Solutions. *Macromolecules*, **11**: 1145-1156.

Sanderson, R.V. and Chien, H.H., 1973. Simultaneous Chemical and Phase Equilibrium Calculation. *Ind. Eng. Chem. Process Des. Develop.*, **12**: 81-85.

Satyro, M.A. and Trebble, M.A., 1996. On the Applicability of the Sandler-Wong Mixing Rules for the Calculations of Thermodynamic Excess Properties - V^E, H^E, S^E and C_p^E. *Fluid Phase Equilibria*, **115**: 135-164.

Seider, W.D., Gautam, R. and White, C.W. III, 1980. Computation of Phase and Chemical Equilibrium: A Review. In Computer Applications to Chemical

Engineering Process Design and Simulation, R.G. Squires and G.V. Reklaitis (Eds.), *American Chemical Society Symposium Series*, **124**: 115-134.

Seider, W.D. and Widagdo, S., 1996. Multiphase Equilibria of Reactive Systems. *Fluid Phase Equilibria*, **123**: 283-303.

Schlijjper, A.G., 1987. Flash Calculations For Polydisperse Fluids: A Variational Approach. *Fluid Phase Equilibria*, **34**: 149-169.

Shibata, S.K., Sandler, S.I. and Behrens, R.A., 1987. Phase Equilibrium Calculations for Continuous and Semicontinuous Mixtures. *Chem. Eng. Sci.*, **42**: 1977-1988.

Smith, J.V., Missen, R.W. and Smith, W.R., 1993. General Optimality Criteria for Multiphase Multireaction Chemical Equilibrium. *AIChE J.*, **39**: 707-710.

Smith, W.R., 1980. The Computation of Chemical Equilibrium in Complex Systems. *Ind. Eng. Chem. Fundam.*, **19**: 1-10.

Smith, W.R. and Missen, R.W., 1968. Calculating Complex Chemical Equilibria by an Improved Reaction Adjustment Method. *Can. J. Chem. Eng.*, **46**: 269-272.

Smith, W.R. and Missen, R.W., 1982. Chemical Reaction Equilibrium Analysis: Theory and Algorithms. John Wiley, New York.

Smith, W.R. and Missen, R.W., 1988. Strategies for Solving the Chemical Equilibrium Problem and an Efficient Microcomputer-Based Algorithm. *Can. J. Chem. Eng.*, **66**: 591-598.

Soave, G., 1986. Infinite-Pressure Excess Functions and VLE *K* Values From Liquid-Phase Activity Coefficients. *Fluid Phase Equilibria*, **31**: 147-152.

Šolc, K., 1970. Cloud-Point Curves of Polymers Solutions. *Macromolecules*, **3**: 665-673.

Šolc, K., 1975. Cloud-Point Curves of Polymers with Logarithmic-Normal Distribution of Molecular Weight. *Macromolecules*, **8**: 819-827.

Tapia, R.A., 1971. The Differentiation and Integration of Nonlinear Operators. In Nonlinear Functional Analysis and Applications, L.B. Rall (Ed.), Academic Press, London, 45-101.

Trebble, M.A. and Bishnoi, P.R., 1987. Development of a New Four-Parameter Cubic Equation of State. *Fluid Phase Equilibria*, **35**: 1-18.

Tsonopoulos, C. and Wilson, G.M., 1983. High-Temperature Mutual Solubilities of Hydrocarbons and Water. Part I: Benzene, Cyclohexane and n-Hexane. *AIChE Journal*, **29**: 990-999.

Ung, S. and Doherty, M.F., 1995. Vapor-Liquid Phase Equilibrium in Systems With Multiple Chemical Reactions. *Chem. Eng. Sci.*, **50**: 23-48.

van Zeggeren, F. and Storey, S.H., 1970. The Computation of Chemical Equilibria, Cambridge University Press, Cambridge.

Villars, D.S., 1959. A Method of Successive Approximations for Computing Combustion Equilibria on a High Speed Digital Computer. *J. Phys. Chem.*, **63**: 521-525.

West, W.A. and Menzies, A.W.C., 1929. The Vapor Pressures of Sulfur between 100° and 550° with the Related Thermal Data. *J. Phys. Chem.*, **33**: 1880-1892.

West, J.R., 1950. Thermodynamic Properties of Sulfur. *Ind. Eng. Chem.*, **42**: 713-718.

White, W.B., Johnson, S.M. and Dantzig, G.B., 1958. Chemical Equilibrium in Complex Mixtures. *J. Chem. Phys.*, **28**: 751-755.

Willman, B.T. and Teja, A.S., 1986. Continuous Thermodynamics of Phase Equilibria Using a Multivariate Distribution Function and an Equation of State. *AIChE J.*, **32**: 2067-2078.

Willman, B.T. and Teja, A.S., 1987a. Prediction of Dew Points of Semicontinuous Natural Gas and Petroleum Mixtures. 1. Characterization by Use of an Effective Carbon Number and Ideal Solution. *Ind. Eng. Chem. Res.*, **26**: 948-952.

Willman, B.T. and Teja, A.S., 1987b. Prediction of Dew Points of Semicontinuous Natural Gas and Petroleum Mixtures. 1. Nonideal Solution Calculations. *Ind. Eng. Chem. Res.*, **26**: 953-957.

Xiao, W., Zhu, K., Yuan, W. and Chien, H.H., 1989. An Algorithm for Simultaneous Chemical and Phase Equilibrium Calculation. *AIChE J.*, **35**: 1813-1820.

Ying, X., Ye., R. and Hu, Y., 1989. Phase Equilibria for Complex Mixtures. Continuous-Thermodynamics Method Based on Spline Fit. *Fluid Phase Equilibria*, **53**: 407-414.

Zeleznik, F.J. and Gordon, S., 1968. Calculation of Complex chemical Equilibria. *Ind. Eng. Chem.*, **60**(6): 27-57.

APPENDIX A - DEVELOPMENT OF THE G^E MIXING RULE

A.1 Introduction

A four parameter equation of state allows a greater flexibility in matching pure component data than a two parameter equation of state. Trebble and Bishnoi (1987) have proposed a four parameter, cubic equation of state, the TB equation of state shown in equation (A.1), which matches pure component data well.

$$P = \frac{RT}{v-b} - \frac{a}{v^2 + (b+c)v - \left(bc + d^2\right)} \tag{A.1}$$

An advantage of this equation of state is that it easily reduces to many of the familiar two or three parameter equations of state. For example, if c=-b and d=b, the van der Waals equation of state results; if c=b and d=0, you get the Peng-Robinson equation of state; if c=d=0, it reduces to the Redlich-Kwong equation of state, and if d=0, the TB equation of state yields the three parameter Patel-Teja equation of state (1982).

When applying an equation of state to mixtures, each of the parameters needs to be determined from the pure component parameters and mole fractions. Work has been done to establish various different types of mixing rules for each parameter. One technique which shows a great potential for giving good mixture behaviour is to use the a

parameter to match excess Gibbs energy as given by an activity coefficient model, such as the NRTL model, at the system temperature.

There have been many papers describing excess free energy mixing rules for two parameter, cubic equations of state, and a review of the literature has been compiled by Heidemann (1995). Huron and Vidal (1979) matched the excess free energies from an activity coefficient model and the modified Redlich-Kwong equation of state at infinite pressure. Since excess free energy models are correlated at low to medium pressures and the Huron-Vidal type mixing rule needs accurate activity coefficients at infinite pressure, Soave (1986) presented a method of estimating infinite pressure activity coefficients for use with these mixing rules. Mollerup (1986) first outlined the alternative route of using a low (or zero) pressure reference state to combine an activity coefficient model with the van der Waals and Redlich-Kwong equations of state. Heidemann and Kokal (1990) presented a zero pressure, excess free energy mixing rule for the van der Waals, Redlich-Kwong and Peng-Robinson equations of state which involved solving a transcendental equation for the mixture reference state. Their method also required an extrapolation for the pure component reference states if the component's reduced temperature was above about 0.85. Other zero pressure excess free energy mixing rules have been proposed by numerous authors such as, but not limited to, Dahl and Michelsen (1990), Michelsen (1990a, 1990b), and Kolár and Kojima (1993). All of the zero pressure excess free energy mixing rules have matched experimental data well at the low pressures where the activity models used were correlated, but their success at higher pressures has varied. Michelsen and Heidemann (1995) have compiled a detailed criticism of the performance of the different excess free energy mixing rules. There has been no published work for similar excess free energy mixing rules incorporated into four parameter, cubic equations of state.

In this appendix, the Heidemann-Kokal mixing rules are extended to the four parameter TB equation of state. As with two parameter equations of state, the mixing rule is "exact" at lower temperatures but must use an extrapolation at higher temperatures. The extrapolation proposed by Heidemann and Kokal (1990) results in a

transcendental equation with no solution at high temperatures or in systems with large positive excess free energies. Therefore, a new high temperature extrapolation is proposed which will alleviate this computational problem. As well, the form of the TB EOS of state dictates that this development of the Heidemann-Kokal mixing rule for the TB EOS given will also yield the equations required for all the other equations of state which are a subset of the TB equation of state.

A.2 Theory

A.2.1 Standard States

A zero pressure liquid volume root must be found for each pure component. These volume roots represent the standard states of the pure components and can only be calculated from equation (A.1) when:

$$\left(\frac{a_i}{b_i RT}-\frac{c_i}{b_i}-1\right)^2 \geq 4\left(\frac{a_i}{b_i RT}-\frac{c_i}{b_i}-\left(\frac{d_i}{b_i}\right)^2\right) \tag{A.2}$$

A dimensionless zero pressure standard state density for each component is defined as $\xi_i = b_i/v_i$. ξ_i can be found from (A.1) at zero pressure as long as (A.2) is satisfied:

$$\xi = \frac{b_i}{v_i} = \frac{\alpha_i - \frac{c_i}{b_i} - 1 + \sqrt{\left(\alpha_i - \frac{c_i}{b_i} - 1\right)^2 - 4\left(\alpha_i - \frac{c_i}{b_i} - \left(\frac{d_i}{b_i}\right)^2\right)}}{2\left(\alpha_i - \frac{c_i}{b_i} - \left(\frac{d_i}{b_i}\right)^2\right)} \tag{A.3}$$

where $\alpha_i = a_i/b_i RT$.

In terms of the compressibility, $h_i = Pv_i/RT$, the zero pressure condition for pure components is:

$$h_i(\xi_i) = \frac{1}{1-\xi_i} - \frac{\alpha_i \xi_i}{1 + \xi_i + \xi_i \frac{c_i}{b_i} - \xi_i^2 \frac{c_i}{b_i} - \xi_i^2 \left(\frac{d_i}{b_i}\right)^2} = 0 \qquad \text{(A.4)}$$

In the case where the zero pressure liquid root does not exist for a pure component, a root can be extrapolated in the same manner by which Heidemann and Kokal (1990) extrapolated one. From equation (A.2), the minimum value of α_i where a liquid root may be found is

$$\alpha_i = 3 + \frac{c_i}{b_i} + 2\sqrt{2 - \left(\frac{d_i}{b_i}\right)^2} \qquad \text{(A.5)}$$

For computational purposes extrapolations will be done when a pure component α value falls below the limiting α value, $\alpha_{i,\lim}$, which will be taken as λ times the minimum as determined from equation (A.5).

$$\alpha_{i,\lim} = \lambda\left(3 + \frac{c_i}{b_i} + 2\sqrt{2 - \left(\frac{d_i}{b_i}\right)^2}\right) \qquad \text{(A.6)}$$

Heidemann and Kokal (1990) suggested 1.15 as an appropriate value for λ, and this same value is again recommended in this work.

For α_i values less than this limiting value, a standard state extrapolation is accomplished by assuming that at $\alpha_i < \alpha_{i,lim}$, the dimensionless standard state densities of the pure component can be approximated by

$$\xi_i(\alpha) = 1 + \beta\alpha^2 + \chi\alpha^3. \qquad \text{(A.7)}$$

The values of β and χ can be found by matching the values of ξ_i and $(\partial\xi_i/\partial\alpha_i)$ as determined from equations (A.3) and (A.7) at $\alpha_i = \alpha_{i,lim}$. That is,

$$\beta = \left[3(\psi_1 - 1) - \psi_2\alpha_{i,\lim}\right]/\alpha_{i,\lim}^2 \qquad \text{(A.8)}$$

$$\chi = -\left[2(\xi_1 - 1) - \psi_2\alpha_{i,\lim}\right]/\alpha_{i,\lim}^3 \qquad \text{(A.9)}$$

where $\psi_1 = \xi_i(\alpha_{i,lim})$ as evaluated by equation (A.3),

$$\psi_2 = \left(\frac{\partial \xi_i}{\partial \alpha_i}\right)\Bigg|_{\alpha_i=\alpha_{i,\lim}} = \left\{\frac{1+\vartheta(\alpha)^{-1/2}\left(\alpha-\frac{c}{b}-3\right)}{2\alpha-2\frac{c}{b}-2\left(\frac{d}{b}\right)^2} - \frac{2\left(\alpha-\frac{c}{b}-1+\vartheta(\alpha)^{1/2}\right)}{\left(2\alpha-2\frac{c}{b}-2\left(\frac{d}{b}\right)^2\right)^2}\right\}\Bigg|_{\alpha=\alpha_{i,\lim}} \quad ,(A.10)$$

and

$$\vartheta(\alpha) = \alpha^2 - 2\alpha\frac{c}{b} + 6\frac{c}{b} + \left(\frac{c}{b}\right)^2 - 6\alpha + 4\left(\frac{d}{b}\right)^2 + 1. \qquad (A.11)$$

The form of equation (A.7) ensures that ξ_i will reflect the Huron-Vidal assumption that $v_i = b_i$ at infinite pressure, and it should be noted that by using an extrapolated standard state, h_i as defined by equation (A.4) does not equal zero.

Having determined the standard state α_i and ξ_i values, the standard state of the mixture can be determined.

A.2.2 Development of the Standard State Transcendental Equations

The excess Helmholtz free energy for an equation of state can be shown to be

$$\frac{\Delta A^E}{RT} = I_m - \sum_{i=1}^{C} x_i\left\{I_i + \ln\left(\frac{v}{v_i}\right)\right\} \qquad (A.12)$$

where

$$I = \int_v^\infty \left(\frac{P}{RT} - \frac{1}{v}\right)dv \qquad (A.13)$$

and the subscript m refers to the mixture properties and the subscript i refers to the pure component properties.

For the TB equation of state, if

$$\delta = 1 + 6\frac{c}{b} + \left(\frac{c}{b}\right)^2 + 4\left(\frac{d}{b}\right)^2 \tag{A.14}$$

then, in the standard states, I is of the form

$$I = \ln\left(\frac{1}{1-\xi}\right) - \alpha\xi g \tag{A.15}$$

where if $\delta > 0$:

$$\xi g = \frac{1}{\sqrt{\delta}} \ln\left(\frac{2 + \left[1 + \frac{c}{b} + \sqrt{\delta}\right]\xi}{2 + \left[1 + \frac{c}{b} - \sqrt{\delta}\right]\xi}\right) \tag{A.16}$$

and if $\delta < 0$:

$$\xi g = \frac{-1}{\sqrt{-\delta}} \left\{ 2\tan^{-1}\left(\frac{2 + \left[1 + \frac{c}{b}\right]\xi}{\xi\sqrt{-\delta}}\right) - \pi \right\} \tag{A.17}$$

Assuming that the excess Helmholtz free energy and the excess Gibbs free energy are equal in the zero pressure standard state, by combining equations (A.12), (A.13) and (A.15)

$$\frac{\Delta G^E}{RT} = \frac{\Delta A^E}{RT} = -\ln\left(\frac{1-\xi}{\xi}\right) - \alpha\xi g + \sum_{i=1}^{C} x_i\left(\alpha_i \xi_i g_i\right) - \sum_{i=1}^{C} x_i \ln\left(\frac{b}{b_i}\right) + \sum_{i=1}^{C} x_i \ln\left(\frac{1-\xi_i}{\xi_i}\right) \tag{A.18}$$

where equations (A.16) and (A.17) define ξg and $\xi_i g_i$ when either the mixture parameters or the pure component parameters, respectively, are used.

$$h(\xi) = \sum_{i=1}^{C} h_i(\xi_i) \tag{A.19}$$

Heidemann and Kokal (1990) used equation (A.19) to force the mixture standard state Helmholtz and Gibbs free energies to be identical and used equations (A.18) and

(A.19) as two equations with two unknowns, α and ξ. Since both equations are linear with respect to α, α could be eliminated between them to give:

$$f(\xi) = \left[1 + \xi + \xi\frac{c}{b} - \xi^2\frac{c}{b} - \xi^2\left(\frac{d}{b}\right)^2\right] g\left[\frac{1}{1-\xi} - \sum_{i=1}^{C} x_i h_i\right] + \ln\left(\frac{1-\xi}{\xi}\right)$$

$$= \frac{-\Delta G^E}{RT} + \sum_{i=1}^{C} x_i \left\{\alpha_i \xi_i g_i + \ln\left(\frac{1-\xi_i}{\xi_i}\right) + \ln\left(\frac{b_i}{b}\right)\right\} \qquad \text{(A.20)}$$

Given an expression for the excess free energy of a mixture and provided a solution exists, this transcendental equation could be solved for ξ using a Newton-Rhapson scheme. The solution exists if the right hand side of equation (A.20) is greater than the minimum possible value of the left hand side, f_{min}. f_{min} is dependent upon x_i, h_i, b, c and d, and Heidemann and Kokal (1990) give approximate expressions for the f_{min} values of some two parameter equations of state. The right hand side is largely dependent upon the non-ideality of the mixture. In fact, for systems with large positive deviations from Raoult's law, no solution to equation (A.20) may exist, especially at higher temperatures where lower α_i values and lower ξ_i values can significantly decrease the value of the equation's right hand side.

To eliminate the hazard of potentially having no solution for the mixture ξ, an alternative method for determining α and ξ has been developed. An extrapolation for the mixture ξ value is used which mirrors the extrapolation for the pure component standard state ξ_i values and which simultaneously solves for the mixture α value.

The two equations which can be used to determine the mixture ξ and α parameters when $\alpha > \alpha_{lim}$ are

$$f_1(\alpha, \xi) = \alpha\xi g + \ln\left(\frac{1-\xi}{\xi}\right) + \frac{\Delta G^E}{RT} - \sum_{i=1}^{C} x_i \left\{\alpha_i \xi_i g_i + \ln\left(\frac{1-\xi_i}{\xi_i}\right) + \ln\left(\frac{b_i}{b}\right)\right\} = 0 \qquad \text{(A.21)}$$

and

$$f_2(\alpha,\xi) = 1+\xi\left(1+\frac{c}{b}\right)-\xi^2\left(\frac{c}{b}-\left(\frac{d}{b}\right)^2\right)-\alpha\xi(1-\xi) = 0. \qquad \text{(A.22)}$$

While if α is less than α_{lim}, when α_{lim} is defined as

$$\alpha_{\lim} = \lambda\left(3+\frac{c}{b}+2\sqrt{2-\left(\frac{d}{b}\right)^2}\right), \qquad \text{(A.23)}$$

then

$$f_2(\alpha,\xi) = \xi-\left(1+\beta\alpha^2+\chi\alpha^3\right) = 0. \qquad \text{(A.24)}$$

In equation (A.23), λ is a scaling factor used to move the limiting α value away from the critical value, and β and χ are as defined by equations (A.8) through (A.11).

Compactly, the new set of two equations in two unknowns, ξ and α, can be written

$$f_1(\alpha,\xi) = \alpha\xi g+\ln\left(\frac{1-\xi}{\xi}\right)+\frac{\Delta G^E}{RT}-\sum_{i=1}^{C}x_i\left\{\alpha_i\xi_i g_i+\ln\left(\frac{1-\xi_i}{\xi_i}\right)+\ln\left(\frac{b_i}{b}\right)\right\} = 0 \qquad \text{(A.25)}$$

$$f_2(\alpha,\xi) = \begin{cases} 1+\xi\left(1+\dfrac{c}{b}\right)-\xi^2\left(\dfrac{c}{b}-\left(\dfrac{d}{b}\right)^2\right)-\alpha\xi(1-\xi) = 0 & ;\ \alpha \geq \alpha_{\lim} \\ \xi-\left(1+\beta\alpha^2+\chi\alpha^3\right) = 0 & ;\ \alpha < \alpha_{\lim} \end{cases}. \qquad \text{(A.26)}$$

To solve equations (A.25) and (A.26), a Newton-Rhapson procedure can be used with initial guesses for ξ and α given by equations (A.27) and (A.28).

$$\alpha^{(0)} = \sum_{i=1}^{C}x_i\alpha_i \qquad \text{(A.27)}$$

$$\xi^{(0)} = \sum_{i=1}^{C}x_i\xi_i \qquad \text{(A.28)}$$

The updating procedure can be summarized as follows:

$$\begin{pmatrix}\alpha\\ \xi\end{pmatrix}^{(k+1)} = \begin{pmatrix}\alpha\\ \xi\end{pmatrix}^{(k)} + \begin{pmatrix}\Delta\alpha\\ \Delta\xi\end{pmatrix}^{(k)} \tag{A.29}$$

where

$$\begin{bmatrix}\left(\partial f_1/\partial\alpha\right) & \left(\partial f_1/\partial\xi\right)\\ \left(\partial f_2/\partial\alpha\right) & \left(\partial f_2/\partial\xi\right)\end{bmatrix}^{(k)} \begin{pmatrix}\Delta\alpha\\ \Delta\xi\end{pmatrix}^{(k)} = -\begin{pmatrix}f_1\\ f_2\end{pmatrix}^{(k)}. \tag{A.30}$$

The Jacobian matrix can be calculated at each iteration along with the residues, f_1 and f_2, and a simple linear solver will give the step change in ξ and α. The required derivatives are given in equations (A.31) through (A.34).

$$\left(\frac{\partial f_1}{\partial\alpha}\right) = \xi g \tag{A.31}$$

$$\left(\frac{\partial f_1}{\partial\xi}\right) = \frac{\alpha}{1+\xi\left(1+\frac{c}{b}\right)-\xi^2\left(\frac{c}{b}+\left(\frac{d}{b}\right)^2\right)} - \frac{1}{\xi(1-\xi)} \tag{A.32}$$

$$\left(\frac{\partial f_2}{\partial\alpha}\right) = \begin{cases}\xi(\xi-1) & ;\ \alpha \geq \alpha_{\lim}\\ -\left(2\beta\alpha+3\chi\alpha^2\right) & ;\ \alpha < \alpha_{\lim}\end{cases} \tag{A.33}$$

$$\left(\frac{\partial f_2}{\partial\xi}\right) = \begin{cases}1+\frac{c}{b}-2\xi\left(\frac{c}{b}+\left(\frac{d}{b}\right)^2\right)+\alpha(2\xi-1) & ;\ \alpha \geq \alpha_{\lim}\\ 1 & ;\ \alpha < \alpha_{\lim}\end{cases} \tag{A.34}$$

A.2.3 Fugacity Coefficients

The partial fugacity coefficients can be expressed as

$$RT\ln\varphi_j = \int_v^\infty\left[\left(\frac{\partial P}{\partial n_j}\right)_{T,V,n} - \frac{RT}{V}\right]dV - RT\ln Z \tag{A.35}$$

which, for the TBS equation of state, can be written in the form:

$$\ln\varphi_j = -\ln\left(\frac{P(v-b)}{RT}\right) + \frac{b_j}{b}\left(\frac{Pv}{RT}-1\right) + g\frac{b}{v}\left[\frac{\alpha}{2\delta}n\left(\frac{\partial\delta}{\partial n_j}\right) - \left(\frac{\partial n\alpha}{\partial n_j}\right)_{T,n}\right] +$$

$$\frac{\alpha\, 2}{v^2+v(b+c)-\left(cb+d^2\right)}\left[c_j b - cb_j - \left(vb+\frac{b^2}{2}+\frac{cb}{2}\right)\frac{n}{\delta}\left(\frac{\partial\delta}{\partial n_j}\right)\right] \qquad \text{(A.36)}$$

where δ is given by equation (A.14), $g(b/v)$ is analogous to $g\xi$ given in equations (A.16) and (A.17), and

$$n\left(\frac{\partial\delta}{\partial n_j}\right) = \frac{1}{b}\left\{-b_j\left(6\frac{c}{b}+2\left(\frac{c}{b}\right)^2+8\left(\frac{d}{b}\right)^2\right)+6c_j+2c_j\frac{c}{b}+8d_j\frac{d}{b}\right\}. \qquad \text{(A.37)}$$

The terms c_j and d_j in the above equations are derivatives of the mixture parameters and will be defined in the next section.

In order to determine the fugacity coefficients, the derivatives $(\partial n\alpha/\partial n_j)$ are needed. Equations (A.25) and (A.26) can be rewritten as

$$f_1(n\alpha,\xi,\mathbf{n}) = n\alpha\xi g + n\ln\left(\frac{1-\xi}{\xi}\right) + \frac{n\Delta G^E}{RT} - \sum_{i=1}^{C} n_i\left\{\alpha_i\xi_i g_i + \ln\left(\frac{1-\xi_i}{\xi_i}\right) + \ln\left(\frac{b_i}{b}\right)\right\} \qquad \text{(A.38)}$$

$$f_2(n\alpha,\xi,\mathbf{n}) = \begin{cases} n + n\xi\left(1+\dfrac{c}{b}\right) - n\xi^2\left(\dfrac{c}{b}-\left(\dfrac{d}{b}\right)^2\right) - n\alpha\xi(1-\xi) & ;\ \alpha \geq \alpha_{\lim} \\ \xi - \left(1+\beta(n\alpha)^2/n^2 + \chi(n\alpha)^3/n^3\right) & ;\ \alpha < \alpha_{\lim} \end{cases} \qquad \text{(A.39)}$$

where $\mathbf{n}$ denotes the vector $\{n_1, n_2, \ldots, n_C\}$. To determine the required partial derivatives, the total derivatives of equations (A.38) and (A.39) are used.

$$\begin{aligned} \left(\frac{\partial f_1}{\partial n\alpha}\right)\left(\frac{\partial n\alpha}{\partial n_j}\right) + \left(\frac{\partial f_1}{\partial \xi}\right)\left(\frac{\partial \xi}{\partial n_j}\right) &= -\left(\frac{\partial f_1}{\partial n_j}\right) \\ \left(\frac{\partial f_2}{\partial n\alpha}\right)\left(\frac{\partial n\alpha}{\partial n_j}\right) + \left(\frac{\partial f_2}{\partial \xi}\right)\left(\frac{\partial \xi}{\partial n_j}\right) &= -\left(\frac{\partial f_2}{\partial n_j}\right) \end{aligned} \qquad \text{(A.40)}$$

When α and ξ have been found, equation set (A.40) defines a linear set of equations in two unknowns, $(\partial n\alpha/\partial n_j)$ and $(\partial\xi/\partial n_j)$, which are easily determined with a linear equation solver. The derivatives which make up the coefficients of this linear system are given in equations (A.41) through (A.46).

$$\left(\frac{\partial f_1}{\partial n\alpha}\right) = \xi g \tag{A.41}$$

$$\left(\frac{\partial f_1}{\partial \xi}\right) = \frac{n\alpha}{1+\xi\left(1+\frac{c}{b}\right)-\xi^2\left(\frac{c}{b}+\left(\frac{d}{b}\right)^2\right)} - \frac{n}{\xi(1-\xi)} \tag{A.42}$$

$$\left(\frac{\partial f_1}{\partial n_j}\right) = n\alpha\left(\frac{\partial \xi g}{\partial n_j}\right) + \ln\left(\frac{1-\xi}{\xi}\right) + \ln\gamma_j - \alpha_j\xi_j g_j - \ln\left(\frac{1-\xi_j}{\xi_j}\right) - \ln\left(\frac{b_j}{b}\right) + \frac{b_j}{b} - 1 \tag{A.43}$$

$$\left(\frac{\partial f_2}{\partial n\alpha}\right) = \begin{cases} \xi(\xi-1) & ;\ \alpha \geq \alpha_{\lim} \\ -\left(2\beta\alpha + 3\chi\alpha^2\right)/n & ;\ \alpha < \alpha_{\lim} \end{cases} \tag{A.44}$$

$$\left(\frac{\partial f_2}{\partial \xi}\right) = \begin{cases} n\left[1+\frac{c}{b}-2\xi\left(\frac{c}{b}+\left(\frac{d}{b}\right)^2\right)+\alpha(2\xi-1)\right] & ;\ \alpha \geq \alpha_{\lim} \\ 1 & ;\ \alpha < \alpha_{\lim} \end{cases} \tag{A.45}$$

$$\left(\frac{\partial f_2}{\partial n_j}\right) = \begin{cases} \frac{\xi}{b}\left[(1-\xi)\left(c_j - c\frac{b_j}{b}\right) - 2\xi\frac{d}{b}\left(d_j - d\frac{b_j}{b}\right)\right] + \\ 1+\xi\left(1+\frac{c}{b}\right)-\xi^2\left(\frac{c}{b}+\left(\frac{d}{b}\right)^2\right) & ;\ \alpha \geq \alpha_{\lim} \\ -(n\alpha)^2\left(\frac{\partial(\beta n^2)}{\partial n_j}\right) - (n\alpha)^3\left(\frac{\partial(\chi n^3)}{\partial n_j}\right) & ;\ \alpha < \alpha_{\lim} \end{cases} \tag{A.46}$$

where

$$\left(\frac{\partial \xi g}{\partial n_j}\right)=\left\{\frac{\xi\left(2+\xi+\xi\frac{c}{b}\right)}{4\delta\left[1+\xi\left(1+\frac{c}{b}\right)-\xi^2\left(\frac{c}{b}+\left(\frac{d}{b}\right)^2\right)\right]}-\frac{\xi g}{2\delta}\right\}\left(\frac{\partial \delta}{\partial n_j}\right)-\frac{\xi^2\left[c_j-c\frac{b_j}{b}\right]}{2bn\left[1+\xi\left(1+\frac{c}{b}\right)-\xi^2\left(\frac{c}{b}+\left(\frac{d}{b}\right)^2\right)\right]} \tag{A.47}$$

The derivatives of β and χ contained in equation (A.46) are given below.

$$\left(\frac{\partial(\beta\, n^2)}{\partial n_j}\right)=\frac{1}{n^2}\left(\frac{\partial \beta}{\partial n_j}\right)-2\frac{\beta}{n^3} \tag{A.48}$$

$$\left(\frac{\partial(\chi\, n^3)}{\partial n_j}\right)=\frac{1}{n^3}\left(\frac{\partial \chi}{\partial n_j}\right)-3\frac{\chi}{n^4} \tag{A.49}$$

$$\left(\frac{\partial \beta}{\partial n_j}\right)=\left\{3\left(\frac{\partial \psi_1}{\partial n_j}\right)-\alpha_{\lim}\left(\frac{\partial \psi_2}{\partial n_j}\right)-\psi_2\left(\frac{\partial \alpha_{\lim}}{\partial n_j}\right)\right\}\Big/\alpha_{\lim}^2-2\frac{\beta}{\alpha_{\lim}}\left(\frac{\partial \alpha_{\lim}}{\partial n_j}\right) \tag{A.50}$$

$$\left(\frac{\partial \chi}{\partial n_j}\right)=-\left\{2\left(\frac{\partial \psi_1}{\partial n_j}\right)-\alpha_{\lim}\left(\frac{\partial \psi_2}{\partial n_j}\right)-\psi_2\left(\frac{\partial \alpha_{\lim}}{\partial n_j}\right)\right\}\Big/\alpha_{\lim}^3-3\frac{\chi}{\alpha_{\lim}}\left(\frac{\partial \alpha_{\lim}}{\partial n_j}\right) \tag{A.51}$$

$$\left(\frac{\partial(c/b)}{\partial n_j}\right)=\frac{1}{nb}\left(c_j-c\frac{b_j}{b}\right) \tag{A.52}$$

$$\left(\frac{\partial(d/b)^2}{\partial n_j}\right)=2\frac{d}{nb^2}\left(d_j-d\frac{b_j}{b}\right) \tag{A.53}$$

$$\left(\frac{\partial \alpha_{\lim}}{\partial n_j}\right)=\lambda\left\{\left(\frac{\partial(c/b)}{\partial n_j}\right)-\left(\frac{\partial(d/b)^2}{\partial n_j}\right)\Big/\sqrt{2-\left(\frac{d}{b}\right)^2}\right\} \tag{A.54}$$

$$\vartheta = \alpha^2 - 2\alpha\frac{c}{b} + 6\frac{c}{b} + \left(\frac{c}{b}\right)^2 - 6\alpha + 4\left(\frac{d}{b}\right)^2 + 1 \tag{A.55}$$

$$\left(\frac{\partial\vartheta}{\partial n_j}\right) = 2\left(\alpha - \frac{c}{b} - 1\right)\left\{\left(\frac{\partial\alpha_{\lim}}{\partial n_j}\right) - \left(\frac{\partial(c/b)}{\partial n_j}\right)\right\} - 4\left\{\left(\frac{\partial\alpha_{\lim}}{\partial n_j}\right) - \left(\frac{\partial(c/b)}{\partial n_j}\right) - \left(\frac{\partial(d/b)^2}{\partial n_j}\right)\right\} \tag{A.56}$$

$$\varepsilon = \alpha - \frac{c}{b} - \left(\frac{d}{b}\right)^2 \tag{A.57}$$

$$\left(\frac{\partial\varepsilon}{\partial n_j}\right) = \left(\frac{\partial\alpha_{\lim}}{\partial n_j}\right) - \left(\frac{\partial(c/b)}{\partial n_j}\right) - \left(\frac{\partial(d/b)^2}{\partial n_j}\right) \tag{A.58}$$

$$\psi_1 = \frac{\alpha - \frac{c}{b} - 1 + \sqrt{\vartheta}}{2\varepsilon} \tag{A.59}$$

$$\psi_2 = \frac{1 + \left(\alpha - \frac{c}{b} - 3\right)\sqrt{\vartheta}}{2\varepsilon} - \frac{\alpha - \frac{c}{b} - 1 + \sqrt{\vartheta}}{2\varepsilon^2} \tag{A.60}$$

$$\left(\frac{\partial\psi_1}{\partial n_j}\right) = \frac{\left(\frac{\partial\alpha_{\lim}}{\partial n_j}\right) - \left(\frac{\partial(c/b)}{\partial n_j}\right) + \frac{1}{2\sqrt{\vartheta}}\left(\frac{\partial\vartheta}{\partial n_j}\right)}{2\varepsilon} - \frac{\alpha - \frac{c}{b} - 1 + \sqrt{\vartheta}}{2\varepsilon^2}\left(\frac{\partial\varepsilon}{\partial n_j}\right) \tag{A.61}$$

$$\left(\frac{\partial\psi_2}{\partial n_j}\right) = \frac{\frac{1}{\sqrt{\vartheta}}\left\{\left(\frac{\partial\alpha_{\lim}}{\partial n_j}\right) - \left(\frac{\partial(c/b)}{\partial n_j}\right)\right\} - \frac{1}{2\vartheta\sqrt{\vartheta}}\left(\alpha - \frac{c}{b} - 3\right)\left(\frac{\partial\vartheta}{\partial n_j}\right)}{2\varepsilon} - \frac{1 + \left(\alpha - \frac{c}{b} - 3\right)\sqrt{\vartheta}}{2\varepsilon^2}\left(\frac{\partial\varepsilon}{\partial n_j}\right) - \left(\frac{\partial\psi_1}{\partial n_j}\right)\Big/\varepsilon + \frac{\alpha - \frac{c}{b} - 1 + \sqrt{\vartheta}}{2\varepsilon^3}\left(\frac{\partial\varepsilon}{\partial n_j}\right) \tag{A.62}$$

These derivatives were found to be correct through numerical differentiation.

A.2.4 Mixing Rules for b, c and d

It is important to recall that in the above development, a linear mixing rule for b was assumed.

$$b = \sum_{i=1}^{C} x_i b_i \tag{A.63}$$

The mixing rules for c and d may be defined in any manner, but it must be noted that when referring to a mixture in the development of equations (A.36) and (A.37)

$$c_j = \frac{\partial nc}{\partial n_j} \tag{A.64}$$

and

$$d_j = \frac{\partial nd}{\partial n_j}. \tag{A.65}$$

For example, in the case where

$$c = \sum_{i=1}^{C} x_i c_i \,, \tag{A.66}$$

then

$$\frac{\partial nc}{\partial n_j} = c_j \tag{A.67}$$

and where

$$d = \sum_{i=1}^{C}\sum_{j=1}^{C} x_i x_j d_i d_j (1 - K_{d_{ij}}) \,, \tag{A.68}$$

then

$$\frac{\partial nd}{\partial n_j} = 2\sum_{i=1}^{C} x_i d_i d_j \left(1 - K_{d_{ij}}\right) - d \tag{A.69}$$

All of the above equations reduce to the same expressions as found by Heidemann and Kokal (1990) when values of c and d are chosen such that the TB EOS reduces to a two parameter equation of state.

A.3 Example Calculations

Two types of example calculations were performed to illustrate the Heidemann-Kokal mixing rules: bubble point curves were generated for methanol-benzene, acetone-water, isopropanol-water and ethanol-water systems, and the three phase line of a benzene-water system was found. For all the calculations save the bubble point curve generation of the ethanol-water system, the Peng-Robinson equation of state was used. For the ethanol-water system, the Trebble-Bishnoi equation of state with modifications described later was utilized with a linear mixing rule for *c* and a quadratic mixing rule for *d*. The pure component TBMC *a* parameter temperature dependence coefficients are summarized in Table A-1 while the pure component critical properties used from the DIPPR data compilation (1984) are summarized in Table A-2. In all the systems studied, the NRTL activity coefficient model was incorporated into the mixing rule.

In the bubble point calculations, a simple temperature dependence was used within the NRTL model which had the form:

$$\tau_{ij} = \tau_{ij}^{o} \frac{T_{ref}}{T} \tag{A.70}$$

where τ_{ij}^{o} is the energy parameter as calculated from the NRTL parameter correlations and T_{ref} is the temperature at which the parameters were correlated. This temperature dependence ensures that the excess free energy of the system goes to zero at infinite temperatures. The NRTL parameters used for each system are summarized in Table A-3.

Component	c_1	c_2	c_3	k
Acetone	0.322455	1.037966	-1.433200	0.322455
Benzene	0.523618	-0.035834	1.004951	0.523618
Ethanol	0.668444	1.761781	-3.200180	0.668444
Methanol	0.573466	1.129855	-2.101343	0.573466
Water	0.402648	0.820637	-1.274822	0.402648
2-Propanol	0.643317	2.631510	-4.655585	0.643317

Table A-1 - TBMC EOS *a* Parameter Temperature Dependence Coefficients.

Component	T_C (K)	P_C (kPa)	v_C (m^3/kmol)	a_C (kPa·m^6/$kmol^2$)	b (m^3/kmol)	c (m^3/kmol)	d (m^3/kmol)
Acetone	508.20	4700.99	0.2090	559.321	0.066410	0.224814	0.066411
Benzene	562.16	4897.99	0.2590	495.516	0.079285	0.119011	0.065550
Ethanol	513.92	6148.00	0.1670	550.069	0.053973	0.156447	0.054577
Methanol	512.64	8097.00	0.1180	571.648	0.037324	0.145862	0.037725
Water	647.13	22054.90	0.0559	558.166	0.016998	0.636846	0.015806
2-Propanol	508.30	4761.99	0.2200	537.154	0.070441	0.178001	0.069025

Table A-2 - Pure Component Critical Properties and TBMC EOS Parameters.

Binary System	T_{ref} (K)	A_{12} (gmol/cal)	A_{21} (gmol/cal)	α_{12}	Original Investigator(s)	DECHEMA Reference (Gmehling and Onker, 1977)
Methanol/Benzene	373.15	-2858.3564	4447.2186	0.0248	Schmidt, 1926	Vol. I, Part 2a, Page 225
Methanol/Water	373.15	-403.5460	1113.1181	0.3004	Griswold & Wong, 1952	Vol. I, Part 1, Page 49
Acetone/Methanol	328.15	284.0402	152.8864	0.3008	Freshwater & Pike, 1967	Vol. I, Part 2a, Page 75
Acetone/Water	333.15	361.8807	1037.8869	0.2908	Taylor, 1900	Vol. I, Part 1, Page 248
2-Propanol/Water	338.19	450.6681	1475.3787	0.5401	Sada & Morisue, 1975	Vol. I, Part 1, Page 323
Ethanol/Water	343.15	-121.2691	1337.8574	0.2974	Mertl, 1972	Vol. I, Part 1, Page 174

Table A-3 - NRTL Parameters and Sources For Binary Mixtures.

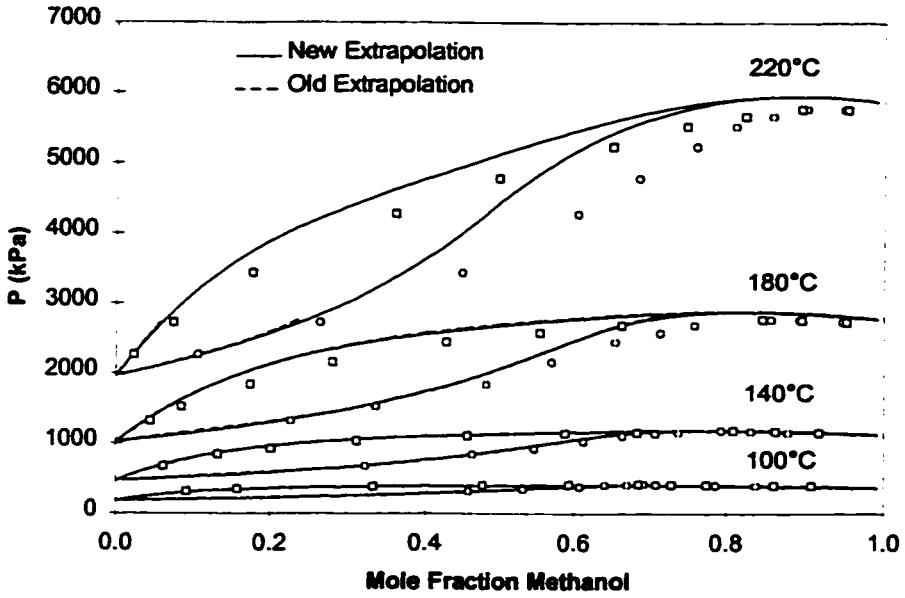

Figure A-1 - Methanol-Benzene VLE Using the Peng-Robinson EOS and Heidemann-Kokal Mixing Rule With the NRTL Activity Model.

A.3.1 VLE Predictions of Typical Binary Systems

Figure A-1 shows the bubble point curve generated for a methanol-benzene system using the Peng-Robinson equation of state and both the previous version of the Heidemann-Kokal mixing rule, and the version presented in this paper. The results show that both versions accurately predict the experimental data by Butcher and Medani (1968) at low temperatures, but at 220°C, the previous method of extrapolation fails to produce a complete result due to lack of a solution of the transcendental. The new extrapolation not only completes the bubble point curve calculations, but shows reasonable agreement with the high temperature experimental data. Similarly, the bubble point curve of the acetone-water system is illustrated in Figure A-2, and it shows that both the new and old extrapolation methods give equally good fits to the data of Griswold and Wong (1952). A further example of the performance of the Heidemann-Kokal mixing rule with the new extrapolation is given in Figure A-3 where the high pressure bubble point curves of an isopropanol-water system are plotted along with the data of Barr-David and Dodge (1959). The predicted bubble point pressures are high at greater temperatures, but it can be seen that the mixing rule is capable of producing acceptable phase equilibrium

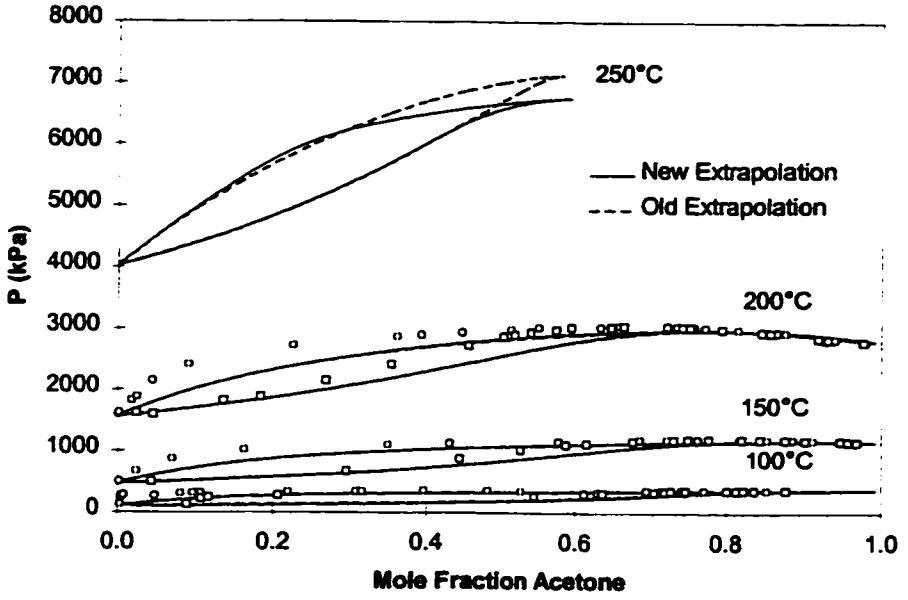

Figure A-2 - Acetone-Water VLE With the Peng-Robinson EOS and Heidemann-Kokal Mixing Rule With the NRTL Activity Model.

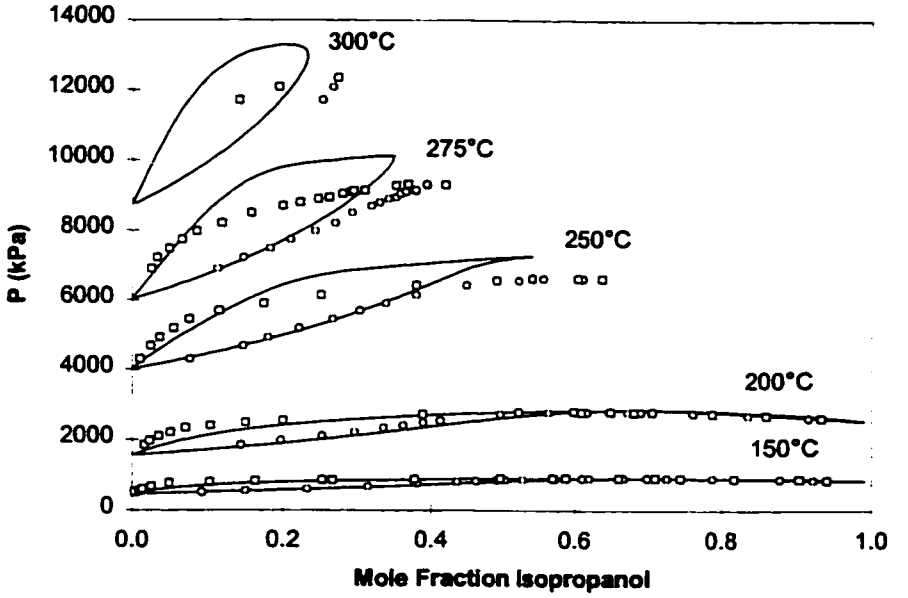

Figure A-3 - Isopropanol-Water VLE Using the Peng-Robinson EOS and Heidemann-Kokal Mixing Rule With the NRTL Activity Model.

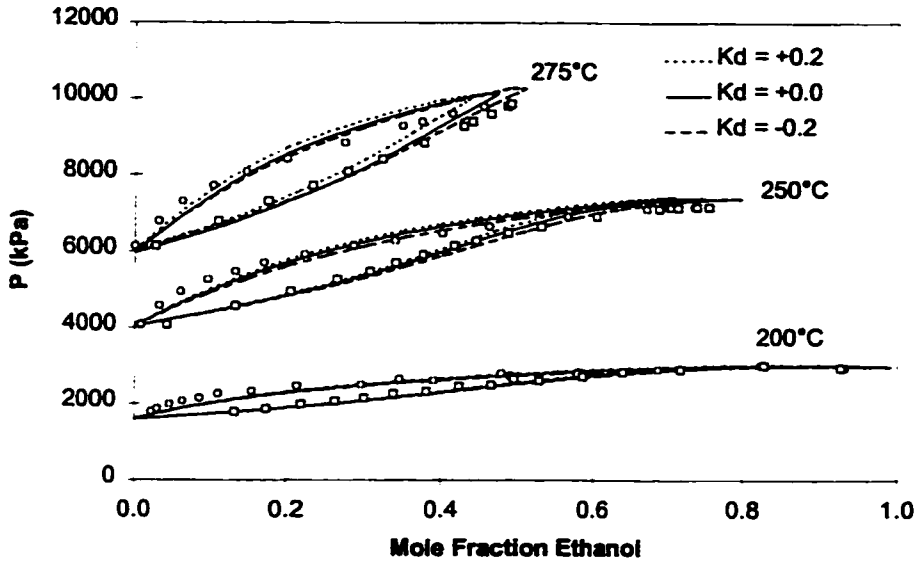

Figure A-4 - Ethanol-Water VLE Using the Trebble-Bishnoi EOS and Heidemann-Kokal Mixing Rule With the NRTL Activity Model.

calculations well past the critical temperature of the isopropanol. By modifying the temperature dependence of the NRTL parameters, it would be possible to arrive at a better fit to the experimental data.

In order to illustrate the added degree of freedom given by the K_d interaction parameter in the Trebble-Bishnoi equation of state, the bubble point curves for an ethanol-water system were generated with K_d values of -0.2, 0.0 and +0.2. This plot is shown in Figure A-4. In order to generate this curve, the pure component equation of state parameters were calculated from pure component critical properties as outlined by the generalized approach Trebble and Bishnoi (1987). In generating the following figure, the temperature dependence is removed from the co-volume parameter as suggested by Salim and Trebble (1991), and the temperature dependence of the a parameter has a Mathias-Copeman form below the critical temperature (Satyro and Trebble, 1996) and the form suggested by Trebble and Bishnoi (1987) above the critical temperature. If a_C is the value of the a parameter at the critical point, then the temperature dependence of a can be summarized as:

$$a = a_C\left(1 + c_1\tau + c_2\tau^2 + c_3\tau^3\right)^2 \qquad \text{for } T_r \le 1 \qquad \text{(A.71)}$$

$$a = a_C \exp\left(k\left[1 - T_r\right]\right) \qquad \text{for } T_r > 1 \qquad \text{(A.72)}$$

where

$$\tau = 1 - \sqrt{T_r}\ . \qquad \text{(A.73)}$$

The coefficients c_1, c_2, c_3, and k are chosen such that the first temperature derivatives of a as determined from equations (A.71) and (A.72) are equal at the critical temperature. The pure component d parameter is correlated in conjunction with the Mathias-Copeman parameters in order to best fit vapour pressure data. The TB equation of state using these modifications will be referred to as the TBMC equation of state.

The bubble point curves in Figure A-4 show that in this case, the general shape of the bubble point curves was not affected by changing K_d, but at the higher temperatures, the lower the interaction parameter, the lower the bubble point pressure. The effect which the interaction parameter had on the location of the curve increased with increasing temperature. In fact, varying K_d seemed to have virtually no effect at 200°C, while there was quite a noticeable change at 275°C. This behaviour could be advantageous if fine tuning of high temperature bubble point pressures was required.

A.3.2 Benzene-Water Three Phase Line Calculations

The example calculations showed that the Heidemann-Kokal mixing rule could be used to generate phase diagrams at high temperatures: temperatures away from where the activity coefficient model was correlated. One instance where activity coefficient models have been more useful than equation of state models alone is in the calculation of phase behaviour in hydrocarbon-water systems. In particular, it has been difficult for equations of state to accurately predict the solubility of hydrocarbons in an aqueous solution. Tsonopoulos and Wilson (1983) have approached the problem of extremely low hydrocarbon solubility in an aqueous phase by determining empirical correlations for these solubilities. Using an equation of state with an excess free energy mixing rule

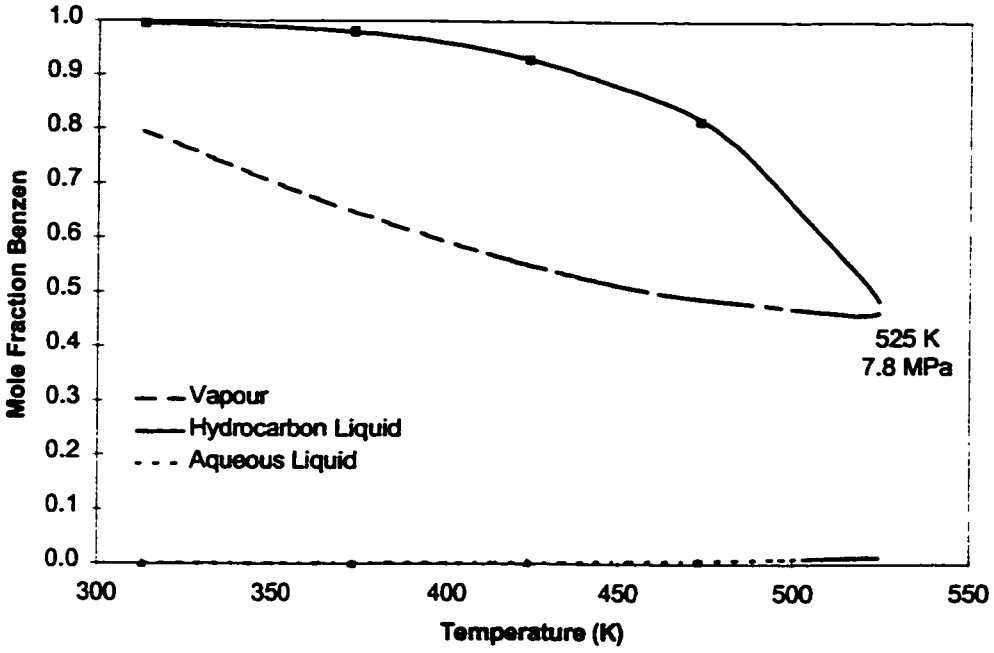

Figure A-5 - Benzene-Water Three Phase Line Compositions. Data from Tsonopoulos and Wilson (1983). Peng-Robinson Equation of State with NRTL Activity Model.

which can reproduce the mutual solubilities of hydrocarbon and water should give the equation of state the ability to reproduce this difficult phase behaviour.

Using the benzene-water three phase data published by Tsonopoulos and Wilson (1983), the NRTL energy parameters τ_{12} and τ_{21} were determined by adjusting the energy parameters as they were used within the Heidemann-Kokal mixing rule to match the fugacities of the liquid phases of the experimental three phase data using a secant method solution algorithm. A non-linear regression of the τ_{ij} values was then done to result in the following two expressions for the NRTL energy parameters:

$$\tau_{12} = \frac{-5671}{T} + \frac{4.303\times10^{6}}{T^{2}} - \frac{6.513\times10^{8}}{T^{3}}$$
$$\tau_{21} = \frac{917.8}{T} + \frac{9.567\times10^{5}}{T^{2}} - \frac{1.868\times10^{8}}{T^{3}} \qquad \text{(A.74)}$$

These two correlations were used in the NRTL model incorporated into a Peng-Robinson equation of state to generate the three phase compositions shown in Figure A-5. Excluding the experimental critical endpoint of the three phase line, the mean error in the

predicted three phase pressures was 3.8%, the mean error of the water mole fraction in the benzene phase was 0.5% and the mean error of the benzene in the water phase was 5.0%. The predicted three phase critical endpoint where the vapour and hydrocarbon phase become critical was at 525K and 7.8 MPa. This is substantially different from the experimental 541K and 9.4 MPa, but it is believed that a better correlation of the NRTL energy parameters would improve this result. Otherwise, the performance of the equation of state with the Heidemann-Kokal mixing rule is more than adequate in predicting this difficult phase behaviour.

A.4 Summary

The Heidemann-Kokal excess free energy mixing rule was extended to include the four parameter TB equation of state. A new method of extrapolating the pure component and mixture standard states to high temperatures was developed. The new extrapolation ensures that a solution to the mixture standard state transcendental equations exist.

The mixing rule was tested on a number of binary systems and it was able to match the vapour-liquid equilibrium data well at low temperatures. At temperatures above where the activity coefficient models were correlated, the mixing rule was still able to match experimental data adequately. The excess free energy mixing rule was also shown to be effective in calculating the simultaneous solubility of water in benzene and the solubility of benzene and water, a calculation which an equation of state with conventional mixing rules cannot do well.

APPENDIX B - DERIVATIVES FOR THE CLOUD AND SHADOW POINT CURVE ALGORITHM

B.1 The Objective Functions

The objective functions for determining a cloud and shadow point of a polymer solvent system using the Sanchez-Lacombe equation of state were

$$g_1 = A_k - A_f = 0 \tag{B.1}$$

$$g_2 = B_k + B_f^{II} - B_f^{I} = 0 \tag{B.2}$$

$$g_3 = \ln K_A - r_A\left\{\frac{1}{\tilde{r}^{II}} - \frac{1}{\tilde{r}^{I}} - \ln\left(\gamma_A^{II}/\gamma_A^{I}\right)\right\} = 0 \tag{B.3}$$

$$g_4 = \frac{\left(1-\psi_B^F\right)\left(1-K_A\right)}{1+\phi\left[K_A-1\right]} + \psi_B^F \int_{r=0}^{\infty}\left\{\frac{W_B^F(r)\left[1-K_B(r)\right]}{1+\phi\left[K_B(r)-1\right]}\right\}dr = 0 \tag{B.4}$$

$$g_5 = \alpha_i - S = 0 \tag{B.5}$$

where

$$A_f = \ln\left(\frac{\tilde{r}^{I}\tilde{b}^{I}}{v^{I}}\right) - \ln\left(\frac{\tilde{r}^{II}\tilde{b}^{II}}{v^{II}}\right), \tag{B.6}$$

$$B_f^i = \frac{2\tilde{b}_B^i}{\tilde{b}^i \tilde{r}^i} - \frac{2\tilde{a}_B^i \bar{r}^i}{v^i RT} - \frac{2}{\bar{r}^i} - \frac{2}{\bar{r}^i \tilde{b}^i}\left[\frac{\tilde{b}_B^i}{\tilde{b}^i} - 1\right]\left(v^i - \bar{r}^i \tilde{b}^i\right)\ln\left(\frac{v^i - \bar{r}^i \tilde{b}^i}{v^i}\right) - \left(\frac{2\tilde{b}_B^i}{\tilde{b}^i} - 1\right)\left[\ln\left(\frac{v^i - \bar{r}^i \tilde{b}^i}{v^i}\right) + 1\right], \tag{B.7}$$

and α_i represents the chosen iteration variable, the i^{th} component of the vector of independent variables, $\alpha = \{\ln K_A, A_K, B_K, \ln T, \ln \psi_B^F\}$.

B.2 The Jacobian Derivatives

The derivatives used in the Jacobian of the Newton-Raphson procedure are listed below.

If $\eta \in \{A_K, B_K\}$,

$$\left(\frac{\partial g_1}{\partial \eta}\right) = \left(\frac{\partial A_K}{\partial \eta}\right) + \frac{1}{\bar{r}^{II}}\left(\frac{\partial \bar{r}^{II}}{\partial \eta}\right) + \frac{1}{\tilde{b}^{II}}\left(\frac{\partial \tilde{b}^{II}}{\partial \eta}\right) - \frac{1}{v^{II}}\left(\frac{\partial v^{II}}{\partial \eta}\right) - \left[\frac{1}{\bar{r}^{I}}\left(\frac{\partial \bar{r}^{I}}{\partial \eta}\right) + \frac{1}{\tilde{b}^{I}}\left(\frac{\partial \tilde{b}^{I}}{\partial \eta}\right) - \frac{1}{v^{I}}\left(\frac{\partial v^{I}}{\partial \eta}\right)\right] \tag{B.8}$$

$$\left(\frac{\partial g_2}{\partial \eta}\right) = \left(\frac{\partial B_K}{\partial \eta}\right) + \left(\frac{\partial B_f^{II}}{\partial \eta}\right) - \left(\frac{\partial B_f^{I}}{\partial \eta}\right) \tag{B.9}$$

$$\left(\frac{\partial g_3}{\partial \eta}\right) = -r_A\left\{\left(\frac{\partial 1\ \bar{r}^{II}}{\partial \eta}\right) - \left(\frac{\partial 1\ \bar{r}^{I}}{\partial \eta}\right) - \left(\frac{\partial \ln \gamma_A^{II}}{\partial \eta}\right) + \left(\frac{\partial \ln \gamma_A^{I}}{\partial \eta}\right)\right\} \tag{B.10}$$

and if $\eta \in \{K_A, T, \psi_B^F\}$,

$$\left(\frac{\partial g_1}{\partial \ln \eta}\right) = \eta\left\{\frac{1}{\bar{r}^{II}}\left(\frac{\partial \bar{r}^{II}}{\partial \eta}\right) + \frac{1}{\tilde{b}^{II}}\left(\frac{\partial \tilde{b}^{II}}{\partial \eta}\right) - \frac{1}{v^{II}}\left(\frac{\partial v^{II}}{\partial \eta}\right) - \left[\frac{1}{\bar{r}^{I}}\left(\frac{\partial \bar{r}^{I}}{\partial \eta}\right) + \frac{1}{\tilde{b}^{I}}\left(\frac{\partial \tilde{b}^{I}}{\partial \eta}\right) - \frac{1}{v^{I}}\left(\frac{\partial v^{I}}{\partial \eta}\right)\right]\right\} \tag{B.11}$$

$$\left(\frac{\partial g_2}{\partial \ln \eta}\right) = \eta\left\{\left(\frac{\partial B_f^{II}}{\partial \eta}\right) - \left(\frac{\partial B_f^{I}}{\partial \eta}\right)\right\} \tag{B.12}$$

$$\left(\frac{\partial g_3}{\partial \ln \eta}\right) = \left(\frac{\partial K_A}{\partial \eta}\right) - \eta r_A \left\{\left(\frac{\partial 1/\bar{r}^{II}}{\partial \eta}\right) - \left(\frac{\partial 1/\bar{r}^{I}}{\partial \eta}\right) - \left(\frac{\partial \ln \gamma_A^{II}}{\partial \eta}\right) + \left(\frac{\partial \ln \gamma_A^{I}}{\partial \eta}\right)\right\} \tag{B.13}$$

The remaining derivatives required for the Jacobian are

$$\left(\frac{\partial g_4}{\partial A_K}\right) = -\psi_B^F \int_{r=0}^{\infty} \frac{W_B^F(r) K_B(r)}{\left(1+\phi\left[K_B(r)-1\right]\right)^2} dr \tag{B.14}$$

$$\left(\frac{\partial g_4}{\partial B_K}\right) = -\psi_B^F \int_{r=0}^{\infty} \frac{r W_B^F(r) K_B(r)}{\left(1+\phi\left[K_B(r)-1\right]\right)^2} dr \tag{B.15}$$

$$\left(\frac{\partial g_4}{\partial \ln K_A}\right) = -K_A \frac{\left(1-\psi_B^F\right)}{\left(1+\phi\left[K_A-1\right]\right)^2} \tag{B.16}$$

$$\left(\frac{\partial g_4}{\partial \ln T}\right) = 0 \tag{B.17}$$

$$\left(\frac{\partial g_4}{\partial \ln \psi_B^F}\right) = \psi_B^F \left\{\int_{r=0}^{\infty} \frac{W_B^F(r)\left[1-K_B(r)\right]}{1+\phi\left[K_B(r)-1\right]} dr - \frac{1-K_A}{1+\phi\left[K_A-1\right]}\right\} \tag{B.18}$$

$$\left(\frac{\partial g_5}{\partial \alpha_i}\right) = \begin{cases} 0 & ; \ i \text{ does not correspond to the iteration variable} \\ 1 & ; \ i \text{ corresponds to the iteration variable} \end{cases} \tag{B.19}$$

B.3 Segment Fraction Derivatives

$$\psi_j^k = \Psi_j^k / \left(\Psi_A^k + \Psi_B^k\right) = \Psi_j^k / n_T^k \tag{B.20}$$

$$\left(\frac{\partial \psi_j^k}{\partial \eta}\right) = \frac{1}{n_T^k}\left(\frac{\partial \Psi_j^k}{\partial \eta}\right) - \frac{\Psi_j^k}{\left(n_T^k\right)^2}\left\{\left(\frac{\partial \Psi_A^k}{\partial \eta}\right) + \left(\frac{\partial \Psi_B^k}{\partial \eta}\right)\right\} \tag{B.21}$$

where $\eta \in \left\{A_K, B_K, K_A, T, \psi_B^F\right\}$.

$$\left(\frac{\partial \Psi_A^I}{\partial A_K}\right)=\left(\frac{\partial \Psi_A^{II}}{\partial A_K}\right)=\left(\frac{\partial \Psi_A^I}{\partial B_K}\right)=\left(\frac{\partial \Psi_A^{II}}{\partial B_K}\right)=\left(\frac{\partial \Psi_B^I}{\partial K_A}\right)=\left(\frac{\partial \Psi_B^{II}}{\partial K_A}\right)=0 \tag{B.22}$$

$$\left(\frac{\partial \Psi_A^I}{\partial T}\right)=\left(\frac{\partial \Psi_A^{II}}{\partial T}\right)=\left(\frac{\partial \Psi_B^I}{\partial T}\right)=\left(\frac{\partial \Psi_B^{II}}{\partial T}\right)=0 \tag{B.23}$$

$$\left(\frac{\partial \Psi_A^I}{\partial K_A}\right)=-\frac{\left(\Psi_A^I\right)^2\phi}{\left(1-\psi_B^F\right)},\quad \left(\frac{\partial \Psi_A^{II}}{\partial K_A}\right)=\Psi_A^I-\frac{\left(\Psi_A^{II}\right)^2\phi}{\left(1-\psi_B^F\right)K_A} \tag{B.24}$$

$$\left(\frac{\partial \Psi_A^I}{\partial \psi_B^F}\right)=-\frac{1}{1+\phi\left[K_A-1\right]},\quad \left(\frac{\partial \Psi_A^{II}}{\partial \psi_B^F}\right)=-\frac{K_A}{1+\phi\left[K_A-1\right]} \tag{B.25}$$

$$\left(\frac{\partial \Psi_B^I}{\partial A_K}\right)=-\psi_B^F\int_{r=0}^{\infty}\frac{W_B^F(r)K_B(r)\phi}{\left(1+\phi\left[K_B(r)-1\right]\right)^2}dr,\quad \left(\frac{\partial \Psi_B^{II}}{\partial A_K}\right)=\psi_B^F\int_{r=0}^{\infty}\frac{W_B^F(r)K_B(r)\left[1-\phi\right]}{\left(1+\phi\left[K_B(r)-1\right]\right)^2}dr \tag{B.26}$$

$$\left(\frac{\partial \Psi_B^I}{\partial B_K}\right)=-\psi_B^F\int_{r=0}^{\infty}\frac{rW_B^F(r)K_B(r)\phi}{\left(1+\phi\left[K_B(r)-1\right]\right)^2}dr,\quad \left(\frac{\partial \Psi_B^{II}}{\partial B_K}\right)=\psi_B^F\int_{r=0}^{\infty}\frac{rW_B^F(r)K_B(r)\left[1-\phi\right]}{\left(1+\phi\left[K_B(r)-1\right]\right)^2}dr \tag{B.27}$$

$$\left(\frac{\partial \Psi_B^I}{\partial \psi_B^F}\right)=\int_{r=0}^{\infty}\frac{W_B^F(r)}{1+\phi\left[K_B(r)-1\right]}dr,\quad \left(\frac{\partial \Psi_B^{II}}{\partial \psi_B^F}\right)=\int_{r=0}^{\infty}\frac{W_B^F(r)K_B(r)}{1+\phi\left[K_B(r)-1\right]}dr \tag{B.28}$$

B.4 Number Average Number of Segments Derivatives

$$\begin{aligned}\left(\frac{\partial \bar{r}^I}{\partial A_K}\right)=-\left(\bar{r}^I\right)^2\left(\frac{\partial 1/\bar{r}^I}{\partial A_K}\right)=-\left(\bar{r}^I\right)^2\Bigg\{&\frac{1}{r_A}\left(\frac{\partial \psi_A^I}{\partial A_K}\right)-\frac{\psi_B^F}{n_T^I}\int_{r=0}^{\infty}\frac{W_B^F(r)K_B(r)\phi}{r\left(1+\phi\left[K_B(r)-1\right]\right)^2}dr\\&-\frac{\psi_B^F}{\left(n_T^I\right)^2}\left\{\left(\frac{\partial \Psi_A^I}{\partial A_K}\right)+\left(\frac{\partial \Psi_B^I}{\partial A_K}\right)\right\}\int_{r=0}^{\infty}\frac{W_B^F(r)}{r\left(1+\phi\left[K_B(r)-1\right]\right)}dr\Bigg\}\end{aligned} \tag{B.29}$$

$$\left(\frac{\partial \bar{r}^{II}}{\partial A_K}\right) = -\left(\bar{r}^{II}\right)^2 \left(\frac{\partial 1/\bar{r}^{II}}{\partial A_K}\right) = -\left(\bar{r}^{II}\right)^2 \left\{ \frac{1}{r_A}\left(\frac{\partial \psi_A^{II}}{\partial A_K}\right) + \frac{\psi_B^F}{n_T^{II}} \int_{r=0}^{\infty} \frac{W_B^F(r) K_B(r)[1-\phi]}{r\left(1+\phi\left[K_B(r)-1\right]\right)^2} dr \right.$$
$$\left. - \frac{\psi_B^F}{\left(n_T^{II}\right)^2} \left\{ \left(\frac{\partial \Psi_A^{II}}{\partial A_K}\right) + \left(\frac{\partial \Psi_B^{II}}{\partial A_K}\right) \right\} \int_{r=0}^{\infty} \frac{W_B^F(r) K_B(r)}{r\left(1+\phi\left[K_B(r)-1\right]\right)} dr \right\} \tag{B.30}$$

$$\left(\frac{\partial \bar{r}^{I}}{\partial B_K}\right) = -\left(\bar{r}^{I}\right)^2 \left(\frac{\partial 1/\bar{r}^{I}}{\partial B_K}\right) = -\left(\bar{r}^{I}\right)^2 \left\{ \frac{1}{r_A}\left(\frac{\partial \psi_A^{I}}{\partial B_K}\right) - \frac{\psi_B^F}{n_T^{I}} \int_{r=0}^{\infty} \frac{W_B^F(r) K_B(r)\phi}{\left(1+\phi\left[K_B(r)-1\right]\right)^2} dr \right.$$
$$\left. - \frac{\psi_B^F}{\left(n_T^{I}\right)^2} \left\{ \left(\frac{\partial \Psi_A^{I}}{\partial B_K}\right) + \left(\frac{\partial \Psi_B^{I}}{\partial B_K}\right) \right\} \int_{r=0}^{\infty} \frac{W_B^F(r)}{r\left(1+\phi\left[K_B(r)-1\right]\right)} dr \right\} \tag{B.31}$$

$$\left(\frac{\partial \bar{r}^{II}}{\partial B_K}\right) = -\left(\bar{r}^{II}\right)^2 \left(\frac{\partial 1/\bar{r}^{II}}{\partial B_K}\right) = -\left(\bar{r}^{II}\right)^2 \left\{ \frac{1}{r_A}\left(\frac{\partial \psi_A^{II}}{\partial B_K}\right) + \frac{\psi_B^F}{n_T^{II}} \int_{r=0}^{\infty} \frac{W_B^F(r) K_B(r)[1-\phi]}{\left(1+\phi\left[K_B(r)-1\right]\right)^2} dr \right.$$
$$\left. - \frac{\psi_B^F}{\left(n_T^{II}\right)^2} \left\{ \left(\frac{\partial \Psi_A^{II}}{\partial B_K}\right) + \left(\frac{\partial \Psi_B^{II}}{\partial B_K}\right) \right\} \int_{r=0}^{\infty} \frac{W_B^F(r) K_B(r)}{r\left(1+\phi\left[K_B(r)-1\right]\right)} dr \right\} \tag{B.32}$$

If $\eta \in \{K_A, T\}$, then

$$\left(\frac{\partial \bar{r}^{I}}{\partial \eta}\right) = -\left(\bar{r}^{I}\right)^2 \left(\frac{\partial 1/\bar{r}^{I}}{\partial \eta}\right) = -\left(\bar{r}^{I}\right)^2 \left\{ \frac{1}{r_A}\left(\frac{\partial \psi_A^{I}}{\partial \eta}\right) \right.$$
$$\left. - \frac{\psi_B^F}{\left(n_T^{I}\right)^2} \left\{ \left(\frac{\partial \Psi_A^{I}}{\partial \eta}\right) + \left(\frac{\partial \Psi_B^{I}}{\partial \eta}\right) \right\} \int_{r=0}^{\infty} \frac{W_B^F(r)}{r\left(1+\phi\left[K_B(r)-1\right]\right)} dr \right\} \tag{B.33}$$

$$\left(\frac{\partial \bar{r}^{II}}{\partial \eta}\right) = -\left(\bar{r}^{II}\right)^2\left(\frac{\partial 1/\bar{r}^{II}}{\partial \eta}\right) = -\left(\bar{r}^{II}\right)^2\left\{\frac{1}{r_A}\left(\frac{\partial \psi_A^{II}}{\partial \eta}\right)\right.$$

$$\left. -\frac{\psi_B^F}{\left(n_T^{II}\right)^2}\left\{\left(\frac{\partial \Psi_A^{II}}{\partial \eta}\right)+\left(\frac{\partial \Psi_B^{II}}{\partial \eta}\right)\right\}\int_{r=0}^{\infty}\frac{W_B^F(r)K_B(r)}{r\left(1+\phi\left[K_B(r)-1\right]\right)}dr\right\} \tag{B.34}$$

$$\left(\frac{\partial \bar{r}^{I}}{\partial \psi_B^F}\right) = -\left(\bar{r}^{I}\right)^2\left(\frac{\partial 1/\bar{r}^{I}}{\partial \psi_B^F}\right) = -\left(\bar{r}^{I}\right)^2\left\{\frac{1}{r_A}\left(\frac{\partial \psi_A^{I}}{\partial \psi_B^F}\right)+\frac{1}{n_T^{I}}\int_{r=0}^{\infty}\frac{W_B^F(r)}{r\left(1+\phi\left[K_B(r)-1\right]\right)}dr\right.$$

$$\left. -\frac{\psi_B^F}{\left(n_T^{I}\right)^2}\left\{\left(\frac{\partial \Psi_A^{I}}{\partial \psi_B^F}\right)+\left(\frac{\partial \Psi_B^{I}}{\partial \psi_B^F}\right)\right\}\int_{r=0}^{\infty}\frac{W_B^F(r)}{r\left(1+\phi\left[K_B(r)-1\right]\right)}dr\right\} \tag{B.35}$$

$$\left(\frac{\partial \bar{r}^{II}}{\partial \psi_B^F}\right) = -\left(\bar{r}^{II}\right)^2\left(\frac{\partial 1/\bar{r}^{II}}{\partial \psi_B^F}\right) = -\left(\bar{r}^{II}\right)^2\left\{\frac{1}{r_A}\left(\frac{\partial \psi_A^{II}}{\partial \psi_B^F}\right)+\frac{1}{n_T^{II}}\int_{r=0}^{\infty}\frac{W_B^F(r)K_B(r)}{r\left(1+\phi\left[K_B(r)-1\right]\right)}dr\right.$$

$$\left. -\frac{\psi_B^F}{\left(n_T^{II}\right)^2}\left\{\left(\frac{\partial \Psi_A^{II}}{\partial \psi_B^F}\right)+\left(\frac{\partial \Psi_B^{II}}{\partial \psi_B^F}\right)\right\}\int_{r=0}^{\infty}\frac{W_B^F(r)K_B(r)}{r\left(1+\phi\left[K_B(r)-1\right]\right)}dr\right\} \tag{B.36}$$

B.5 Derivatives of the Sanchez Lacombe Activity Coefficients.

Let $\eta \in \left\{A_K, B_K, K_A, T, \psi_B^F\right\}$, then for each phase,

$$\tau \equiv \left(\frac{\partial\left[\ln\left(\bar{r}\tilde{b}\ v\right)\right]}{\partial \eta}\right) = \frac{1}{\bar{r}}\left(\frac{\partial \bar{r}}{\partial \eta}\right)+\frac{1}{\tilde{b}}\left(\frac{\partial \tilde{b}}{\partial \eta}\right)-\frac{1}{v}\left(\frac{\partial v}{\partial \eta}\right) \tag{B.37}$$

$$\left(\frac{\partial \ln \gamma_A}{\partial \eta}\right) = \frac{\tau}{r_A} + \frac{2}{\bar{r}\tilde{b}}\left\{\frac{1}{\bar{r}}\left(\frac{\partial \bar{r}}{\partial \eta}\right) + \frac{1}{\tilde{b}}\left(\frac{\partial \tilde{b}}{\partial \eta}\right)\right\}\left[\frac{\tilde{b}_A}{\tilde{b}} - 1\right]\left(v - \bar{r}\tilde{b}\right)\ln\left(\frac{v - \bar{r}\tilde{b}}{v}\right)$$
$$- \frac{2}{\bar{r}\tilde{b}}\left\{\frac{1}{\tilde{b}}\left(\frac{\partial \tilde{b}_A}{\partial \eta}\right) - \frac{\tilde{b}_A}{\tilde{b}^2}\left(\frac{\partial \tilde{b}}{\partial \eta}\right)\right\}\left(v - \bar{r}\tilde{b}\right)\ln\left(\frac{v - \bar{r}\tilde{b}}{v}\right)$$
$$- \frac{2}{\bar{r}\tilde{b}}\left[\frac{\tilde{b}_A}{\tilde{b}} - 1\right]\left\{\left(\frac{\partial v}{\partial \eta}\right) - \tilde{b}\left(\frac{\partial \bar{r}}{\partial \eta}\right) - \bar{r}\left(\frac{\partial \tilde{b}}{\partial \eta}\right)\right\}\ln\left(\frac{v - \bar{r}\tilde{b}}{v}\right) + 2\tau\left[\frac{\tilde{b}_A}{\tilde{b}} - 1\right]$$
$$- \frac{2\tilde{b}_A}{\tilde{b}}\left\{\frac{1}{\tilde{b}_A}\left(\frac{\partial \tilde{b}_A}{\partial \eta}\right) - \frac{1}{\tilde{b}}\left(\frac{\partial \tilde{b}}{\partial \eta}\right)\right\}\left[\ln\left(\frac{v - \bar{r}\tilde{b}}{v}\right) + 1\right] + \left(\frac{2\tilde{b}_A}{\tilde{b}} - 1\right)\frac{\bar{r}\tilde{b}\tau}{v - \bar{r}\tilde{b}}$$
$$- \frac{2\tilde{a}_A\bar{r}}{vRT}\left\{\frac{1}{\tilde{a}_A}\left(\frac{\partial \tilde{a}_A}{\partial \eta}\right) + \frac{1}{\bar{r}}\left(\frac{\partial \bar{r}}{\partial \eta}\right) - \frac{1}{v}\left(\frac{\partial v}{\partial \eta}\right)\right\}$$
$$- \frac{2\tilde{b}_A}{\tilde{b}\bar{r}}\left\{\frac{1}{\bar{r}}\left(\frac{\partial \bar{r}}{\partial \eta}\right) + \frac{1}{\tilde{b}}\left(\frac{\partial \tilde{b}}{\partial \eta}\right) - \frac{1}{\tilde{b}_A}\left(\frac{\partial \tilde{b}_A}{\partial \eta}\right)\right\} + \frac{1}{\bar{r}^2}\left(\frac{\partial \bar{r}}{\partial \eta}\right) + \frac{2\tilde{a}_A\bar{r}}{vRT^2}\left(\frac{\partial T}{\partial \eta}\right) \tag{B.38}$$

$$\left(\frac{\partial B_f}{\partial \eta}\right) = \frac{2}{\bar{r}\tilde{b}}\left\{\frac{1}{\bar{r}}\left(\frac{\partial \bar{r}}{\partial \eta}\right) + \frac{1}{\tilde{b}}\left(\frac{\partial \tilde{b}}{\partial \eta}\right)\right\}\left[\frac{\tilde{b}_B}{\tilde{b}} - 1\right]\left(v - \bar{r}\tilde{b}\right)\ln\left(\frac{v - \bar{r}\tilde{b}}{v}\right)$$
$$- \frac{2}{\bar{r}\tilde{b}}\left\{\frac{1}{\tilde{b}}\left(\frac{\partial \tilde{b}_B}{\partial \eta}\right) - \frac{\tilde{b}_B}{\tilde{b}^2}\left(\frac{\partial \tilde{b}}{\partial \eta}\right)\right\}\left(v - \bar{r}\tilde{b}\right)\ln\left(\frac{v - \bar{r}\tilde{b}}{v}\right)$$
$$- \frac{2}{\bar{r}\tilde{b}}\left[\frac{\tilde{b}_B}{\tilde{b}} - 1\right]\left\{\left(\frac{\partial v}{\partial \eta}\right) - \tilde{b}\left(\frac{\partial \bar{r}}{\partial \eta}\right) - \bar{r}\left(\frac{\partial \tilde{b}}{\partial \eta}\right)\right\}\ln\left(\frac{v - \bar{r}\tilde{b}}{v}\right) + 2\tau\left[\frac{\tilde{b}_B}{\tilde{b}} - 1\right]$$
$$- \frac{2\tilde{b}_B}{\tilde{b}}\left\{\frac{1}{\tilde{b}_B}\left(\frac{\partial \tilde{b}_B}{\partial \eta}\right) - \frac{1}{\tilde{b}}\left(\frac{\partial \tilde{b}}{\partial \eta}\right)\right\}\left[\ln\left(\frac{v - \bar{r}\tilde{b}}{v}\right) + 1\right] + \left(\frac{2\tilde{b}_B}{\tilde{b}} - 1\right)\frac{\bar{r}\tilde{b}\tau}{v - \bar{r}\tilde{b}}$$
$$- \frac{2\tilde{a}_B\bar{r}}{vRT}\left\{\frac{1}{\tilde{a}_B}\left(\frac{\partial \tilde{a}_B}{\partial \eta}\right) + \frac{1}{\bar{r}}\left(\frac{\partial \bar{r}}{\partial \eta}\right) - \frac{1}{v}\left(\frac{\partial v}{\partial \eta}\right)\right\}$$
$$- \frac{2\tilde{b}_B}{\tilde{b}\bar{r}}\left\{\frac{1}{\bar{r}}\left(\frac{\partial \bar{r}}{\partial \eta}\right) + \frac{1}{\tilde{b}}\left(\frac{\partial \tilde{b}}{\partial \eta}\right) - \frac{1}{\tilde{b}_B}\left(\frac{\partial \tilde{b}_B}{\partial \eta}\right)\right\} + \frac{2}{\bar{r}^2}\left(\frac{\partial \bar{r}}{\partial \eta}\right) + \frac{2\tilde{a}_B\bar{r}}{vRT^2}\left(\frac{\partial T}{\partial \eta}\right) \tag{B.39}$$

B.6 Volume Derivatives for the Sanchez-Lacombe Equation of State

$$\left(\frac{\partial v}{\partial \eta}\right)_P = \left\{\frac{1}{vRT}\left(\frac{\partial \tilde{a}}{\partial \eta}\right) + \left(\frac{\partial \bar{r}}{\partial \eta}\right) - \frac{v}{\tilde{b}^2}\left(\frac{\partial \tilde{b}}{\partial \eta}\right)\ln\left(\frac{v - \bar{r}\tilde{b}}{v}\right) - \frac{v}{RT^2}\left[\frac{\tilde{a}}{v^2} + P\right]\left(\frac{\partial T}{\partial \eta}\right)\right.$$
$$\left. - \frac{v}{\tilde{b}\left(v - \bar{r}\tilde{b}\right)}\left[\tilde{b}\left(\frac{\partial \bar{r}}{\partial \eta}\right) + \bar{r}\left(\frac{\partial \tilde{b}}{\partial \eta}\right)\right]\right\} \Bigg/ \left\{\frac{2\tilde{a}}{v^2RT} - \frac{(1 - \bar{r})}{v} - \frac{\bar{r}}{v - \bar{r}\tilde{b}}\right\} \tag{B.40}$$

B.7 Mixture Parameter Derivatives for the Sanchez-Lacombe Equation of State

$$\left(\frac{\partial \tilde{a}}{\partial \eta}\right) = 2\bar{r}^2\left\{\left[\psi_A\varepsilon_{AA}v_{AA} + \psi_B\varepsilon_{AB}v_{AB}\right]\left(\frac{\partial \psi_A}{\partial \eta}\right) + \left[\psi_A\varepsilon_{AB}v_{AB} + \psi_B\varepsilon_{BB}v_{BB}\right]\left(\frac{\partial \psi_B}{\partial \eta}\right)\right\} + \frac{2\tilde{a}}{\bar{r}}\left(\frac{\partial \bar{r}}{\partial \eta}\right) \tag{B.41}$$

$$\left(\frac{\partial \tilde{a}_A}{\partial \eta}\right) = \varepsilon_{AA}v_{AA}\left(\frac{\partial \psi_A}{\partial \eta}\right) + \varepsilon_{AB}v_{AB}\left(\frac{\partial \psi_B}{\partial \eta}\right) \tag{B.42}$$

$$\left(\frac{\partial \tilde{a}_B}{\partial \eta}\right) = \varepsilon_{AB}v_{AB}\left(\frac{\partial \psi_A}{\partial \eta}\right) + \varepsilon_{BB}v_{BB}\left(\frac{\partial \psi_B}{\partial \eta}\right) \tag{B.43}$$

$$\left(\frac{\partial \tilde{b}}{\partial \eta}\right) = 2\left\{\left[\psi_A v_{AA} + \psi_B v_{AB}\right]\left(\frac{\partial \psi_A}{\partial \eta}\right) + \left[\psi_A v_{AB} + \psi_B v_{BB}\right]\left(\frac{\partial \psi_B}{\partial \eta}\right)\right\} \tag{B.44}$$

$$\left(\frac{\partial \tilde{b}_A}{\partial \eta}\right) = v_{AA}\left(\frac{\partial \psi_A}{\partial \eta}\right) + v_{AB}\left(\frac{\partial \psi_B}{\partial \eta}\right) \tag{B.45}$$

$$\left(\frac{\partial \tilde{b}_B}{\partial \eta}\right) = v_{AB}\left(\frac{\partial \psi_A}{\partial \eta}\right) + v_{BB}\left(\frac{\partial \psi_B}{\partial \eta}\right) \tag{B.46}$$

where $\eta \in \left\{A_K, B_K, K_A, T, \psi_B^F\right\}$.

APPENDIX C - DERIVATIVES FOR THE NEWTON-RAPHSON FLASH ALGORITHM

C.1 The Objective Functions

The necessary conditions for phase equilibrium in a π phase, C component polymer PT-flash where the first n_d components are discrete can be stated as

$$\begin{aligned} h_{Bij} &= \ln K_{Bij} + B_{ij} - \hat{B}_i = 0 \quad ; \ 1 \le i \le C, \ 1 \le j \le \pi \\ h_{Aj} &= \ln K_{Aj} + A_j - \hat{A} - \theta_j = 0 \quad ; \ 1 \le j \le \pi \\ l_j &= 1 - \sum_{i=1}^{C} \Psi_{ij} \begin{cases} = 0 & ; \ \beta_j > 0 \\ > 0 & ; \ \beta_j = 0 \end{cases} \quad ; \ 1 \le j \le \pi \end{aligned} \tag{C.1}$$

where

$$\Psi_{ij} = \begin{cases} \psi_{iF} K_{ij} / E_i & ; \ 1 \le i \le n_d \\ \psi_{iF} \displaystyle\int_{r=0}^{\infty} \frac{W_{iF}(r) K_{ij}(r)}{E_i(r)} dr & ; \ n_d < i \le C \end{cases} \tag{C.2}$$

$$\begin{aligned} \ln K_{ij} &= \ln K_{Aj} + r_i \ln K_{Bij} \quad ; \ 1 \le i \le n_d \\ \ln K_{ij}(r) &= \ln K_{Aj} + r \ln K_{Bij} \quad ; \ n_d < i \le C \end{aligned} \tag{C.3}$$

$$E_i = \sum_{j=1}^{\pi} \beta_j K_{ij} \qquad ; \; 1 \le i \le n_d$$

and

$$E_i(r) = \sum_{j=1}^{\pi} \beta_j K_{ij}(r) \quad ; \; n_d < i \le C \qquad \text{(C.4)}$$

The variables in this system are $\ln K_{Bij}$, $\ln K_{Aj}$ and the segment fractions in each phase, β_j. This gives $(C + 2)\pi$ unknowns in the same number of equations.

C.2 The Jacobian

The Jacobian matrix will have the generalized form:

$$\mathbf{J} = \begin{bmatrix} \left(\frac{\partial \mathbf{h_B}}{\partial \mathbf{nK_B}}\right) & \left(\frac{\partial \mathbf{h_B}}{\partial \mathbf{nK_A}}\right) & \left(\frac{\partial \mathbf{h_B}}{\partial \beta}\right) \\ \left(\frac{\partial \mathbf{h_A}}{\partial \mathbf{nK_B}}\right) & \left(\frac{\partial \mathbf{h_A}}{\partial \mathbf{nK_A}}\right) & \left(\frac{\partial \mathbf{h_A}}{\partial \beta}\right) \\ \left(\frac{\partial \mathbf{l}}{\partial \mathbf{nK_B}}\right) & \left(\frac{\partial \mathbf{l}}{\partial \mathbf{nK_A}}\right) & \left(\frac{\partial \mathbf{l}}{\partial \beta}\right) \end{bmatrix} \qquad \text{(C.5)}$$

where

$$\mathbf{h_B} = \left[h_{B11}, h_{B21}, \ldots, h_{BC1}, h_{B12}, \ldots, h_{BC\pi}\right]^T, \qquad \text{(C.6)}$$

$$\mathbf{h_A} = \left[h_{A1}, h_{A2}, \ldots, h_{A\pi}\right]^T, \qquad \text{(C.7)}$$

$$\mathbf{l} = \left[l_1, l_2, \ldots, l_\pi\right]^T, \qquad \text{(C.8)}$$

$$\mathbf{lnK_B} = \left[\ln K_{B11}, \ln K_{B21}, \ldots, \ln K_{BC1}, \ln K_{B12}, \ldots, \ln K_{BC\pi}\right]^T, \qquad \text{(C.9)}$$

$$\mathbf{lnK_A} = \left[\ln K_{A1}, \ln K_{A2}, \ldots, \ln K_{A\pi}\right]^T \qquad \text{(C.10)}$$

and $$\beta = \left[\beta_1, \beta_2, \ldots, \beta_\pi\right]^T. \qquad \text{(C.11)}$$

The derivatives in the Jacobian matrix are:

$$\left(\frac{\partial h_{Bij}}{\partial \ln K_{Blm}}\right) = \delta(i-l, j-m) + \left(\frac{\partial B_{ij}}{\partial \ln K_{Blm}}\right) - \left(\frac{\partial \hat{B}_i}{\partial \ln K_{Blm}}\right) \quad ; \; 1 \le i,l \le C \qquad \text{(C.12)}$$

$$\left(\frac{\partial h_{Bij}}{\partial \ln K_{Am}}\right)=\left(\frac{\partial B_{ij}}{\partial \ln K_{Am}}\right)-\left(\frac{\partial \hat{B}_i}{\partial \ln K_{Am}}\right) \quad ; \; 1\le i\le C \tag{C.13}$$

$$\left(\frac{\partial h_{Bij}}{\partial \beta_m}\right)=\left(\frac{\partial B_{ij}}{\partial \beta_m}\right)-\left(\frac{\partial \hat{B}_i}{\partial \beta_m}\right) \quad ; \; 1\le i\le C \tag{C.14}$$

$$\left(\frac{\partial h_{Aj}}{\partial \ln K_{Blm}}\right)=\left(\frac{\partial A_j}{\partial \ln K_{Blm}}\right)-\left(\frac{\partial \hat{A}}{\partial \ln K_{Blm}}\right)+\left[\sum_{k=1}^{C}\left(\frac{\partial \Psi_{kj}}{\partial \ln K_{Blm}}\right)\right]\Big/\sum_{k=1}^{C}\Psi_{kj} \quad ; \; 1\le i,l\le C \tag{C.15}$$

$$\left(\frac{\partial h_{Aj}}{\partial \ln K_{Am}}\right)=\delta(j-m)+\left(\frac{\partial A_j}{\partial \ln K_{Am}}\right)-\left(\frac{\partial \hat{A}}{\partial \ln K_{Am}}\right)+\left[\sum_{k=1}^{C}\left(\frac{\partial \Psi_{kj}}{\partial \ln K_{Am}}\right)\right]\Big/\sum_{k=1}^{C}\Psi_{kj} \tag{C.16}$$

$$\left(\frac{\partial h_{Aj}}{\partial \beta_m}\right)=\left(\frac{\partial A_j}{\partial \beta_m}\right)-\left(\frac{\partial \hat{A}}{\partial \beta_m}\right)+\left[\sum_{k=1}^{C}\left(\frac{\partial \Psi_{kj}}{\partial \beta_m}\right)\right]\Big/\sum_{k=1}^{C}\Psi_{kj} \tag{C.17}$$

$$\left(\frac{\partial l_j}{\partial \ln K_{Blm}}\right)=-\left(\frac{\partial \Psi_{lj}}{\partial \ln K_{Blm}}\right) \quad ; \; 1\le l\le C \tag{C.18}$$

$$\left(\frac{\partial l_j}{\partial \ln K_{Am}}\right)=-\sum_{i=1}^{C}\left(\frac{\partial \Psi_{ij}}{\partial \ln K_{Am}}\right) \tag{C.19}$$

and $$\left(\frac{\partial l_j}{\partial \beta_m}\right)=-\sum_{i=1}^{C}\left(\frac{\partial \Psi_{ij}}{\partial \beta_m}\right) \tag{C.20}$$

where m and j are phase indices which may vary from 1 to π.

C.3 Segment Fraction Derivatives

The derivatives of the unnormalized segment fractions, Ψ_{ij}, are given by:

$$\left(\frac{\partial \Psi_{ij}}{\partial \ln K_{Blm}}\right)=\begin{cases}\delta(i-l)\dfrac{\psi_{lF}K_{lm}}{E_l}\left[\delta(j-m)-\dfrac{K_{lj}\beta_m}{E_l}\right] & ; \; 1\le i\le n_d \\ \delta(i-l)\psi_{lF}\displaystyle\int_{r=0}^{\infty}\frac{rW_{lF}(r)K_{lm}(r)}{E_l(r)}\left[\delta(j-m)-\frac{K_{lj}(r)\beta_m}{E_l(r)}\right]dr & ; \; n_d<i\le C\end{cases} \tag{C.21}$$

$$\left(\frac{\partial \Psi_{ij}}{\partial \ln K_{Am}}\right) = \Psi_{im}\delta(j-m) + \left(\frac{\partial \Psi_{ij}}{\partial \beta_m}\right)\beta_m \quad ; \; 1 \le i \le C \tag{C.22}$$

and

$$\left(\frac{\partial \Psi_{ij}}{\partial \beta_m}\right) = \begin{cases} -\dfrac{\Psi_{ij}\Psi_{im}}{\psi_{iF}} & ; \; 1 \le i \le n_d \\ -\psi_{iF}\displaystyle\int_{r=0}^{\infty} \frac{W_{iF}(r)K_{ij}(r)K_{im}(r)}{E_i^2(r)}dr & ; \; n_d < i \le C \end{cases}, \tag{C.23}$$

From these, the derivatives of the normalized mole fractions, ψ_{ij}, can be found from

$$\left(\frac{\partial \psi_{ij}}{\partial \eta}\right) = \left\{\left(\frac{\partial \Psi_{ij}}{\partial \eta}\right) - \psi_{ij}\sum_{n=1}^{C}\left(\frac{\partial \Psi_{nj}}{\partial \eta}\right)\right\} \Big/ \sum_{n=1}^{C}\Psi_{nj} \tag{C.24}$$

where η represents any one of $\ln K_{Blm}$, $\ln K_{Am}$ or β_m.

C.4 Number Average Number of Segments Derivatives

The derivatives of the number average number of segments in each phase, $\bar{r}_j$, can be expressed as

$$\begin{aligned} -\frac{1}{\bar{r}_j^2}\left(\frac{\partial \bar{r}_j}{\partial \ln K_{Blm}}\right) &= \left(\frac{\partial 1/\bar{r}_j}{\partial \ln K_{Blm}}\right) \\ &= \begin{cases} \left(\dfrac{1}{r_l} - \dfrac{1}{\bar{r}_j}\right)\left(\dfrac{\partial \Psi_{lj}}{\partial \ln K_{Blm}}\right) \Big/ \displaystyle\sum_{n=1}^{C}\Psi_{nj} & ; \; 1 \le l \le n_d \\ \left[\left(\dfrac{\partial \Psi_{lj}}{\partial \ln K_{Am}}\right) - \dfrac{1}{\bar{r}_j}\left(\dfrac{\partial \Psi_{lj}}{\partial \ln K_{Blm}}\right)\right] \Big/ \displaystyle\sum_{n=1}^{C}\Psi_{nj} & ; \; n_d < l \le C \end{cases} \end{aligned} \tag{C.25}$$

$$\begin{aligned} -\frac{1}{\bar{r}_j^2}\left(\frac{\partial \bar{r}_j}{\partial \ln K_{Am}}\right) &= \left(\frac{\partial 1/\bar{r}_j}{\partial \ln K_{Am}}\right) \\ &= \left\{\sum_{i=n_d+1}^{C}\int_{r=0}^{\infty}\frac{\psi_{iF}W_{iF}(r)K_{im}(r)}{rE_i(r)}\left(\delta(j-m) - \frac{K_{ij}(r)\beta_m}{E_i(r)}\right)dr\right. \\ &\quad \left. + \sum_{i=1}^{n_d}\frac{1}{r_i}\left(\frac{\partial \Psi_{ij}}{\partial \ln K_{Am}}\right) - \frac{1}{\bar{r}_j}\sum_{i=1}^{C}\left(\frac{\partial \Psi_{ij}}{\partial \ln K_{Am}}\right)\right\} \Big/ \sum_{n=1}^{C}\Psi_{nj} \end{aligned} \tag{C.26}$$

and

$$-\frac{1}{\bar{r}_j^2}\left(\frac{\partial \bar{r}_j}{\partial \beta_m}\right)=\left(\frac{\partial 1/\bar{r}_j}{\partial \beta_m}\right)$$
$$=\left\{\sum_{i=1}^{n_d}\frac{1}{r_i}\left(\frac{\partial \Psi_{ij}}{\partial \beta_m}\right)-\sum_{i=n_d+1}^{C}\int_{r=0}^{\infty}\frac{\psi_{iF}W_{iF}(r)K_{ij}(r)K_{im}(r)}{rE_i^2(r)}dr\right.$$
$$\left.-\frac{1}{\bar{r}_j}\sum_{i=1}^{C}\left(\frac{\partial \Psi_{ij}}{\partial \beta_m}\right)\right\}\Bigg/\sum_{n=1}^{C}\Psi_{nj} \qquad \text{(C.27)}$$

C.5 *Reference Phase Derivatives*

The reference phase is defined by the two variables, $\hat{A}$ and $\hat{B}_i$, such that

$$\hat{A}=\sum_{j=1}^{\pi}\beta_j\left[\ln K_{Aj}+A_j-\ln\left(\sum_{n=1}^{C}\Psi_{nj}\right)\right] \qquad \text{(C.28)}$$

and

$$\hat{B}_i=\sum_{j=1}^{\pi}\beta_j\left[\ln K_{Bij}+B_{ij}\right]\quad ;\ 1\le i\le C. \qquad \text{(C.29)}$$

The required derivatives of these variables are

$$\left(\frac{\partial \hat{A}}{\partial \ln K_{Blm}}\right)=\sum_{j=1}^{\pi}\beta_j\left\{\left(\frac{\partial A_j}{\partial \ln K_{Blm}}\right)-\sum_{k=1}^{C}\left(\frac{\partial \Psi_{kj}}{\partial \ln K_{Blm}}\right)\Bigg/\sum_{n=1}^{C}\Psi_{nj}\right\}\quad ;\ 1\le l\le C \qquad \text{(C.30)}$$

$$\left(\frac{\partial \hat{A}}{\partial \ln K_{Am}}\right)=\sum_{j=1}^{\pi}\beta_j\left\{\delta(j-m)+\left(\frac{\partial A_j}{\partial \ln K_{Am}}\right)-\sum_{k=1}^{C}\left(\frac{\partial \Psi_{kj}}{\partial \ln K_{Am}}\right)\Bigg/\sum_{n=1}^{C}\Psi_{nj}\right\} \qquad \text{(C.31)}$$

$$\left(\frac{\partial \hat{A}}{\partial \beta_m}\right)=\sum_{j=1}^{\pi}\beta_j\left\{\left(\frac{\partial A_j}{\partial \beta_m}\right)-\sum_{k=1}^{C}\left(\frac{\partial \Psi_{kj}}{\partial \beta_m}\right)\Bigg/\sum_{n=1}^{C}\Psi_{nj}\right\}+\ln K_{Am}+A_m-\ln\left(\sum_{k=1}^{C}\Psi_{km}\right) \qquad \text{(C.32)}$$

$$\left(\frac{\partial \hat{B}_i}{\partial \ln K_{Blm}}\right)=\sum_{j=1}^{\pi}\beta_j\left\{\delta(i-l,j-m)+\left(\frac{\partial B_{ij}}{\partial \ln K_{Blm}}\right)\right\}\quad ;\ 1\le i,l\le C \qquad \text{(C.33)}$$

$$\left(\frac{\partial \hat{B}_i}{\partial \ln K_{Am}}\right)=\sum_{j=1}^{\pi}\beta_j\left(\frac{\partial B_{ij}}{\partial \ln K_{Am}}\right)\quad ;\ 1\le i\le C \qquad \text{(C.34)}$$

and

$$\left(\frac{\partial \hat{B}_i}{\partial \beta_m}\right) = \sum_{j=1}^{x} \beta_j \left(\frac{\partial B_{ij}}{\partial \beta_m}\right) + \ln K_{Bim} + B_{im} \quad ; \; 1 \le i \le C \tag{C.35}$$

C.6 *Volume Derivatives*

$$\left(\frac{\partial v_j}{\partial \eta}\right)_{T,P} = \left\{ \frac{1}{vRT}\left(\frac{\partial \tilde{a}_j}{\partial \eta}\right) + \left(\frac{\partial \bar{r}_j}{\partial \eta}\right) - \frac{v_j}{\tilde{b}_j^2}\left(\frac{\partial \tilde{b}_j}{\partial \eta}\right) \ln\left(\frac{v_j - \bar{r}_j \tilde{b}_j}{v_j}\right) - \frac{v_j}{\tilde{b}_j\left(v_j - \bar{r}_j \tilde{b}_j\right)}\left[\tilde{b}_j\left(\frac{\partial \bar{r}_j}{\partial \eta}\right) + \bar{r}_j\left(\frac{\partial \tilde{b}_j}{\partial \eta}\right)\right]\right\} \Bigg/ \left\{ \frac{2\tilde{a}_j}{v_j^2 RT} - \frac{\left(1-\bar{r}_j\right)}{v_j} - \frac{\bar{r}_j}{v_j - \bar{r}_j \tilde{b}_j} \right\} \tag{C.36}$$

C.7 *Derivatives of the Sanchez-Lacombe Equation of State*

$$\left(\frac{\partial A_j}{\partial \eta}\right) = \frac{1}{\bar{r}_j}\left(\frac{\partial \bar{r}_j}{\partial \eta}\right) + \frac{1}{\tilde{b}_j}\left(\frac{\partial \tilde{b}_j}{\partial \eta}\right) - \frac{1}{v_j}\left(\frac{\partial v_j}{\partial \eta}\right) \tag{C.37}$$

$$\begin{aligned}
\left(\frac{\partial B_{ij}}{\partial \eta}\right) = {} & \frac{2}{\bar{r}_j \tilde{b}_j}\left\{\frac{1}{\bar{r}_j}\left(\frac{\partial \bar{r}_j}{\partial \eta}\right) + \frac{1}{\tilde{b}_j}\left(\frac{\partial \tilde{b}_j}{\partial \eta}\right)\right\}\left[\frac{\tilde{b}_{ij}}{\tilde{b}_j} - 1\right]\left(v_j - \bar{r}_j \tilde{b}_j\right)\ln\left(\frac{v_j - \bar{r}_j \tilde{b}_j}{v_j}\right) \\
& - \frac{2}{\bar{r}_j \tilde{b}_j}\left\{\frac{1}{\tilde{b}_j}\left(\frac{\partial \tilde{b}_{ij}}{\partial \eta}\right) - \frac{\tilde{b}_{ij}}{\tilde{b}_j^2}\left(\frac{\partial \tilde{b}_j}{\partial \eta}\right)\right\}\left(v_j - \bar{r}_j \tilde{b}_j\right)\ln\left(\frac{v_j - \bar{r}_j \tilde{b}_j}{v_j}\right) \\
& - \frac{2}{\bar{r}_j \tilde{b}_j}\left[\frac{\tilde{b}_{ij}}{\tilde{b}_j} - 1\right]\left\{\left(\frac{\partial v_j}{\partial \eta}\right) - \tilde{b}_j\left(\frac{\partial \bar{r}_j}{\partial \eta}\right) - \bar{r}_j\left(\frac{\partial \tilde{b}_j}{\partial \eta}\right)\right\}\ln\left(\frac{v_j - \bar{r}_j \tilde{b}_j}{v_j}\right) + 2\left(\frac{\partial A_j}{\partial \eta}\right)\left[\frac{\tilde{b}_{ij}}{\tilde{b}_j} - 1\right] \\
& - \frac{2\tilde{b}_{ij}}{\tilde{b}_j}\left\{\frac{1}{\tilde{b}_{ij}}\left(\frac{\partial \tilde{b}_{ij}}{\partial \eta}\right) - \frac{1}{\tilde{b}_j}\left(\frac{\partial \tilde{b}_j}{\partial \eta}\right)\right\}\left[\ln\left(\frac{v_j - \bar{r}_j \tilde{b}_j}{v_j}\right) + 1\right] + \left(\frac{2\tilde{b}_{ij}}{\tilde{b}_j} - 1\right)\frac{\bar{r}_j \tilde{b}_j}{v_j - \bar{r}_j \tilde{b}_j}\left(\frac{\partial A_j}{\partial \eta}\right) \\
& - \frac{2\tilde{a}_{ij}\bar{r}_j}{v_j RT}\left\{\frac{1}{\tilde{a}_{ij}}\left(\frac{\partial \tilde{a}_{ij}}{\partial \eta}\right) + \frac{1}{\bar{r}_j}\left(\frac{\partial \bar{r}_j}{\partial \eta}\right) - \frac{1}{v_j}\left(\frac{\partial v_j}{\partial \eta}\right)\right\} \\
& - \frac{2\tilde{b}_{ij}}{\tilde{b}_j \bar{r}_j}\left\{\frac{1}{\bar{r}_j}\left(\frac{\partial \bar{r}_j}{\partial \eta}\right) + \frac{1}{\tilde{b}_j}\left(\frac{\partial \tilde{b}_j}{\partial \eta}\right) - \frac{1}{\tilde{b}_{ij}}\left(\frac{\partial \tilde{b}_{ij}}{\partial \eta}\right)\right\} + \frac{2}{\bar{r}_j^2}\left(\frac{\partial \bar{r}_j}{\partial \eta}\right)
\end{aligned} \tag{C.38}$$

C.8 *Derivatives of the Sanchez-Lacombe Equation of State Parameters*

$$\left(\frac{\partial \tilde{a}_j}{\partial \eta}\right) = 2\frac{\tilde{a}_j}{\tilde{r}_j}\left(\frac{\partial \tilde{r}_j}{\partial \eta}\right) + \tilde{r}_j^2 \sum_{i=1}^{C}\sum_{k=1}^{C}\left\{\left(\frac{\partial \psi_{ij}}{\partial \eta}\right)\psi_{kj} + \psi_{ij}\left(\frac{\partial \psi_{kj}}{\partial \eta}\right)\right\}\varepsilon_{ik}\nu_{ik} \tag{C.39}$$

$$\left(\frac{\partial \tilde{a}_{ij}}{\partial \eta}\right) = \sum_{k=1}^{C}\left(\frac{\partial \psi_{kj}}{\partial \eta}\right)\varepsilon_{ik}\nu_{ik} \tag{C.40}$$

$$\left(\frac{\partial \tilde{b}_j}{\partial \eta}\right) = \sum_{i=1}^{C}\sum_{k=1}^{C}\left\{\left(\frac{\partial \psi_{ij}}{\partial \eta}\right)\psi_{kj} + \psi_{ij}\left(\frac{\partial \psi_{kj}}{\partial \eta}\right)\right\}\nu_{ik} \tag{C.41}$$

$$\left(\frac{\partial \tilde{b}_{ij}}{\partial \eta}\right) = \sum_{k=1}^{C}\left(\frac{\partial \psi_{kj}}{\partial \eta}\right)\nu_{ik}\,. \tag{C.42}$$

IMAGE EVALUATION TEST TARGET (QA-3)

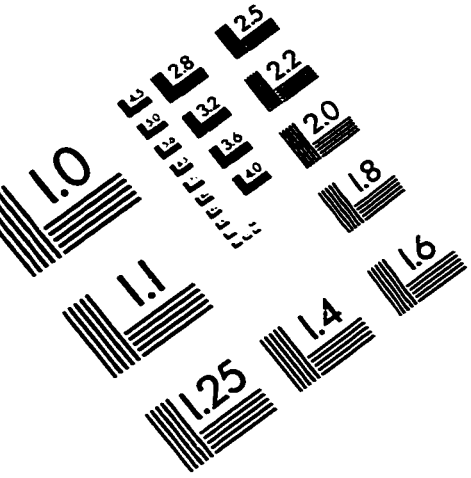

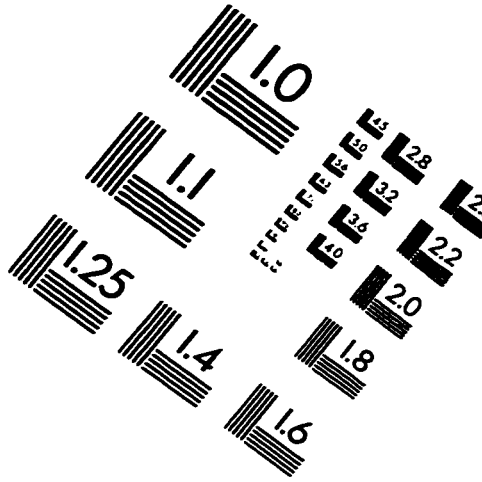

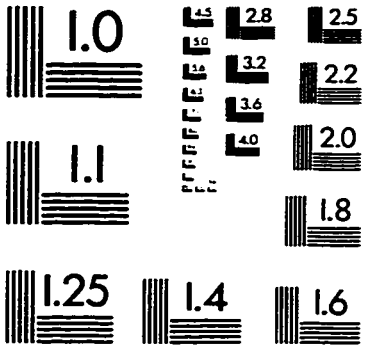

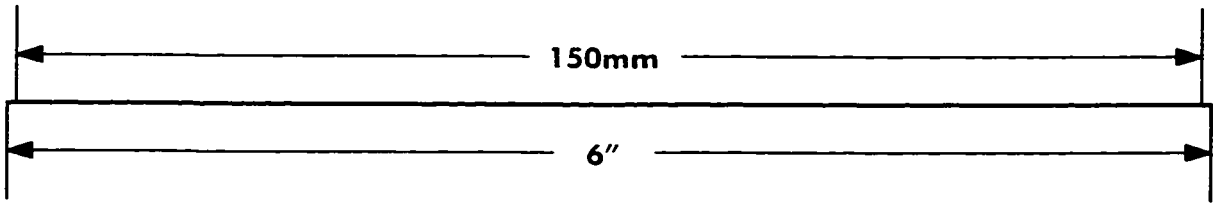

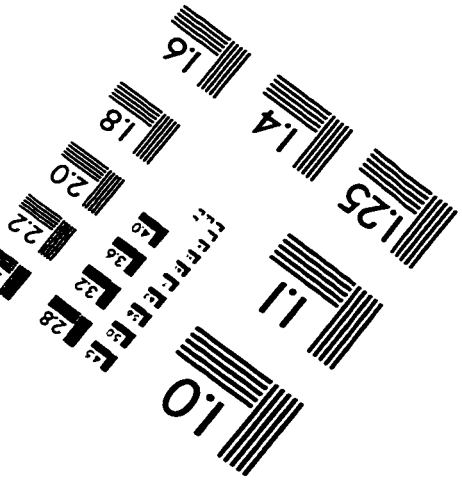

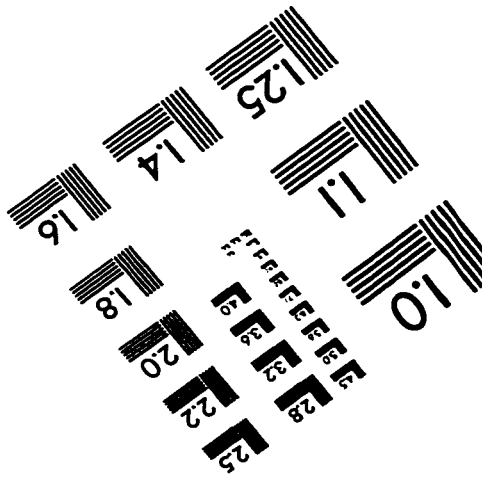

APPLIED IMAGE, Inc
1653 East Main Street
Rochester, NY 14609 USA
Phone: 716/482-0300
Fax: 716/288-5989